

Solid State Theory

Spring Semester 2014

Manfred Sigrist
Institut für Theoretische Physik HIT K23.8
Tel.: 044-633-2584
Email: sigrist@itp.phys.ethz.ch
Website: <http://www.itp.phys.ethz.ch/research/condmat/strong/>

Lecture Website:
<http://www.itp.phys.ethz.ch/education/fs14/sst>

Literature:

- N.W. Ashcroft and N.D. Mermin: *Solid State Physics*, HRW International Editions, 1976.
- C. Kittel: *Einführung in die Festkörperphysik*, R. Oldenburg Verlag, 1983.
- C. Kittel: *Quantentheorie der Festkörper*, R. Oldenburg, 1970.
- O. Madelung: *Introduction to solid-state theory*, Springer 1981; auch in Deutsch in drei Bänden: *Festkörperphysik I-III*, Springer.
- J.M. Ziman: *Principles of the Theory of Solids*, Cambridge University Press, London, 1972.
- M.P. Marder: *Condensed Matter Physics*, John Wiley & Sons, 2000.
- G. Grosso & G.P. Parravicini: *Solid State Physics*, Academic Press, 2000.
- G. Czychol: *Theoretische Festkörperphysik*, Springer 2004.
- P.L. Taylor & O. Heinonen, *A Quantum Approach to Condensed Matter Physics*, Cambridge Press 2002.
- G.D. Mahan, *Condensed Matter in a Nutshell*, Princeton University Press 2011.
- numerous specialized books.

Contents

| | |
|--|-----------|
| Introduction | 5 |
| 1 Electrons in the periodic crystal - band structure | 8 |
| 1.1 Symmetries of crystals | 8 |
| 1.1.1 Space groups of crystals | 8 |
| 1.1.2 Reciprocal lattice | 10 |
| 1.2 Bloch's theorem and Bloch functions | 11 |
| 1.3 Nearly free electron approximation | 12 |
| 1.4 Tight-binding approximation | 14 |
| 1.4.1 Linear combination of atomic orbitals - LCAO | 16 |
| 1.4.2 Band structure of s-orbitals | 17 |
| 1.4.3 Band structure of p-orbitals | 17 |
| 1.4.4 Wannier functions | 19 |
| 1.4.5 Tight binding model in second quantization formulation | 21 |
| 1.5 Symmetry properties of the band structure | 21 |
| 1.6 Band-filling and materials properties | 24 |
| 1.6.1 Electron count and band filling | 24 |
| 1.6.2 Metals, semiconductors and insulators | 25 |
| 1.7 Semi-classical description | 27 |
| 1.7.1 Equations of motion | 27 |
| 1.7.2 Bloch oscillations | 28 |
| 1.7.3 Current densities | 29 |
| 1.8 Appendix: Approximative band structure calculations | 30 |
| 1.8.1 Pseudo-potential | 30 |
| 1.8.2 Augmented plane wave | 33 |
| 2 Semiconductors | 35 |
| 2.1 The band structure in group IV | 36 |
| 2.1.1 Crystal and band structure | 36 |
| 2.2 Elementary excitations | 38 |
| 2.2.1 Electron-hole excitations | 39 |
| 2.2.2 Excitons | 40 |
| 2.2.3 Optical properties | 43 |
| 2.3 Doping semiconductors | 44 |
| 2.3.1 Impurity state | 44 |
| 2.3.2 Carrier concentration | 46 |
| 2.4 Semiconductor devices | 46 |
| 2.4.1 pn-contacts | 46 |
| 2.4.2 Diodes | 48 |
| 2.4.3 MOSFET | 49 |

| | | |
|----------|---|------------|
| 3 | Metals | 51 |
| 3.1 | The Jellium model | 51 |
| 3.1.1 | Theory of metals - Sommerfeld and Pauli | 52 |
| 3.1.2 | Stability of metals - a Hartree-Fock approach | 54 |
| 3.2 | Charge excitations | 57 |
| 3.2.1 | Dielectric response and Lindhard function | 58 |
| 3.2.2 | Electron-hole excitation | 60 |
| 3.2.3 | Collective excitation - Plasmon | 60 |
| 3.2.4 | Screening | 63 |
| 3.3 | Phonons | 66 |
| 3.3.1 | Vibration of a isotropic continuous medium | 66 |
| 3.3.2 | Phonons in metals | 68 |
| 3.3.3 | Peierls instability in one dimension | 69 |
| 3.3.4 | Dynamics of phonons and the dielectric function | 74 |
| 4 | Itinerant electrons in a magnetic field | 76 |
| 4.1 | The de Haas-van Alphen effect | 76 |
| 4.1.1 | Landau levels | 76 |
| 4.1.2 | Oscillatory behavior of the magnetization | 78 |
| 4.1.3 | Onsager equation | 79 |
| 4.2 | Quantum Hall Effect | 80 |
| 4.2.1 | Hall effect of the two-dimensional electron gas | 82 |
| 4.2.2 | Integer Quantum Hall Effect | 83 |
| 4.2.3 | Fractional Quantum Hall Effect | 89 |
| 5 | Landau's Theory of Fermi Liquids | 93 |
| 5.1 | Lifetime of quasiparticles | 93 |
| 5.2 | Phenomenological Theory of Fermi Liquids | 96 |
| 5.2.1 | Specific heat | 98 |
| 5.2.2 | Compressibility | 100 |
| 5.2.3 | Spin susceptibility | 101 |
| 5.2.4 | Galilei invariance | 102 |
| 5.2.5 | Stability of the Fermi liquid | 103 |
| 5.3 | Microscopic considerations | 105 |
| 5.3.1 | Landau parameters | 106 |
| 5.3.2 | Distribution function | 108 |
| 5.3.3 | Fermi liquid in one dimension? | 109 |
| 6 | Transport properties of metals | 111 |
| 6.1 | Electrical conductivity | 111 |
| 6.2 | Transport equations and relaxation time | 113 |
| 6.2.1 | The Boltzmann equation | 113 |
| 6.2.2 | The Drude form | 115 |
| 6.2.3 | The relaxation time | 118 |
| 6.3 | Impurity scattering | 119 |
| 6.3.1 | Potential scattering | 119 |
| 6.3.2 | Kondo effect | 121 |
| 6.4 | Electron-phonon interaction | 122 |
| 6.5 | Electron-electron scattering | 125 |
| 6.6 | Matthiessen's rule and the Ioffe-Regel limit | 127 |
| 6.7 | General transport coefficients | 128 |
| 6.7.1 | Generalized Boltzmann equation | 128 |
| 6.7.2 | Thermoelectric effect | 130 |

| | | |
|----------|--|------------|
| 6.8 | Anderson localization | 133 |
| 6.8.1 | Landauer Formula for a single impurity | 133 |
| 6.8.2 | Scattering at two impurities | 135 |
| 6.8.3 | Anderson localization | 136 |
| 7 | Magnetism in metals | 138 |
| 7.1 | Stoner instability | 139 |
| 7.1.1 | Stoner model within the mean field approximation | 139 |
| 7.1.2 | Stoner criterion | 140 |
| 7.1.3 | Spin susceptibility for $T > T_C$ | 143 |
| 7.2 | General spin susceptibility and magnetic instabilities | 144 |
| 7.2.1 | General dynamic spin susceptibility | 144 |
| 7.2.2 | Instability with finite wave vector \mathbf{Q} | 147 |
| 7.2.3 | Influence of the band structure | 148 |
| 7.3 | Stoner excitations | 150 |
| 8 | Magnetism of localized moments | 153 |
| 8.1 | Mott transition | 154 |
| 8.1.1 | Hubbard model | 154 |
| 8.1.2 | Insulating state | 155 |
| 8.1.3 | The metallic state | 156 |
| 8.1.4 | Fermi liquid properties of the metallic state | 158 |
| 8.2 | The Mott insulator as a quantum spin system | 160 |
| 8.2.1 | The effective Hamiltonian | 160 |
| 8.2.2 | Mean field approximation of the anti-ferromagnet | 161 |
| 8.3 | Collective modes – spin wave excitations | 163 |

Introduction

Solid state physics (or condensed matter physics) is one of the most active and versatile branches of modern physics that have developed in the wake of the discovery of quantum mechanics. It deals with problems concerning the properties of materials and, more generally, systems with many degrees of freedom, ranging from fundamental questions to technological applications. This richness of topics has turned solid state physics into the largest subfield of physics; furthermore, it has arguably contributed most to technological development in industrialized countries.

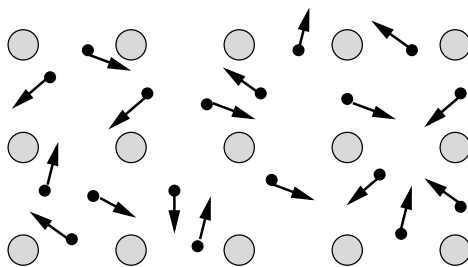


Figure 1: Atom cores and the surrounding electrons.

Condensed matter (solid bodies) consists of atomic nuclei (ions), usually arranged in a regular (elastic) lattice, and of electrons (see Figure 1). As the macroscopic behavior of a solid is determined by the dynamics of these constituents, the description of the system requires the use of quantum mechanics. Thus, we introduce the Hamiltonian describing nuclei and electrons,

$$\hat{H} = \hat{H}_e + \hat{H}_n + \hat{H}_{n-e}, \quad (1)$$

with

$$\begin{aligned} \hat{H}_e &= \sum_i \frac{\hat{\mathbf{p}}_i^2}{2m} + \frac{1}{2} \sum_{i \neq i'} \frac{e^2}{|\mathbf{r}_i - \mathbf{r}_{i'}|}, \\ \hat{H}_n &= \sum_j \frac{\hat{\mathbf{P}}_j^2}{2M_j} + \frac{1}{2} \sum_{j \neq j'} \frac{Z_j Z_{j'} e^2}{|\mathbf{R}_j - \mathbf{R}_{j'}|}, \\ \hat{H}_{n-e} &= - \sum_{i,j} \frac{Z_j e^2}{|\mathbf{r}_i - \mathbf{R}_j|}, \end{aligned} \quad (2)$$

where \hat{H}_e (\hat{H}_n) describes the dynamics of the electrons (nuclei) and their mutual interaction and \hat{H}_{n-e} includes the interaction between ions and electrons. The parameters appearing are

| | | |
|-------|---|------------------------------------|
| m | free electron mass | $9.1094 \times 10^{-31} \text{kg}$ |
| e | elementary charge | $1.6022 \times 10^{-19} \text{As}$ |
| M_j | mass of j -th nucleus | $\sim 10^3 - 10^4 \times m$ |
| Z_j | atomic (charge) number of j -th nucleus | |

The characteristic scales known from atomic and molecular systems are

| | |
|---------------------|--|
| Length: Bohr radius | $a_B = \hbar^2/me^2 \approx 0.5 \times 10^{-10} \text{m}$ |
| Energy: Hartree | $e^2/a_B = me^4/\hbar^2 = mc^2\alpha^2 \approx 27\text{eV} = 2\text{Ry}$ |

with the fine structure constant $\alpha = e^2/\hbar c = 1/137$. The energy scale of one Hartree is much less than the (relativistic) rest mass of an electron ($\sim 0.5\text{MeV}$), which in turn is considered small in particle physics. In fact, in high-energy physics even physics at the Planck scale is considered, at least theoretically. The Planck scale is an energy scale so large that even gravity is thought to be affected by quantum effects, as

$$E_{\text{Planck}} = c^2 \sqrt{\frac{\hbar c}{G}} \sim 10^{19} \text{GeV}, \quad l_{\text{Planck}} = \sqrt{\frac{\hbar G}{c^3}} \sim 1.6 \times 10^{-35} \text{m}, \quad (3)$$

where $G = 6.673 \times 10^{-11} \text{m}^3 \text{kg}^{-1} \text{s}^{-2}$ is the gravitational constant. This is the realm of the GUT (grand unified theory) and string theory. The goal is not to provide a better description of electrons or atomic cores, but to find the most fundamental theory of physics.

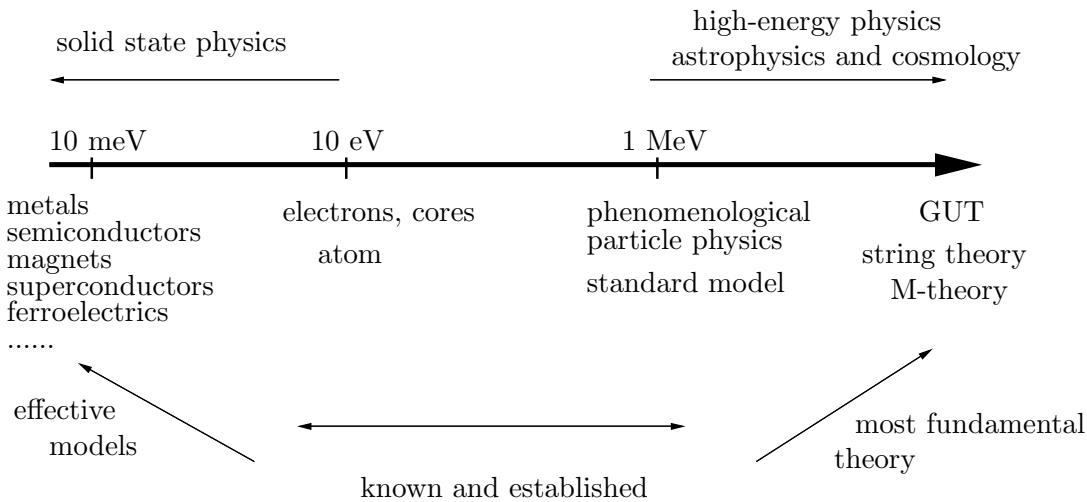


Figure 2: Energy scales in physics.

In contrast, in solid state physics we are dealing with phenomena occurring at room temperature ($T \sim 300\text{K}$) or below, i.e., at characteristic energies of about $E \sim k_B T \sim 0.03\text{eV} = 30\text{meV}$, which is even much smaller than the energy scale of one Hartree. Correspondingly, the important length scales are given by the extension of the system or of the electronic wave functions. The focus is thus quite different from the one of high-energy physics.

There, a highly successful phenomenological theory for low energies, the so-called standard model, exists, whereas the underlying theory for higher energies is unknown. In solid state physics, the situation is reversed. The Hamiltonian (1) describes the known 'high-energy' physics (on the energy scale of Hartree), and one aims at describing the low-energy properties using reduced (effective, phenomenological) theories. Both tasks are far from trivial.

Among the various states of condensed matter that solid state theory seeks to describe are metals, semiconductors, and insulators. Furthermore, there are phenomena such as magnetism, superconductivity, ferroelectricity, charge ordering, and the quantum Hall effect. All of these states share a common origin: Electrons interacting among themselves and with the ions through the Coulomb interaction. More often than not, the microscopic formulation in (1) is too complicated to allow an understanding of the low-energy behavior from first principles. Consequently, the formulation of effective (reduced) theories is an important step in condensed matter theory. On the one hand, characterizing the ground state of a system is an important goal in itself. However, measurable quantities are determined by excited states, so that the concept of 'elementary excitations' takes on a central role. Some celebrated examples are Landau's quasiparticles for

Fermi liquids, the phonons connected to lattice vibrations, and magnons in ferromagnets. The idea is to treat the ground state as an effective vacuum in the sense of second quantization, with the elementary excitations as particles on that vacuum. Depending on the system, the vacuum may be the Fermi sea or some state with a broken symmetry, like a ferromagnet, a superconductor, or the crystal lattice itself.

According to P. W. Anderson,¹ the description of the properties of materials rests on two principles: The principle of *adiabatic continuity* and the principle of *spontaneously broken symmetry*. By adiabatic continuity we mean that complicated systems may be replaced by simpler systems that have the same essential properties in the sense that the two systems may be adiabatically deformed into each other without changing qualitative properties. Arguably the most impressive example is Landau's Fermi liquid theory mentioned above. The low-energy properties of strongly interacting electrons are the same as those of non-interacting fermions with renormalized parameters. On the other hand, phase transitions into states with qualitatively different properties can often be characterized by broken symmetries. In magnetically ordered states the rotational symmetry and the time-reversal invariance are broken, whereas in the superconducting state the global gauge symmetry is. In many cases the violation of a symmetry is a guiding principle which helps to simplify the theoretical description considerably. Moreover, in recent years some systems have been recognized as having topological order which may be considered as a further principle to characterize low-energy states of matter. A famous example for this is found in the context of the Quantum Hall effect.

The goal of these lectures is to introduce these basic concepts on which virtually all more elaborate methods are building up. In the course of this, we will cover a wide range of frequently encountered ground states, starting with the theory of metals and semiconductors, proceeding with magnets, Mott insulators, and finally superconductors.

¹P.W. Anderson: *Basic Notions of Condensed Matter Physics*, Frontiers in Physics Lecture Notes Series, Addison-Wesley (1984).

Chapter 1

Electrons in the periodic crystal - band structure

One of the characteristic features of many solids is the regular arrangement of their atoms forming a crystal. Electrons moving in such a crystal are subject to a *periodic potential* which originates from the lattice of ions and an averaged electron-electron interaction (like Hartree-Fock approximation). The spectrum of extended electronic states, i.e. delocalized eigenstates of the Schrödinger equation, form bands of allowed energies and gaps of "forbidden" energies.

There are two limiting starting points towards the understanding of the band formation: (1) the *free electron gas* whose continuous spectrum is broken up into bands under the influence of a periodic potential (electrons undergo Bragg scattering); (2) *independent atoms* are brought together into a lattice until the outer-most electronic states overlap and lead to delocalized states turning a discrete set of states into continua of electronic energies - bands. In this chapter we will address the emergence of band structures from these two limiting cases. The band structure of electrons is essential for the basic classification of materials into metals and insulators (semiconductors).

1.1 Symmetries of crystals

1.1.1 Space groups of crystals

Most solids consist of a regular lattice of atoms with perfectly repeating structures. The minimal repeating unit of such a lattice is the *unit cell*. The symmetries of a crystal are contained in the *space group* \mathcal{R} , a group of symmetry operations (translations, rotations, the inversion or combinations) under which the crystal is left invariant. In three dimensions, there are 230 different space groups¹ (cf. Table 1.1).

¹All symmetry transformations form together a set which has the properties of a group. A group \mathcal{G} combined with a multiplication "*" has the following properties:

- the product of two elements of \mathcal{G} is also in \mathcal{G} : $a, b \in \mathcal{G} \Rightarrow a * b = c \in \mathcal{G}$.
- multiplications are associative: $a * (b * c) = (a * b) * c$.
- a unit element $e \in \mathcal{G}$ exists with: $e * a = a * e = a$ for all $a \in \mathcal{G}$.
- for every element $a \in \mathcal{G}$ there is an inverse $a^{-1} \in \mathcal{G}$ with $a^{-1} * a = a * a^{-1} = e$.

A group with $a * b = b * a$ for all pairs of element is called Abelian group, otherwise it is non-Abelian. A subset $\mathcal{G}' \subset \mathcal{G}$ is called a subgroup of \mathcal{G} , if it is a group as well.

Guides to group theory in the context of condensed matter physics can be found in the textbooks

- Mildred S. Dresselhaus, Gene Dresselhaus and Ado Jorio: *Group Theory - Application to the Physics of Condensed Matter*
- Peter Y. Yu and Manuel Cardona: *Fundamentals of Semiconductors*, Springer.

We consider here a crystal displayed as a point lattice, each point either symbolizing an atom or a whole unit cell (Fig.1.1 for a square lattice). Translations in the space group are represented by linear combinations of a basic set of translation vectors $\{\mathbf{a}_i\}$ (primitive lattice vectors) connecting lattice points. Any translation that maps the lattice onto itself is a linear combination of the $\{\mathbf{a}_i\}$ with integer coefficients,

$$\mathbf{R}_n = n_1\mathbf{a}_1 + n_2\mathbf{a}_2 + n_3\mathbf{a}_3. \quad (1.1)$$

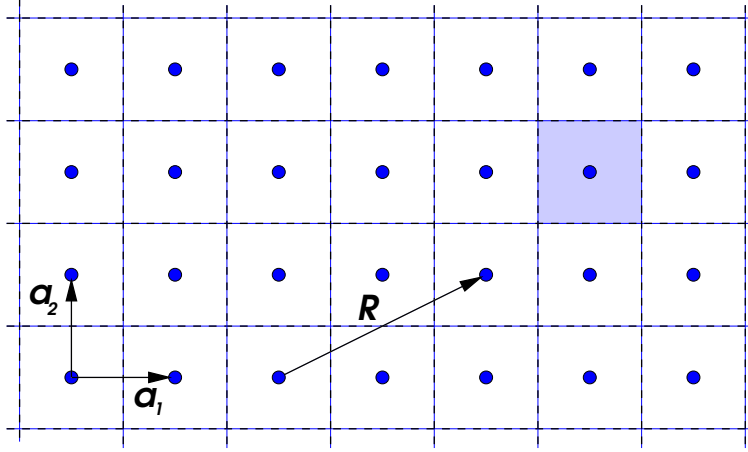


Figure 1.1: Crystal point lattice in two dimensions: the vectors \mathbf{a}_1 and \mathbf{a}_2 form the basic set of translations and $\mathbf{R} = 2\mathbf{a}_1 + \mathbf{a}_2$ in the figure. The shaded area is the Wigner-Seitz cell which is obtained by drawing perpendicular lines (planes in three dimensions) through the center of all lines connecting neighboring lattice points. The Wigner-Seitz cell also constitutes a unit cell of the lattice.

General symmetry transformations including general elements of the space group may be written in the notation due to Wigner,

$$\mathbf{r}' = g\mathbf{r} + \mathbf{a} = \{g|\mathbf{a}\}\mathbf{r}, \quad (1.2)$$

where g represents a rotation, reflection or inversion with respect to lattice points, axes or planes. The elements g form the generating *point group* \mathcal{P} . In three dimensions there are 32 point groups. We distinguish the following basic symmetry operations:

| | |
|------------------------------------|---------------------|
| basic translations | $\{E \mathbf{a}\},$ |
| rotations, reflections, inversions | $\{g \mathbf{0}\},$ |
| screw axes, glide planes | $\{g \mathbf{a}\},$ |

where E is the unit element (identity) of \mathcal{P} . A screw axis is a symmetry operation of a rotation followed by a translation along the rotation axis. A glide plane is a symmetry operation with reflection at a plane followed by a translation along the same plane. The symmetry operations $\{g|\mathbf{a}\}$, together with the associative multiplication

$$\{g|\mathbf{a}\}\{g'|\mathbf{a}'\} = \{gg'|\mathbf{a}' + \mathbf{a}\} \quad (1.3)$$

form a group with unit element $\{E|\mathbf{0}\}$. In general, these groups are non-Abelian, i.e., the group elements do not commute with each other. However, there is always an Abelian subgroup of \mathcal{R} , the group of translations $\{E|\mathbf{a}\}$. The elements $g \in \mathcal{P}$ do not necessarily form a subgroup,

because some of these elements (e.g., screw axes or glide planes) leave the lattice invariant only in combination with a translation. Nevertheless, the relation

$$\{g|\mathbf{a}\}\{E|\mathbf{a}'\}\{g|\mathbf{a}\}^{-1} = \{E|g\mathbf{a}'\} \quad (1.4)$$

$$\{g|\mathbf{a}\}^{-1}\{E|\mathbf{a}'\}\{g|\mathbf{a}\} = \{E|g^{-1}\mathbf{a}'\} \quad (1.5)$$

holds generally. If \mathcal{P} is a subgroup of \mathcal{R} , then \mathcal{R} is said to be *symmorphic*. In this case, the space group contains only primitive translations $\{E|\mathbf{a}\}$ and neither screw axes nor glide planes. The 14 Bravais lattices² are symmorphic. Among the 230 space groups 73 are symmorphic and 157 are non-symmorphic.

| crystal system (# point groups, # space groups) | point groups Schönflies symbols | space group numbers international tables |
|--|--|---|
| triclinic (2,2) | C_1, C_1 | 1-2 |
| monoclinic (3,13) | C_2, C_s, C_{2h} | 3-15 |
| orthorhombic (3,59) | D_2, C_{2v}, D_{2h} | 16-74 |
| tetragonal (7,68) | $C_4, S_4, C_{4h}, D_4, C_{4v}, D_{2d}, D_{4h}$ | 75-142 |
| trigonal (5,25) | $C_3, S_6, D_3, C_{3v}, D_{3d}$ | 143-167 |
| hexagonal (7,27) | $C_6, C_{3h}, C_{6h}, D_6, C_{6v}, D_{3h}, D_{6h}$ | 168-194 |
| cubic (5, 36) | T, T_h, O, T_d, O_h | 195-230 |

Table 1.1: List of the point and space groups for each crystal system in three dimensions.

1.1.2 Reciprocal lattice

We define now the reciprocal lattice which is of importance for the electron band structure and x-ray diffraction on a periodic lattice. The reciprocal lattice is also perfectly periodic with a translation symmetry with a basic set $\{\mathbf{b}_i\}$ defining arbitrary reciprocal lattice vectors as

$$\mathbf{G}_m = m_1\mathbf{b}_1 + m_2\mathbf{b}_2 + m_3\mathbf{b}_3, \quad (1.6)$$

where m_i are integers and

$$\mathbf{a}_i \cdot \mathbf{b}_j = 2\pi\delta_{ij}, \quad i, j = 1, 2, 3, \quad (1.7)$$

such that

$$\mathbf{b}_i = 2\pi \frac{\mathbf{a}_j \times \mathbf{a}_k}{\mathbf{a}_i \cdot (\mathbf{a}_j \times \mathbf{a}_k)} \quad \text{and} \quad \mathbf{a}_i = 2\pi \frac{\mathbf{b}_j \times \mathbf{b}_k}{\mathbf{b}_i \cdot (\mathbf{b}_j \times \mathbf{b}_k)}. \quad (1.8)$$

The reciprocal lattice of a simple cubic lattice is simple cubic. However, a body centered cubic (bcc) lattice has a face centered cubic (fcc) reciprocal lattice and vice versa (see slides).

It follows that any real space lattice vector \mathbf{R}_n and any reciprocal lattice vector \mathbf{G}_m have the property that

$$\mathbf{G}_m \cdot \mathbf{R}_n = 2\pi(m_1n_1 + m_2n_2 + m_3n_3) = 2\pi N \quad (1.9)$$

²Crystal systems, crystals, Bravais lattices are discussed in more detail in

- Czocholl, *Theoretische Festkörperphysik*, Springer

with N being an integer. This allows us to expand any function $f(\mathbf{r})$ periodically in the real lattice as

$$f(\mathbf{r}) = \sum_{\mathbf{G}} f_{\mathbf{G}} e^{i\mathbf{G}\cdot\mathbf{r}} \quad (1.10)$$

with the obvious property: $f(\mathbf{r} + \mathbf{R}) = f(\mathbf{r})$. The coefficients are given by

$$f_{\mathbf{G}} = \frac{1}{\Omega_{\text{UC}}} \int_{\text{UC}} d^3r f(\mathbf{r}) e^{-i\mathbf{G}\cdot\mathbf{r}} \quad (1.11)$$

where the integral runs over the unit cell of the periodic lattice with the volume Ω_{UC} . Finally, we define the (first) Brillouin zone as the "Wigner-Seitz cell" constructed in the reciprocal lattice (see Fig.1.1 and 1.2).

1.2 Bloch's theorem and Bloch functions

We consider a Hamiltonian \mathcal{H} of electrons invariant under a discrete set of lattice translations $\{\{E|\mathbf{a}\}\}$, a symmetry introduced by a periodic potential. This implies that the corresponding translation operator $\hat{T}_{\mathbf{a}}$ on the Hilbert space commutes with the Hamiltonian $\mathcal{H} = \mathcal{H}_e + \mathcal{H}_{ie}$ (purely electronic Hamiltonian \mathcal{H}_e , interaction between electrons and ions \mathcal{H}_{ie}),

$$[\hat{T}_{\mathbf{a}}, \mathcal{H}] = 0. \quad (1.12)$$

This translation operator is defined through $\hat{T}_{\mathbf{a}}|\mathbf{r}\rangle = |\mathbf{r} + \mathbf{a}\rangle$ and $\langle\mathbf{r}|\hat{T}_{\mathbf{a}} = \langle\mathbf{r} - \mathbf{a}|$. Neglecting the interactions among electrons, which would be contained in \mathcal{H}_e , we are left with a single particle problem

$$\mathcal{H} \rightarrow \mathcal{H}_0 = \frac{\hat{\mathbf{p}}^2}{2m} + V(\hat{\mathbf{r}}), \quad (1.13)$$

where $\hat{\mathbf{r}}$ and $\hat{\mathbf{p}}$ are position and momentum operators, and

$$V(\mathbf{r}) = \sum_j V_{\text{ion}}(\mathbf{r} - \mathbf{R}_j), \quad (1.14)$$

describes the potential landscape of the single particle in the ionic background. With \mathbf{R}_j being the position of the j -th ion, the potential $V(\mathbf{r})$ is by construction periodic, with $V(\mathbf{r} + \mathbf{a}) = V(\mathbf{r})$ for all lattice vectors \mathbf{a} , and represents \mathcal{H}_{ie} . Therefore, \mathcal{H}_0 commutes with $\hat{T}_{\mathbf{a}}$. For a Hamiltonian \mathcal{H}_0 commuting with the translation operator $\hat{T}_{\mathbf{a}}$, the eigenstates of \mathcal{H}_0 are simultaneously eigenstates of $\hat{T}_{\mathbf{a}}$.

Bloch's theorem states that the eigenvalues of $\hat{T}_{\mathbf{a}}$ lie on the unit circle of the complex plane, which ensures that these states are extended. This means³

$$\hat{T}_{\mathbf{a}}\psi(\mathbf{r}) = \psi(\mathbf{r} - \mathbf{a}) = \lambda_{\mathbf{a}}\psi(\mathbf{r}), \quad \hat{T}_{l\mathbf{a}}\psi(\mathbf{r}) = \psi(\mathbf{r} - l\mathbf{a}) = \hat{T}_{\mathbf{a}}^l\psi(\mathbf{r}) = \lambda_{\mathbf{a}}^l\psi(\mathbf{r}) \quad (1.16)$$

with l an integer (positive or negative). In order to be bounded (renormalizable) and delocalized in the periodic potential the wave function satisfies,

$$|\psi(\mathbf{r})|^2 = |\psi(\mathbf{r} - l\mathbf{a})|^2 = |\lambda_{\mathbf{a}}^l|^2 |\psi(\mathbf{r})|^2 = |\lambda_{\mathbf{a}}|^{2l} |\psi(\mathbf{r})|^2, \quad (1.17)$$

requiring

$$|\lambda_{\mathbf{a}}| = 1 \quad \Rightarrow \quad \lambda_{\mathbf{a}} = e^{i\varphi_{\mathbf{a}}}. \quad (1.18)$$

³Transformation of wave function:

$$|\psi'\rangle = \hat{T}_{\mathbf{a}}|\psi\rangle \quad \Rightarrow \quad \psi'(\mathbf{r}) = \langle\mathbf{r}|\psi'\rangle = \langle\mathbf{r}|\hat{T}_{\mathbf{a}}|\psi\rangle = \langle\mathbf{r} - \mathbf{a}|\psi\rangle = \psi(\mathbf{r} - \mathbf{a}). \quad (1.15)$$

This condition is satisfied if we express the wave function as product of a plane wave $e^{i\mathbf{k}\cdot\mathbf{r}}$ and a periodic Bloch function $u_{\mathbf{k}}(\mathbf{r})$

$$\psi_{n,\mathbf{k}}(\mathbf{r}) = \frac{1}{\sqrt{\Omega}} e^{i\mathbf{k}\cdot\mathbf{r}} u_{n,\mathbf{k}}(\mathbf{r}). \quad (1.19)$$

with

$$\widehat{T}_{\mathbf{a}} u_{n,\mathbf{k}}(\mathbf{r}) = u_{n,\mathbf{k}}(\mathbf{r} - \mathbf{a}) = u_{n,\mathbf{k}}(\mathbf{r}), \quad (1.20)$$

$$\widehat{T}_{\mathbf{a}} \psi_{n,\mathbf{k}}(\mathbf{r}) = \psi_{n,\mathbf{k}}(\mathbf{r} - \mathbf{a}) = e^{-i\mathbf{k}\cdot\mathbf{a}} \psi_{n,\mathbf{k}}(\mathbf{r}), \quad (1.21)$$

$$\mathcal{H}_0 \psi_{n,\mathbf{k}}(\mathbf{r}) = \epsilon_{n,\mathbf{k}} \psi_{n,\mathbf{k}}(\mathbf{r}). \quad (1.22)$$

The integer n is a quantum number called band index, \mathbf{k} is the pseudo-momentum (wave vector) and Ω represents the volume of the system. Note that the eigenvalue of $\psi_{n,\mathbf{k}}(\mathbf{r})$ with respect to $\widehat{T}_{\mathbf{a}}$, $e^{-i\mathbf{k}\cdot\mathbf{a}}$, implies periodicity in the reciprocal space, the \mathbf{k} -space, because $e^{i(\mathbf{k}+\mathbf{G})\cdot\mathbf{a}} = e^{i\mathbf{k}\cdot\mathbf{a}}$ for all reciprocal lattice vectors \mathbf{G} . We may, therefore, restrict \mathbf{k} to the first Brillouin zone and $\epsilon_{n,\mathbf{k}+\mathbf{G}} = \epsilon_{n,\mathbf{k}}$.

Bloch's theorem simplifies the initial problem to the so-called Bloch equation for the periodic function $u_{\mathbf{k}}$,

$$\left(\frac{(\widehat{\mathbf{p}} + \hbar\mathbf{k})^2}{2m} + V(\widehat{\mathbf{r}}) \right) u_{\mathbf{k}}(\mathbf{r}) = \epsilon_{\mathbf{k}} u_{\mathbf{k}}(\mathbf{r}), \quad (1.23)$$

where we suppress the band index to simplify the notation. This equation follows from the relation

$$\widehat{\mathbf{p}} e^{i\mathbf{k}\cdot\mathbf{r}} u_{\mathbf{k}}(\mathbf{r}) = e^{i\mathbf{k}\cdot\mathbf{r}} (\widehat{\mathbf{p}} + \hbar\mathbf{k}) u_{\mathbf{k}}(\mathbf{r}), \quad (1.24)$$

which can be used for more complex forms of the Hamiltonian as well. There are various numerical methods which allow to compute rather efficiently the band energies $\epsilon_{\mathbf{k}}$ for a given Hamiltonian \mathcal{H} .

1.3 Nearly free electron approximation

We start here from the limit of free electrons assuming the periodic potential $V(\mathbf{r})$ is weak. Using Eqs.(1.10) and (1.11) we expand the periodic potential,

$$V(\mathbf{r}) = \sum_{\mathbf{G}} V_{\mathbf{G}} e^{i\mathbf{G}\cdot\mathbf{r}}, \quad (1.25)$$

$$V_{\mathbf{G}} = \frac{1}{\Omega_{\text{UC}}} \int_{\text{UC}} d^3r V(\mathbf{r}) e^{-i\mathbf{G}\cdot\mathbf{r}}. \quad (1.26)$$

The potential is real and we assume it also to be invariant under inversion ($V(\mathbf{r}) = V(-\mathbf{r})$) with $\mathbf{r} = 0$ being an inversion center of the crystal lattice, leading to $V_{\mathbf{G}} = V_{-\mathbf{G}}^* = V_{-\mathbf{G}}$. Note that the uniform component V_0 corresponds to an irrelevant energy shift and may be set to zero. Because of its periodicity, the Bloch function $u_{\mathbf{k}}(\mathbf{r})$ is expressed in the same way,

$$u_{\mathbf{k}}(\mathbf{r}) = \sum_{\mathbf{G}} c_{\mathbf{G}} e^{-i\mathbf{G}\cdot\mathbf{r}}, \quad (1.27)$$

where the coefficients $c_{\mathbf{G}} = c_{\mathbf{G}}(\mathbf{k})$ are functions of \mathbf{k} , in general. Inserting this Ansatz and the expansion (1.25) into the Bloch equation, (1.23), we obtain a linear eigenvalue problem for the band energies $\epsilon_{\mathbf{k}}$,

$$\left(\frac{\hbar^2}{2m} (\mathbf{k} - \mathbf{G})^2 - \epsilon_{\mathbf{k}} \right) c_{\mathbf{G}} + \sum_{\mathbf{G}'} V_{\mathbf{G}'-\mathbf{G}} c_{\mathbf{G}'} = 0. \quad (1.28)$$

This represents an eigenvalue problem in infinite dimensions with eigenvectors $c_{\mathbf{G}}(\mathbf{k})$ and eigenvalues $\epsilon_{\mathbf{k}}$ as band energies. These $\epsilon_{\mathbf{k}}$ include corrections to the bare parabolic dispersion, $\epsilon_{\mathbf{k}}^{(0)} = \hbar^2 \mathbf{k}^2 / 2m$, due to the potential $V(\mathbf{r})$. Obviously, the dispersion $\epsilon_{\mathbf{k}}^{(0)}$ is naturally parabolic in absence of the potential $V(\mathbf{r})$ whereby the eigenstates would be simply plane waves. As a lowest order approach we obtain the approximative energy spectrum within the first Brillouin zone, considering only all parabolic bands of the type $\epsilon_{\mathbf{k}}(\mathbf{G}) = \hbar^2 (\mathbf{k} - \mathbf{G})^2 / 2m$ centered around the reciprocal wave vectors \mathbf{G} (see dashed line in Fig.1.2)).

Example: 1-dimensional system

We illustrate here the nearly free electron method using the case of a one-dimensional lattice. Assuming that the periodic modulation of the potential is weak, say $|V_G| \ll \hbar^2 G^2 / 2m$ (taking G as a characteristic wavevector in the periodic system), the problem (1.28) can be simplified. Let us start with the lowest energy values around the center of the first Brillouin zone, i.e. $k \approx 0$ ($|k| \ll \pi/a$). For the lowest energy eigenvalue we solve Eq.(1.28) by

$$c_G \approx \begin{cases} 1 & \text{for } G = 0 \\ -\frac{2mV_G}{\hbar^2\{(k-G)^2 - k^2\}} \ll 1 & \text{for } G \neq 0 \end{cases} \quad (1.29)$$

leading to the energy eigenvalue

$$\epsilon_k \approx \frac{\hbar^2 k^2}{2m} - \sum_{G \neq 0} \frac{|V_G|^2}{\frac{\hbar^2}{2m} [(k-G)^2 - k^2]} \approx \frac{\hbar^2 k^2}{2m^*} + E_0 \quad (1.30)$$

with

$$E_0 = - \sum_{G \neq 0} |\lambda_G|^2 \frac{\hbar^2}{2m} G^2 \quad (1.31)$$

and

$$\frac{1}{m^*} = \frac{1}{m} \left\{ 1 - 4 \sum_{G \neq 0} |\lambda_G|^2 \right\} \quad (1.32)$$

with $\lambda_G = V_G / \{\hbar^2 G^2 / 2m\}$ ($|\lambda_G| \ll 1$). We observe that ϵ_k is parabolic with a slightly modified (effective) mass, $m \rightarrow m^* > m$. Note that this result resembles the lowest order corrections in the Rayleigh-Schrödinger perturbation theory for a non-degenerate state. This solution corresponds to the lowest branch of the band structure within this approach (see Fig.1.2). The parabolic approximation of the band structure at a symmetry point with an effective mass m^* , is a standard way to approximate band tops or bottoms. It is called $\mathbf{k} \cdot \mathbf{p}$ -approximation ("k-dot-p").

We stay at the zone center and address the next eigenstates which are dominated by the parabola originating from $G_{\pm} = \pm 2\pi/a = \pm \tilde{G}$ which cross for $k = 0$ at a value $\hbar^2 \tilde{G}^2 / 2m$. Restricting ourselves to these two components we obtain the two-dimensional eigenvalue equation system,

$$\begin{pmatrix} \frac{\hbar^2}{2m} (k - \tilde{G})^2 - \epsilon_k & V_{-2\tilde{G}} \\ V_{2\tilde{G}} & \frac{\hbar^2}{2m} (k + \tilde{G})^2 - \epsilon_k \end{pmatrix} \begin{pmatrix} c_{\tilde{G}} \\ c_{-\tilde{G}} \end{pmatrix} = 0. \quad (1.33)$$

The eigenvalues are obtained through the secular equation,

$$\det \begin{bmatrix} \frac{\hbar^2}{2m} (k - \tilde{G})^2 - \epsilon_k & V_{2\tilde{G}}^* \\ V_{2\tilde{G}} & \frac{\hbar^2}{2m} (k + \tilde{G})^2 - \epsilon_k \end{bmatrix} = 0, \quad (1.34)$$

leading to

$$\begin{aligned}\epsilon_{k\pm} &= \frac{1}{2} \left[\frac{\hbar^2}{2m} \left\{ (k + \tilde{G})^2 + (k - \tilde{G})^2 \right\} \pm \sqrt{\left(\frac{\hbar^2}{2m} \left\{ (k + \tilde{G})^2 - (k - \tilde{G})^2 \right\} \right)^2 + 4|V_{2\tilde{G}}|^2} \right] \\ &= \frac{\hbar^2}{2m} \tilde{G}^2 \pm |V_{2\tilde{G}}| + \frac{\hbar^2}{2m_{\pm}^*} k^2\end{aligned}\tag{1.35}$$

with the effective mass

$$\frac{1}{m_{\pm}^*} \approx \frac{1}{m} (1 \pm 2|\lambda_{\tilde{G}}|^{-1})\tag{1.36}$$

where $m_+^* > 0$ and $m_-^* < 0$ as $|\lambda_{\tilde{G}}| \ll 1$. We observe a energy band gap separating two bands with opposite curvature (see Fig.1.2). Note that the curvature diverges for $V_{2\tilde{G}} \rightarrow 0$ as $m_{\pm}^* \rightarrow 0$. The wavefunctions at $k = 0$ are given by

$$c_{-\tilde{G}}^{(\pm)} = \mp \frac{V_{2\tilde{G}}^*}{|V_{2\tilde{G}}|} c_{+\tilde{G}}^{(\pm)} = \mp c_{+\tilde{G}}^{(\pm)}\tag{1.37}$$

where we have chosen $V_{2\tilde{G}}$ to be real and positive. Thus,

$$u_{k=0}(x) = \begin{cases} \sin \tilde{G}x & \text{for } \epsilon_{k=0,+} \\ \cos \tilde{G}x & \text{for } \epsilon_{k=0,-} \end{cases}\tag{1.38}$$

one being even and the other odd under parity operation $x \rightarrow -x$.

A similar analysis can be done at the boundary of the first Brillouin zone where two energy parabolas cross. For example at $k = \pm\pi/a$ we find the two dominant contributions originate from $G = +2\pi/a$ and $-2\pi/a$, respectively, together with $G = 0$. Also here the energy eigenvalues show a band gap with parabolic bands centered at $k = \pm\pi/a$ (boundary of the first Brillouin zone in one-dimension) with positive and negative effective mass (see Fig.1.2). Analogous as for the band center we can distinguish the wavefunction with even and odd parity for the two bands at the Brillouin zone boundary. Indeed every crossing energy parabola centered around different reciprocal lattice points contributes to a band gap. By construction we can extend the band structure beyond the first Brillouin zone and find a periodic energy spectrum with

$$\epsilon_{k+G} = \epsilon_k\tag{1.39}$$

where G is a reciprocal lattice "vector". Moreover, we find in Fig.1.2 that $\epsilon_{-k} = \epsilon_k$ due to parity as well as time reversal symmetry, like for free electrons.

1.4 Tight-binding approximation

We consider now a regular lattice of atoms which are well separated such that their atomic orbitals have small overlaps only. Therefore, in a good approximation the electronic states are rather well represented by localized atomic orbitals, $\phi_n(\mathbf{r})$. The discrete spectrum of the atoms is obtained with the atomic Hamiltonian,

$$\mathcal{H}_a(\mathbf{R})\phi_n(\mathbf{r} - \mathbf{R}) = \epsilon_n\phi_n(\mathbf{r} - \mathbf{R}),\tag{1.40}$$

for an atom located at position \mathbf{R} , so that

$$\mathcal{H}_a(\mathbf{R}) = \frac{\hat{\mathbf{p}}^2}{2m} + V_a(\mathbf{r} - \mathbf{R})\tag{1.41}$$

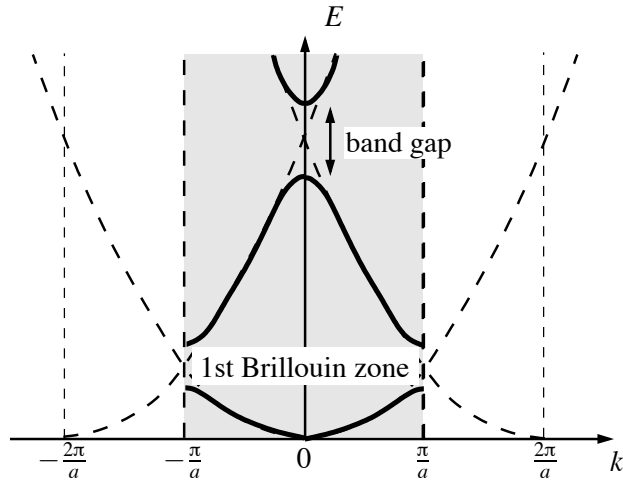


Figure 1.2: Band structure obtained by the nearly free electron approximation for a regular one-dimensional lattice.

with $V_a(\mathbf{r})$ as the rotation symmetric atomic potential as shown in Fig.1.3 a). The index n shall include all necessary quantum numbers, besides the principal quantum number also angular momentum (l, m) and spin. The single-particle Hamiltonian combines all the potentials of the atoms on the regular lattice (see Fig.1.3 b)),

$$\mathcal{H} = \frac{\hat{\mathbf{p}}^2}{2m} + \sum_{\mathbf{R}_j} V_a(\mathbf{r} - \mathbf{R}_j) = \mathcal{H}_a(\mathbf{R}_j) + \Delta V_{\mathbf{R}_j}(\mathbf{r}) \quad (1.42)$$

where we single out one atomic potential (the choice of \mathbf{R}_j is arbitrary) and introduce the correction

$$\Delta V_{\mathbf{R}_j}(\mathbf{r}) = \sum_{\mathbf{R}_{j'} \neq \mathbf{R}_j} V_a(\mathbf{r} - \mathbf{R}_{j'}) . \quad (1.43)$$

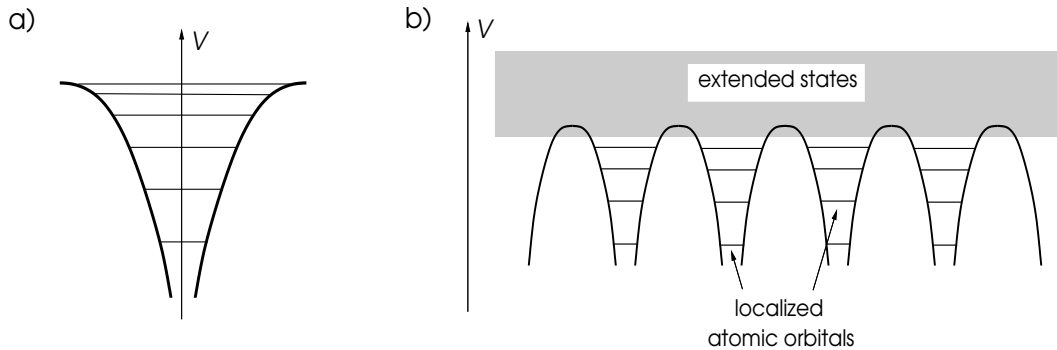


Figure 1.3: Potential landscape: a) a single atomic Coulomb potential yields a discrete spectrum electronic states; b) atoms arranged in a regular lattice give rise to a periodic potential which close to the atom sites look much like the attractive Coulomb-like potential. Electron states of low energy can be considered as practically localized at the atom sites, as the extension of their wave functions is very small. The higher energy states, however, extend further and can delocalize to form itinerant electron states which form bands.

1.4.1 Linear combination of atomic orbitals - LCAO

We use here a linear combination of atomic orbitals (LCAO) to approximate the extended Bloch states

$$\psi_{\tilde{n}\mathbf{k}}(\mathbf{r}) = \frac{1}{\sqrt{N}} \sum_{\mathbf{R}_j} e^{i\mathbf{k}\cdot\mathbf{R}_j} \phi_{\tilde{n}}(\mathbf{r} - \mathbf{R}_j), \quad (1.44)$$

where N denotes the number of lattice sites. This superposition has obviously the properties of a Bloch function through $\psi_{\tilde{n}\mathbf{k}}(\mathbf{r} - \mathbf{a}) = e^{-i\mathbf{k}\cdot\mathbf{a}}\psi_{\tilde{n}\mathbf{k}}(\mathbf{r})$ for all lattice vectors \mathbf{a} .⁴ Note that this is similar to the Hund-Mullikan ansatz for molecular orbitals.

First we determine the norm of this Bloch function,

$$\begin{aligned} \langle 1 \rangle_{\tilde{n}\tilde{n}'}(\mathbf{k}) &= \int d^3r \psi_{\tilde{n}\mathbf{k}}(\mathbf{r})^* \psi_{\tilde{n}'\mathbf{k}}(\mathbf{r}) = \frac{1}{N} \sum_{\mathbf{R}_j, \mathbf{R}_{j'}} \int d^3r e^{i\mathbf{k}\cdot(\mathbf{R}_{j'} - \mathbf{R}_j)} \phi_{\tilde{n}}^*(\mathbf{r} - \mathbf{R}_j) \phi_{\tilde{n}'}(\mathbf{r} - \mathbf{R}_{j'}) \\ &= \sum_{\mathbf{R}_j} \int d^3r e^{-i\mathbf{k}\cdot\mathbf{R}_j} \phi_{\tilde{n}}^*(\mathbf{r} - \mathbf{R}_j) \phi_{\tilde{n}'}(\mathbf{r}) \\ &= \delta_{\tilde{n}\tilde{n}'} + \sum_{\mathbf{R}_j \neq 0} e^{-i\mathbf{k}\cdot\mathbf{R}_j} \alpha_{\tilde{n}\tilde{n}'}(\mathbf{R}_j) \end{aligned} \quad (1.46)$$

where due to translational invariance in the lattice we may set $\mathbf{R}_{j'} = 0$ eliminating the sum over $\mathbf{R}_{j'}$ and dropping the factor $1/N$. To estimate the energy we calculate,

$$\begin{aligned} \langle \mathcal{H} \rangle_{\tilde{n}\tilde{n}'}(\mathbf{k}) &= \frac{1}{N} \sum_{\mathbf{R}_j, \mathbf{R}_{j'}} \int d^3r e^{i\mathbf{k}\cdot(\mathbf{R}_{j'} - \mathbf{R}_j)} \phi_{\tilde{n}}^*(\mathbf{r} - \mathbf{R}_j) \{H_a(\mathbf{R}_{j'}) + \Delta V_{\mathbf{R}_{j'}}(\mathbf{r})\} \phi_{\tilde{n}'}(\mathbf{r} - \mathbf{R}_{j'}) \\ &= E_{\tilde{n}'} \langle 1 \rangle_{\tilde{n}\tilde{n}'}(\mathbf{k}) + \frac{1}{N} \sum_{\mathbf{R}_j, \mathbf{R}_{j'}} \int d^3r e^{i\mathbf{k}\cdot(\mathbf{R}_{j'} - \mathbf{R}_j)} \phi_{\tilde{n}}^*(\mathbf{r} - \mathbf{R}_j) \Delta V_{\mathbf{R}_{j'}}(\mathbf{r}) \phi_{\tilde{n}'}(\mathbf{r} - \mathbf{R}_{j'}) \\ &= E_{\tilde{n}'} \langle 1 \rangle_{\tilde{n}\tilde{n}'}(\mathbf{k}) + \Delta E_{\tilde{n}\tilde{n}'} + \sum_{\mathbf{R}_j \neq 0} e^{-i\mathbf{k}\cdot\mathbf{R}_j} \gamma_{\tilde{n}\tilde{n}'}(\mathbf{R}_j) \end{aligned} \quad (1.47)$$

where

$$\Delta E_{\tilde{n}\tilde{n}'} = \int d^3r \phi_{\tilde{n}}^*(\mathbf{r}) \Delta V_{\mathbf{R}_{j'}=0}(\mathbf{r}) \phi_{\tilde{n}'}(\mathbf{r}) \quad (1.48)$$

and

$$\gamma_{\tilde{n}\tilde{n}'}(\mathbf{R}_j) = \int d^3r \phi_{\tilde{n}}^*(\mathbf{r} - \mathbf{R}_j) \Delta V_{\mathbf{R}_{j'}=0}(\mathbf{r}) \phi_{\tilde{n}'}(\mathbf{r}). \quad (1.49)$$

From this we can now calculate the band energies through the secular equation,

$$\det [\langle \mathcal{H} \rangle_{\tilde{n}\tilde{n}'}(\mathbf{k}) - \epsilon_{\mathbf{k}} \langle 1 \rangle_{\tilde{n}\tilde{n}'}(\mathbf{k})] = 0. \quad (1.50)$$

The merit of the approach is that the tightly bound atomic orbitals have only weak overlap such that both $\alpha_{\tilde{n}\tilde{n}'}(\mathbf{R}_j)$ and $\gamma_{\tilde{n}\tilde{n}'}(\mathbf{R}_j)$ fall off very quickly with growing \mathbf{R}_j . Mostly it is sufficient to

⁴We apply the translation operation to the wave function (1.44),

$$\begin{aligned} \hat{T}_{\mathbf{a}} \psi_{\tilde{n}\mathbf{k}}(\mathbf{r}) &= \psi_{\tilde{n}\mathbf{k}}(\mathbf{r} - \mathbf{a}) = \frac{1}{\sqrt{N}} \sum_{\mathbf{R}_j} e^{i\mathbf{k}\cdot\mathbf{R}_j} \phi_{\tilde{n}}(\mathbf{r} - \underbrace{\mathbf{a} - \mathbf{R}_j}_{\mathbf{R}'_j}) = \frac{1}{\sqrt{N}} \sum_{\mathbf{R}_j} e^{i\mathbf{k}\cdot(\mathbf{R}'_j - \mathbf{a})} \phi_{\tilde{n}}(\mathbf{r} - \mathbf{R}'_j) \\ &= e^{-i\mathbf{k}\cdot\mathbf{a}} \frac{1}{\sqrt{N}} \sum_{\mathbf{R}'_j} e^{i\mathbf{k}\cdot\mathbf{R}'_j} \phi_{\tilde{n}}(\mathbf{r} - \mathbf{R}'_j) = e^{-i\mathbf{k}\cdot\mathbf{a}} \psi_{\tilde{n}\mathbf{k}}(\mathbf{r}). \end{aligned} \quad (1.45)$$

take \mathbf{R}_j connecting nearest-neighbor and sometimes next-nearest-neighbor lattice sites. This is for example fine for bands derived from 3d-orbitals among the transition metals such as Mn, Fe or Co etc.. Also transition metal oxides are well represented in the tight-binding formulation. Alkali metals in the first row of the periodic table, Li, Na, K etc. are not suitable because their outermost s-orbitals have generally a large overlap. Note that the construction of the Hamiltonian matrix ensures that $\mathbf{k} \rightarrow \mathbf{k} + \mathbf{G}$ does not change $\epsilon_{\mathbf{k}}$, if \mathbf{G} is a reciprocal lattice vector.

1.4.2 Band structure of s-orbitals

The most simple case of a non-degenerate atomic orbital is the s-orbital with vanishing angular momentum ($\ell = 0$). Since these orbitals have rotation symmetric wavefunctions, $\phi_s(\mathbf{r}) = \phi_s(|\mathbf{r}|)$, the matrix elements only depend on the distance between sites, $|\mathbf{R}_j|$. As an example we consider a simple cubic lattice taking nearest-neighbor ($\mathbf{R}_j = \pm(a, 0, 0)$, $\pm(0, a, 0)$ and $\pm(0, 0, a)$) and next-nearest-neighbor coupling ($\mathbf{R}_j = (\pm a, \pm a, 0)$, $(\pm a, 0, \pm a)$, $(0, \pm a, \pm a)$) into account. For simplicity we will neglect the overlap integrals $\alpha_{ss}(\mathbf{R}_j)$, as they are not important to describe the essential feature of the band structure.

$$\gamma_{ss}(\mathbf{R}_j) = \begin{cases} -t & \mathbf{R}_j \text{ connects nearest neighbors} \\ -t' & \mathbf{R}_j \text{ connects next nearest neighbors} \end{cases} \quad (1.51)$$

which leads immediately to

$$\begin{aligned} \epsilon_{\mathbf{k}} &= E_s + \Delta E_s - t \sum_{\mathbf{R}_j}^{n.n.} e^{-i\mathbf{k}\cdot\mathbf{R}_j} - t' \sum_{\mathbf{R}_j}^{n.n.n.} e^{-i\mathbf{k}\cdot\mathbf{R}_j} \\ &= E_s + \Delta E_s - 2t\{\cos(k_x a) + \cos(k_y a) + \cos(k_z a)\} \\ &\quad - 4t'[\cos(k_x a) \cos(k_y a) + \cos(k_y a) \cos(k_z a) + \cos(k_z a) \cos(k_x a)] \end{aligned} \quad (1.52)$$

Note that $\Delta V_{\mathbf{R}_j}(\mathbf{r}) \leq 0$ in most cases due to the attractive ionic potentials. Therefore $t, t' > 0$. There is a single band resulting from this s-orbital, as shown in Fig.1.4. We may also consider the $\mathbf{k} \cdot \mathbf{p}$ -approximation at $\mathbf{k} = 0$ which yields an effective mass

$$\epsilon_{\mathbf{k}} = E_s + \Delta E_s + 6t + 12t' + \frac{\hbar^2}{2m^*} \mathbf{k}^2 + \dots \quad (1.53)$$

with

$$\frac{1}{m^*} = \frac{2}{\hbar^2} (t + 4t') . \quad (1.54)$$

Note that t and t' shrink quickly, if with growing lattice constant a the overlap of atomic orbitals decreases.

1.4.3 Band structure of p-orbitals

We turn to the case of degenerate orbitals. The most simple case is the p-orbital with angular momentum $l = 1$ which is three-fold degenerate, represented by the atomic orbital wavefunctions of the form,

$$\phi_x(\mathbf{r}) = x\varphi(r), \quad \phi_y(\mathbf{r}) = y\varphi(r), \quad \phi_z(\mathbf{r}) = z\varphi(r) , \quad (1.55)$$

with $\varphi(r)$ being a rotation symmetric function. Note that $\{x, y, z\}$ can be represented by spherical harmonics $Y_{1,m}$. We assume again a simple cubic lattice such that these atomic orbitals remain degenerate. Analyzing the properties of the integrals by symmetry, we find,

$$E_x = E_y = E_z = E_p \quad \text{and} \quad \Delta E_{\tilde{n}\tilde{n}'} = \Delta E_p \delta_{\tilde{n}\tilde{n}'} . \quad (1.56)$$

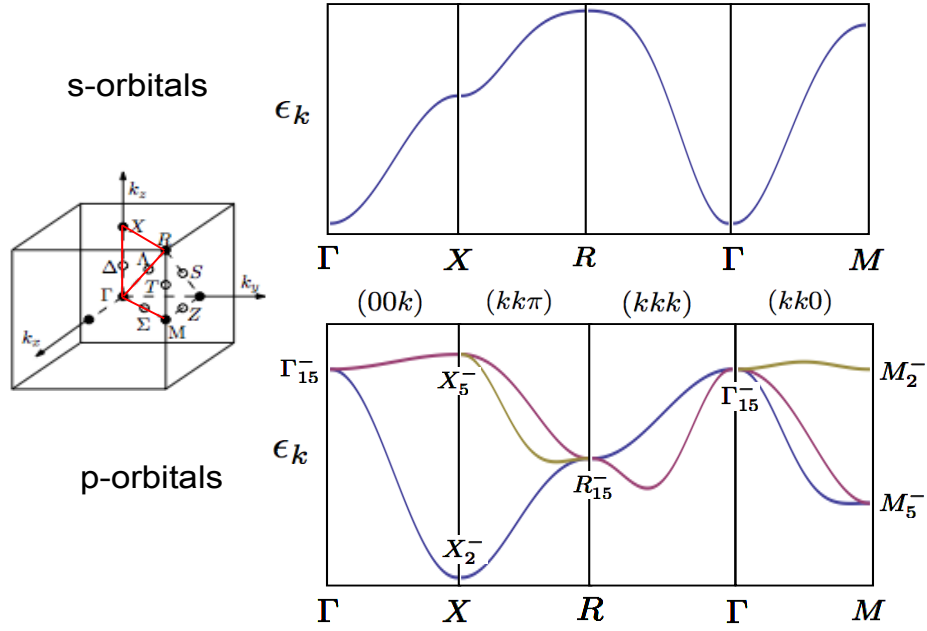


Figure 1.4: Band structures derived from atomic orbitals with s- (one band, upper panel) and p-symmetry (three bands, lower panel) in a simple cubic lattice. Left side: First Brillouin zone of the simple cubic lattice. Dispersion given along the k -line connecting $\Gamma - X - R - \Gamma - M$. We choose the parameters: $t' = 0.2t$ for the s-orbitals; $t' = 0.2t$, $\tilde{t} = 0.1t$, $\tilde{t}' = 0.05t$ and $\tilde{t}'' = 0.15t$. For the band derived from atomic p-orbitals, the irreducible representations of the bands are given at the symmetry points: Γ_{15}^- ($d = 3$); X_2^- ($d = 1$), X_5^- ($d = 2$); R_{15}^- ($d = 3$); M_2^- ($d = 1$), M_5^- ($d = 2$) where d is the dimension of the representation showing the degeneracy.

The overlaps Eq.(1.49) for nearest neighbors,

$$\gamma_{xx}(\mathbf{R}_j) = \begin{cases} t & \mathbf{R}_j = (\pm a, 0, 0) \parallel \hat{x} \quad (\sigma - \text{bonding}) \\ -t' & \mathbf{R}_j = (0, \pm a, 0), (0, 0, \pm a) \perp \hat{x} \quad (\pi - \text{bonding}) \end{cases} \quad (1.57)$$

and analogous for γ_{yy} and γ_{zz} , while $\gamma_{\tilde{n}\tilde{n}'} = 0$, if $\tilde{n} \neq \tilde{n}'$. For next-nearest neighbors by symmetry we obtain,

$$\gamma_{xx}(\mathbf{R}_j) = \begin{cases} \tilde{t} & \mathbf{R}_j = (\pm a, \pm a, 0), (\pm a, 0, \pm a) \\ -\tilde{t}' & \mathbf{R}_j = (0, \pm a, \pm a) \end{cases} \quad (1.58)$$

and analogous for γ_{yy} and γ_{zz} . Next-nearest neighbor coupling also allows for inter-orbital matrix elements, e.g.

$$\gamma_{xy}(\mathbf{R}_j) = \gamma_{yx}(\mathbf{R}_j) = \tilde{t}'' \text{sign}(R_{nx}R_{ny}) \quad (1.59)$$

for $\mathbf{R}_j = (\pm a, \pm a, 0)$ and analogous for $\gamma_{yz}(\mathbf{R}_j)$ and $\gamma_{zx}(\mathbf{R}_j)$. The different configuration of nearest- and next-nearest-neighbor coupling is shown in Fig.1.5.

Now we may setup the coupling matrix,

$$\langle \mathcal{H} \rangle_{\tilde{n}\tilde{n}'} = \begin{pmatrix} E_x(\mathbf{k}) & -4\tilde{t}'' \sin(k_x a) \sin(k_y a) & -4\tilde{t}'' \sin(k_x a) \sin(k_z a) \\ -4\tilde{t}'' \sin(k_x a) \sin(k_y a) & E_y(\mathbf{k}) & -4\tilde{t}'' \sin(k_y a) \sin(k_z a) \\ -4\tilde{t}'' \sin(k_x a) \sin(k_z a) & -4\tilde{t}'' \sin(k_y a) \sin(k_z a) & E_z(\mathbf{k}) \end{pmatrix} \quad (1.60)$$

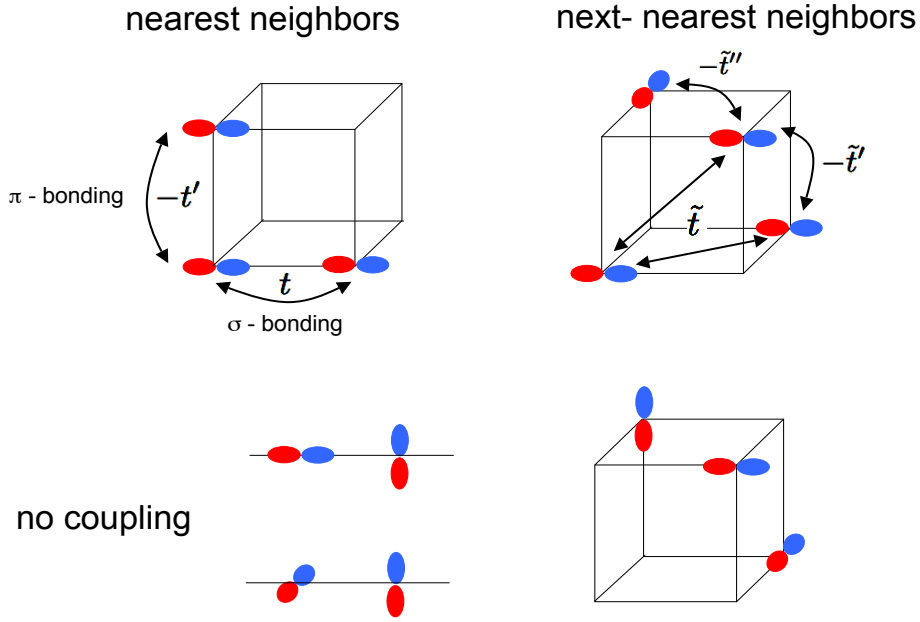


Figure 1.5: The configurations for nearest- and next-nearest-neighbor coupling between p-orbitals on different sites. The p-orbitals are depicted by the dumb-bell structured wavefunction with positive (blue) and negative (red) lobes. For nearest-neighbor couplings we distinguish here σ -bonding (full rotation symmetry around connecting axis) and π -bonding (two-fold rotation symmetry around connecting axis). Generally the coupling is weaker for π - than for σ -bonding. No coupling for symmetry reasons are obtained between orbitals in the lower panel.

with

$$E_x(\mathbf{k}) = E_p + \Delta E_p + 2t \cos(k_x a) - 2t' (\cos(k_y a) + \cos(k_z a)) + 4\tilde{t} \cos(k_x a) (\cos(k_y a) + \cos(k_z a)) - 4\tilde{t}' \cos(k_y a) \cos(k_z a) \quad (1.61)$$

and analogous for $E_y(\mathbf{k})$, $E_z(\mathbf{k})$. The three bands derived from the atomic p-orbitals are obtained by solving the secular equation of the type Eq.(1.50) and shown in Fig.1.4.

Also in this case we may consider a $\mathbf{k} \cdot \mathbf{p}$ -approximation around a symmetry point in the Brillouin zone. For the Γ -point we find the expansion around $\mathbf{k} = 0$:

$$\langle \mathcal{H} \rangle_{\tilde{n}\tilde{n}'} = E_\Gamma + \begin{pmatrix} Ak_x^2 + B(k_y^2 + k_z^2) & Ck_x k_y & Ck_x k_z \\ Ck_x k_y & Ak_y^2 + B(k_z^2 + k_x^2) & Ck_y k_z \\ Ck_x k_z & Ck_y k_z & Ak_z^2 + B(k_x^2 + k_y^2) \end{pmatrix} \quad (1.62)$$

with $E_\Gamma = E_p + \Delta E_p + 2t - 4t' + 4\tilde{t} - 4\tilde{t}'$, $A = -a^2(t + 4\tilde{t})$, $B = a^2(t' - 2\tilde{t} + 2\tilde{t}')$ and $C = -4\tilde{t}''$. These band energies have to be determined through the secular equations and lead to three bands with anisotropic effective masses.

1.4.4 Wannier functions

An alternative approach to the tight-binding approximation is through Wannier functions. These are defined as the Fourier transformation of the Bloch wave functions,

$$\psi_{\mathbf{k}}(\mathbf{r}) = \frac{1}{\sqrt{N}} \sum_{\mathbf{R}} e^{i\mathbf{k} \cdot \mathbf{R}} w(\mathbf{r} - \mathbf{R}) \quad w(\mathbf{r} - \mathbf{R}) = \frac{1}{\sqrt{N}} \sum_{\mathbf{k}} e^{-i\mathbf{k} \cdot \mathbf{R}} \psi_{\mathbf{k}}(\mathbf{r}) \quad (1.63)$$

where the Wannier function $w(\mathbf{r} - \mathbf{R})$ ⁵ is centered on the real-space lattice site \mathbf{R} . We consider here the situation of a non-degenerate band analogous to the atomic s-orbital case, such that there is only one Wannier function per site. Wannier functions obey the orthogonality relation

$$\begin{aligned} \int d^3r w^*(\mathbf{r} - \mathbf{R}')w(\mathbf{r} - \mathbf{R}) &= \frac{1}{N} \sum_{\mathbf{k}, \mathbf{k}'} e^{i\mathbf{k} \cdot \mathbf{R} - i\mathbf{k}' \cdot \mathbf{R}'} \int d^3r \psi_{\mathbf{k}'}^*(\mathbf{r})\psi_{\mathbf{k}}(\mathbf{r}) \\ &= \frac{1}{N} \sum_{\mathbf{k}, \mathbf{k}'} e^{i\mathbf{k} \cdot \mathbf{R} - i\mathbf{k}' \cdot \mathbf{R}'} \delta_{\mathbf{k}\mathbf{k}'} = \delta_{\mathbf{R}\mathbf{R}'} . \end{aligned} \quad (1.65)$$

We consider the one-particle Hamiltonian to be of the form $\mathcal{H} = -\hbar^2 \nabla^2 / 2m + V(\mathbf{r})$, with a periodic potential $V(\mathbf{r})$. Then, $\epsilon_{\mathbf{k}}$ can be expressed through

$$\begin{aligned} \epsilon_{\mathbf{k}} &= \int d^3r \psi_{\mathbf{k}}^*(\mathbf{r})\mathcal{H}\psi_{\mathbf{k}}(\mathbf{r}) = \frac{1}{N} \sum_{\mathbf{R}, \mathbf{R}'} e^{-i\mathbf{k} \cdot (\mathbf{R}' - \mathbf{R})} \int d^3r w^*(\mathbf{r} - \mathbf{R}')\mathcal{H}w(\mathbf{r} - \mathbf{R}) \\ &= \sum_{\mathbf{R}} e^{-i\mathbf{k} \cdot \mathbf{R}} \int d^3r w^*(\mathbf{r} - \mathbf{R})\mathcal{H}w(\mathbf{r}) , \end{aligned} \quad (1.66)$$

where we took translational invariance of the lattice into account. With the definitions

$$\epsilon_0 = \int d^3r w^*(\mathbf{r})\mathcal{H}w(\mathbf{r}), \quad (1.67)$$

$$t(\mathbf{R}) = \int d^3r w^*(\mathbf{r} - \mathbf{R})\mathcal{H}w(\mathbf{r}) \quad \text{for } \mathbf{R} \neq 0 \quad (1.68)$$

the band energy can be written as

$$\epsilon_{\mathbf{k}} = \epsilon_0 + \sum_{\mathbf{R}} t(\mathbf{R})e^{-i\mathbf{k} \cdot \mathbf{R}} . \quad (1.69)$$

This is the same type of tight-binding band structure as we have derived above from the LCAO view point.

We can extend the Wannier function to the case of several bands, like the p-orbital bands. Then we define

$$\psi_{n\mathbf{k}}(\mathbf{r}) = \frac{1}{\sqrt{N}} \sum_{\mathbf{R}, \tilde{n}} e^{i\mathbf{k} \cdot \mathbf{R}} c_{n\tilde{n}}(\mathbf{k})w_{\tilde{n}}(\mathbf{r} - \mathbf{R}) \quad (1.70)$$

where for all \mathbf{k} ,

$$\sum_{\tilde{n}} c_{n\tilde{n}}(\mathbf{k})c_{\tilde{n}n'}(\mathbf{k})^* = \delta_{nn'} . \quad (1.71)$$

The matrix $c_{n\tilde{n}}(\mathbf{k})$ rotates the Wannier function from the band basis into the atomic orbital basis, i.e. for p-bands into the three Wannier function with symmetry like $\{x, y, z\}$.

⁵Ambiguity of the Wannier functions: The Wannier function is not uniquely defined, because there is a "gauge freedom" for the Bloch function which can be multiplied by a phase factor

$$\psi_{\mathbf{k}}(\mathbf{r}) \rightarrow e^{i\chi(\mathbf{k})}\psi_{\mathbf{k}}(\mathbf{r}) \quad (1.64)$$

where $\chi(\mathbf{k})$ is an arbitrary real function. In particular, we find different degrees of localization of $w(\mathbf{r} - \mathbf{R})$ around its center \mathbf{R} depending on the choice of $\chi(\mathbf{k})$.

Again we can express the band energy in terms of a tight-binding Hamiltonian,

$$\begin{aligned}
\epsilon_{n\mathbf{k}} &= \int d^3r \psi_{n\mathbf{k}}^*(\mathbf{r}) \mathcal{H} \psi_{n\mathbf{k}}(\mathbf{r}) \\
&= \sum_{\mathbf{R}} \sum_{\tilde{n}, \tilde{n}'} c_{\tilde{n}'n}^*(\mathbf{k}) c_{n\tilde{n}}(\mathbf{k}) e^{-i\mathbf{k}\cdot\mathbf{R}} \int d^3r w_{\tilde{n}'}^*(\mathbf{r}-\mathbf{R}) H w_{\tilde{n}}(\mathbf{r}) \\
&= \sum_{\mathbf{R}} \sum_{\tilde{n}, \tilde{n}'} c_{\tilde{n}'n}^*(\mathbf{k}) c_{n\tilde{n}}(\mathbf{k}) e^{-i\mathbf{k}\cdot\mathbf{R}} t_{\tilde{n}'\tilde{n}}(\mathbf{R}) .
\end{aligned} \tag{1.72}$$

1.4.5 Tight binding model in second quantization formulation

The tight-binding formulation of band electrons can also be implemented very easily in second quantization language and provides a rather intuitive interpretation. For simplicity we restrict ourselves to the single-orbital case and define the following Fermionic operators,

$$\hat{c}_{j,s}^\dagger \quad \text{creates an electron of spin } s \text{ on lattice site } \mathbf{R}_j , \tag{1.73}$$

$$\hat{c}_{j,s} \quad \text{annihilates an electron of spin } s \text{ on lattice site } \mathbf{R}_j ,$$

in the corresponding Wannier states. We introduce the following Hamiltonian,

$$\mathcal{H} = \sum_{j,s} \epsilon_0 \hat{c}_{j,s}^\dagger \hat{c}_{j,s} + \sum_{i,j} t_{ij} \hat{c}_{i,s}^\dagger \hat{c}_{j,s} \tag{1.74}$$

with $t_{ij} = t_{ji}$ real. These coefficients t_{ij} are called "hopping matrix elements", since $\hat{c}_{i,s}^\dagger \hat{c}_{j,s}$ annihilates an electron on site \mathbf{R}_j and creates one on site \mathbf{R}_i , in this way an electron moves (hops) from \mathbf{R}_j to \mathbf{R}_i . Thus, this Hamiltonian represents the "kinetic energy" of the electron. Let us now diagonalize this Hamiltonian by following Fourier transformation, equivalent to the transformation between Bloch and Wannier functions,

$$\hat{c}_{j,s}^\dagger = \frac{1}{\sqrt{N}} \sum_{\mathbf{k}} \hat{a}_{\mathbf{k}s}^\dagger e^{-i\mathbf{k}\cdot\mathbf{R}_j} \quad \text{and} \quad \hat{c}_{j,s} = \frac{1}{\sqrt{N}} \sum_{\mathbf{k}} \hat{a}_{\mathbf{k}s} e^{i\mathbf{k}\cdot\mathbf{R}_j} \tag{1.75}$$

where $\hat{a}_{\mathbf{k}s}^\dagger$ ($\hat{a}_{\mathbf{k}s}$) creates (annihilates) an electron in the Bloch state with pseudo-momentum \mathbf{k} and spin s . Inserting Eq.(1.75) into the Hamiltonian (1.74) leads to

$$\mathcal{H} = \sum_{\mathbf{k}, \mathbf{k}', s} \left\{ \frac{1}{N} \sum_i \epsilon_0 e^{i(\mathbf{k}-\mathbf{k}')\cdot\mathbf{R}_i} + \frac{1}{N} \sum_{i,j} t_{ij} e^{i\mathbf{k}\cdot\mathbf{R}_j - i\mathbf{k}'\cdot\mathbf{R}_i} \right\} \hat{a}_{\mathbf{k}'s}^\dagger \hat{a}_{\mathbf{k}s} = \sum_{\mathbf{k}, s} \epsilon_{\mathbf{k}} \hat{a}_{\mathbf{k}s}^\dagger \hat{a}_{\mathbf{k}s} \tag{1.76}$$

where $\hat{a}_{\mathbf{k}s}^\dagger \hat{a}_{\mathbf{k}s} = \hat{n}_{\mathbf{k}s}$ constitutes the number operator for electrons. The band energy is the same as obtained above from the tight-binding approach. The Hamiltonian (1.74) will be used later for the Hubbard model where a real-space formulation is helpful.

The real-space formulation of the kinetic energy allows also for the introduction of disorder, non-periodicity which can be most straightforwardly implemented by site dependent potentials $\epsilon_0 \rightarrow \epsilon_{0i}$ and to spatially (bond) dependent hopping matrix elements $t_{ij} = t(\mathbf{R}_i, \mathbf{R}_j) \neq t(\mathbf{R}_i - \mathbf{R}_j)$.

1.5 Symmetry properties of the band structure

The symmetry properties of crystals are a helpful tool for the analysis of their band structure. They emerge from the symmetry group (space and point group) of the crystal lattice. Consider the action $\hat{S}_{\{g|\mathbf{a}\}}$ of an element $\{g|\mathbf{a}\}$ of the space group on a Bloch wave function $\psi_{\mathbf{k}}(\mathbf{r})$ ⁶

⁶In Dirac notation we write for the Bloch state with pseudo-momentum \mathbf{k} as

$$\psi_{\mathbf{k}}(\mathbf{r}) = \langle \mathbf{r} | \psi_{\mathbf{k}} \rangle . \tag{1.77}$$

$$\widehat{S}_{\{g|\mathbf{a}\}}\psi_{\mathbf{k}}(\mathbf{r}) = \psi_{\mathbf{k}}(\{g|\mathbf{a}\}^{-1}\mathbf{r}) = \psi_{\mathbf{k}}(g^{-1}\mathbf{r} - g^{-1}\mathbf{a}). \quad (1.81)$$

Because $\{g|\mathbf{a}\}$ belongs to the space group of the crystal, we have $[\widehat{S}_{\{g|\mathbf{a}\}}, \mathcal{H}_0] = 0$. Applying a pure translation $\widehat{T}_{\mathbf{a}'} = \widehat{S}_{\{E|\mathbf{a}'\}}$ to this new wave function and using Eq.(1.5)

$$\begin{aligned} \widehat{T}_{\mathbf{a}'}\widehat{S}_{\{g|\mathbf{a}\}}\psi_{\mathbf{k}}(\mathbf{r}) &= \widehat{S}_{\{g|\mathbf{a}\}}\widehat{T}_{g^{-1}\mathbf{a}'}\psi_{\mathbf{k}}(\mathbf{r}) = \widehat{S}_{\{g|\mathbf{a}\}}e^{-i\mathbf{k}\cdot(g^{-1}\mathbf{a}')} \psi_{\mathbf{k}}(\mathbf{r}) \\ &= \widehat{S}_{\{g|\mathbf{a}\}}e^{-i(g\mathbf{k})\cdot\mathbf{a}'} \psi_{\mathbf{k}}(\mathbf{r}) \\ &= e^{-i(g\mathbf{k})\cdot\mathbf{a}'} \widehat{S}_{\{g|\mathbf{a}\}}\psi_{\mathbf{k}}(\mathbf{r}), \end{aligned} \quad (1.82)$$

the latter is found to be an eigenfunction of $\widehat{T}_{\mathbf{a}'}$ with eigenvalue $e^{-i(g\mathbf{k})\cdot\mathbf{a}'}$. Remember, that, according to the Bloch theorem, we chose a basis $\{\psi_{\mathbf{k}}\}$ diagonalizing both $\widehat{T}_{\mathbf{a}}$ and \mathcal{H}_0 . Thus, apart from a phase factor, the action of a symmetry transformation $\{g|\mathbf{a}\}$ on the wave function⁷ corresponds to a rotation from \mathbf{k} to $g\mathbf{k}$.

$$\widehat{S}_{\{g|\mathbf{a}\}}\psi_{\mathbf{k}}(\mathbf{r}) = \lambda_{\{g|\mathbf{a}\}}\psi_{g\mathbf{k}}(\mathbf{r}), \quad (1.84)$$

with $|\lambda_{\{g|\mathbf{a}\}}|^2 = 1$, or

$$\widehat{S}_{\{g|\mathbf{a}\}}|\mathbf{k}\rangle = \lambda_{\{g|\mathbf{a}\}}|g\mathbf{k}\rangle. \quad (1.85)$$

in Dirac notation. Then it is easy to see that

$$\epsilon_{g\mathbf{k}} = \langle g\mathbf{k}|\mathcal{H}_0|g\mathbf{k}\rangle = \langle \mathbf{k}|\widehat{S}_{\{g|\mathbf{a}\}}^{-1}\mathcal{H}_0\widehat{S}_{\{g|\mathbf{a}\}}|\mathbf{k}\rangle = \langle \mathbf{k}|\mathcal{H}_0|\mathbf{k}\rangle = \epsilon_{\mathbf{k}}. \quad (1.86)$$

Consequently, there is a star-like structure of equivalent points $g\mathbf{k}$ with the same band energy (\rightarrow degeneracy) for each \mathbf{k} in the Brillouin zone (cf. Fig. 1.6).

For a general point \mathbf{k} the number of equivalent points in the star equals the number of point

The action of the operator $\widehat{S}_{\{g|\mathbf{a}\}}$ on the state $|\mathbf{r}\rangle$ is given by

$$\widehat{S}_{\{g|\mathbf{a}\}}|\mathbf{r}\rangle = |g\mathbf{r} + \mathbf{a}\rangle \quad \text{and} \quad \langle \mathbf{r}|\widehat{S}_{\{g|\mathbf{a}\}} = \langle g^{-1}\mathbf{r} - g^{-1}\mathbf{a}|, \quad (1.78)$$

such that

$$\langle \mathbf{r}|\widehat{S}_{\{g|\mathbf{a}\}}|\psi_{\mathbf{k}}\rangle = \psi_{\mathbf{k}}(g^{-1}\mathbf{r} - g^{-1}\mathbf{a}). \quad (1.79)$$

The same holds for pure translations.

Note that this definition has also implications on the sequential application of transformation operators such as

$$\begin{aligned} \widehat{S}_{\{g_1|\mathbf{a}_1\}}\widehat{S}_{\{g_2|\mathbf{a}_2\}}\psi_{\mathbf{k}}(\mathbf{r}) &= \langle \mathbf{r}|\widehat{S}_{\{g_1|\mathbf{a}_1\}}\widehat{S}_{\{g_2|\mathbf{a}_2\}}|\psi_{\mathbf{k}}\rangle = \langle \{g_1|\mathbf{a}_1\}^{-1}\mathbf{r}|\widehat{S}_{\{g_2|\mathbf{a}_2\}}|\psi_{\mathbf{k}}\rangle \\ &= \langle \{g_2|\mathbf{a}_2\}^{-1}\{g_1|\mathbf{a}_1\}^{-1}\mathbf{r}|\psi_{\mathbf{k}}\rangle = \psi_{\mathbf{k}}(\{g_2|\mathbf{a}_2\}^{-1}\{g_1|\mathbf{a}_1\}^{-1}\mathbf{r}). \end{aligned} \quad (1.80)$$

This is important in the context of Eq.(1.82).

⁷Symmetry behavior of the wave function.

$$\begin{aligned} \widehat{S}_{\{g|\mathbf{a}\}}\psi_{\mathbf{k}}(\mathbf{r}) &= \frac{1}{\sqrt{\Omega}}\widehat{S}_{\{g|\mathbf{a}\}}e^{i\mathbf{k}\cdot\mathbf{r}} \sum_{\mathbf{G}} c_{\mathbf{G}}(\mathbf{k}) e^{i\mathbf{G}\cdot\mathbf{r}} = \frac{1}{\sqrt{\Omega}}e^{i\mathbf{k}\cdot(g^{-1}\mathbf{r}-g^{-1}\mathbf{a})} \sum_{\mathbf{G}} c_{\mathbf{G}}(\mathbf{k}) e^{i\mathbf{G}\cdot(g^{-1}\mathbf{r}-g^{-1}\mathbf{a})} \\ &= \frac{1}{\sqrt{\Omega}}e^{-i(g\mathbf{k})\cdot\mathbf{a}} e^{i(g\mathbf{k})\cdot\mathbf{r}} \sum_{\mathbf{G}} c_{\mathbf{G}}(\mathbf{k}) e^{i(g\mathbf{G})\cdot\mathbf{r}} = e^{-i(g\mathbf{k})\cdot\mathbf{a}} \frac{1}{\sqrt{\Omega}} e^{i(g\mathbf{k})\cdot\mathbf{r}} \sum_{\mathbf{G}} c_{g^{-1}\mathbf{G}}(\mathbf{k}) e^{i\mathbf{G}\cdot\mathbf{r}} \\ &= e^{-i(g\mathbf{k})\cdot\mathbf{a}} \frac{1}{\sqrt{\Omega}} e^{i(g\mathbf{k})\cdot\mathbf{r}} \sum_{\mathbf{G}} c_{\mathbf{G}}(g\mathbf{k}) e^{i\mathbf{G}\cdot\mathbf{r}} = \lambda_{\{g|\mathbf{a}\}}\psi_{g\mathbf{k}}(\mathbf{r}), \end{aligned} \quad (1.83)$$

where we use the fact that $c_{\mathbf{G}} = c_{\mathbf{G}}(\mathbf{k})$ is a function of \mathbf{k} with the property $c_{g^{-1}\mathbf{G}}(\mathbf{k}) = c_{\mathbf{G}}(g\mathbf{k})$ i.e. $\widehat{S}_{\{g|\mathbf{a}\}}u_{\mathbf{k}}(\mathbf{r}) = u_{g\mathbf{k}}(\mathbf{r})$.

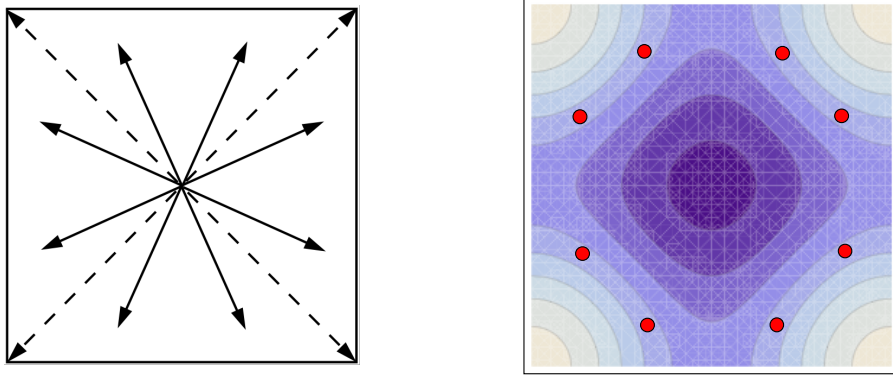


Figure 1.6: Star of \mathbf{k} -points in the Brillouin zone with degenerate band energies: Left panel: Star of \mathbf{k} ; Right panel: contour plot of a two dimensional band $\epsilon_{\mathbf{k}} = -2t\{\cos(k_x a) + \cos(k_y a)\} + 4t' \cos(k_x a) \cos(k_y a)$. The dots correspond to the star of \mathbf{k} with degenerate energy values, demonstrating $\epsilon_{n\mathbf{k}} = \epsilon_{n,g\mathbf{k}}$.

group elements for this \mathbf{k} (without inversion). If \mathbf{k} lies on points or lines of higher symmetry, it is left invariant under a subgroup of the point group. Consequently, the number of beams of the star is smaller. The subgroup of the point group leaving \mathbf{k} unchanged is called *little group* of \mathbf{k} . If inversion is part of the point group, $-\mathbf{k}$ is always contained in the star of \mathbf{k} . In summary, we have the simple relations

$$\epsilon_{n\mathbf{k}} = \epsilon_{n,g\mathbf{k}}, \quad \epsilon_{n\mathbf{k}} = \epsilon_{n,-\mathbf{k}}, \quad \epsilon_{n\mathbf{k}} = \epsilon_{n,\mathbf{k}+\mathbf{G}}. \quad (1.87)$$

We can also use symmetries to characterize Bloch states for given pseudo-momentum \mathbf{k} . Let us take a set of degenerate Bloch states belonging to the band n , $\{|\gamma; n, \mathbf{k}\rangle\}$ satisfying the eigenvalue equation,

$$\mathcal{H}|\gamma; n, \mathbf{k}\rangle = \epsilon_{n\mathbf{k}}|\gamma; n, \mathbf{k}\rangle \quad (1.88)$$

For given \mathbf{k} we consider the little group operations. Operating an element g of the little group on a state $|\gamma; n, \mathbf{k}\rangle$ we obtain again an eigenstate of the Hamiltonian \mathcal{H} , as $\hat{S}_{\{g, \mathbf{0}\}}$ commutes with \mathcal{H} ,

$$\hat{S}_{\{g, \mathbf{0}\}}|\gamma; n, \mathbf{k}\rangle = \sum_{\gamma'} |\gamma', n, \mathbf{k}\rangle \underbrace{\langle \gamma', n, \mathbf{k} | \hat{S}_{\{g, \mathbf{0}\}} | \gamma; n, \mathbf{k} \rangle}_{=M_{\gamma', \gamma}(g)}. \quad (1.89)$$

We transform only within the subspace of degenerate states $|\gamma, n, \mathbf{k}\rangle$ and the matrix $M_{\gamma', \gamma}(g)$ is a representation of the group element g on the vector space of eigenstates $\{|\gamma, n, \mathbf{k}\rangle\}$. If this representation is irreducible then its dimension corresponds to the degeneracy of the corresponding set of Bloch states.

Looking back to the example of tight-binding bands derived from atomic p-orbitals (Fig.1.4). The symmetry at the Γ -point ($\mathbf{k} = 0$) is the full crystal point group O_h (simple cubic lattice). The representation Γ_{15}^- is three-dimensional corresponding to a basis set $\{x, y, z\}$ (p-orbital). At the X -point (symmetry point on the Brillouin zone boundary) the group is reduced to D_{4h} (tetragonal) and the representations appearing are X_2^- (one-dimensional corresponding to z) and X_5^- (two-dimensional corresponding to $\{x, y\}$). Note that generally the little group of \mathbf{k} has lower symmetry and leads to splitting of degeneracies as can be seen on the line $\Gamma - M$ where the bands, degenerate at the Γ -point split up into three and combine again at the M -point into two level of degeneracy one and two, respectively. The symmetry group of the M -point is D_{4h} while for arbitrary $\mathbf{k} \parallel [110]$ it is C_{2v} containing only four elements leaving \mathbf{k} invariant: $C_{2v} \subset D_{4h} \subset O_h$.

1.6 Band-filling and materials properties

Due to the fermionic character of electrons each of the band states $|n, \mathbf{k}, s\rangle$ can be occupied with one electron taking also the spin quantum number into account with spin $s = \uparrow$ and \downarrow (Pauli exclusion principle). The count of electrons has profound implications on the properties of materials. Here we would like to look at the most simple classification of materials based on independent electrons.

1.6.1 Electron count and band filling

We consider here a most simple band structure in the one-dimensional tight-binding model with nearest-neighbor coupling. The lattice has N sites (N even) and we assume periodic boundary conditions. The Hamiltonian is given by

$$\mathcal{H} = -t \sum_{j=1}^N \sum_{s=\uparrow, \downarrow} \{ \hat{c}_{j+1,s}^\dagger \hat{c}_{j,s} + \hat{c}_{j,s}^\dagger \hat{c}_{j+1,s} \} \quad (1.90)$$

where we impose the equivalence $j + N = j$ (periodic boundary conditions). This Hamiltonian can be diagonalized by the Fourier transform

$$\hat{c}_{j,s} = \frac{1}{\sqrt{N}} \sum_k \hat{a}_{k,s} e^{iR_j k} \quad (1.91)$$

leading to

$$\mathcal{H} = \sum_{k,s} \epsilon_k \hat{a}_{k,s}^\dagger \hat{a}_{k,s} \quad \text{with} \quad \epsilon_k = -2t \cos ka . \quad (1.92)$$

Now we request

$$e^{iR_j k} = e^{i(R_j + L)k} \quad \Rightarrow \quad Lk = Nak = 2\pi n \quad \Rightarrow \quad k = \frac{2\pi}{L}n = \frac{2\pi}{a} \frac{n}{N} \quad (1.93)$$

with the pseudo-momentum k within the first Brillouin zone ($-\frac{\pi}{a} < k < \frac{\pi}{a}$) and n being an integer. On the real-space lattice an electron can take $2N$ different states. Thus, for k we find that n should take the values, $n + N/2 = 1, 2, \dots, N-1, N$. Note that $k = -\pi/a$ and $k = +\pi/a$ differ by a reciprocal lattice vector $G = 2\pi/a$ and are therefore identical. This provides the same number of states ($2N$), since per k we have two spins (see Fig.1.7).

We can fill these states with electrons following the Pauli exclusion principle. In Fig.1.7 we show the two typical situations: (1) N electrons corresponding to half of the possible electrons which can be accommodated leading to a half-filled band and (2) $2N$ electrons exhausting all possible states representing a completely filled band. In the case of half-filling we define the Fermi energy as the energy ϵ_F of the highest occupied state, here $\epsilon_F = 0$. This corresponds to the chemical potential, the energy necessary to add an electron to the system at $T = 0K$.

An important difference between (1) and (2) is that the former allows for many different states which may be separated from each other by a very small energy. For example, considering the ground state (as in Fig.1.7) and the excited states obtained by moving one electron from $k = \pi/2a$ ($n = N/4$) to $k' = 2\pi(1 + N/4)/Na$ ($n = 1 + N/4$), we find the energy difference

$$\Delta E = \epsilon_{k'} - \epsilon_k \approx 2t \frac{2\pi}{N} \propto \frac{1}{N} \quad (1.94)$$

which shrinks to zero for $N \rightarrow \infty$. On the other hand, for case (2) there is only one electron configuration possible and no excitations within the one-band picture.

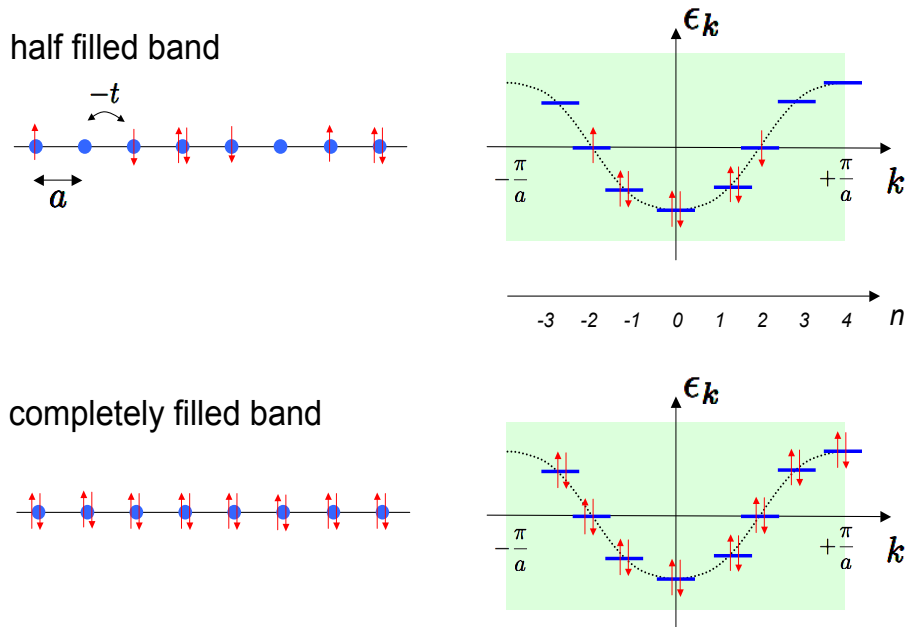


Figure 1.7: One-dimensional tight-binding model with $N = 8$ and periodic boundary conditions. The dispersion has eight different k -levels whereby it has to be noticed that $+\pi/a$ and $-\pi/a$ are equivalent. The condition of half-filling and complete filling are shown, where for half-filling a ground state configuration is shown (note there are 4 degenerate states). For the completely filled band all k levels are occupied by two electrons of opposite spin. This means in real space that also all sites are occupied by two electrons. This is a non-degenerate state.

1.6.2 Metals, semiconductors and insulators

The two situations depicted in Fig.1.7 are typical as each atom (site) in a lattice contributes an integer number of electrons to the system. So we distinguish the case that there is an *odd* or an *even* number of electrons per unit cell. Note that the unit cell may contain more than one atom, unlike the situation shown in our tight-binding example.

- The bands can be either completely filled or empty when the number of electrons per atom (unit cell) is even. Thus taking the complete set of energy bands into account, the chemical potential cannot be identified with a Fermi energy but lies within the energy gap separating highest filled and the lowest empty band (see Fig.1.8). There is a finite energy needed to add, to remove or to excite an electron. If the band gap E_g is much smaller than the bandwidth, we call the material a *semiconductor*. for E_g of the order of the bandwidth, it is an (*band*) *insulator*. In both cases, for temperatures $T \ll E_g/k_B$ the application of a small electric voltage will not produce an electric transport. The highest filled band is called *valence* band, whereas the lowest empty band is termed *conduction* band. Examples for insulators are *C* as diamond and for semiconductors *Si* and *Ge*. They have diamond lattice structure with two atoms per unit cell. As these atoms belong to the group IV in the periodic table, each provides an even number of electrons suitable for completely filling bands. Note that we will encounter another form of an insulator, the Mott insulator, whose insulating behavior is not governed by a band structure effect, but by a correlation effect through strong Coulomb interaction.
- If the number of electrons per unit cell is odd, the uppermost non-empty band is half filled (see Figure 1.8). Then the system is a *metal*, in which electrons can move and

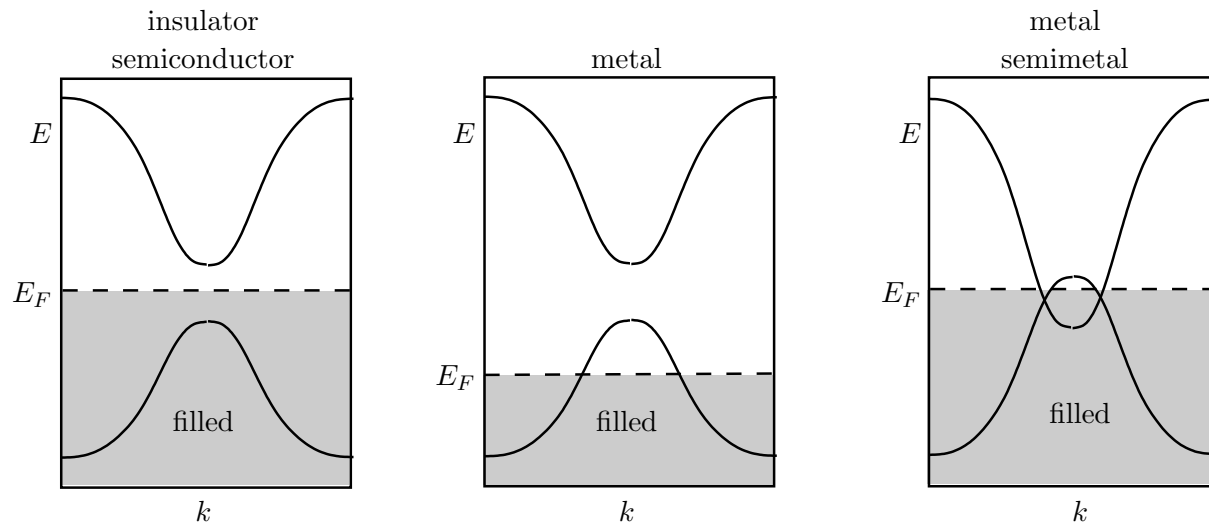


Figure 1.8: Material classes according to band filling: left panel: insulator or semiconductor (partially filled bands with the Fermi level in band gap); center panel: metal (Fermi level inside band); right panel: metal or semimetal (Fermi level inside two overlapping bands).

excitations with arbitrarily small energies are possible. The electrons remain mobile down to arbitrarily low temperatures. The standard example of a metal are the Alkali metals in the first column of the periodic table (Li, Na, K, Rb, Cs), as all of them have the configuration [noble gas] $(ns)^1$, i.e., one mobile electron per ion.

- In general, band structures are more complex. Different bands need not to be separated by energy gaps, but can overlap instead. In particular, this happens, if different orbitals are involved in the structure of the bands. In these systems, bands can have any fractional filling (not just filled or half-filled). The earth alkaline metals are an example for this (second column of the periodic table, Be, Mg, Ca, Sr, Ba), which are metallic despite having two (n, s) -electrons per unit cell. Systems, where two bands overlap at the Fermi energy but the overlap is small, are termed *semi-metals*. The extreme case, where valence and conduction band touch in isolated points so that there are no electrons at the Fermi energy and still the band gap is zero, is realized in graphene.

The electronic structure is also responsible for the cohesive forces necessary for the formation of a regular crystal. We may also classify materials according to relevant forces. We distinguish four major types of crystals:

Molecular crystals are formed from atoms or molecules with closed-shell atomic structures such as the noble gases He, Ne etc. which become solid under pressure. Here the van der Waals forces generate the binding interactions.

Ionic crystals combine different atoms, A and B, where A has a small ionization energy while B has a large electron affinity. Thus, electrons are transferred from A to B giving a positively charged A^+ and a negatively charge B^- . In a regular (alternating) lattice the energy gained through Coulomb interaction can overcome the energy expense for the charge transfer stabilizing the crystal. A famous example is NaCl where one electron leaves Na ($[\text{Ne}] 3s$) and is added to Cl ($[\text{Ne}] 3s^2 3p^5$) as to bring both atoms to closed-shell electronic configuration.

Covalent-bonded crystals form through chemical binding, like in the case of the H_2 , where neighboring atoms share electrons through the large overlap of the electron orbital wavefunction. Insulators like diamond C or semiconductors like Si or GaAs are important

examples of this type as we will discuss later. Note that electrons of covalent bonds are localized between the atoms.

Metallic bonding is based on delocalized electrons (in contrast to the covalent bonds) stripped from their atoms. The stability of simple metals like the alkaly metals Li, Na, K etc will be discussed later. Note that many metals, such as the noble metals Au or Pt, can also involve aspects of covalent or molecular bonding through overlapping but more localized electronic orbitals.

1.7 Dynamics of band electrons - semiclassical approach

In quantum mechanics, the Ehrenfest theorem shows that the expectation values of the position and momentum operators obey equations similar to the equation of motion in Newtonian mechanics.⁸ An analogous formulation holds for electrons in a periodic potential, where we assume that the electron may be described as a wave packet of the form

$$\psi_{\mathbf{k}}(\mathbf{r}, t) = \sum_{\mathbf{k}'} g_{\mathbf{k}}(\mathbf{k}') e^{i\mathbf{k}' \cdot \mathbf{r} - i\epsilon_{\mathbf{k}'} t}, \quad (1.98)$$

where $g_{\mathbf{k}}(\mathbf{k}')$ is centered around \mathbf{k} in reciprocal space and has a width of Δk . Δk should be much smaller than the size of the Brillouin zone for this Ansatz to make sense, i.e., $\Delta k \ll 2\pi/a$. Therefore, the wave packet is spread over many unit cells of the lattice since Heisenberg's uncertainty principle $(\Delta k)(\Delta x) > 1$ implies $\Delta x \gg a/2\pi$. In this way, the pseudo-momentum \mathbf{k} of the wave packet remains well defined. Furthermore, the applied electric and magnetic fields have to be small enough not to induce transitions between different bands. The latter condition is not very restrictive in practice.

1.7.1 Semi-classical equations of motion

We introduce the rules of the semi-classical motion of electrons with applied electric and magnetic fields without proof:

- The band index of an electron is conserved, i.e., there are no transitions between the bands.

⁸Ehrenfest theorem for free electrons with the Hamiltonian,

$$\mathcal{H} = \frac{\hat{\mathbf{p}}^2}{2m} + V(\hat{\mathbf{r}}) \quad (1.95)$$

states for the expectation values for a particle represented by a wave packet,

$$\frac{d}{dt} \langle \hat{\mathbf{r}} \rangle = \frac{i}{\hbar} \langle [\mathcal{H}, \hat{\mathbf{r}}] \rangle = \frac{\langle \hat{\mathbf{p}} \rangle}{m} \quad (1.96)$$

and

$$\frac{d}{dt} \langle \hat{\mathbf{p}} \rangle = \frac{i}{\hbar} \langle [\mathcal{H}, \hat{\mathbf{p}}] \rangle = -\langle \nabla V(\hat{\mathbf{r}}) \rangle \quad (1.97)$$

which has a form similar to Newtons equations with the restriction $-\langle \nabla V(\hat{\mathbf{r}}) \rangle \neq \nabla V(\langle \hat{\mathbf{r}} \rangle)$.

- The equations of motion read⁹

$$\dot{\mathbf{r}} = \mathbf{v}_n(\mathbf{k}) = \frac{\partial \epsilon_n \mathbf{k}}{\partial \hbar \mathbf{k}}, \quad (1.101)$$

$$\hbar \dot{\mathbf{k}} = -e \mathbf{E}(\mathbf{r}, t) - \frac{e}{c} \mathbf{v}_n(\mathbf{k}) \times \mathbf{H}(\mathbf{r}, t). \quad (1.102)$$

- All electronic states have a wave vector that lies in the first Brillouin zone, as \mathbf{k} and $\mathbf{k} + \mathbf{G}$ label the same state for all reciprocal lattice vectors \mathbf{G} .
- In thermal equilibrium, the electron density per spin in the n -th band in the volume element $d^3k/(2\pi)^3$ around \mathbf{k} is given by

$$n_F[\epsilon_n(\mathbf{k})] = \frac{1}{e^{[\epsilon_n(\mathbf{k}) - \mu]/k_B T} + 1}. \quad (1.103)$$

Each state of given \mathbf{k} and spin can be occupied only once (Pauli principle).

Note that $\hbar \mathbf{k}$ is not the momentum of the electron, but the so-called lattice momentum or pseudo momentum in the Bloch theory of bands. It is connected with the eigenvalue of the translation operator on the state. Consequently, the right-hand side of the equation (1.102) is not the force that acts on the electron, as the forces exerted by the periodic lattice potential is not included. The latter effect is contained implicitly through the form of the band energy $\epsilon(\mathbf{k})$, which governs the first equation.

1.7.2 Bloch oscillations

The fact that the band energy is a periodic function of \mathbf{k} leads to a strange oscillatory behavior of the electron motion in a static electric field. For illustration, consider a one-dimensional system where the band energy $\epsilon_k = -2 \cos ka$ leads to the solution of the semi-classical equations (1.101,1.102)

$$\hbar \dot{k} = -eE \quad (1.104)$$

$$\Rightarrow k = -\frac{eEt}{\hbar} \quad (1.105)$$

$$\Rightarrow \dot{x} = -\frac{2a}{\hbar} \sin\left(\frac{eEat}{\hbar}\right), \quad (1.106)$$

in the presence of a homogenous electric field E . It follows immediately, that the position x of the electron oscillates like

$$x(t) = \frac{2}{eE} \cos\left(\frac{eEat}{\hbar}\right). \quad (1.107)$$

This behavior is called *Bloch oscillation* and means that the electron oscillates around its initial position rather than moving in one direction when subjected to a static electric field. This effect can only be observed under very special conditions where the probe is absolutely clean. The effect is easily destroyed by damping or scattering.

⁹A plausibility argument concerning the conservation of energy leading to the equation (1.102) is given here. The time derivative of the energy (kinetic and potential)

$$E = \epsilon_n(\mathbf{k}(t)) - e\phi(\mathbf{r}(t)) \quad (1.99)$$

has to vanish, i.e.,

$$0 = \frac{dE}{dt} = \frac{\partial \epsilon_n(\mathbf{k})}{\partial \mathbf{k}} \cdot \dot{\mathbf{k}} - e \nabla \phi \cdot \dot{\mathbf{r}} = \mathbf{v}_n(\mathbf{k}) \cdot (\hbar \dot{\mathbf{k}} - e \nabla \phi). \quad (1.100)$$

From this, equation (1.102) follows directly for the electric field $\mathbf{E} = -\nabla \phi$ and the Lorentz force is allowed because the force is always perpendicular to the velocity \mathbf{v}_n .

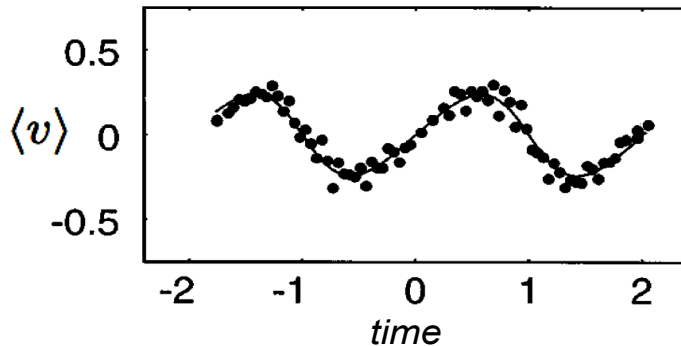


Figure 1.9: Experimental observation of Bloch oscillation for accelerated cesium atoms trapped in an periodic optical lattice generated by standing waves of laser light: mean velocity $\langle v \rangle$ versus time [M.B. Dahan et al, Phys. Rev. Lett. 76, 4508 (1996)].

1.7.3 Current densities

We will see in chapter 6 that homogenous steady current carrying states of electron systems can be described by the momentum distribution $n(\mathbf{k})$. Assuming this property, the current density follows from

$$\mathbf{j} = -2e \int_{\text{BZ}} \frac{d^3k}{(2\pi)^3} \mathbf{v}(\mathbf{k}) n(\mathbf{k}) = -2e \int_{\text{BZ}} \frac{d^3k}{(2\pi)^3} n(\mathbf{k}) \frac{\partial \epsilon(\mathbf{k})}{\partial \hbar \mathbf{k}}, \quad (1.108)$$

where the integral extends over all \mathbf{k} in the Brillouin zone (BZ) and the factor 2 originates from the two possible spin states of the electrons. Note that for a finite current density \mathbf{j} , the momentum distribution $n(\mathbf{k})$ has to deviate from the equilibrium Fermi-Dirac distribution in equation (1.103). It is straight forward to show that the current density vanishes for an empty band. The same holds true for a completely filled band ($n(\mathbf{k}) = 1$) where equation (1.101) implies

$$\mathbf{j} = -2e \int_{\text{BZ}} \frac{d^3k}{(2\pi)^3} \frac{1}{\hbar} \frac{\partial \epsilon(\mathbf{k})}{\partial \mathbf{k}} = 0 \quad (1.109)$$

because $\epsilon(\mathbf{k})$ is periodic in the Brillouin zone, i.e., $\epsilon(\mathbf{k} + \mathbf{G}) = \epsilon(\mathbf{k})$ when \mathbf{G} is a reciprocal lattice vector. Thus, neither empty nor completely filled bands can carry currents.

An interesting aspect of band theory is the picture of holes. We compute the current density for a partially filled band in the framework of the semi-classical approximation,

$$\mathbf{j} = -2e \int_{\text{BZ}} \frac{d^3k}{(2\pi)^3} n(\mathbf{k}) \mathbf{v}(\mathbf{k}) \quad (1.110)$$

$$= -2e \left[\int_{\text{BZ}} \frac{d^3k}{(2\pi)^3} \mathbf{v}(\mathbf{k}) - \int_{\text{BZ}} \frac{d^3k}{4\pi^3} [1 - n(\mathbf{k})] \mathbf{v}(\mathbf{k}) \right] \quad (1.111)$$

$$= +2e \int_{\text{BZ}} \frac{d^3k}{(2\pi)^3} [1 - n(\mathbf{k})] \mathbf{v}(\mathbf{k}). \quad (1.112)$$

This suggests that the current density comes either from electrons in filled states with charge $-e$ or from 'holes', missing electrons carrying positive charge and sitting in the unoccupied electronic states. In band theory, both descriptions are equivalent. However, it is usually easier to work with holes, if a band is almost filled, and with electrons if the filling of an energy band is small.

1.8 Appendix: Approximative band structure calculations

While the approximation of nearly free electrons gives a qualitative picture of the band structure, it rests on the assumption that the periodic potential is weak, and, thus, may be treated as a small perturbation. Only few states connected with different reciprocal lattice vectors are sufficient within this approximation. However, in reality the ionic potential is strong compared to the electrons' kinetic energy. This leads to strong modulations of the wave function around the ions, which is not well described by slightly perturbed plane waves.

1.8.1 Pseudo-potential

In order to overcome this weakness of the plane wave solution, we would have to superpose a very large number of plane waves, which is not an easy task to put into practice. Alternatively, we can divide the electronic states into the ones corresponding to filled low-lying energy states, which are concentrated around the ionic core (core states), and into extended (and more weakly modulated) states, which form the valence and conduction bands. The core electron states may be approximated by atomic orbitals of isolated atoms. For a metal such as aluminum (Al: $1s^2 2s^2 2p^6 3s^2 3p$) the core electrons correspond to the $1s$ -, $2s$ -, and $2p$ -orbitals, whereas the $3s$ - and $3p$ -orbitals contribute dominantly to the extended states of the valence- and conduction bands. We will focus on the latter, as they determine the low-energy physics of the electrons. The core electrons are deeply bound and can be considered inert.

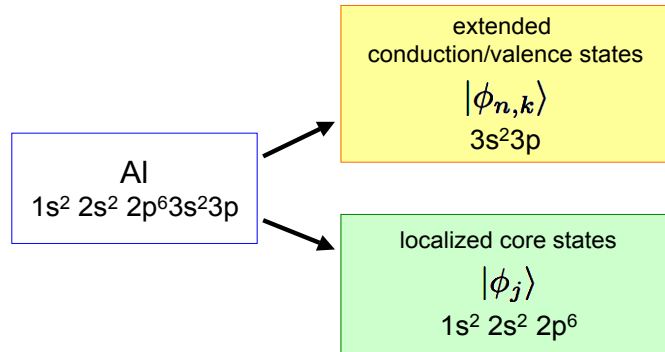


Figure 1.10: Separation into extended and core electronic states (example Aluminium).

We introduce the core electron states as $|\phi_j\rangle$, with $\mathcal{H}|\phi_j\rangle = E_j|\phi_j\rangle$ where \mathcal{H} is the Hamiltonian of the single atom. The remaining states have to be orthogonal to these core states, so that we make the Ansatz

$$|\phi_{n,\mathbf{k}}\rangle = |\chi_{n\mathbf{k}}\rangle - \sum_j |\phi_j\rangle \langle \phi_j | \chi_{n,\mathbf{k}} \rangle, \quad (1.113)$$

with $|\chi_{n,\mathbf{k}}\rangle$ an orthonormal set of states. Then, $\langle \phi_{n,\mathbf{k}} | \phi_j \rangle = 0$ holds for all j . If we choose plane waves for the $|\chi_{n\mathbf{k}}\rangle$, the resulting $|\phi_{n,\mathbf{k}}\rangle$ are so-called orthogonalized plane waves (OPW). The Bloch functions are superpositions of these OPW,

$$|\psi_{n,\mathbf{k}}\rangle = \sum_{\mathbf{G}} b_{\mathbf{k}+\mathbf{G}} |\phi_{n,\mathbf{k}+\mathbf{G}}\rangle, \quad (1.114)$$

where the coefficients $b_{\mathbf{k}+\mathbf{G}}$ converge rapidly, such that, hopefully, only a small number of OPWs is needed for a good description.

First, we again consider an arbitrary $|\chi_{n\mathbf{k}}\rangle$ and insert it into the eigenvalue equation $\mathcal{H}|\phi_{n\mathbf{k}}\rangle = E_{n\mathbf{k}}|\phi_{n\mathbf{k}}\rangle$,

$$\mathcal{H}|\chi_{n\mathbf{k}}\rangle - \sum_j \mathcal{H}|\phi_j\rangle\langle\phi_j|\chi_{n,\mathbf{k}}\rangle = E_{n\mathbf{k}}\left(|\chi_{n\mathbf{k}}\rangle - \sum_j |\phi_j\rangle\langle\phi_j|\chi_{n,\mathbf{k}}\rangle\right) \quad (1.115)$$

or

$$\mathcal{H}|\chi_{n\mathbf{k}}\rangle + \sum_j (E_{n\mathbf{k}} - E_j)|\phi_j\rangle\langle\phi_j|\chi_{n,\mathbf{k}}\rangle = E_{n\mathbf{k}}|\chi_{n\mathbf{k}}\rangle. \quad (1.116)$$

We introduce the integral operator in real space $\widehat{V}' = \sum_j (E_{n\mathbf{k}} - E_j)|\phi_j\rangle\langle\phi_j|$, describing a non-local and energy-dependent potential. With this operator we can rewrite the eigenvalue equation in the form

$$(\mathcal{H} + \widehat{V}')|\chi_{n,\mathbf{k}}\rangle = (\mathcal{H}_0 + \widehat{V} + \widehat{V}')|\chi_{n,\mathbf{k}}\rangle = (\mathcal{H} + \widehat{V}_{\text{ps}})|\chi_{n,\mathbf{k}}\rangle = E_{n\mathbf{k}}|\chi_{n\mathbf{k}}\rangle. \quad (1.117)$$

This is an eigenvalue equation for the so-called pseudo-wave function (or pseudo-state) $|\chi_{n\mathbf{k}}\rangle$, instead of the Bloch state $|\psi_{n\mathbf{k}}\rangle$, where the modified potential $\widehat{V}_{\text{ps}} = \widehat{V} + \widehat{V}'$ is called *pseudo-potential*. The attractive core potential $\widehat{V} = V(\widehat{\mathbf{r}})$ is always negative. On the other hand, $E_{n\mathbf{k}} > E_j$, such that \widehat{V}' is positive. It follows that \widehat{V}_{ps} is weaker than both \widehat{V} and \widehat{V}' . An arbitrary number of core states $\sum_j a_j|\psi_j\rangle$ may be added to $|\chi_{n\mathbf{k}}\rangle$ without violating the orthogonality condition (1.113). Consequently, neither the pseudo-potential nor the pseudo-states are uniquely determined and may be optimized variationally with respect to the set $\{a_j\}$ in order to optimally reduce the spatial modulation of either the pseudo-potential or the wave-function.

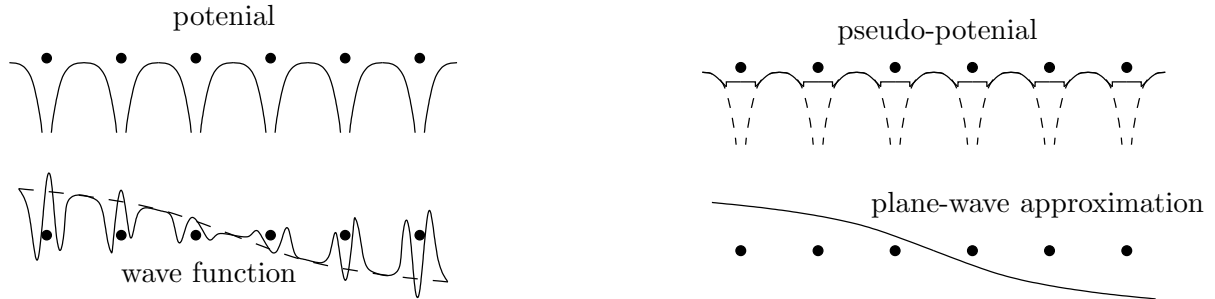


Figure 1.11: Illustration of the pseudo-potential.

If we are only interested in states inside a small energy window, the energy dependence of the pseudo-potential can be neglected, and V_{ps} may be approximated by a standard potential (see Figure 1.11). Such a simple Ansatz is exemplified by the atomic pseudo-potential, proposed by Ashcroft, Heine and Abarenkov (AHA). The potential of a single ion is assumed to be of the form

$$v_{\text{ps}}(r) = \begin{cases} V_0 & r < R_c, \\ -\frac{Z_{\text{ion}}e^2}{r} & r > R_c, \end{cases} \quad (1.118)$$

where Z_{ion} is the charge of the ionic core and R_c its effective radius (determined by the core electrons). The constants R_c and V_0 are chosen such that the energy levels of the outermost electrons are reproduced correctly for the single-atom calculations. For example, the $1s$ -, $2s$ -, and $2p$ -electrons of Na form the ionic core. R_c and V_0 are adjusted such that the one-particle problem $\mathbf{p}^2/2m + v_{\text{ps}}(r)$ leads to the correct ionization energy of the $3s$ -electron. More flexible

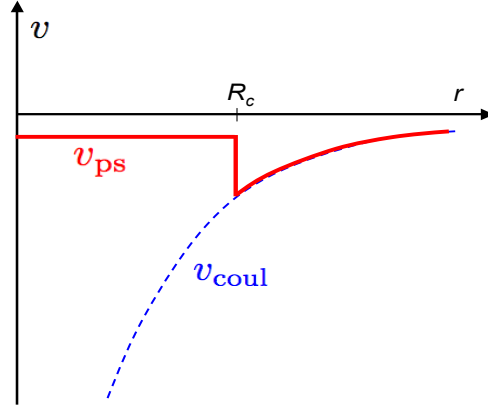


Figure 1.12: Pseudopotential: Ashcroft, Heine and Abarenkov form.

approaches allow for the incorporation of more experimental input into the pseudo-potential. The full pseudo-potential of the lattice can be constructed from the contribution of the individual atoms,

$$V_{\text{ps}}(\mathbf{r}) = \sum_n v_{\text{ps}}(|\mathbf{r} - \mathbf{R}_j|), \quad (1.119)$$

where \mathbf{R}_j is the lattice vector. For the method of nearly free electrons we need the Fourier transform of the potential evaluated at the reciprocal lattice vectors,

$$V_{\text{ps},\mathbf{G}} = \frac{1}{\Omega} \int d^3r V_{\text{ps}}(\mathbf{r}) e^{-i\mathbf{G}\cdot\mathbf{r}} = \frac{N}{\Omega} \int d^3r v_{\text{ps}}(\mathbf{r}) e^{-i\mathbf{G}\cdot\mathbf{r}}. \quad (1.120)$$

For the AHA form (1.118), this is given by

$$V_{\text{ps},\mathbf{G}} = -\frac{4\pi Z_{\text{ion}} e^2}{G^2} \left(\cos(GR_c) + \frac{V_0}{Z_{\text{ion}} e^2 G} \left((R_c^2 G^2 - 2) \cos(GR_c) + 2 - 2R_c G \sin(GR_c) \right) \right). \quad (1.121)$$

For small reciprocal lattice vectors, the zeroes of the trigonometric functions on the right-hand side of (1.121) reduce the strength of the potential. For large G , the pseudo-potential decays $\propto 1/G^2$. It is thus clear that the pseudo-potential is always weaker than the original potential. Extending this theory for complex unit cells containing more than one atom, the pseudo-potential may be written as

$$V_{\text{ps}}(\mathbf{r}) = \sum_{n,\alpha} v_{\text{ps}}^\alpha(|\mathbf{r} - (\mathbf{R}_j + \mathbf{R}_\alpha)|), \quad (1.122)$$

where \mathbf{R}_α denotes the position of the α -th base atom in the unit cell. Here, v_{ps}^α is the pseudo-potential of the α -th ion. In reciprocal space,

$$V_{\text{ps},\mathbf{G}} = \frac{N}{\Omega} \sum_\alpha e^{-i\mathbf{G}\cdot\mathbf{R}_\alpha} \int d^3r v_{\text{ps}}^\alpha(|\mathbf{r}|) e^{-i\mathbf{G}\cdot\mathbf{r}} \quad (1.123)$$

$$= \sum_\alpha e^{-i\mathbf{G}\cdot\mathbf{R}_\alpha} F_{\alpha,\mathbf{G}}. \quad (1.124)$$

The form factor $F_{\alpha,\mathbf{G}}$ contains the information of the base atoms and may be calculated or obtained by fitting experimental data.

1.8.2 Augmented plane wave

We now consider a method introduced by Slater in 1937. It is an extension of the so-called Wigner-Seitz cell method (1933) and consists of approximating the crystal potential by a so-called muffin-tin potential. The latter is a periodic potential, which is taken to be spherically symmetric and position dependent around each atom up to a distance r_s , and constant for larger distances. The spheres of radius r_s are taken to be non-overlapping and are contained completely in the Wigner-Seitz cell¹⁰ (Figure 1.13).

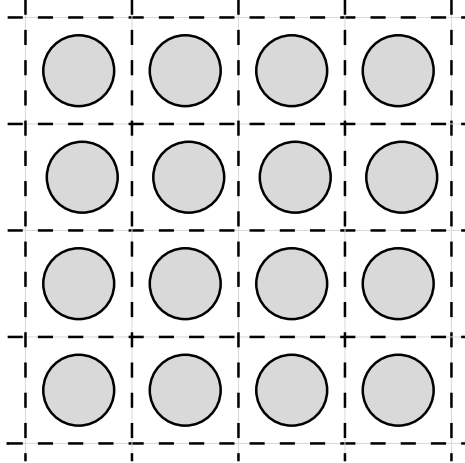


Figure 1.13: Muffin-tin potential.

The advantage of this decomposition is that the problem can be solved using a divide-and-conquer strategy. Inside the muffin-tin radius we solve the spherically symmetric problem, while the solutions on the outside are given by plane waves; the remaining task is to match the solutions at the boundaries.

The spherically symmetric problem for $|\mathbf{r}| < r_s$ is solved with the standard Ansatz

$$\varphi(\mathbf{r}) = \frac{u_l(r)}{r} Y_{lm}(\theta, \phi), \quad (1.125)$$

where (r, θ, ϕ) are the spherical coordinates of \mathbf{r} and the radial part $u_l(r)$ of the wave function obeys the differential equation

$$\left[-\frac{\hbar^2}{2m} \frac{d^2}{dr^2} + \frac{\hbar^2 l(l+1)}{2mr^2} + V(r) - E \right] u_l(r, E) = 0. \quad (1.126)$$

We define an augmented plane wave (APW) $A(\mathbf{k}, \mathbf{r}, E)$, which is a pure plane wave with wave vector \mathbf{k} outside the Muffin-tin sphere. For this, we employ the representation of plane waves by spherical harmonics,

$$e^{i\mathbf{k}\cdot\mathbf{r}} = 4\pi \sum_{l=0}^{\infty} \sum_{m=-l}^l i^l j_l(kr) Y_{lm}^*(\hat{\mathbf{k}}) Y_{lm}(\hat{\mathbf{r}}), \quad (1.127)$$

¹⁰The Wigner-Seitz cell is the analogue of the Brillouin zone in real space. One draws planes cutting each line joining two atoms in the middle, and orthogonal to them. The smallest cell bounded by these planes is the Wigner-Seitz cell.

where $j_l(x)$ is the l -th spherical Bessel function. We parametrize

$$A(\mathbf{k}, \mathbf{r}, E) = \begin{cases} \frac{4\pi}{\sqrt{\Omega_{\text{UC}}}} \sum_{l,m} i^l j_l(kr_s) \frac{r_s u_l(r, E)}{r u_l(r_s, E)} Y_{lm}^*(\hat{\mathbf{k}}) Y_{lm}(\hat{\mathbf{r}}), & r < r_s, \\ \frac{4\pi}{\sqrt{\Omega_{\text{UC}}}} \sum_{l,m} i^l j_l(kr) Y_{lm}^*(\hat{\mathbf{k}}) Y_{lm}(\hat{\mathbf{r}}), & r > r_s, \end{cases} \quad (1.128)$$

where Ω_{UC} is the volume of the unit cell. Note that the wave function is always continuous at $r = r_s$, but that its derivatives are in general not continuous. We can use an expansion of the wave function $\psi_{\mathbf{k}}(\mathbf{r})$ similar to the one in the nearly free electron approximation (see equations (1.19) and (1.27)),

$$\psi_{\mathbf{k}}(\mathbf{r}) = \sum_{\mathbf{G}} c_{\mathbf{G}}(\mathbf{k}) A(\mathbf{k} + \mathbf{G}, \mathbf{r}, E), \quad (1.129)$$

where the \mathbf{G} are reciprocal lattice vectors. The unknown coefficients can be determined variationally by solving the system of equations

$$\sum_{\mathbf{G}} \langle A_{\mathbf{k}}(E) | \mathcal{H} - E | A_{\mathbf{k}+\mathbf{G}}(E) \rangle c_{\mathbf{G}}(\mathbf{k}) = 0, \quad (1.130)$$

where

$$\langle A_{\mathbf{k}}(E) | \mathcal{H} - E | A_{\mathbf{k}'}(E) \rangle = \left(\frac{\hbar^2 \mathbf{k} \cdot \mathbf{k}'}{2m} - E \right) \Omega_{\text{UC}} \delta_{\mathbf{k}, \mathbf{k}'} + V_{\mathbf{k}, \mathbf{k}'} \quad (1.131)$$

with

$$V_{\mathbf{k}, \mathbf{k}'} = 4\pi r_s^2 \left[- \left(\frac{\hbar^2 \mathbf{k} \cdot \mathbf{k}'}{2m} - E \right) \frac{j_1(|\mathbf{k} - \mathbf{k}'| r_s)}{|\mathbf{k} - \mathbf{k}'|} + \sum_{l=0}^{\infty} \frac{\hbar^2}{2m} (2l+1) P_l(\hat{\mathbf{k}} \cdot \hat{\mathbf{k}}') j_l(kr_s) j_l(k'r_s) \frac{u'_l(r_s, E)}{u_l(r_s, E)} \right]. \quad (1.132)$$

Here, $P_l(z)$ is the l -th Legendre polynomial and $u' = du/dr$. The solution of (1.130) yields the energy bands. The most difficult parts are the approximation of the crystal potential by the muffin-tin potential and the computation of the matrix elements in (1.130). The rapid convergence of the method is its big advantage: just a few dozens of \mathbf{G} -vectors are needed and the largest angular momentum needed is about $l = 5$. Another positive aspect is the fact that the APW-method allows the interpolation between the two extremes of extended, weakly bound electronic states and tightly bound states.

Chapter 2

Semiconductors

The technological relevance of semiconductors can hardly be overstated. In this chapter, we review some of their basic properties. Regarding the electric conductivity, semiconductors are placed in between metals and insulators. Normal metals are good conductors at all temperatures, and the conductivity usually increases with decreasing temperature. On the other hand, for semiconductors and insulators the conductivity decreases upon cooling (see Figure 2.1).

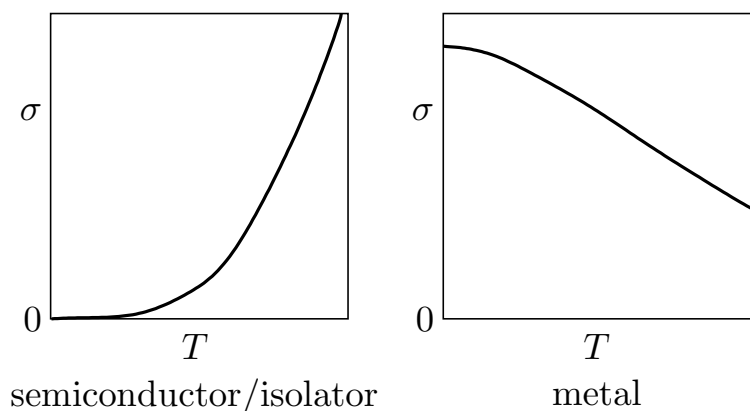


Figure 2.1: Schematic temperature dependence of the electric conductivity for semiconductors and metals.

We will see that the conductivity may be written in the Drude form as

$$\sigma = \frac{ne^2\tau}{m}, \quad (2.1)$$

where n is the density of mobile electrons, τ is the average time between two scattering events of the electrons (transport life time of electrons) and m and e are the electronic mass and charge, respectively. In metals, n is essentially independent of temperature, whereas the scattering time τ decreases with increasing temperature. Thus, τ determines mainly the temperature dependence of the conductivity in metals. On the other hand, insulators and semiconductors have no mobile charges at $T = 0$. At finite temperature, charges are induced by thermal excitations which have to overcome the band gap¹ E_g between the valence and the conduction

¹Actually, one has to count both the excited electrons in the conduction band and the resulting holes in the valence band, as both contribute to the current,

$$\mathbf{j} = (\sigma_+ + \sigma_-)\mathbf{E}, \quad \text{with} \quad \sigma_{\pm} = \frac{n_{\pm}e^2\tau_{\pm}}{m_{\pm}}, \quad (2.2)$$

where $+$ and $-$ stand for holes and electrons, respectively, and $n_+ = n_-$ holds for thermal excitation. Note that, in general, the effective masses and scattering times are not the same for the valence and conduction bands.

band, yielding

$$n \sim n_0 \left(\frac{T}{T_0} \right)^{3/2} e^{-E_g/2k_B T}, \quad (2.3)$$

where $T_0 = 300\text{K}$ and the electron density in the material n_0 is typically 10^{20} cm^{-3} . For insulators, the energy gap is huge, e.g., 5.5 eV for diamond. Consequently, the charge carrier density at room temperature $T = 300\text{K}$ is around $n \sim 10^{-27} \text{ cm}^{-3}$. For a higher charge carrier density $n \sim 10^3 - 10^{11} \text{ cm}^{-3}$, smaller gaps $E_g \sim 0.5 - 1\text{eV}$ are necessary. Materials with a band gap in this regime are not fully isolating and, therefore, are termed semiconductors. However, the carrier densities of both insulators and semiconductors are dwarfed by the electron density in metals contributing to current transport ($n_{\text{metal}} \sim 10^{23} - 10^{24} \text{ cm}^{-3}$). Adding a small amount of impurities in semiconductors, a process called doping with acceptors or donors, their conductivity can be engineered in various ways, rendering them useful as components in innumerable applications.

2.1 The band structure of the elements in group IV

2.1.1 Crystal and band structure

The most important semiconductor for technological applications is silicon (Si) that – like carbon (C), germanium (Ge) and tin (Sn) – belongs to the group IV of the periodic table. These elements have four electrons in their outermost shell in the configuration $(ns)^2(np)^2$ ($n=2$ for C, $n=3$ for Si, $n=4$ for Ge, and $n=5$ for Sn). All four elements form crystals with a diamond structure (cf. Figure 2.2), i.e., a face-centered cubic lattice with a unit cell containing two atoms located at $(0, 0, 0)$ and $(\frac{1}{4}, \frac{1}{4}, \frac{1}{4})$ (for Sn this is called α -Sn). The crystal structure is stabilized by hybridization of the four valence electrons, leading to covalent bonding of oriented orbitals,

$$\begin{aligned} |\psi_1\rangle &= |ns\rangle + |np_x\rangle + |np_y\rangle + |np_z\rangle, & |\psi_2\rangle &= |ns\rangle + |np_x\rangle - |np_y\rangle - |np_z\rangle, \\ |\psi_3\rangle &= |ns\rangle - |np_x\rangle + |np_y\rangle - |np_z\rangle, & |\psi_4\rangle &= |ns\rangle - |np_x\rangle - |np_y\rangle + |np_z\rangle. \end{aligned} \quad (2.4)$$

Locally, the nearest neighbors of each atom form a tetrahedron around it, which leads to the diamond structure of the lattice.

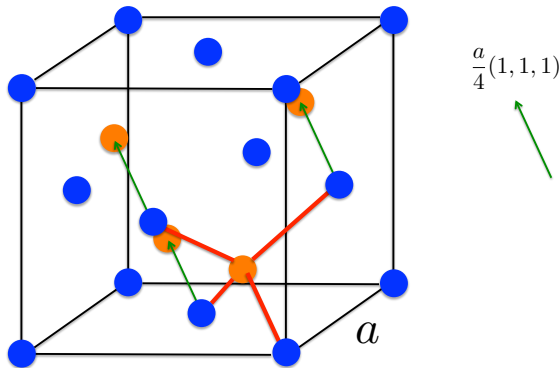


Figure 2.2: The crystal structure of diamond corresponds to two face-centered cubic lattices shifted by a quarter of lattice spacing along the $(1,1,1)$ direction (2 sublattices blue and orange).

The electron band structure of this system is represented in the Brillouin zone of the fcc lattice (Fig. 2.3). In Fig. 2.4 the approximate band structures of both carbon C and silicon Si are displayed. They are rather similar. Focussing on the Γ -point we find the lowest band belongs to the trivial representation Γ_1 of the cubic point group and is, consequently non-degenerate.

Next we find the three-fold degenerate bands belonging to the three-dimensional representation Γ_{25} . Here the Γ -point is the band top. There is a finite energy gap to the next higher bands which at the Γ -point are also three-fold degenerate belonging to Γ_{15} . This is, however, neither a band bottom nor top. The lowest point of these bands lies between the Γ -point and the Brillouin zone boundary at the X -point (Fig. 2.3) with $\mathbf{k}_0 \approx (100)\mathbf{k}_0$ and five other equivalent directions.

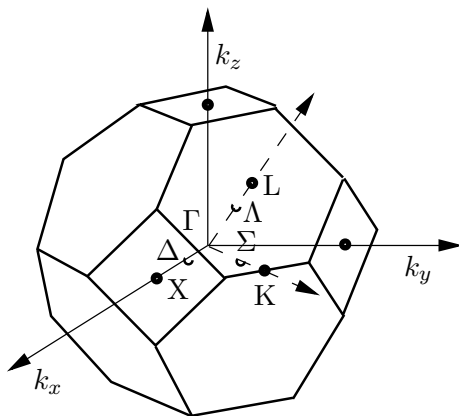


Figure 2.3: The Brillouin zone of a face-centered cubic crystal (in real space) is embedded in a bcc lattice.

Let us look now at the electron count. The two atoms per unit cell provide together eight valence electrons. With these we can fill four bands completely (Sect. 1.6). Thus, in the ground state the lowest four bands constitute the completely filled *valence bands*, while all the upper ones are empty and represent *conduction bands*. The energy gap between the valence and conduction bands (top of valence band at $\mathbf{k} = 0$ and bottom of conduction bands at $\mathbf{k}_0 \neq 0$) is smallest for a non-vanishing connecting k -vector. We call this an *indirect gap*. This is the case for both C and Si. A typical example for a *direct gap* semiconductor is GaAs where the two sub lattices of the crystal structure in Fig. 2.2 are occupied by an atom of the group III and V, respectively, in the periodic table.

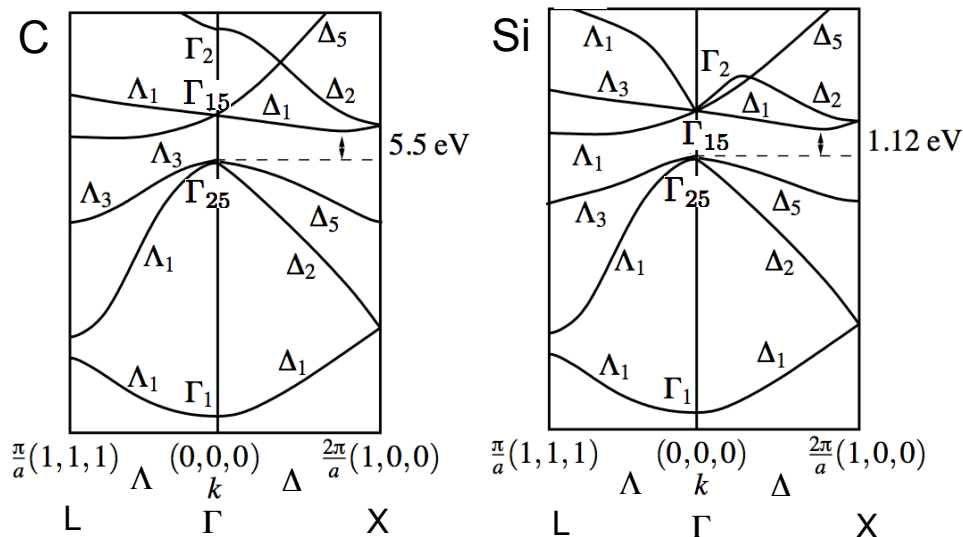


Figure 2.4: Band structure of C and Si.

Note that generally energy gaps in semiconductors and insulators are classified to be *direct* if the wave-vector connecting the maximum of the valence band and the minimum of the conduction band vanishes. Otherwise a gap is called *indirect* (see Fig. 2.5).

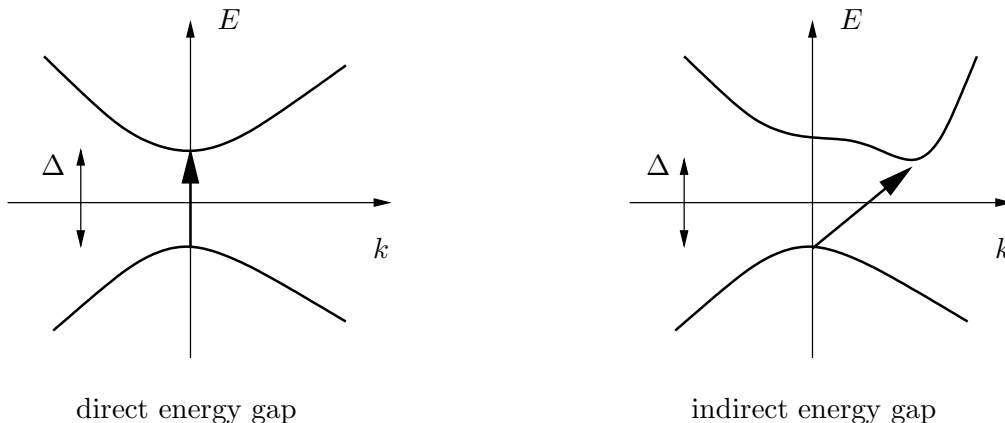


Figure 2.5: Illustration of direct and indirect band gaps.

List of some facts about these materials of the group IV and compounds combining group III and V:

- Carbon has an energy gap of around 5.5eV in the diamond structure. Thus, in this configuration it is not a semiconductor but an insulator. The large energy gap causes the transparency of diamond in the visible range (1.5 - 3.5eV), as the electromagnetic energy in this range cannot be absorbed by the electrons.
- The energy gap of silicon is 1.12eV and thus much smaller; furthermore, it is indirect.
- Germanium has an indirect gap of 0.67eV.
- GaAs and GaN have a direct energy gap of 1.43eV and 3.5eV, respectively.

2.2 Elementary excitations in semiconductors

We consider a simple two-band model to illustrate the most basic properties of the excitation spectrum of a semiconductor. The Hamiltonian is given by

$$\mathcal{H} = \sum_{\mathbf{k},s} \epsilon_{V,\mathbf{k}} \hat{c}_{V,\mathbf{k},s}^\dagger \hat{c}_{V,\mathbf{k},s} + \sum_{\mathbf{k},s} \epsilon_{C,\mathbf{k}} \hat{c}_{C,\mathbf{k},s}^\dagger \hat{c}_{C,\mathbf{k},s}, \quad (2.5)$$

where $\epsilon_{V,\mathbf{k}}$ and $\epsilon_{C,\mathbf{k}}$ are the band energies of the valence band and conduction band, respectively (Fig. 2.6).

The operator $c_{n\mathbf{k}s}^\dagger$ ($c_{n\mathbf{k}s}$) creates (annihilates) an electron with (pseudo-)momentum \mathbf{k} and spin s in the band n , $n \in \{V, C\}$. In the ground state $|\Phi_0\rangle$,

$$|\Phi_0\rangle = \prod_{\mathbf{k},s} \hat{c}_{V,\mathbf{k},s}^\dagger |0\rangle, \quad (2.6)$$

the valence band is completely filled, whereas the conduction band is empty. The product on the right-hand side runs over all wave vectors in the first Brillouin zone. The ground state energy is given by

$$E_0 = 2 \sum_{\mathbf{k}} \epsilon_{V,\mathbf{k}}. \quad (2.7)$$

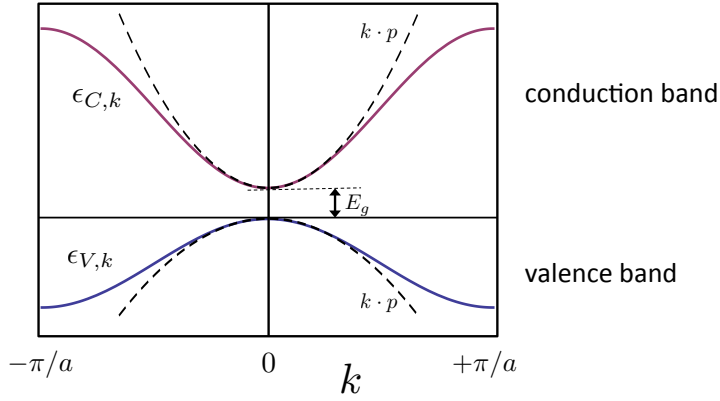


Figure 2.6: Schematic band structure of a direct-gap semiconductor with a $\mathbf{k} \cdot \mathbf{p}$ -approximation around the top of the valence and the bottom of the conduction band.

The total momentum and spin of the ground state vanish. We next consider single electron excitations from that ground state.²

2.2.1 Electron-hole excitations

A simple excitation of the system consists of removing an electron (i.e., creating a hole) from the valence band and inserting it into the conduction band. We write such an excitation as

$$|\mathbf{k} + \mathbf{q}, s; \mathbf{k}, s'\rangle = \hat{c}_{C, \mathbf{k} + \mathbf{q}, s}^\dagger \hat{c}_{V, \mathbf{k}, s'} |\Phi_0\rangle = \hat{\rho}_{\mathbf{k}, \mathbf{q}, s s'} |\Phi_0\rangle, \quad (2.12)$$

where we remove an electron with pseudo-momentum \mathbf{k} and spin s' in the valence band and replace it by an electron with $\mathbf{k} + \mathbf{q}$ and s in the conduction band. The possibility of changing the spin from s' to s and of shifting the wave vector of conduction electrons by \mathbf{q} is included.

²Where is the chemical potential? We assume a simple band structure for a direct-gap semiconductor based on the $\mathbf{k} \cdot \mathbf{p}$ approximation (Fig. 2.6):

$$\epsilon_{V, \mathbf{k}} = -\frac{\hbar^2 \mathbf{k}^2}{2m_V} \quad \text{and} \quad \epsilon_{C, \mathbf{k}} = E_g + \frac{\hbar^2 \mathbf{k}^2}{2m_C} \quad (2.8)$$

Now we calculate the electron distribution. The overall electron density is n :

$$n = \sum_{\mathbf{k} \in \text{BZ}} \sum_s 1 = 2 \int_{\text{BZ}} \frac{d^3 k}{(2\pi)^3} 1. \quad (2.9)$$

The density of electrons in the conduction and valence band for small finite temperature are given by

$$\begin{aligned} n_C &= 2 \int_{\text{BZ}} \frac{d^3 k}{(2\pi)^3} n_F(\epsilon_{C, \mathbf{k}}) = \int_{\text{BZ}} \frac{d^3 k}{4\pi^3} \frac{1}{e^{\beta(\epsilon_{C, \mathbf{k}} - \mu)} + 1} \approx \int_{\text{BZ}} \frac{d^3 k}{4\pi^3} e^{-\beta(\epsilon_{C, \mathbf{k}} - \mu)} = \frac{e^{\beta(\mu - E_g)}}{4\pi^3} (2\pi m_C k_B T)^{3/2}, \\ n - n_V &= \int_{\text{BZ}} \frac{d^3 k}{4\pi^3} (1 - n_F(\epsilon_{V, \mathbf{k}})) = \int_{\text{BZ}} \frac{d^3 k}{4\pi^3} \frac{1}{e^{-\beta(\epsilon_{V, \mathbf{k}} - \mu)} + 1} \approx \int_{\text{BZ}} \frac{d^3 k}{4\pi^3} e^{\beta(\epsilon_{V, \mathbf{k}} - \mu)} = \frac{e^{-\beta\mu}}{4\pi^3} (2\pi m_V k_B T)^{3/2}. \end{aligned} \quad (2.10)$$

Here we assumed that both μ and $E_g - \mu$ are much larger than $k_B T$ ($\beta = 1/k_B T$). Now we see that electron count gives $n_C + n_V = n$ such that we can set the two lines of the above equation equal to obtain for the chemical potential,

$$\mu = \frac{E_g}{2} + \frac{3}{4} k_B T \ln \left(\frac{m_V}{m_C} \right). \quad (2.11)$$

At $T = 0$ the chemical potential is exactly in the center of the band gap and then moves with increasing T , if the effective masses are different. Note also that for small temperatures the thermally activated carriers, electrons and holes, are well described by the classical Maxwell-Boltzmann distribution, as was used in the approximation of the integrals.

Furthermore $|\mathbf{k} + \mathbf{q}, s; \mathbf{k}, s'\rangle$ is assumed to be normalized. The electron-hole pair may either be in a spin-singlet (pure charge excitation $s = s'$) or a spin-triplet state (spin excitation $s \neq s'$). Apart from spin, the state is characterized by the wave vectors \mathbf{k} and \mathbf{q} . The excitation energy can be obtained by

$$E_{\mathbf{k},\mathbf{q},ss'}|\mathbf{k} + \mathbf{q}, s; \mathbf{k}, s'\rangle = [\mathcal{H}, \hat{\rho}_{\mathbf{k},\mathbf{q},ss'}]|\Phi_0\rangle = \mathcal{H}|\mathbf{k} + \mathbf{q}, s; \mathbf{k}, s'\rangle - \underbrace{\hat{\rho}_{\mathbf{k},\mathbf{q},ss'}\mathcal{H}|\Phi_0\rangle}_{E_0|\mathbf{k}+\mathbf{q},s;\mathbf{k},s'\rangle}, \quad (2.13)$$

such that,

$$E_{\mathbf{k},\mathbf{q},ss'} = \epsilon_{C,\mathbf{k}+\mathbf{q}} - \epsilon_{V,\mathbf{k}}. \quad (2.14)$$

The spectrum of the electron-hole excitations with fixed \mathbf{q} is determined by the spectral function

$$I(\mathbf{q}, E) = \sum_{\mathbf{k},s,s'} |\langle \mathbf{k} + \mathbf{q}, s; \mathbf{k}, s' | \hat{c}_{C,\mathbf{k}+\mathbf{q},s}^\dagger \hat{c}_{V,\mathbf{k},s'} |\Phi_0\rangle|^2 \delta(E - (\epsilon_{C,\mathbf{k}+\mathbf{q}} - \epsilon_{V,\mathbf{k}})). \quad (2.15)$$

Excitations exist for all pairs E and \mathbf{q} for which $I(\mathbf{q}, E)$ does not vanish, thus, only above a \mathbf{q} -dependent threshold, which is minimal for $\mathbf{q} = \mathbf{k}_0$, where $\mathbf{k}_0 = 0$ ($\mathbf{k}_0 \neq 0$) for a direct (indirect) energy gap. As \mathbf{k} is arbitrary, there is a continuum of excited states above the threshold for each \mathbf{q} (see Figure 2.7).

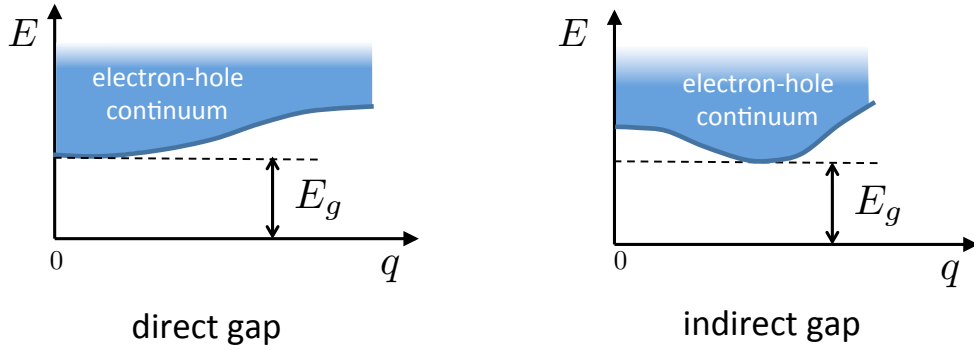


Figure 2.7: Electron-hole excitation spectrum for direct and indirect gap semiconductors, excitation energy E versus "momentum" transfer q . Excitations exist in the shaded region, where $I(q, E) \neq 0$.

For the electron-hole excitations considered here, interactions among them was assumed to be irrelevant, and the electrons involved are treated as non-interacting particles. Note the analogy with the Dirac-sea in relativistic quantum mechanics: The electron-hole excitations of a semiconductor correspond to electron-positron pair creation in the Dirac theory.

2.2.2 Excitons

Taking into account the Coulomb interaction between the electrons, there is another class of excitations called excitons. In order to discuss them, we extend the Hamiltonian (2.5) by the Coulomb interaction,

$$\hat{V} = \sum_{s,s'} \int d^3r d^3r' \hat{\Psi}_s^\dagger(\mathbf{r}) \hat{\Psi}_{s'}^\dagger(\mathbf{r}') \frac{e^2}{|\mathbf{r} - \mathbf{r}'|} \hat{\Psi}_{s'}(\mathbf{r}') \hat{\Psi}_s(\mathbf{r}), \quad (2.16)$$

where the field operators are defined by

$$\widehat{\Psi}_s(\mathbf{r}) = \frac{1}{\sqrt{\Omega}} \sum_{n=V,C} \sum_{\mathbf{k}} u_{n,\mathbf{k}}(\mathbf{r}) e^{i\mathbf{k}\cdot\mathbf{r}} \widehat{c}_{n,\mathbf{k}s}, \quad (2.17)$$

where $u_{n,\mathbf{k}}(\mathbf{r})$ are the Bloch functions of the band $n = C, V$. Now, we consider a general particle-hole state,

$$|\Phi_{\mathbf{q}}\rangle = \sum_{\mathbf{k}} A(\mathbf{k}) \widehat{c}_{C,\mathbf{k}+\mathbf{q},s}^\dagger \widehat{c}_{V,\mathbf{k},s'} |\Phi_0\rangle = \sum_{\mathbf{k}} A(\mathbf{k}) |\mathbf{k} + \mathbf{q}, s; \mathbf{k}, s'\rangle, \quad (2.18)$$

and demand that it satisfies the stationary Schrödinger equation $(\mathcal{H} + \widehat{V})|\Phi_{\mathbf{q}}\rangle = (E_0 + E_{\mathbf{q}})|\Phi_{\mathbf{q}}\rangle$. This two-body problem can be expressed as

$$\sum_{\mathbf{k}'} \langle \mathbf{k} + \mathbf{q}, s; \mathbf{k}, s' | \mathcal{H} + \widehat{V} | \mathbf{k}' + \mathbf{q}, s; \mathbf{k}', s' \rangle A(\mathbf{k}') = (E_0 + E_{\mathbf{q}}) A(\mathbf{k}). \quad (2.19)$$

The matrix elements are given by

$$\langle \mathbf{k} + \mathbf{q}, s; \mathbf{k}, s' | \mathcal{H} | \mathbf{k}' + \mathbf{q}, s; \mathbf{k}', s' \rangle = \delta_{\mathbf{k},\mathbf{k}'} \{ E_0 + \epsilon_{C,\mathbf{k}+\mathbf{q}} - \epsilon_{V,\mathbf{k}} \} \quad (2.20)$$

and

$$\begin{aligned} \langle \mathbf{k} + \mathbf{q}, s; \mathbf{k}, s' | \widehat{V} | \mathbf{k}' + \mathbf{q}, s; \mathbf{k}', s' \rangle = & \\ & \frac{2\delta_{ss'}}{\Omega^2} \int d^3r d^3r' u_{C,\mathbf{k}+\mathbf{q}}^*(\mathbf{r}) u_{V,\mathbf{k}}(\mathbf{r}) u_{C,\mathbf{k}'+\mathbf{q}}(\mathbf{r}') u_{V,\mathbf{k}'}^*(\mathbf{r}') e^{-i\mathbf{q}\cdot(\mathbf{r}-\mathbf{r}')} \frac{e^2}{|\mathbf{r}-\mathbf{r}'|} \\ & - \frac{1}{\Omega^2} \int d^3r d^3r' u_{C,\mathbf{k}+\mathbf{q}}^*(\mathbf{r}) u_{V,\mathbf{k}}(\mathbf{r}') u_{C,\mathbf{k}'+\mathbf{q}}(\mathbf{r}) u_{V,\mathbf{k}'}^*(\mathbf{r}') e^{i(\mathbf{k}'-\mathbf{k})\cdot(\mathbf{r}-\mathbf{r}')} \frac{e^2}{|\mathbf{r}-\mathbf{r}'|}, \end{aligned} \quad (2.21)$$

The first term is the exchange term, and the second term the direct term of the Coulomb interaction. Now we consider a semiconductor with a direct energy gap at the Γ -point. Thus, the most important wave vectors are those around $\mathbf{k} = 0$. We approximate

$$u_{n,\mathbf{k}'}^*(\mathbf{r}) u_{n,\mathbf{k}}(\mathbf{r}) \approx \frac{1}{\Omega} \int d^3r u_{n,\mathbf{k}'}^*(\mathbf{r}) u_{n,\mathbf{k}}(\mathbf{r}) = \frac{1}{\Omega} \langle u_{n,\mathbf{k}'} | u_{n,\mathbf{k}} \rangle \approx 1, \quad (2.22)$$

which is reasonable for $\mathbf{k} \approx \mathbf{k}' (= \mathbf{k} + \mathbf{q})$. In the same manner, we see that

$$u_{C,\mathbf{k}+\mathbf{q}}^*(\mathbf{r}) u_{V,\mathbf{k}}(\mathbf{r}) \approx \frac{1}{\Omega} \langle u_{C,\mathbf{k}+\mathbf{q}} | u_{V,\mathbf{k}} \rangle \approx \frac{1}{\Omega} \langle u_{C,\mathbf{k}} | u_{V,\mathbf{k}} \rangle = 0. \quad (2.23)$$

Note that the semiconductor is a dielectric medium with a dielectric constant ϵ ($\mathbf{D} = \epsilon \mathbf{E}$). Classical electrodynamics states that

$$\nabla \cdot \mathbf{E} = \frac{4\pi\rho}{\epsilon}, \quad (2.24)$$

i.e., the Coulomb potential is partially screened due to dielectric polarization. Including this effect in the Schrödinger equation phenomenologically, the matrix element (2.21) takes on the form

$$\langle \mathbf{k} + \mathbf{q}, s; \mathbf{k}, s' | \widehat{V} | \mathbf{k}' + \mathbf{q}, s; \mathbf{k}', s' \rangle = -\frac{4\pi e^2}{\Omega \epsilon |\mathbf{k} - \mathbf{k}'|^2}. \quad (2.25)$$

Thus, we can write the stationary equation (2.19) as

$$\left(\epsilon_{C,\mathbf{k}+\mathbf{q}} - \epsilon_{V,\mathbf{k}} - E \right) A(\mathbf{k}) - \frac{1}{\Omega} \sum_{\mathbf{k}'} \frac{4\pi e^2}{\epsilon |\mathbf{k} - \mathbf{k}'|^2} A(\mathbf{k}') = 0. \quad (2.26)$$

We include the band structure using the $\mathbf{k} \cdot \mathbf{p}$ -approximation which, for a direct energy gap, leads to

$$\epsilon_{C,\mathbf{k}} = \frac{\hbar^2 \mathbf{k}^2}{2m_C} + E_g \quad \text{and} \quad \epsilon_{V,\mathbf{k}} = -\frac{\hbar^2 \mathbf{k}^2}{2m_V}. \quad (2.27)$$

For simplicity we assume now that $m_V = m_C = m^*$, We define a so-called envelope function $F(\mathbf{r})$ by

$$F(\mathbf{r}) = \frac{1}{\sqrt{\Omega}} \sum_{\mathbf{k}} A(\mathbf{k}) e^{i\mathbf{k} \cdot \mathbf{r}}. \quad (2.28)$$

This function satisfies the differential equation

$$\left[-\frac{\hbar^2 \nabla^2}{2\mu_{\text{ex}}} - \frac{e^2}{\varepsilon|\mathbf{r}|} \right] F(\mathbf{r}) = \left\{ E - E_g - \frac{\hbar^2 \mathbf{q}^2}{2M_{\text{ex}}} \right\} F(\mathbf{r}), \quad (2.29)$$

where μ_{ex} is the reduced mass, i.e., $\mu_{\text{ex}}^{-1} = 2/m^*$ and total mass $M_{\text{ex}} = 2m^*$. The stationary equation (2.29) is equivalent to the Schrödinger equation of a hydrogen atom. The energy levels then are given by

$$E_{\mathbf{q}} = E_g - \frac{\mu_{\text{ex}} e^4}{2\varepsilon^2 \hbar^2 n^2} + \frac{\hbar^2 \mathbf{q}^2}{2M_{\text{ex}}}, \quad (2.30)$$

which implies that there are excitations below the particle-hole continuum, corresponding to particle-hole bound states. This excitation spectrum is discrete and there is a well-defined relation between energy and momentum (\mathbf{q}), which is the wave vector corresponding to the center of mass of the particle-hole pair. This non-trivial quasiparticle is called *exciton*. In the present approximation it takes on the form of a simple two-particle state. In fact, however, it may be viewed as a collective excitation, as the dielectric constant includes the polarization by all electrons. When the screening is neglected, the excitonic states would not make sense as their energies would not be within the band gap but much below. For the case of weak binding considered above, the excitation is called a *Wannier exciton*. The typical binding energy is

$$E_b \sim \frac{\mu_{\text{ex}}}{m\varepsilon^2} Ry. \quad (2.31)$$

Typical values of the constants on the right-hand side are $\varepsilon \sim 10$ and $\mu_{\text{ex}} \sim m/10$, so that the binding energy is in the meV range. This energy is much smaller than the energy gap, such that the excitons are inside the gap, as shown schematically in Figure 2.8.

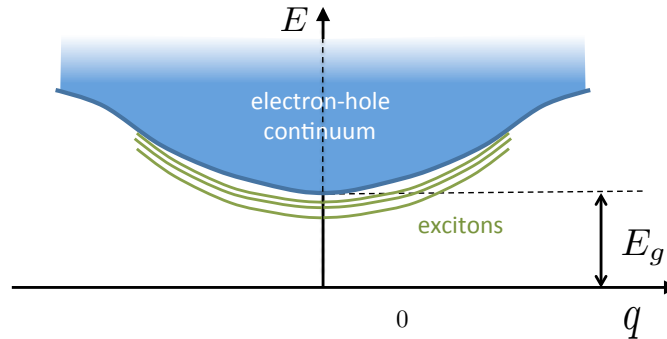


Figure 2.8: Qualitative form of the exciton spectrum below the electron-hole continuum.

The exciton levels are dispersive and their spectrum becomes increasingly dense with increasing energy, similar to the hydrogen atom. When they merge with the particle-hole continuum the

bound state is ‘ionized’, i.e., the electron and the hole dissociate and behave like independent particles.

Strongly bound excitons are called *Frenkel excitons*. In the limit of strong binding, the pair is almost local, so that the excitation is restricted to a single atom rather than involving the whole semiconductor band structure.

Excitons are mobile, but they carry no charge, as they consist of an electron and a hole with opposite charges. Their spin quantum number depends on s and s' . If $s = s'$ the exciton is a spin singlet, while for $s \neq s'$ it has spin triplet character, both corresponding to integer spin quasiparticles. For small densities they approximately obey Bose-Einstein statistics, as they are made from two fermions. In special cases, Bose-Einstein condensation of excitons can be observed experimentally.

2.2.3 Optical properties

Excitation in semiconductors can occur via the absorption of electromagnetic radiation. The energy and momentum transferred by a photon is $\hbar\omega$ and $\hbar\mathbf{q}$, respectively. With the linear light dispersion relation $\omega = c|\mathbf{q}|$ and the approximation $E_g \sim 1\text{eV} \sim e^2/a$, we can estimate this momentum transfer in a semiconductor

$$q = \frac{\omega}{c} = \frac{\hbar\omega}{\hbar c} 2\pi \sim \frac{e^2}{\hbar c} \frac{2\pi}{a} = \alpha \frac{2\pi}{a} \ll \frac{2\pi}{a}, \quad (2.32)$$

where c denotes the speed of light, a the lattice constant, and $\alpha \approx 1/137$ the fine structure constant. With this, the momentum transfer from a photon to the excited electron can be ignored. In other words, pure electromagnetic excitations lead only to ‘direct’ excitations. For semiconductors with a direct energy gap (e.g., GaAs) the photo-induced electron-hole excitation is most easy and yields absorption rates with the characteristics

$$\Gamma_{\text{abs}}(\omega) \propto \begin{cases} (\hbar\omega - E_g)^{1/2}, & \text{dipole-allowed,} \\ (\hbar\omega - E_g)^{3/2}, & \text{dipole-forbidden.} \end{cases} \quad (2.33)$$

Here, the terms ‘dipole-allowed’ and ‘dipole-forbidden’ have a similar meaning as in the excitation of atoms regarding whether matrix elements of the type $\langle u_{V,\mathbf{k}} | \mathbf{r} | u_{C,\mathbf{k}} \rangle$ are finite or vanish, respectively. Obviously, dipole-allowed transitions occur at a higher rate for photon energies immediately above the energy gap E_g , than for dipole-forbidden transitions.

For semiconductors with indirect energy gap (e.g., Si and Ge), the lowest energy transition connecting the top of the valence band to the bottom of the conduction band is not allowed without the help of phonons (lattice vibrations), which contribute little energy but much momentum transfer, as $\hbar\omega_{\mathbf{Q}} \ll \hbar\omega$ with $\omega_{\mathbf{Q}} = c_s|\mathbf{Q}|$ and the sound velocity $c_s \ll c$. The requirement of a phonon assisting in the transition reduces the transition rate to

$$\Gamma_{\text{abs}}(\omega) \propto c_+(\hbar\omega + \hbar\omega_{\mathbf{Q}} - E_g)^2 + c_-(\hbar\omega - \hbar\omega_{\mathbf{Q}} - E_g)^2, \quad (2.34)$$

where c_{\pm} are constants and \mathbf{Q} corresponds to the wave vector of the phonon connecting the top of the valence band and the bottom of the conduction band. There are two relevant processes: either the phonon is absorbed (c_+ -process) or it is emitted (c_- -process) (see Figure 2.9).

In addition to the absorption into the particle-hole spectrum, absorption processes inducing exciton states exist. They lead to discrete absorption peaks below the absorption continuum.

In Figure 2.10, we show the situation for a direct-gap semiconductor.

Naturally, the recombination of electrons and holes is important as well; in particular, if it is a radiative recombination, i.e., leads to the emission of a photon. Additionally, other recombination channels such as recombination at impurities, interfaces and through Auger processes are possible. The radiative recombination for the direct-gap semiconductors is most relevant for applications. The photon emission rate follows the approximate law

$$\Gamma_{\text{em}}(\omega) \propto [N_{\gamma}(\omega) + 1](\hbar\omega - E_g)^{1/2} e^{-\hbar\omega/k_B T}, \quad (2.35)$$

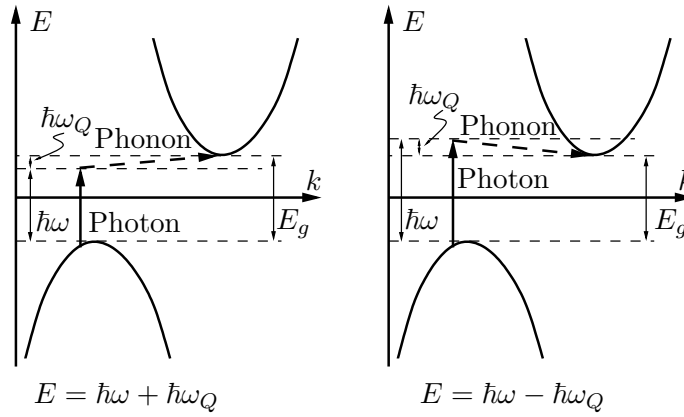


Figure 2.9: Phonon-assisted photon absorption in a semiconductor with indirect gap: phonon absorption (left panel) and phonon emission (right panel).

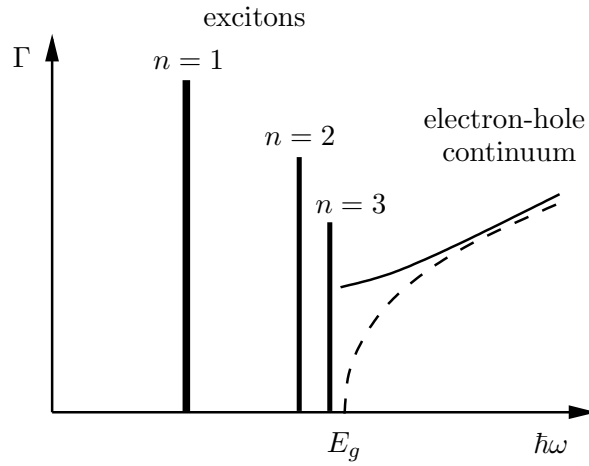


Figure 2.10: Absorption spectrum including the exciton states for a direct-gap semiconductor with dipole-allowed transitions. The exciton states appear as sharp lines below the electron-hole continuum starting at $\hbar\omega = E_g$.

with the photon density $N_\gamma(\omega)$. This yields the dominant rate for $\hbar\omega$ very close to E_g .

2.3 Doping semiconductors

Let us replace a Si atom in a Si semiconductor by aluminum Al (group III) or phosphorus P (group V), which then act as impurities in the crystal lattice. Both Al and P are in the same row of the periodic table, and their electron configurations are given by

$$\begin{aligned} \text{Al} : & \quad [(1s)^2(2s)^2(2p)^6] \underline{(3s)^2(3p)}, \\ \text{P} : & \quad [(1s)^2(2s)^2(2p)^6] \underline{(3s)^2(3p)^3}. \end{aligned}$$

The compound Al (P) has one electron less (more) than Si.

2.3.1 Impurity state

We consider the case of a P-impurity contributing an additional electron whose dynamics is governed by the conduction band of the semiconductor. For the sake of simplicity, we describe

the conduction band by a single isotropic band with effective mass m_C ,

$$\epsilon_{\mathbf{k}} = \frac{\hbar^2 \mathbf{k}^2}{2m_C} + E_g. \quad (2.36)$$

In the neutral Si background, the phosphorus (P) ion represents a positively charged center, which attracts its additional electron. In the simplest model, this situation is described by the so-called Wannier equation

$$\left\{ -\frac{\hbar^2 \nabla^2}{2m_C} - \frac{e^2}{\epsilon |\mathbf{r}'|} \right\} F(\mathbf{r}) = EF(\mathbf{r}), \quad (2.37)$$

which is nothing else than the static Schrödinger equation for the hydrogen atom, where the dielectric constant ϵ measures the screening of the ionic potential by the surrounding electrons. Analogous to the discussion of the exciton states, $F(\mathbf{r})$ is an envelope wave function of the electron. Therefore, the low energy states of the additional electron are bound states around the P ion. The electron may become mobile when this “reduced hydrogen atom” is ionized. The binding energy relative to the minimum of the conduction band given by

$$E_n - E_g = -\frac{m_C e^4}{2\hbar^2 \epsilon^2 n^2} = -\frac{m_C}{m \epsilon^2 n^2} \text{Ry}, \quad (2.38)$$

for $n \in \mathbb{N}$ and the effective radius (corresponding to the renormalized Bohr radius in the material) of the lowest bound state reads

$$r_1 = \frac{\hbar^2 \epsilon}{m^* e^2} = \frac{\epsilon m}{m_C} a_B, \quad (2.39)$$

where $a_B = 0.53 \text{Å}$ is the Bohr radius for the hydrogen atom. For Si we find $m_C \approx 0.2m$ and $\epsilon \approx 12$, such that

$$E_1 \approx -20 \text{meV} \quad (2.40)$$

and

$$r_1 \approx 30 \text{Å}. \quad (2.41)$$

Thus, the resulting states are weakly bound, with energies inside the band gap. We conclude that the net effect of the P-impurities is to introduce additional electrons into the crystal, whose energies lie just below the conduction band ($E_g \sim 1\text{eV}$ while $E_g - E_1 \sim 10\text{meV}$). Therefore, they can easily be transferred to the conduction band by thermal excitation (ionization). One speaks of an *n-doped* semiconductor (n: negative charge). In full analogy one can consider Al-impurities, thereby replacing electrons with holes: An Al-atom introduces an additional hole into the lattice which is weakly bound to the Al-ion (its energy is slightly above the band edge of the valence band) and may dissociate from the impurity by thermal excitation. This case is called *p-doping* (p: positive charge). In both cases, the chemical potential is tied to the dopand levels, i.e., it lies between the dopand level and the valence band for p-doping and between the dopand level and the conduction band in case of n-doping (Figure 2.11).

The electric conductivity of semiconductors (in particular at room temperature) can be tuned strongly by doping with so-called ‘donors’ (n-doping) and ‘acceptors’ (p-doping). Practically all dopand atoms are ionized, with the electrons/holes becoming mobile. Combining differently doped semiconductors, the possibility to engineer electronic properties is enhanced even more. This is the basic reason for the semiconductors being ubiquitous in modern electronics.

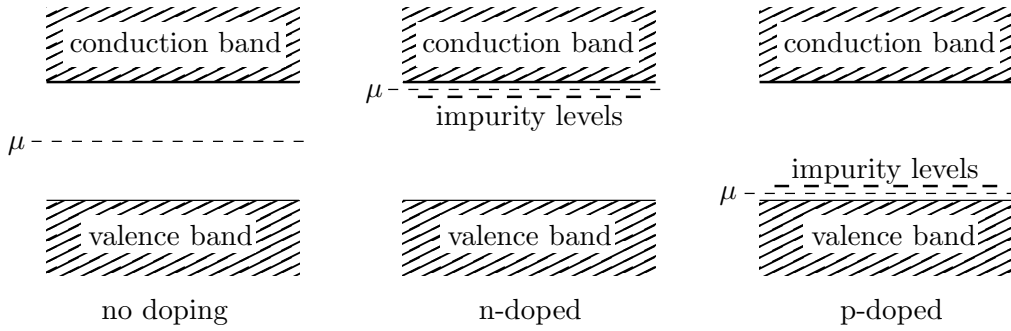


Figure 2.11: Position of the chemical potential in semiconductors.

2.3.2 Carrier concentration

Let us briefly compare the carrier concentration in doped and undoped semiconductors at room temperature. Carriers are always created in form of electron hole pairs, following the “reaction formula”



where γ denotes a photon which is absorbed (e - h -creation) or emitted (e - h -recombination) and accounts for the energy balance. The carrier concentration is described by a mass action law of the form,

$$n_e n_h = n_0^2 \left(\frac{T}{T_0} \right)^3 e^{-E_g/k_B T} = n^2(T), \quad (2.43)$$

where T_0 , n_0 and E_g are parameters specific to the semiconductor. In the case of undoped silicon at $T = 300\text{K}$, $n_e n_h \approx 10^{20} (\text{cm}^{-3})^2$. Thus, for the undoped semiconductor we find $n_e = n_h \approx 10^{10} \text{cm}^{-3}$. On the other hand, for n-doped Si with a typical donor concentration of $n_D \approx 10^{17} \text{cm}^{-3}$ we can assume that most of the donors are ionized at room temperature such that

$$n_e \approx n_D \approx 10^{17} \text{cm}^{-3} \quad (2.44)$$

and

$$n_h = \frac{n^2(T)}{n_e} \approx 10^3 \text{cm}^{-3}. \quad (2.45)$$

We conclude, that in n-doped semiconductors the vast majority of mobile carriers are electrons, while the hole carriers are negligible. The opposite is true for p-doped Si.

2.4 Semiconductor devices

Semiconductors are among the most important components of current high-technology. In this section, we consider a few basic examples of semiconductor devices.

2.4.1 pn-contacts

The so-called pn-junctions, made by bringing in contact a p-doped and an n-doped version of the same semiconductor, are used as rectifiers.³ When contacting the two types of doped

³dt. Gleichrichter

semiconductors the chemical potential, which is pinned by the dopand (impurity) levels, determines the behavior of the electrons at the interface. In electrostatic equilibrium, the chemical potential is constant across the interface. This is accompanied by a “band bending” leading to the ionization of the impurity levels in the interface region (see Figure 2.12). Consequently, these ions produce an electric dipole layer which induces an electrostatic potential shift across the interface. Additionally, the carrier concentration is strongly reduced in the interface region (depletion layer).

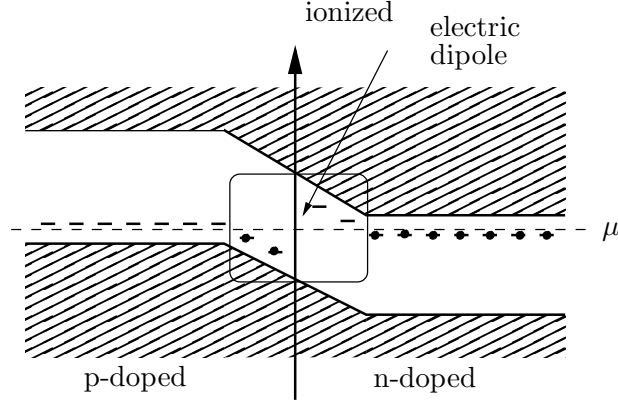


Figure 2.12: Occupation of the impurity levels of a pn-junction.

In the absence of a voltage U over the junction, the net current flow vanishes because the dipole is in electrostatic equilibrium. This can also be interpreted as the equilibrium of two oppositely directed currents, called the drift current J_{drift} and the diffusion current J_{diff} . From the point of view of the electrons, the dipole field exerts a force pulling the electrons from the p-side to the n-side. This leads to the drift current J_{drift} . On the other hand, the electron concentration gradient leads to the diffusion current J_{diff} from the n-side to the p-side. The diffusion current is directed against the potential gradient, so that the diffusing electrons have to overcome a potential step. The equilibrium condition for $U = 0$ is given by

$$0 = J_{\text{tot}}(U = 0) = J_{\text{diff}} + J_{\text{drift}} \propto C_1(T)e^{-E_g/k_B T} - C_2(T)e^{-E_g/k_B T} = 0, \quad (2.46)$$

where $C_1 = C_2 = C$. Both currents are essentially determined by the factor $C(T)e^{-E_g/k_B T}$. For the drift current, the exponential behavior $e^{-E_g/k_B T}$ stems from the dependence of the current on the concentration of mobile charge carriers (electrons and holes on the p-side and n-side, respectively), which are created by thermal excitation (Boltzmann factor). Applying a voltage does not change this contribution significantly. For the diffusion current however, the factor $C(T)e^{-E_g/k_B T}$ describes the thermal activation over the dipole barrier, which in turn strongly depends on the applied voltage U . For zero voltage, the height of the barrier E_b is essentially given by the energy gap $E_b \approx E_g$. With an applied voltage, this is modified according to $E_b \approx E_g - eU$, where $eU = \mu_n - \mu_p$ is the difference of the chemical potentials between the n-side and the p-side. From these considerations, the well-known current-voltage characteristic of the pn-junctions follows directly as

$$J_{\text{tot}}(U) = C(T)e^{-E_g/k_B T} \left(e^{eU/k_B T} - 1 \right). \quad (2.47)$$

For $U > 0$, the current is rapidly enhanced with increasing voltage. This is called forward bias. By contrast, charge transport is suppressed for $U < 0$ (reverse bias), leading to small currents only. The current-voltage characteristics $J(U)$ (see Figure 2.13) shows a clearly asymmetric behavior, which can be used to rectify ac-currents. Rectifiers (or diodes) are an important component of many integrated circuits.

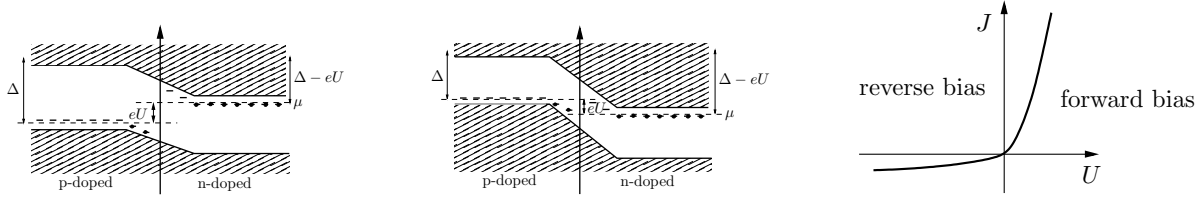


Figure 2.13: The pn-junction with an applied voltage and the resulting J - U characteristics.

2.4.2 Semiconductor diodes

Light emitting diode

As mentioned above, the recombination of electrons and holes can lead to the emission of photons (radiative recombination) with a rather well-defined frequency essentially corresponding to the energy gap E_g . An excess of electron-hole pairs can be produced in pn-diodes by running a current in forward direction. Using different semiconductors with different energy gaps allows to tune the color of the emitted light. Direct-gap semiconductors are most suitable for this kind of devices. Well-known are the semiconductors of the GaAs-GaN series (see table 2.1). These techniques are commonly used in LED (light emitting diode) lamps.

There appear efficiency problems concerning the emission of light by semiconductors. In

| semiconductor | GaAs | GaAs _{0.6} P _{0.4} | GaAs _{0.4} P _{0.6} | GaP | GaN |
|------------------|----------|--------------------------------------|--------------------------------------|-------|-------------|
| wave length (nm) | 940 | 660 | 620 | 550 | 340 |
| color | infrared | red | yellow | green | ultraviolet |

Table 2.1: Materials commonly used for LEDs and their light emitting properties.

particular, the difference in refractive indices inside $n_{\text{SC}} \approx 3$ and outside $n_{\text{air}} \approx 1$ the device leads to large reflective losses. Thus, the efficacy of diode light sources, defined as the number of photons emitted per created particle-hole pair, is small, but still larger than the efficiency of conventional dissipative light bulbs.

Solar cell

Inversely to the previous consideration, the population of charge carriers can be changed by the absorption of light. Suppose that the n-side of a diode is exposed to irradiation by light, which leads to an excess of hole carriers (minority charge carriers). Some of these holes will diffuse towards the pn-interface and will be drawn to the p-side by the dipole field. In this way, they induce an additional current J_L modifying the current-voltage characteristics to

$$J_{\text{tot}} = J_{pn} - J_L = J_s(e^{eU/k_B T} - 1) - J_L. \quad (2.48)$$

It is important for the successful migration of the holes to the interface dipole that they do not recombine too quickly. When $J_{\text{tot}} = 0$, the voltage drop across the diode is

$$U_L = \frac{k_B T}{e} \ln \left(\frac{J_L}{J_s} + 1 \right). \quad (2.49)$$

The maximum efficiency is reached by applying an external voltage $U_c < U_L$ such that the product $J_c U_c$ is maximized, where $J_c = J_{\text{tot}}(U = U_c)$ (cf. Figure 2.14).

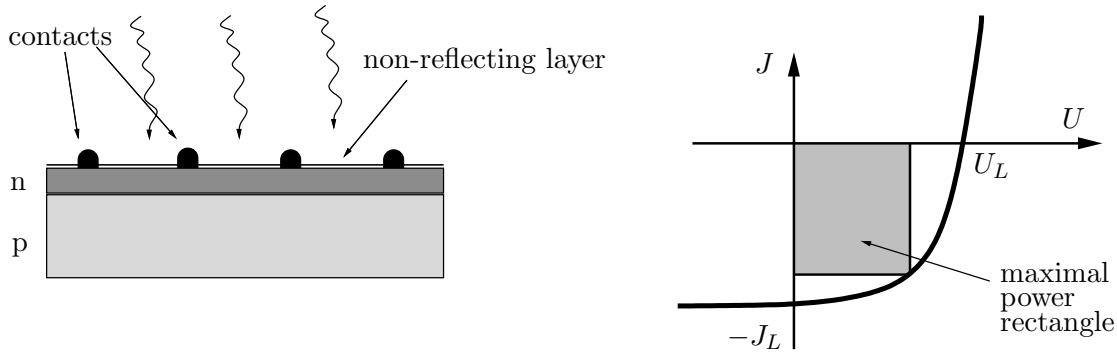


Figure 2.14: Solar cell design and shifted current-voltage characteristics. The efficiency is maximal for a maximal area of the power rectangle.

2.4.3 MOSFET

The arguably most important application of semiconductors is the transistor, an element existing with different architectures. Here we shortly introduce the MOSFET (Metal-Oxide-Semiconductor-Field-Effect-Transistor). A transistor is a switch allowing to control the current through the device by switching a small control voltage. In the MOSFET, this is achieved by changing the charge carrier concentration in a p-doped semiconductor using a metallic gate. The basic design of a MOSFET is as follows (see Figure 2.15): A thin layer of SiO_2 is deposited on the surface of a p-type semiconductor. SiO_2 is a good insulator that is compatible with the lattice structure of Si. Next, a metallic layer, used as a gate electrode, is deposited on top of the insulating layer.

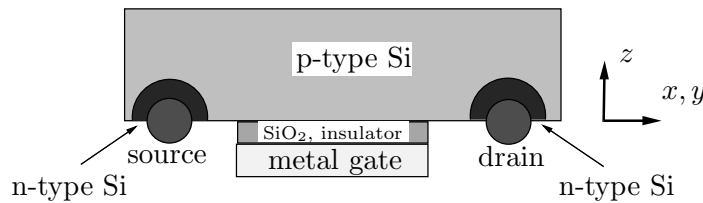


Figure 2.15: Schematic design of a MOSFET device.

The voltage between the Si semiconductor and the metal electrode is called gate voltage U_G . The insulating SiO_2 layer ensures that no currents flow between the electrode and the semiconductor when a gate voltage is applied. The switchable currents in the MOSFET flow between the source and the drain which are heavily n-doped semiconductor regions.

Depending on the applied gate voltage U_G three different regimes can be realized:

1. $U_G = 0$

Virtually no current flows, as the conduction band of the p-doped semiconductor is empty. The doping states (acceptor levels) are occupied by thermal excitations.

2. $0 < \frac{eU_G}{E_g} < 1$

In this case, the energy of the Si bands is lowered, such that in a narrow region within the p-doped Si the acceptor levels drops below the chemical potential and the states are filled with electrons (or, equivalently, holes are removed). This depletion layer has the extension d measured from the Si- SiO_2 interface. The negative charge of the acceptors leads to a position-dependent

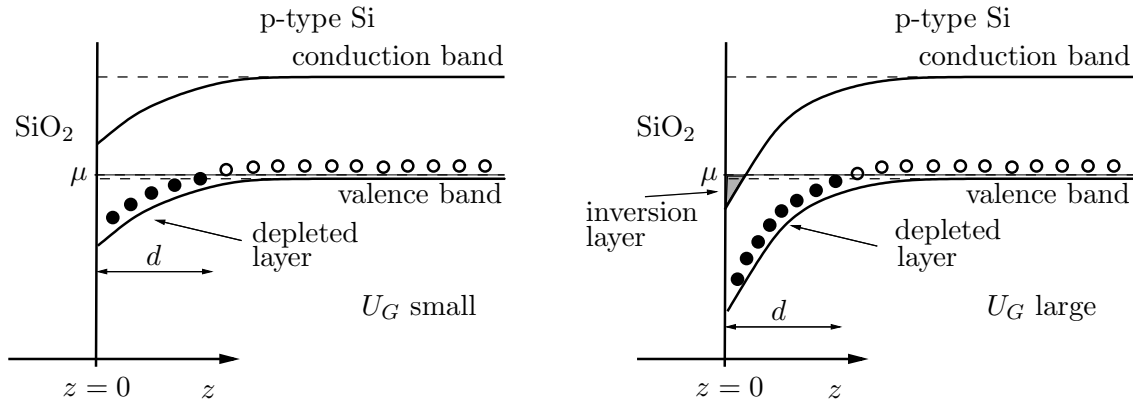


Figure 2.16: Depletion layer at the SiO₂-Si interface for $0 < eU_G < E_g$ (left panel) and the inversion layer $E_g < eU_G$ (right panel).

potential $\Phi(z)$, where z is the distance from the boundary between SiO₂ and Si. This potential $\Phi(z)$ satisfies the simple one-dimensional Poisson equation

$$\frac{d^2}{dz^2}\Phi(z) = \frac{4\pi\rho(z)}{\varepsilon}, \quad (2.50)$$

where the charge density originates in the occupied acceptor levels,

$$\rho(z) = \begin{cases} -en_A, & z < d, \\ 0, & z > d, \end{cases} \quad (2.51)$$

and n_A is the density of acceptors. The boundary conditions are given by

$$\Phi(z=0) = U_G \quad \text{and} \quad \Phi(z=d) = 0. \quad (2.52)$$

The solution for $0 \leq z \leq d$ then reads

$$\Phi(z) = \frac{2\pi en_A}{\varepsilon}(z-d)^2, \quad \text{with} \quad d^2 = \frac{\varepsilon U_G}{2\pi en_A}. \quad (2.53)$$

The thickness of the depletion layer increases with increasing gate voltage $d^2 \propto U_G$.

3. $1 < \frac{eU_G}{E_g}$

When the applied gate voltage is sufficiently large, a so-called inversion layer is created (cf. Figure 2.16). Close to the boundary, the conduction band is bent down so that its lower edge lies below the chemical potential. The electrons accumulating in this inversion layer providing carriers connecting the n-type source and drain electrodes and producing a large, nearly metallic, current between source and drain. Conduction band electrons accumulating in the inversion layer behave like a two-dimensional electron gas. In such a system, the quantum Hall effect (QHE), which is characterized by highly unusual charge transport properties in the presence of a large magnetic field, can occur.

Chapter 3

Metals

The electronic states in a periodic atomic lattice are extended and have an energy spectrum forming energy bands. In the ground state these energy states are filled successively starting at the bottom of the electronic spectrum until the number of electrons is exhausted. Metallic behavior occurs whenever in this way a band is only partially filled. The fundamental difference that distinguishes metals from insulators and semiconductors is the absence of a gap for electron-hole excitations. In metals, the ground state can be excited at arbitrarily small energies which has profound phenomenological consequences.

We will consider a basic model suitable for the description of simple metals like the Alkali metals Li, Na, or K, where the (atomic) electron configuration consists of closed shell cores and one single valence electron in an ns-orbital. Neglecting the core electrons (completely filled bands), we consider the valence electrons only and apply the approximation of nearly free electrons. The lowest band around the Γ -point is then half-filled. First, we will also neglect the influence of the periodic lattice potential and consider the problem of a free electron gas subject to mutual (repulsive) Coulomb interaction.

3.1 The Jellium model of the metallic state

The Jellium¹ model is the probably simplest possible model of a metal that is able to describe qualitative and to some extent even quantitative aspects of simple metals. The main simplification made is to replace the ionic lattice by a homogeneous positively charged background (Jellium). The uniform charge density en_{ion} is chosen such that the whole system – electrons and ionic background – is charge neutral, i.e. $n_{\text{ion}} = n$, where n is the electron density. In this fully translational invariant system, the plane waves

$$\psi_{\mathbf{k},s}(\mathbf{r}) = \frac{1}{\sqrt{\Omega}} e^{i\mathbf{k}\cdot\mathbf{r}} \quad (3.1)$$

represent the single-particle wave functions of the free electrons. Here Ω is the volume of the system, \mathbf{k} and $s \in \{\uparrow, \downarrow\}$ denote the wave vector and spin, respectively. Assuming a cubic system of side length L and volume $\Omega = L^3$ we impose periodic boundary conditions for the wave function

$$\psi_{\mathbf{k},s}(\mathbf{r} + (L, 0, 0)) = \psi_{\mathbf{k},s}(\mathbf{r} + (0, L, 0)) = \psi_{\mathbf{k},s}(\mathbf{r} + (0, 0, L)) = \psi_{\mathbf{k},s}(\mathbf{r}) \quad (3.2)$$

such that the reciprocal space is discretized as

$$\mathbf{k} = \frac{2\pi}{L}(n_x, n_y, n_z) \quad (3.3)$$

¹Jellium originates from the word jelly (gelatin) and was first introduced by Conyers Herring.

where $(n_x, n_y, n_z) \in \mathbb{Z}^3$. The energy of a single-electron state is given by $\epsilon_{\mathbf{k}} = \hbar^2 \mathbf{k}^2 / 2m$ (free particle). The ground state of non-interacting electrons is obtained by filling all single particle states up to the Fermi energy with two electrons. In the language of second quantization the ground state is, thus, given by

$$|\Psi_0\rangle = \prod_{|\mathbf{k}| \leq k_F} \prod_s \hat{c}_{\mathbf{k},s}^\dagger |0\rangle \quad (3.4)$$

where the operators $\hat{c}_{\mathbf{k},s}^\dagger$ ($\hat{c}_{\mathbf{k},s}$) create (annihilate) an electron with wave vector \mathbf{k} and spin s . The Fermi wave vector k_F with the corresponding Fermi energy $\epsilon_F = \hbar^2 k_F^2 / 2m$ is determined by equating the filled electronic states with the electron density n . We have

$$n = \frac{1}{\Omega} \sum_{|\mathbf{k}| \leq k_F, s} 1 = 2 \int \frac{d^3 k}{(2\pi)^3} 1 = 2 \frac{4\pi}{3} \frac{k_F^3}{(2\pi)^3}, \quad (3.5)$$

which results in

$$k_F = (3\pi^2 n)^{1/3}. \quad (3.6)$$

Note k_F is the radius of the Fermi sphere in k -space around $\mathbf{k} = 0$.²

3.1.1 Theory of metals - Sommerfeld and Pauli

In a first step we neglect the interaction among the electrons and consider the electrons in the metal simply as a Fermi gas. Then thermodynamic properties can be described by using the Fermi-Dirac distribution function,

$$f(\epsilon_{\mathbf{k}}) = \frac{1}{e^{(\epsilon_{\mathbf{k}} - \mu)/k_B T} + 1} \quad (3.7)$$

and the density of states

$$\begin{aligned} N(E) &= \sum_{\mathbf{k}, s} \delta(E - \epsilon_{\mathbf{k}}) = 2\Omega \int \frac{d^3 k}{(2\pi)^3} \delta\left(E - \frac{\hbar^2 \mathbf{k}^2}{2m}\right) = \frac{\Omega}{4\pi^3} \int d\Omega_{\mathbf{k}} dk k^2 \frac{m}{\hbar^2 k} \delta\left(k - \frac{\sqrt{2mE}}{\hbar}\right) \\ &= \frac{\Omega}{2\pi^2} \left(\frac{2m}{\hbar^2}\right)^{3/2} E^{1/2} = \frac{3}{2} \frac{N}{\epsilon_F} \left(\frac{E}{\epsilon_F}\right)^{1/2}, \end{aligned} \quad (3.8)$$

for $E > 0$ with $N = n\Omega$ as the total number of electrons. We first address the temperature dependence of the chemical potential up second power in T for fixed electron number N , by using the equation

$$N = \sum_{\mathbf{k}, s} f(\epsilon_{\mathbf{k}}) = \int_0^{+\infty} dE f(E) N(E) = \int_0^{\mu} dE N(E) + \frac{\pi^2}{6} (k_B T)^2 N'(\mu) + \dots, \quad (3.9)$$

where we used the Sommerfeld expansion assuming $T \ll T_F = \epsilon_F / k_B$.³ We now use

$$\int_0^{\mu} dE N(E) \approx \int_0^{\epsilon_F} dE N(E) + (\mu - \epsilon_F) N(\epsilon_F) = N + (\mu - \epsilon_F) N(\epsilon_F) \quad (3.14)$$

²Note that the function $k_F(n) \propto n^{(1/d)}$ depends on the dimensionality d of the system.

³*Sommerfeld expansion*: In the limit $k_B T \ll \epsilon_F$ the derivative $\partial f(E) / \partial E$ is well concentrated around $E = \mu$. We consider

$$\begin{aligned} \int_{-\infty}^{+\infty} dE g(E) \left(-\frac{\partial f(E)}{\partial E}\right) &= \int_{-\infty}^{+\infty} dE \left\{ g(\mu) + (E - \mu)g'(\mu) + \frac{(E - \mu)^2}{2} g''(\mu) + \dots \right\} \left(-\frac{\partial f(E)}{\partial E}\right) \\ &= g(\mu) + \frac{g''(\mu)}{2} \int_{-\infty}^{+\infty} dE (E - \mu)^2 \left(-\frac{\partial f(E)}{\partial E}\right) + \dots = g(\mu) + \frac{\pi^2}{6} g''(\mu) (k_B T)^2 + \dots \end{aligned} \quad (3.10)$$

leading to

$$N \approx N + (\mu - \epsilon_F)N(\epsilon_F) + \frac{\pi^2}{6}(k_B T)^2 N'(\epsilon_F) \quad \Rightarrow \quad \mu(T) = \epsilon_F - \frac{\pi^2}{6}(k_B T)^2 \frac{N'(\epsilon_F)}{N(\epsilon_F)} + \dots \quad (3.15)$$

with $N'(\epsilon_F)/N(\epsilon_F) = 1/2\epsilon_F$. Now we also determine the internal energy

$$\begin{aligned} U(T) &= \int_0^\infty dE EN(E)f(E) \approx \int_0^\mu dE EN(E) + \frac{\pi^2}{6}(k_B T)^2 \{ \mu N'(\mu) + N(\mu) \} \\ &\approx \int_0^{\epsilon_F} dE EN(E) + \underbrace{\epsilon_F \left\{ (\mu - \epsilon_F)N(\epsilon_F) + \frac{\pi^2}{6}(k_B T)^2 N'(\epsilon_F) \right\}}_{=0} + \frac{\pi^2}{6}(k_B T)^2 N(\epsilon_F) \\ &= U_0 + \frac{\pi^2}{6}(k_B T)^2 N(\epsilon_F), \end{aligned} \quad (3.16)$$

where we used Eq.3.15. The specific heat is then given by

$$C = \frac{1}{\Omega} \frac{\partial U}{\partial T} = \frac{\pi^2}{3\Omega} k_B^2 T N(\epsilon_F) = \gamma T \quad (3.17)$$

and shows a T -linear behavior where γ is the Sommerfeld coefficient, proportional to the density of states at the Fermi energy.

Next we consider the effect of a magnetic field coupling to the electron spin, so that $\epsilon_{\mathbf{k}} \rightarrow \epsilon_{\mathbf{k},s} = \epsilon_{\mathbf{k}} - \mu_B s H$ with μ_B the Bohr magneton and $s = \pm 1$. We consider the magnetization due to the spin polarization of the electrons,

$$\begin{aligned} M &= \mu_B (N_+ - N_-) = \frac{\mu_B}{2} \left\{ \int_0^\infty dE N(E) f(E - \mu_B H) - \int_0^\infty dE N(E) f(E + \mu_B H) \right\} \\ &\approx \frac{\mu_B}{2} \int_0^\infty dE N(E) \left(-\frac{\partial f(E)}{\partial E} \right) 2\mu_B H \approx \mu_B^2 H N(\epsilon_F) \int_0^\infty dE \left(-\frac{\partial f(E)}{\partial E} \right) = \mu_B^2 H N(\epsilon_F). \end{aligned} \quad (3.18)$$

By taking the derivative with respect to H we find for the susceptibility,

$$\chi_p = \frac{\partial M}{\partial H} = \mu_B^2 N(\epsilon_F). \quad (3.19)$$

This is the Pauli paramagnetic susceptibility which is to lowest order temperature independent and proportional to the density of states at the Fermi energy, like γ^4 .

and analogous

$$\int_{-\infty}^{+\infty} dE \left(\frac{\partial g(E)}{\partial E} \right) f(E) = g(\mu) + \frac{\pi^2}{6} g''(\mu) (k_B T)^2 + \dots \quad (3.11)$$

With the definition

$$g(E) = \int_{-\infty}^E dE' \Gamma(E') \quad \Rightarrow \quad \int_{-\infty}^{+\infty} dE \Gamma(E) f(E) = \int_{-\infty}^\mu dE \Gamma(E) + \frac{\pi^2}{6} (k_B T)^2 \Gamma'(\mu) + \dots \quad (3.12)$$

Note that

$$\int_{-\infty}^{+\infty} dx \frac{\beta x^2 e^{\beta x}}{(e^{\beta x} + 1)^2} = \frac{\pi^2}{3\beta^2}. \quad (3.13)$$

⁴ *Temperature dependence of the χ_p* : In Eq.(3.18) we go beyond the lowest order approximation using Eq.(3.10),

$$M \approx \mu_B^2 H \int_0^\infty dE N(E) \left(-\frac{\partial f(E)}{\partial E} \right) = \mu_B^2 H \left\{ N(\mu) + \frac{\pi^2}{6} (k_B T)^2 N''(\mu) \right\} \quad (3.20)$$

3.1.2 Stability of metals - a Hartree-Fock approach

Now we would like to examine the stability of the Jellium model. For this purpose, we compute the ground state energy of the Jellium system variationally, using the density n as a variational parameter, which is equivalent to the variation of the lattice constant. In this way, we will obtain an understanding of the stability of a metal, i.e. the cohesion of the ion lattice through the itinerant electrons (in contrast to semiconductors where the stability was due to covalent chemical bonding). The variational ground state shall be $|\Psi_0\rangle$ from Eq.(3.4) for given k_F . The Hamiltonian splits into four terms

$$\mathcal{H} = \mathcal{H}_{\text{kin}} + \mathcal{H}_{ee} + \mathcal{H}_{ei} + \mathcal{H}_{ii} \quad (3.23)$$

with

$$\mathcal{H}_{\text{kin}} = \sum_{\mathbf{k},s} \epsilon_{\mathbf{k}} \hat{c}_{\mathbf{k}s}^\dagger \hat{c}_{\mathbf{k}s} \quad (3.24)$$

$$\mathcal{H}_{ee} = \frac{1}{2} \sum_{s,s'} \int d^3r d^3r' \hat{\Psi}_s^\dagger(\mathbf{r}) \hat{\Psi}_{s'}^\dagger(\mathbf{r}') \frac{e^2}{|\mathbf{r} - \mathbf{r}'|} \hat{\Psi}_{s'}(\mathbf{r}') \hat{\Psi}_s(\mathbf{r}) \quad (3.25)$$

$$\mathcal{H}_{ei} = - \sum_s \int d^3r d^3r' \frac{ne^2}{|\mathbf{r} - \mathbf{r}'|} \hat{\Psi}_s^\dagger(\mathbf{r}) \hat{\Psi}_s(\mathbf{r}) \quad (3.26)$$

$$\mathcal{H}_{ii} = \frac{1}{2} \int d^3r d^3r' \frac{n^2 e^2}{|\mathbf{r} - \mathbf{r}'|}, \quad (3.27)$$

where we have used in second quantization language the electron field operators

$$\hat{\Psi}_s^\dagger(\mathbf{r}) = \frac{1}{\sqrt{\Omega}} \sum_{\mathbf{k}} \hat{c}_{\mathbf{k},s}^\dagger e^{-i\mathbf{k}\cdot\mathbf{r}} \quad (3.28)$$

$$\hat{\Psi}_s(\mathbf{r}) = \frac{1}{\sqrt{\Omega}} \sum_{\mathbf{k}} \hat{c}_{\mathbf{k},s} e^{i\mathbf{k}\cdot\mathbf{r}} \quad (3.29)$$

The variational energy – which we want to minimize with respect to n – can be computed from $E_g = \langle \Psi_0 | \mathcal{H} | \Psi_0 \rangle$ and consists of four different contributions:

First we have the kinetic energy

$$E_{\text{kin}} = \langle \Psi_0 | \mathcal{H}_{\text{kin}} | \Psi_0 \rangle = \sum_{\mathbf{k},s} \epsilon_{\mathbf{k}} \underbrace{\langle \Psi_0 | \hat{c}_{\mathbf{k}s}^\dagger \hat{c}_{\mathbf{k}s} | \Psi_0 \rangle}_{= n_{\mathbf{k}s}} \quad (3.30)$$

$$= 2\Omega \int \frac{d^3k}{(2\pi)^3} \epsilon_{\mathbf{k}} n_{\mathbf{k}s} = N \frac{3}{5} \epsilon_F \quad (3.31)$$

where we used $N = \Omega n$ the number of valence electrons and

$$n_{\mathbf{k}s} = \begin{cases} 1 & |\mathbf{k}| \leq k_F \\ 0 & |\mathbf{k}| > k_F \end{cases}. \quad (3.32)$$

With Eq.(3.15) we write

$$N(\mu) \approx N \left(\epsilon_F - \frac{\pi^2}{6} (k_B T)^2 \frac{N'(\epsilon_F)}{N(\epsilon_F)} \right) \approx N(\epsilon_F) - \frac{\pi^2}{6} (k_B T)^2 \frac{N'(\epsilon_F)^2}{N(\epsilon_F)}, \quad (3.21)$$

which leads to

$$M \approx \mu_B^2 H N(\epsilon_F) \left[1 - \frac{\pi^2}{6} (k_B T)^2 \left\{ \left(\frac{N'(\epsilon_F)}{N(\epsilon_F)} \right)^2 - \frac{N''(\epsilon_F)}{N(\epsilon_F)} \right\} \right] = \chi_p(T) H, \quad (3.22)$$

and defines the temperature dependent spin susceptibility, which depends on details of the density of states.

Secondly, there is the energy resulting from the Coulomb repulsion between the electrons,

$$E_{ee} = \frac{1}{2} \int d^3r d^3r' \frac{e^2}{|\mathbf{r} - \mathbf{r}'|} \sum_{s,s'} \langle \Psi_0 | \widehat{\Psi}_s^\dagger(\mathbf{r}) \widehat{\Psi}_{s'}^\dagger(\mathbf{r}') \widehat{\Psi}_{s'}(\mathbf{r}') \widehat{\Psi}_s(\mathbf{r}) | \Psi_0 \rangle \quad (3.33)$$

$$= \frac{1}{2} \int d^3r d^3r' \frac{e^2}{|\mathbf{r} - \mathbf{r}'|} (n^2 - G(\mathbf{r} - \mathbf{r}')) = E_{\text{Hartree}} + E_{\text{Fock}}. \quad (3.34)$$

For this contribution we used the fact, that the two-particle correlation function from equation (3.33) may be expressed⁵ as

$$\sum_{s,s'} \langle \Psi_0 | \widehat{\Psi}_s^\dagger(\mathbf{r}) \widehat{\Psi}_{s'}^\dagger(\mathbf{r}') \widehat{\Psi}_{s'}(\mathbf{r}') \widehat{\Psi}_s(\mathbf{r}) | \Psi_0 \rangle = n^2 - G(\mathbf{r} - \mathbf{r}') \quad (3.42)$$

where

$$G(\mathbf{r}) = \frac{9n^2}{2} \left(\frac{k_F |\mathbf{r}| \cos k_F |\mathbf{r}| - \sin k_F |\mathbf{r}|}{(k_F |\mathbf{r}|)^3} \right)^2. \quad (3.43)$$

The Coulomb repulsion \mathcal{H}_{ee} between the electrons leads to two terms, called the *direct* or Hartree term describing the Coulomb energy of a uniformly spread charge distribution, and the *exchange* or Fock term resulting from the exchange hole that follows from the Fermi-Dirac statistics (Pauli exclusion principle).

The third contribution originates in the attractive interaction between the (uniform) ionic background and the electrons,

$$E_{ei} = - \int d^3r d^3r' \frac{e^2}{|\mathbf{r} - \mathbf{r}'|} n \sum_s \langle \Psi_0 | \widehat{\Psi}_s^\dagger(\mathbf{r}) \widehat{\Psi}_s(\mathbf{r}') | \Psi_0 \rangle \quad (3.44)$$

$$= - \int d^3r d^3r' \frac{e^2}{|\mathbf{r} - \mathbf{r}'|} n^2. \quad (3.45)$$

⁵We shortly sketch the derivation of the pair correlation function. Using equations (3.28) and (3.29) we find

$$\langle \Psi_0 | \widehat{\Psi}_s^\dagger(\mathbf{r}) \widehat{\Psi}_{s'}^\dagger(\mathbf{r}') \widehat{\Psi}_{s'}(\mathbf{r}') \widehat{\Psi}_s(\mathbf{r}) | \Psi_0 \rangle = \frac{1}{\Omega^2} \sum_{\mathbf{k}, \mathbf{k}', \mathbf{q}, \mathbf{q}'} e^{-i(\mathbf{k}-\mathbf{k}') \cdot \mathbf{r}} e^{-i(\mathbf{q}-\mathbf{q}') \cdot \mathbf{r}'} \langle \Phi_0 | \widehat{c}_{\mathbf{k}s}^\dagger \widehat{c}_{\mathbf{q}s'}^\dagger \widehat{c}_{\mathbf{q}'s'} \widehat{c}_{\mathbf{k}'s} | \Phi_0 \rangle. \quad (3.35)$$

We distinguish two cases:

First, consider $s \neq s'$,

$$\langle \Phi_0 | \widehat{c}_{\mathbf{k}s}^\dagger \widehat{c}_{\mathbf{q}s'}^\dagger \widehat{c}_{\mathbf{q}'s'} \widehat{c}_{\mathbf{k}'s} | \Phi_0 \rangle = \delta_{\mathbf{k}\mathbf{k}'} \delta_{\mathbf{q}\mathbf{q}'} n_{\mathbf{k}s} n_{\mathbf{q}s'} \quad (3.36)$$

leading to

$$\langle \Psi_0 | \widehat{\Psi}_s^\dagger(\mathbf{r}) \widehat{\Psi}_{s'}^\dagger(\mathbf{r}') \widehat{\Psi}_{s'}(\mathbf{r}') \widehat{\Psi}_s(\mathbf{r}) | \Psi_0 \rangle = \frac{1}{\Omega^2} \sum_{\mathbf{k}, \mathbf{q}} n_{\mathbf{k}s} n_{\mathbf{q},s'} = \frac{n^2}{4}. \quad (3.37)$$

Secondly, assume $s = s'$ such that

$$\langle \Phi_0 | \widehat{c}_{\mathbf{k}s}^\dagger \widehat{c}_{\mathbf{q}s}^\dagger \widehat{c}_{\mathbf{q}'s} \widehat{c}_{\mathbf{k}'s} | \Phi_0 \rangle = (\delta_{\mathbf{k}\mathbf{k}'} \delta_{\mathbf{q}\mathbf{q}'} - \delta_{\mathbf{k}\mathbf{q}'} \delta_{\mathbf{q}\mathbf{k}'}) n_{\mathbf{k}s} n_{\mathbf{q}s}, \quad (3.38)$$

which in turn leads to

$$\langle \Psi_0 | \widehat{\Psi}_s^\dagger(\mathbf{r}) \widehat{\Psi}_s^\dagger(\mathbf{r}') \widehat{\Psi}_s(\mathbf{r}') \widehat{\Psi}_s(\mathbf{r}) | \Psi_0 \rangle = \frac{1}{\Omega^2} \sum_{\mathbf{k}, \mathbf{q}} \left(1 - e^{i(\mathbf{q}-\mathbf{k}) \cdot (\mathbf{r}-\mathbf{r}')} \right) n_{\mathbf{k}s} n_{\mathbf{q},s}. \quad (3.39)$$

Both cases eventually lead to the result in equation (3.42) with

$$G(\mathbf{r}) = 2 \left(\frac{1}{\Omega} \sum_{\mathbf{k}} e^{i\mathbf{k} \cdot \mathbf{r}} n_{\mathbf{k}s} \right)^2 = 2 \left(\int_{|\mathbf{k}| \leq k_F} \frac{d^3k}{(2\pi)^3} e^{i\mathbf{k} \cdot \mathbf{r}} \right)^2 \quad (3.40)$$

$$= 2 \left(\frac{1}{2\pi^2 r} \int_0^{k_F} dk k \sin kr \right)^2 = 2 \left(\frac{1}{2\pi^2} \frac{\sin k_F r - k_F r \cos k_F r}{r^3} \right)^2 \quad (3.41)$$

and $n = k_F^3/3\pi^2$ ($k = |\mathbf{k}|$ and $r = |\mathbf{r}|$).

Were the expectation value $\langle \Psi_0 | \hat{\Psi}_s^\dagger(\mathbf{r}) \Psi_s(\mathbf{r}) | \Psi_0 \rangle$ corresponds to the uniform density n , as is easily calculated from the definitions (3.28) and (3.29).

Finally we have the repulsive ion-ion interaction

$$E_{ii} = \langle \Psi_0 | \mathcal{H}_{ii} | \Psi_0 \rangle = \frac{1}{2} \int d^3r d^3r' \frac{n^2 e^2}{|\mathbf{r} - \mathbf{r}'|}. \quad (3.46)$$

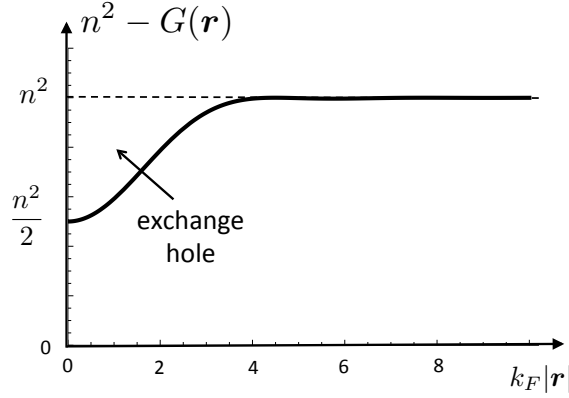


Figure 3.1: Pair correlation function $n^2 - G(\mathbf{r} - \mathbf{r}') = \langle \Psi_0 | \hat{\Psi}_s^\dagger(\mathbf{r}) \hat{\Psi}_{s'}^\dagger(\mathbf{r}') \hat{\Psi}_{s'}(\mathbf{r}') \hat{\Psi}_s(\mathbf{r}) | \Psi_0 \rangle$.

It is easy to verify that the three contributions E_{Hartree} , E_{ei} , and E_{ii} compensate each other to exactly zero. Note that these three terms are the only ones that would arise in a classical electrostatic calculation, implying that the stability of metals relies purely on quantum effect. The remaining terms are the kinetic energy and the Fock term. The latter is negative and reads

$$E_{\text{Fock}} = -\Omega \frac{9n^2}{4} \int d^3r \frac{e^2}{|\mathbf{r}|} \left(\frac{\sin k_F |\mathbf{r}| - k_F |\mathbf{r}| \cos k_F |\mathbf{r}|}{(k_F |\mathbf{r}|)^3} \right)^2 = -N \frac{3e^2}{4\pi} k_F. \quad (3.47)$$

Eventually, the total energy per electron is given by

$$\frac{E_g}{N} = \frac{3}{5} \frac{\hbar^2 k_F^2}{2m} - \frac{3e^2}{4\pi} k_F = \left(\frac{2.21}{r_s^2} - \frac{0.916}{r_s} \right) \text{Ry} \quad (3.48)$$

where $1\text{Ry} = e^2/2a_B$ and the dimensionless quantity r_s is defined via

$$n = \frac{3}{4\pi d^3} \quad (3.49)$$

and

$$r_s = \frac{d}{a_B} = \left(\frac{9\pi}{4} \right)^{1/3} \frac{me^2}{\hbar^2 k_F}. \quad (3.50)$$

The length d is the average radius of the volume occupied by one electron. Minimizing the energy per electron with respect to n is equivalent to minimize it with respect to r_s , yielding $r_{s,\text{min}} = 4.83$, $d \approx 2.5\text{\AA}$ (see Fig.3.2) and a density of $n_0 \approx 1.5 \times 10^{24} \text{ cm}^{-3}$. This corresponds to a lattice constant of $a = (4\pi/3)^{1/3} d \approx 4\text{\AA}$. This estimate is roughly in agreement with the lattice constants of the Alkali metals: $r_{s,\text{Li}} = 3.22$, $r_{s,\text{Na}} = 3.96$, $r_{s,\text{K}} = 4.86$. Note that in metals the delocalized electrons are responsible for the cohesion of the positive background yielding a stable solid.

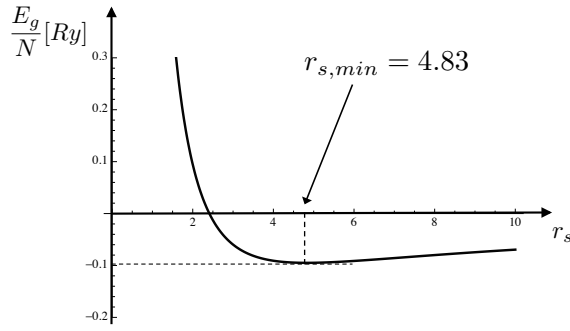


Figure 3.2: Total ground state Hartree-Fock energy as a function of r_s . A minimum exists at $r_{s,min} = 4.83$.

The good agreement of this simple estimate with the experimental values is due to the fact that the Alkali metals have only one valence electron in an s-orbital that is delocalized, whereas the the core electrons are in a noble gas configuration and, thus, relatively inert. In the variational approach outlined above correlation effects among the electrons due to the Coulomb repulsion have been neglected. In particular, electrons can be expected to 'avoid' each other not just because of the Pauli principle, but also as a result of the repulsive interaction. However, for the problem under consideration the correlation corrections turn out to be small for $r_s \sim r_{s,min}$:

$$\frac{E_{\text{tot}}}{N} = \left(\frac{2.21}{r_s^2} - \frac{0.916}{r_s} + 0.062 \ln r_s - 0.096 + \dots \right) \text{Ry} \quad (3.51)$$

which can be obtained from a more sophisticated quantum field theoretical analysis.

3.2 Charge excitations and the dielectric function

In analogy to semiconductors, the elementary excitations of metallic systems are the electron-hole excitations, which for metals, however, can have arbitrarily small energies. One particularly drastic consequence of this behavior is the strong screening of the long-ranged Coulomb potential. As we will see, a negative test charge in a metal reduces the electron density in its vicinity, and the induced cloud of positive charges, relative to the uniform charge density, weaken the Coulomb potential as,

$$V(r) \propto \frac{1}{r} \quad \longrightarrow \quad V'(r) \propto \frac{e^{-r/l}}{r} \quad (3.52)$$

i.e. the Coulomb potential is modified into the short-ranged Yukawa potential with screening length l . In contrast to metals, the finite energy gap for electron-hole excitations the charge distribution in semiconductors reduces the adaption of the system to perturbations, so that the screened Coulomb potential remains long-ranged,

$$V(r) \propto \frac{1}{r} \quad \longrightarrow \quad V'(r) \propto \frac{1}{\epsilon r}. \quad (3.53)$$

As mentioned earlier, the semiconductor acts as a dielectric medium and its screening effects are accounted for by the polarization of localized electric dipoles, i.e., the Coulomb potential inside a semiconductor is renormalized by the dielectric constant ϵ .

3.2.1 Dielectric response and Lindhard function

We will now investigate the response of an electron gas to a time- and position-dependent weak external potential $V_a(\mathbf{r}, t)$ in more detail based on the equation of motion. We introduce the Hamiltonian

$$\mathcal{H} = \mathcal{H}_{\text{kin}} + \mathcal{H}_V = \sum_{\mathbf{k}, s} \epsilon_{\mathbf{k}} \hat{c}_{\mathbf{k}s}^\dagger \hat{c}_{\mathbf{k}s} + \sum_s \int d^3r V_a(\mathbf{r}, t) \hat{\Psi}_s^\dagger(\mathbf{r}) \hat{\Psi}_s(\mathbf{r}) \quad (3.54)$$

where the second term is considered as a small perturbation. In a first step we consider the linear response of the system to the external potential. On this level we restrict ourself to one Fourier component in the spatial and time dependence of the potential,

$$V_a(\mathbf{r}, t) = V_a(\mathbf{q}, \omega) e^{i\mathbf{q}\cdot\mathbf{r} - i\omega t} e^{\eta t}, \quad (3.55)$$

where $\eta \rightarrow 0_+$ includes the adiabatic switching on of the potential. To linear response this potential induces a small modulation of the electron density of the form $n_{\text{ind}}(\mathbf{r}, t) = n_0 + \delta n_{\text{ind}}(\mathbf{r}, t)$ with

$$\delta n_{\text{ind}}(\mathbf{r}, t) = \delta n_{\text{ind}}(\mathbf{q}, \omega) e^{i\mathbf{q}\cdot\mathbf{r} - i\omega t}. \quad (3.56)$$

Using equations (3.28) and (3.29) we obtain for the density operator in momentum space,

$$\hat{\rho}_{\mathbf{q}} = \sum_s \int d^3r \hat{\Psi}_s^\dagger(\mathbf{r}) \hat{\Psi}_s(\mathbf{r}) e^{-i\mathbf{q}\cdot\mathbf{r}} = \frac{1}{\Omega} \sum_{\mathbf{k}, s} \hat{c}_{\mathbf{k}s}^\dagger \hat{c}_{\mathbf{k}+\mathbf{q}s} = \frac{1}{\Omega} \sum_{\mathbf{k}, s} \hat{\rho}_{\mathbf{k}, \mathbf{q}, s}, \quad (3.57)$$

where we define $\hat{\rho}_{\mathbf{k}, \mathbf{q}, s} = \hat{c}_{\mathbf{k}s}^\dagger \hat{c}_{\mathbf{k}+\mathbf{q}s}$. The perturbation term \mathcal{H}_V now reads

$$\mathcal{H}_V = \sum_s \int d^3r V_a(\mathbf{r}, t) \hat{\Psi}_s^\dagger(\mathbf{r}) \hat{\Psi}_s(\mathbf{r}) = \hat{\rho}_{\mathbf{q}}^\dagger V_a(\mathbf{q}, \omega) e^{-i\omega t} e^{\eta t} = \frac{1}{\Omega} \sum_{\mathbf{k}, s} \hat{\rho}_{\mathbf{k}, \mathbf{q}, s}^\dagger V_a(\mathbf{q}, \omega) e^{-i\omega t} e^{\eta t}. \quad (3.58)$$

The density operator $\hat{\rho}_{\mathbf{q}}(t)$ in Heisenberg representation is the relevant quantity needed to describe the electron density in the metal.

Linear response

We introduce the equation of motion for $\hat{\rho}_{\mathbf{k}, \mathbf{q}, s}(t)$:

$$i\hbar \frac{d}{dt} \hat{\rho}_{\mathbf{k}, \mathbf{q}, s} = [\hat{\rho}_{\mathbf{k}, \mathbf{q}, s}, \mathcal{H}] = [\hat{\rho}_{\mathbf{k}, \mathbf{q}, s}, \mathcal{H}_{\text{kin}} + \mathcal{H}_V] \quad (3.59)$$

$$= (\epsilon_{\mathbf{k}+\mathbf{q}} - \epsilon_{\mathbf{k}}) \hat{\rho}_{\mathbf{k}, \mathbf{q}, s} + (\hat{c}_{\mathbf{k}s}^\dagger \hat{c}_{\mathbf{k}s} - \hat{c}_{\mathbf{k}+\mathbf{q}s}^\dagger \hat{c}_{\mathbf{k}+\mathbf{q}s}) V_a(\mathbf{q}, \omega) e^{-i\omega t} e^{\eta t}. \quad (3.60)$$

We now take the thermal average $\langle \hat{A} \rangle = \text{Tr}[\hat{A} e^{-\beta \mathcal{H}}] / \text{Tr}[e^{-\beta \mathcal{H}}]$ and follow the linear response scheme by assuming the same time dependence for $\langle \hat{\rho}_{\mathbf{k}, \mathbf{q}, s}(t) \rangle \propto e^{-i\omega t + \eta t}$ as for the potential, so that the equation of motion reads,

$$(\hbar\omega + i\hbar\eta) \langle \hat{\rho}_{\mathbf{k}, \mathbf{q}, s} \rangle = (\epsilon_{\mathbf{k}+\mathbf{q}} - \epsilon_{\mathbf{k}}) \langle \hat{\rho}_{\mathbf{k}, \mathbf{q}, s} \rangle + (n_{0\mathbf{k}, s} - n_{0\mathbf{k}+\mathbf{q}, s}) V_a(\mathbf{q}, \omega) \quad (3.61)$$

where $n_{0\mathbf{k}, s} = \langle \hat{c}_{\mathbf{k}s}^\dagger \hat{c}_{\mathbf{k}s} \rangle$ and, therefore,

$$\delta n_{\text{ind}}(\mathbf{q}, \omega) = \frac{1}{\Omega} \sum_{\mathbf{k}, s} \langle \hat{\rho}_{\mathbf{k}, \mathbf{q}, s} \rangle = \frac{1}{\Omega} \sum_{\mathbf{k}, s} \frac{n_{0\mathbf{k}+\mathbf{q}, s} - n_{0\mathbf{k}, s}}{\epsilon_{\mathbf{k}+\mathbf{q}} - \epsilon_{\mathbf{k}} - \hbar\omega - i\hbar\eta} V_a(\mathbf{q}, \omega). \quad (3.62)$$

With this, we define the dynamical linear response function as

$$\chi_0(\mathbf{q}, \omega) = \frac{1}{\Omega} \sum_{\mathbf{k}, s} \frac{n_{0\mathbf{k}+\mathbf{q}, s} - n_{0\mathbf{k}, s}}{\epsilon_{\mathbf{k}+\mathbf{q}} - \epsilon_{\mathbf{k}} - \hbar\omega - i\hbar\eta} \quad (3.63)$$

such that $\delta n_{\text{ind}}(\mathbf{q}, \omega) = \chi_0(\mathbf{q}, \omega) V_a(\mathbf{q}, \omega)$, where $\chi_0(\mathbf{q}, \omega)$ is known to be the Lindhard function.

Coulomb interaction - Random phase approximation

So far we treated the linear response of the system to an external perturbation without considering "feedback effects" due to the interaction among electrons. In fact, the density fluctuation $\delta n(\mathbf{r}, t)$ can be thought as a source for an additional Coulomb potential $V_{\delta n}$ which can be determined by means of the Poisson equation,

$$\nabla^2 V_{\delta n}(\mathbf{r}, t) = -4\pi e^2 \delta n(\mathbf{r}, t) \quad (3.64)$$

or in Fourier space

$$V_{\delta n}(\mathbf{q}, \omega) = \frac{4\pi e^2}{q^2} \delta n(\mathbf{q}, \omega). \quad (3.65)$$

If we allow feedback effects in our system with external perturbation $V_a(\mathbf{q}, \omega)$, the effective potential V felt by the electrons is determined self-consistently via

$$V(\mathbf{q}, \omega) = V_a(\mathbf{q}, \omega) + V_{\delta n}(\mathbf{q}, \omega) \quad (3.66)$$

$$= V_a(\mathbf{q}, \omega) + \frac{4\pi e^2}{q^2} \delta n(\mathbf{q}, \omega), \quad (3.67)$$

where

$$\delta n(\mathbf{q}, \omega) = \chi_0(\mathbf{q}, \omega) V(\mathbf{q}, \omega). \quad (3.68)$$

The relation between V and V_a may then be written as

$$V(\mathbf{q}, \omega) = \frac{V_a(\mathbf{q}, \omega)}{\varepsilon(\mathbf{q}, \omega)} \quad (3.69)$$

with

$$\varepsilon(\mathbf{q}, \omega) = 1 - \frac{4\pi e^2}{q^2} \chi_0(\mathbf{q}, \omega), \quad (3.70)$$

where $\varepsilon(\mathbf{q}, \omega)$ is termed the dynamical dielectric function and describes the renormalization of the external potential due to the dynamical response of the electrons in the metal. Extending Eq.(3.68) to

$$\delta n(\mathbf{q}, \omega) = \chi_0(\mathbf{q}, \omega) V(\mathbf{q}, \omega) = \chi(\mathbf{q}, \omega) V_a(\mathbf{q}, \omega). \quad (3.71)$$

we define the response function $\chi(\mathbf{q}, \omega)$ within "random phase approximation"⁶ to be

$$\chi(\mathbf{q}, \omega) = \frac{\chi_0(\mathbf{q}, \omega)}{\varepsilon(\mathbf{q}, \omega)} = \frac{\chi_0(\mathbf{q}, \omega)}{1 - \frac{4\pi e^2}{q^2} \chi_0(\mathbf{q}, \omega)}. \quad (3.73)$$

This response function $\chi(\mathbf{q}, \omega)$ contains also effects of electron-electron interaction and comprises information not only about the renormalization of potentials, but also on the excitation spectrum of the metal.

⁶The equation (3.73) can be written in the form of a geometric series,

$$\chi(\mathbf{q}, \omega) = \chi_0(\mathbf{q}, \omega) \left[1 + \frac{4\pi e^2}{q^2} \chi_0(\mathbf{q}, \omega) + \left(\frac{4\pi e^2}{q^2} \chi_0(\mathbf{q}, \omega) \right)^2 + \dots \right]. \quad (3.72)$$

From the point of view of perturbation theory, this series corresponds to summing a limited subset of perturbative terms to infinite order. This approximation is called Random Phase Approximation (RPA) and is based on the assumption the phase relation between different particle-hole excitations entering the perturbation series are random such that interference terms vanish on the average. This approximation is used quite frequently, in particular, in the discussion of instabilities of a system towards an ordered phase.

3.2.2 Electron-hole excitation

For simple particle-hole excitations in metals, neglecting Coulomb interaction between the electrons, it is sufficient to study the bare response function $\chi_0(\mathbf{q}, \omega)$. We may separate χ_0 into its real and imaginary part, $\chi_0(\mathbf{q}, \omega) = \chi_{01}(\mathbf{q}, \omega) + i\chi_{02}(\mathbf{q}, \omega)$. Using the relation

$$\lim_{\eta \rightarrow 0^+} \frac{1}{z - i\eta} = \mathcal{P} \left(\frac{1}{z} \right) + i\pi\delta(z) \quad (3.74)$$

where the Cauchy principal value \mathcal{P} of the first term has to be taken, we separate the Lindhard function (3.63) into

$$\chi_{01}(\mathbf{q}, \omega) = \frac{1}{\Omega} \sum_{\mathbf{k}, s} \mathcal{P} \left(\frac{n_{0, \mathbf{k}+\mathbf{q}} - n_{0, \mathbf{k}}}{\epsilon_{\mathbf{k}+\mathbf{q}} - \epsilon_{\mathbf{k}} - \hbar\omega} \right) \quad (3.75)$$

$$\chi_{02}(\mathbf{q}, \omega) = \frac{\pi}{\Omega} \sum_{\mathbf{k}, s} (n_{0, \mathbf{k}+\mathbf{q}} - n_{0, \mathbf{k}}) \delta(\epsilon_{\mathbf{k}+\mathbf{q}} - \epsilon_{\mathbf{k}} - \hbar\omega) \quad (3.76)$$

The real part will be important later in the context of instabilities of metals. The excitation spectrum is visible in the imaginary part which relates to the absorption of energy by the electrons subject to a time-dependent external perturbation.⁷ Note that $\chi_{02}(\mathbf{q}, \omega)$ corresponds to Fermi's golden rule known from time-dependent perturbation theory, i.e. the transition rate from the ground state to an excited state of energy $\hbar\omega$ and momentum \mathbf{q} .

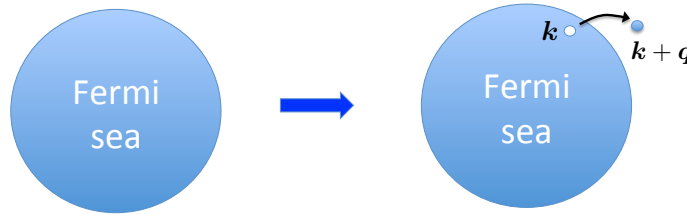


Figure 3.3: Electron-hole excitation: hole with momentum \mathbf{k} and electron with momentum $\mathbf{k} + \mathbf{q}$.

The relevant excitations originating from the Lindhard function are particle-hole excitations. Starting from the ground state of a completely filled Fermi sea, one electron with momentum \mathbf{k} is removed and inserted again outside the Fermi sea in some state with momentum $\mathbf{k} + \mathbf{q}$ (see Figure 3.3). The energy difference is then given by

$$E_{\mathbf{k}, \mathbf{q}} = \epsilon_{\mathbf{k}+\mathbf{q}} - \epsilon_{\mathbf{k}} > 0. \quad (3.77)$$

In analogy to the semiconducting case, there is a continuum of particle-hole excitation spectrum in the energy-momentum plane – sketched in Figure 3.4. Note the absence of an energy gap for excitations.

3.2.3 Collective excitation

For the electron-hole excitations the Coulomb interaction was ignored (by using $\chi_0(\mathbf{q}, \omega)$ instead of $\chi(\mathbf{q}, \omega)$), such that the bare Lindhard function provides information about the single particle

⁷See Chapter 6 “Linear response theory” of the course “Statistical Physics” FS09.

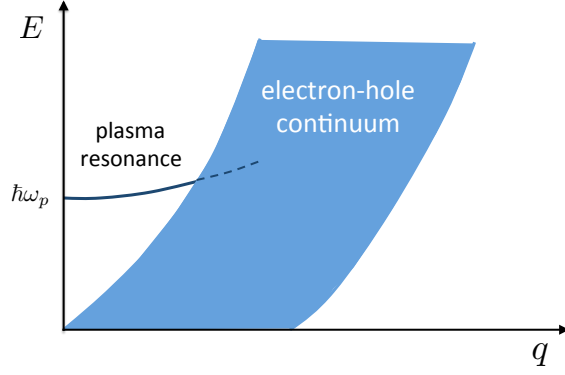


Figure 3.4: Excitation spectrum in the E - q -plane. The large shaded region corresponds to the electron-hole continuum and the sharp line outside the continuum represents the plasma resonance which is damped when entering the continuum.

spectrum. Including the Coulomb interaction a new collective excitation will arise, the so-called plasma resonance. For a long-ranged interaction like the Coulomb interaction this resonance appears at finite frequency for small momenta \mathbf{q} . We derive it here using the response function $\chi(\mathbf{q}, \omega)$. Assuming $|\mathbf{q}| \ll k_F$ we expand $\chi_0(\mathbf{q}, \omega)$ in \mathbf{q} , starting with

$$\epsilon_{\mathbf{k}+\mathbf{q}} = \epsilon_{\mathbf{k}} + \mathbf{q} \cdot \nabla_{\mathbf{k}} \epsilon_{\mathbf{k}} + \dots \quad (3.78)$$

$$n_{0,\mathbf{k}+\mathbf{q}} = n_{0,\mathbf{k}} + \frac{\partial n_0}{\partial \epsilon} \mathbf{q} \cdot \nabla_{\mathbf{k}} \epsilon_{\mathbf{k}} + \dots \quad (3.79)$$

Note that $\partial n_0 / \partial \epsilon_{\mathbf{k}} = -\delta(\epsilon_{\mathbf{k}} - \epsilon_F)$ at $T = 0$ and $\nabla_{\mathbf{k}} \epsilon_{\mathbf{k}} = \hbar \mathbf{v}_{\mathbf{k}}$ is the velocity. Since we will deal with states located at the Fermi energy here, $\mathbf{v}_{\mathbf{k}} = v_F \mathbf{k} / |\mathbf{k}|$ is the Fermi velocity. This leads to the approximation

$$\begin{aligned} \chi_0(\mathbf{q}, \omega) &\approx -2 \int \frac{d^3 k}{(2\pi)^3} \frac{\mathbf{q} \cdot \mathbf{v}_F \delta(\epsilon_{\mathbf{k}} - \mu)}{\mathbf{q} \cdot \mathbf{v}_F - \omega - i\eta} \\ &= \frac{2}{(2\pi)^2} \int_{-1}^{+1} d \cos \theta \frac{k_F^2}{\hbar v_F} \left[\frac{q v_F \cos \theta}{\omega + i\eta} + \left(\frac{q v_F \cos \theta}{\omega + i\eta} \right)^2 + \left(\frac{q v_F \cos \theta}{\omega + i\eta} \right)^3 + \dots \right] \end{aligned} \quad (3.80)$$

$$\approx \frac{k_F^3 q^2}{3\pi^2 m (\omega + i\eta)^2} \left(1 + \frac{3}{5} \frac{v_F^2 q^2}{(\omega + i\eta)^2} \right) \quad (3.81)$$

$$= \frac{n_0 q^2}{m (\omega + i\eta)^2} \left(1 + \frac{3}{5} \frac{v_F^2 q^2}{(\omega + i\eta)^2} \right). \quad (3.82)$$

According to equation (3.70), we find

$$\lim_{|\mathbf{q}| \rightarrow 0} \varepsilon(\mathbf{q}, \omega) = 1 - \frac{\omega_p^2}{\omega^2} \quad (3.83)$$

for the dielectric function in the long wavelength limit ($|\mathbf{q}| \rightarrow 0$), with

$$\omega_p^2 = \frac{4\pi e^2 n_0}{m}. \quad (3.84)$$

We now use the result in Eq.(3.82) to approximate $\chi(\mathbf{q}, \omega)$,

$$\chi(\mathbf{q}, \omega) \approx \frac{n_0 q^2 R(q, \omega)^2}{m (\omega + i\eta)^2 - 4\pi e^2 n_0^2 R(q, \omega)^2} \quad (3.85)$$

$$= \frac{n_0 q^2 R(q, \omega)}{2m\omega_p} \left\{ \frac{1}{\omega + i\eta - \omega_p R(q, \omega)} - \frac{1}{\omega + i\eta + \omega_p R(q, \omega)} \right\} \quad (3.86)$$

where we introduced

$$R(q, \omega)^2 = \left(1 + \frac{3v_F^2 q^2}{5\omega^2}\right). \quad (3.87)$$

Applying the relation (3.74) in Eq.(3.82) we obtain

$$\text{Im}[\chi(\mathbf{q}, \omega)] \approx \frac{\pi n_0 q^2 R(q, \omega_p)}{\omega_p} \left[\delta(\omega - \omega_p R(q, \omega_p)) - \delta(\omega + \omega_p R(q, \omega_p)) \right] \quad (3.88)$$

which yields a sharp excitation mode,

$$\omega(\mathbf{q}) = \omega_p R(q, \omega_p) = \omega_p \left\{ 1 + \frac{3v_F^2 q^2}{10\omega_p^2} + \dots \right\}, \quad (3.89)$$

which is called *plasma resonance* with ω_p as the *plasma frequency*. Similar to the exciton, the plasma excitation has a well-defined energy-momentum relation and may consequently be viewed as a quasiparticle (*plasmon*) which has bosonic character. When the plasmon dispersion merges with the electron-hole continuum it is damped (Landau damping) because of the allowed decay into electron-hole excitations. This results in a finite life-time of the plasmons within the electron-hole continuum corresponding to a finite width of the resonance of the collective excitation.

| metal | $\omega_p^{(\text{exp})}$ [eV] | $\omega_p^{(\text{theo})}$ [eV] |
|-------|--------------------------------|---------------------------------|
| Li | 7.1 | 8.5 |
| Na | 5.7 | 6.2 |
| K | 3.7 | 4.6 |
| Mg | 10.6 | - |
| Al | 15.3 | - |

Table 3.1: Experimental values of the plasma frequency for different compounds. For the alkali metals a theoretically determined ω_p is given for comparison, using equation (3.84) with m the free electron mass and n determined through $r_{s,\text{Li}} = 3.22$, $r_{s,\text{Na}} = 3.96$ and $r_{s,\text{K}} = 4.86$.

It is possible to understand the plasma excitation in a classical picture. Consider negatively charged electrons in a positively charged ionic background. When the electrons are shifted uniformly by \mathbf{r} with respect to the ions, a polarization $\mathbf{P} = -n_0 e \mathbf{r}$ results. The polarization causes an electric field $\mathbf{E} = -4\pi \mathbf{P}$ which acts as a restoring force. The equation of motion for an individual electron describes harmonic oscillations

$$m \frac{d^2}{dt^2} \mathbf{r} = -e \mathbf{E} = -4\pi e^2 n_0 \mathbf{r}. \quad (3.90)$$

with the same oscillation frequency as in Eq.(3.84), the plasma frequency,

$$\omega_p^2 = \frac{4\pi e^2 n_0}{m}. \quad (3.91)$$

Classically, the plasma resonance can therefore be thought as an oscillation of the whole electron gas cloud on top of a positively charged background.

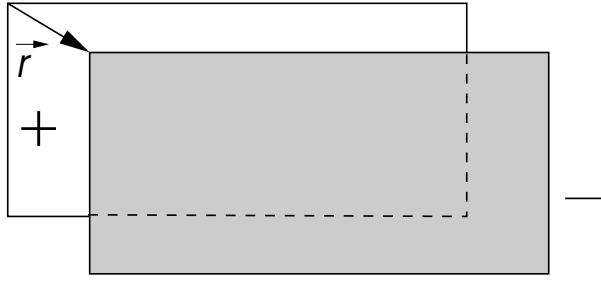


Figure 3.5: Classical understanding of the plasma excitation.

3.2.4 Screening

Thomas-Fermi screening

Next, we analyze the potential V felt by the electrons exposed to a static field ($\omega \rightarrow 0$). Using the expansion (3.79) we obtain

$$\chi_0(\mathbf{q}, 0) = -\frac{1}{\Omega} \sum_{\mathbf{k}, s} \delta(\epsilon_{\mathbf{k}} - \epsilon_F) = -\frac{1}{\pi^2} \frac{k_F^2}{\hbar v_F} = -\frac{3n_0}{2\epsilon_F} \quad (3.92)$$

and thus

$$\epsilon(\mathbf{q}, 0) = 1 + \frac{k_{TF}^2}{q^2} \quad (3.93)$$

with the so-called Thomas-Fermi wave vector $k_{TF}^2 = 6\pi e^2 n_0 / \epsilon_F$. The effect of the renormalized \mathbf{q} -dependence of the dielectric function can best be understood by considering a bare point charge $V_a(\mathbf{r}) = e^2/r$ (or $V_a(\mathbf{q}) = 4\pi e^2/q^2$) and its renormalization in momentum space

$$V(\mathbf{q}) = \frac{V_a(\mathbf{q})}{\epsilon(\mathbf{q}, 0)} = \frac{4\pi e^2}{q^2 + k_{TF}^2} \quad (3.94)$$

or in real space

$$V(\mathbf{r}) = \frac{e^2}{r} e^{-k_{TF} r}. \quad (3.95)$$

The potential is screened by a rearrangement of the electrons and this turns the long-ranged Coulomb potential into a Yukawa potential with exponential decay. The new length scale is k_{TF}^{-1} , the so-called Thomas-Fermi screening length. In ordinary metals k_{TF} is typically of the same order of magnitude as k_F , i.e. the screening length is of order 5\AA comparable to the distance between neighboring atoms.⁸ As a consequence also external electric fields cannot penetrate a metal, but are screened on this length $1/k_{TF}$. This legitimates one of the basic assumptions used in electrostatics with metals.

⁸The Thomas-Fermi approach for electron gas is sketched in the following. The Thomas-Fermi theory for the charge distributions slowly varying in space is based on the approximation that locally the electrons form a Fermi gas with Fermi energy ϵ_F and electron density $n_e(\epsilon_F)$ neutralizing the ionic background. The electrostatic potential $\Phi(\mathbf{r})$ of an external charge distribution $\rho_{\text{ex}}(\mathbf{r})$ induces a charge redistribution $\rho_{\text{ind}}(\mathbf{r})$ relative to $n_e(\epsilon_F)$. Within Thomas-Fermi approximation the induced charge distribution can then be written as

$$\rho_{\text{ind}}(\mathbf{r}) = -e[n_e(\epsilon_F + e\Phi(\vec{r})) - n_e(\epsilon_F)] \quad (3.96)$$

with

$$n_e(\epsilon_F) = \frac{k_F^3}{3\pi^2} = \frac{1}{3\pi^2 \hbar^2} (2m\epsilon_F)^{3/2} \quad (3.97)$$

where $\epsilon_F = \hbar^2 k_F^2 / 2m$. This approach is justified, if the spacial change of the potential $\Phi(\mathbf{r})$ is slow compared to k_F^{-1} , so that locally we may describe the electron gas as a filled Fermi sphere of corresponding electron density.

Friedel oscillations

The static dielectric function can be evaluated exactly for a system of free electrons, resulting for 3 dimensions in

$$\varepsilon(\mathbf{q}, 0) = 1 + \frac{4e^2 m k_F}{\pi q^2} \left\{ \frac{1}{2} + \frac{4k_F^2 - q^2}{8k_F q} \ln \left| \frac{2k_F + q}{2k_F - q} \right| \right\}. \quad (3.102)$$

Noticeably the dielectric function varies little for small $\mathbf{q} \ll k_F$. At $q = \pm 2k_F$ there is, however, a logarithmic singularity. This is a consequence of the sharpness of the Fermi surface in k -space. Consider the induced charge of a point charge at the origin: $en_a(r) = en_{a0}\delta(\mathbf{r})$ which is Fourier transformed is $n_a(\mathbf{q}) = n_{a0}$.⁹

$$\delta n(\mathbf{r}) = \int \frac{d^3q}{(2\pi)^3} \left\{ \frac{1}{\varepsilon(q)} - 1 \right\} n_a(\mathbf{q}) e^{i\mathbf{q}\cdot\mathbf{r}} = -\frac{1}{r} \int_0^\infty g(q) n_a(\mathbf{q}) \sin qr \, dq \quad (3.104)$$

with

$$g(q) = \frac{q}{2\pi^2} \frac{\varepsilon(q) - 1}{\varepsilon(q)}. \quad (3.105)$$

Note that $g(q)$ vanishes for both $q \rightarrow 0$ and $q \rightarrow \infty$. Using partial integration twice, we find

$$\delta n(\mathbf{r}) = \frac{n_{a0}}{r^3} \int_0^\infty g''(q) \sin qr \, dq \quad (3.106)$$

where

$$g'(q) \approx A \ln|q - 2k_F| \quad (3.107)$$

and

$$g''(q) \approx \frac{A}{q - 2k_F} \quad (3.108)$$

The Poisson equation may now be formulated as

$$\nabla^2 \Phi(\mathbf{r}) = -4\pi[\rho_{\text{ind}}(\mathbf{r}) + \rho_{\text{ex}}(\mathbf{r})] \approx 4\pi \left[e^2 \Phi(\mathbf{r}) \frac{\partial n_e(\epsilon)}{\partial \epsilon} \Big|_{\epsilon=\epsilon_F} - \rho_{\text{ex}}(\mathbf{r}) \right] \quad (3.98)$$

$$= k_{TF}^2 \Phi(\mathbf{r}) - 4\pi \rho_{\text{ex}}(\mathbf{r}) \quad (3.99)$$

with the Thomas-Fermi momentum k_{TF} defined as,

$$k_{TF}^2 = 4\pi e^2 \frac{\partial n_e(\epsilon)}{\partial \epsilon} \Big|_{\epsilon=\epsilon_F} = \frac{6\pi e^2 n_e}{\epsilon_F}. \quad (3.100)$$

and $n_e = n_e(\epsilon_F)$. For a point charge Q located at the origin we obtain,

$$\Phi(\mathbf{r}) = Q \frac{e^{-rk_{TF}}}{r}. \quad (3.101)$$

This is the Yukawa potential as obtained above.

⁹The charge distribution can be deduced from the Poisson equation (3.65):

$$e\delta n(\mathbf{q}) = \frac{q^2}{4\pi e^2} V_{\delta n}(\mathbf{q}) = \chi_0(\mathbf{q}, 0) V(\mathbf{q}) = \chi_0(\mathbf{q}, 0) \frac{V_a(\mathbf{q})}{\varepsilon(\mathbf{q}, 0)} = \frac{1 - \varepsilon(\mathbf{q}, 0)}{\varepsilon(\mathbf{q}, 0)} n_a(\mathbf{q}, 0) \quad (3.103)$$

The charge distribution in real space can be obtained by Fourier transformation.

dominate around $q \sim 2k_F$. Hence, for $k_F r \gg 1$,

$$\delta n(r) \approx \frac{An_{a0}}{r^3} \int_{2k_F-\Lambda}^{2k_F+\Lambda} \frac{\sin[(q-2k_F)r] \cos 2k_F r + \cos[(q-2k_F)r] \sin 2k_F r}{q-2k_F} dq \quad (3.109)$$

$$\rightarrow \pi An_{a0} \frac{\cos 2k_F r}{r^3}. \quad (3.110)$$

with a cutoff $\Lambda \rightarrow \infty$. The induced charge distribution exhibits so-called *Friedel oscillations*. Finally we may ask what is the total electron charge displaced around the point charge $en_{a0}\delta(\mathbf{r})$. We take Eq.(charge-displace) and integrate over \mathbf{r} .

$$\delta Q = e\delta n = e \int d^3r \delta n(\mathbf{r}) = \lim_{\mathbf{q} \rightarrow 0} \left\{ \frac{1}{\epsilon(\mathbf{q})} - 1 \right\} n_a(\mathbf{q}) = -en_{a0} \quad (3.111)$$

where we used $1/\epsilon(\mathbf{q}) \rightarrow 0$ for $\mathbf{q} \rightarrow 0$. The charge displacement corresponds to the exact opposite amount of charge of the point charge. Thus we find a perfect compensation which corresponds to perfect screening.

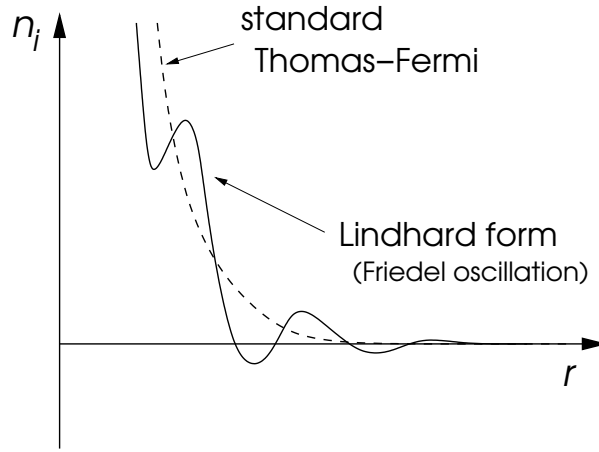


Figure 3.6: Friedel oscillations of the charge distribution.

Dielectric function in various dimensions

Above we have treated the dielectric function for a three-dimensional parabolic band. Similar calculations can be performed for one- and two-dimensional systems. In general, the static susceptibility is given by

$$\chi_0(q, \omega = 0) = \begin{cases} -\frac{1}{2\pi q} \ln \left| \frac{s+2}{s-2} \right|, & 1\text{D} \\ -\frac{1}{2\pi} \left\{ 1 - \left(1 - \frac{4}{s^2} \right)^{1/2} \theta(s-2) \right\}, & 2\text{D} \\ -\frac{k_F}{2\pi^2} \left\{ 1 - \frac{s}{4} \left(1 - \frac{4}{s^2} \right) \ln \left| \frac{s+2}{s-2} \right| \right\}, & 3\text{D} \end{cases} \quad (3.112)$$

where $s = q/k_F$. Interestingly $\chi_0(q, 0)$ has a singularity at $q = 2k_F$ in all dimensions. The singularity becomes weaker as the dimensionality is increased. In one dimension, there is a logarithmic divergence, in two dimensions there is a kink, and in three dimensions only the derivative diverges. Later we will see that these singularities may lead to instabilities of the metallic state, in particular for the one-dimensional case.

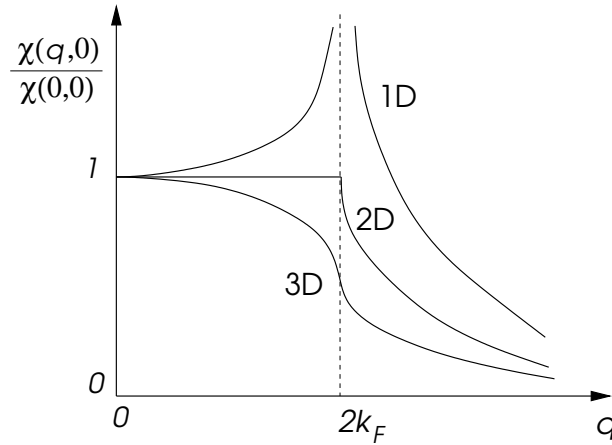


Figure 3.7: Lindhard functions for different dimensions. The lower the dimension the stronger the singularity at $q = 2k_F$.

3.3 Lattice vibrations - Phonons

The atoms in a lattice of a solid are not immobile but vibrate around their equilibrium positions. We will describe this new degree of freedom by treating the lattice as a continuous elastic medium (Jellium with elastic modulus λ). This approximation is sufficient to obtain some essential features of the interaction between lattice vibrations and electrons. In particular, renormalized screening effects will be found. Our approach here is, however, limited to mono-atomic unit cells because the internal structure of a unit cell is neglected.

3.3.1 Vibration of an isotropic continuous medium

The deformation of an elastic medium can be described by the displacement of the infinitesimal volume element d^3r around a point \mathbf{r} to a different point $\mathbf{r}'(\mathbf{r})$. We can introduce here the so-called *displacement field* $\mathbf{u}(\mathbf{r}) = \mathbf{r}'(\mathbf{r}) - \mathbf{r}$ as function of \mathbf{r} . In general, \mathbf{u} is also a function of time. In the simplest form of an isotropic medium the elastic energy for small deformations is given by

$$E_{\text{el}} = \frac{\lambda}{2} \int d^3r (\nabla \cdot \mathbf{u}(\mathbf{r}, t))^2 \quad (3.113)$$

where λ is the elastic modulus (note that there is no deformation energy, if the medium is just shifted uniformly). This energy term produces a restoring force trying to bring the system back to the undeformed state. In this model we are neglecting the shear contributions.¹⁰ The continuum form above is valid for deformation wavelengths that are much longer than the lattice constant, so that details of the arrangement of atoms in the lattice can be neglected. The kinetic energy of the motion of the medium is given by

$$E_{\text{kin}} = \frac{\rho_0}{2} \int d^3r \left(\frac{\partial \mathbf{u}(\mathbf{r}, t)}{\partial t} \right)^2 \quad (3.115)$$

¹⁰Note that the most general form of the elastic energy of an isotropic medium takes the form

$$E_{\text{el}} = \int d^3r \sum_{\alpha, \beta=x, y, z} \left[\frac{\lambda}{2} (\partial_\alpha u_\alpha) (\partial_\beta u_\beta) + \mu (\partial_\alpha u_\beta) (\partial_\alpha u_\beta) \right], \quad (3.114)$$

where $\partial_\alpha = \partial/\partial r_\alpha$. The *Lamé coefficients* λ and μ characterize the elastic properties. The elastic constant λ describes density modulations leading to longitudinal elastic waves, whereas μ corresponds to shear deformations connected with transversely polarized elastic waves. Note that transverse elastic waves are not important for the coupling of electrons and lattice vibrations.

where $\rho_0 = M_i n_i$ is the mass density with the ionic mass M_i and the ionic density n_i . Variation of the Lagrangian functional $L[\mathbf{u}] = E_{\text{kin}} - E_{\text{el}}$ with respect to $\mathbf{u}(\mathbf{r}, t)$ leads to the equation of motion

$$\frac{1}{c_s^2} \frac{\partial^2}{\partial t^2} \mathbf{u}(\mathbf{r}, t) - \nabla(\nabla \cdot \mathbf{u}(\mathbf{r}, t)) = 0, \quad (3.116)$$

which is a wave equation with sound velocity $c_s^2 = \lambda/\rho_0$. The resulting displacement field can be expanded into normal modes,

$$\mathbf{u}(\mathbf{r}, t) = \frac{1}{\sqrt{\Omega}} \sum_{\mathbf{k}} \mathbf{e}_{\mathbf{k}} \left(q_{\mathbf{k}}(t) e^{i\mathbf{k} \cdot \mathbf{r}} + q_{\mathbf{k}}^*(t) e^{-i\mathbf{k} \cdot \mathbf{r}} \right) \quad (3.117)$$

where every $q_{\mathbf{k}}(t)$ satisfies the equation

$$\frac{d^2}{dt^2} q_{\mathbf{k}} + \omega_{\mathbf{k}}^2 q_{\mathbf{k}} = 0, \quad (3.118)$$

with the frequency $\omega_{\mathbf{k}} = c_s |\mathbf{k}| = c_s k$ and the polarization vector $\mathbf{e}_{\mathbf{k}}$ has unit length. Note that within our simplification for the elastic energy (3.114), all modes correspond to longitudinal waves, i.e. $\nabla \times \mathbf{u}(\mathbf{r}, t) = 0$ and $\mathbf{e}_{\mathbf{k}} \parallel \mathbf{k}$. The total energy expressed in terms of the normal modes reads

$$E = \sum_{\mathbf{k}} \rho_0 \omega_{\mathbf{k}}^2 [q_{\mathbf{k}}(t) q_{\mathbf{k}}^*(t) + q_{\mathbf{k}}^*(t) q_{\mathbf{k}}(t)]. \quad (3.119)$$

Next, we switch from a Lagrangian to a Hamiltonian description by defining the new variables

$$Q_{\mathbf{k}} = \sqrt{\rho_0} (q_{\mathbf{k}} + q_{\mathbf{k}}^*) \quad (3.120)$$

$$P_{\mathbf{k}} = \frac{d}{dt} Q_{\mathbf{k}} = -i\omega_{\mathbf{k}} \sqrt{\rho_0} (q_{\mathbf{k}} - q_{\mathbf{k}}^*) \quad (3.121)$$

in terms of which the energy is given by

$$E = \frac{1}{2} \sum_{\mathbf{k}} (P_{\mathbf{k}}^2 + \omega_{\mathbf{k}}^2 Q_{\mathbf{k}}^2). \quad (3.122)$$

Thus, the system is equivalent to an ensemble of independent harmonic oscillators, one for each normal mode \mathbf{k} . Consequently, the system may be quantized by defining the canonical conjugate operators $P_{\mathbf{k}} \rightarrow \hat{P}_{\mathbf{k}}$ and $Q_{\mathbf{k}} \rightarrow \hat{Q}_{\mathbf{k}}$ which obey, by definition, the commutation relation,

$$[\hat{Q}_{\mathbf{k}}, \hat{P}_{\mathbf{k}'}] = i\hbar \delta_{\mathbf{k}, \mathbf{k}'}. \quad (3.123)$$

As it is usually done for quantum harmonic oscillators, we define the raising and lowering operators

$$\hat{b}_{\mathbf{k}} = \frac{1}{\sqrt{2\hbar\omega_{\mathbf{k}}}} \left(\omega_{\mathbf{k}} \hat{Q}_{\mathbf{k}} + i\hat{P}_{\mathbf{k}} \right) \quad (3.124)$$

$$\hat{b}_{\mathbf{k}}^\dagger = \frac{1}{\sqrt{2\hbar\omega_{\mathbf{k}}}} \left(\omega_{\mathbf{k}} \hat{Q}_{\mathbf{k}} - i\hat{P}_{\mathbf{k}} \right), \quad (3.125)$$

satisfying the commutation relations

$$[\hat{b}_{\mathbf{k}}, \hat{b}_{\mathbf{k}'}^\dagger] = \delta_{\mathbf{k}, \mathbf{k}'}, \quad (3.126)$$

$$[\hat{b}_{\mathbf{k}}, \hat{b}_{\mathbf{k}'}] = 0, \quad (3.127)$$

$$[\hat{b}_{\mathbf{k}}^\dagger, \hat{b}_{\mathbf{k}'}^\dagger] = 0. \quad (3.128)$$

These relations can be interpreted in a way that these operators create and annihilate quasi-particles following the Bose-Einstein statistics. According to the correspondence principle, the quantum mechanical Hamiltonian corresponding to the energy (3.122) is

$$\mathcal{H} = \sum_{\mathbf{k}} \hbar\omega_{\mathbf{k}} \left(\widehat{b}_{\mathbf{k}}^\dagger \widehat{b}_{\mathbf{k}} + \frac{1}{2} \right). \quad (3.129)$$

In analogy to the treatment of the electrons in second quantization we say that the operators $\widehat{b}_{\mathbf{k}}^\dagger$ ($\widehat{b}_{\mathbf{k}}$) create (annihilate) a *phonon*, a quasiparticle with well-defined energy-momentum relation, $\omega_{\mathbf{k}} = c_s |\mathbf{k}|$. Using Eqs.(3.118, 3.121, and 3.125) the displacement field operator $\widehat{\mathbf{u}}(\mathbf{r})$ can now be defined as

$$\widehat{\mathbf{u}}(\mathbf{r}) = \frac{1}{\sqrt{\Omega}} \sum_{\mathbf{k}} \mathbf{e}_{\mathbf{k}} \sqrt{\frac{\hbar}{2\rho_0\omega_{\mathbf{k}}}} \left[\widehat{b}_{\mathbf{k}} e^{i\mathbf{k}\cdot\mathbf{r}} + \widehat{b}_{\mathbf{k}}^\dagger e^{-i\mathbf{k}\cdot\mathbf{r}} \right]. \quad (3.130)$$

As mentioned above, the continuum approximation is valid for long wavelengths (small \mathbf{k}) only. For wavevectors with $\mathbf{k} \approx \pi/a$ the discreteness of the lattice appears in the form of corrections to the linear dispersion $\omega_{\mathbf{k}} \propto |\mathbf{k}|$. Since the number of degrees of freedom is limited to $3N_i$ (N_i number of atoms), there is a maximal wave vector called the Debye wavevector¹¹ k_D . We can now define the corresponding Debye frequency $\omega_D = c_s k_D$ and the Debye temperature $\Theta_D = \hbar\omega_D/k_B$. In the continuous medium approximation there are only acoustic phonons. For the inclusion of optical phonons, the arrangement of the atoms within a unit cell has to be considered, which goes beyond this simple picture.

3.3.2 Phonons in metals

The consideration above is certainly valid for semiconductors, where ionic interactions are mediated via covalent chemical bonds and oscillations around the equilibrium position may be approximated by a harmonic potential, so that the form of the elastic energy above is well motivated. The situation is more subtle for metals, where the ions interact through the long-ranged Coulomb interaction and are held to together through an intricate interplay with the mobile conduction electrons.

First, neglecting the gluey effect of the electrons, the positively charged background can itself be treated as an ionic gas. Similar to the electronic gas (3.84), the background exhibits a well-defined collective plasma excitation at the ionic plasma frequency

$$\Omega_p^2 = \frac{4\pi n_i (Z_i e)^2}{M_i}, \quad (3.131)$$

For equation (3.131) we used the formula (3.84) with $n_0 \rightarrow n_i = n_0/Z_i$ the density of ions with charge number Z_i , $e \rightarrow Z_i e$, and $m \rightarrow M_i$ the atomic mass. Apparently the excitation energy does not vanish as $\mathbf{k} \rightarrow 0$. So far, the background of the metallic system can not be described as an elastic medium where the excitation spectrum is expected to be linear in k , $\omega_{\mathbf{k}} \propto |\mathbf{k}|$.

The shortcoming in this discussion is that we neglected the feedback effects of the electrons that react nearly instantaneously to the slow ionic motion, due to their much smaller mass. The finite plasma frequency is a consequence of the long-range nature of the Coulomb potential (as mentioned earlier), but as we have seen above the electrons tend to screen these potentials, in particular for small wavevectors \mathbf{k} . The “bare” ionic plasma frequency Ω_p is thus renormalized to

$$\omega_{\mathbf{k}}^2 = \frac{\Omega_p^2}{\varepsilon(\mathbf{k}, 0)} = \frac{k^2 \Omega_p^2}{k^2 + k_{TF}^2} \approx (c_s k)^2, \quad (3.132)$$

¹¹See course of Statistical Physics HS09.

where the presence of the electrons leads to a renormalization of the Coulomb potential by a factor $1/\varepsilon(\mathbf{k}, \omega)$. Having included the back-reaction of the electrons, a linear dispersion of a sound wave ($\omega_{\mathbf{k}} = c_s |\mathbf{k}|$) is finally recovered, and the renormalized velocity of sound c_s reads

$$c_s^2 \approx \frac{\Omega_p^2}{k_{TF}^2} = \frac{Zm\omega_p^2}{M_i k_{TF}^2} = \frac{1}{3} Z \frac{m}{M_i} v_F^2. \quad (3.133)$$

For the comparison of the energy scales we find,

$$\frac{\Theta_D}{T_F} \sim \frac{c_s}{v_F} = \sqrt{\frac{1}{3} Z \frac{m}{M_i}} \ll 1, \quad (3.134)$$

where we used $k_B T_F = \epsilon_F$ and $k_D \approx k_F$.

Kohn anomaly

Notice that phonon frequencies are much smaller than the (electronic) plasma frequency, so that the approximation

$$\omega_{\mathbf{k}}^2 = \frac{\Omega_p^2}{\varepsilon(\mathbf{k}, 0)} \quad (3.135)$$

is valid even for larger wavevectors. Employing the Lindhard form of $\varepsilon(\mathbf{k}, 0)$, we deduce that the phonon frequency is singular at $|\mathbf{k}| = 2k_F$. More explicitly we find

$$\frac{\partial \omega_{\mathbf{k}}}{\partial \mathbf{k}} \rightarrow \infty \quad (3.136)$$

in the limit $k \rightarrow 2k_F$. This behavior is called the *Kohn anomaly* and results from the interaction between electrons and phonons. This effect is not contained in the previous elastic medium model that neglected ion-electron interactions.

3.3.3 Peierls instability in one dimension

The Kohn anomaly has particularly drastic effects in (quasi) one-dimensional electron systems, where the electron-phonon coupling leads to an instability of the metallic state. We consider a one-dimensional Jellium model where the ionic background is treated as an elastic medium with a displacement field u along the extended direction (x -axis). We neglect both the electron-electron interaction and the slow time evolution of the background modulation so that the Hamiltonian reads,

$$\mathcal{H} = \mathcal{H}_{\text{isol}} + \mathcal{H}_{\text{int}}, \quad (3.137)$$

where contributions of the isolated electronic and ionic systems are included in

$$\mathcal{H}_{\text{isol}} = \sum_{k,s} \frac{\hbar^2 k^2}{2m} c_{k,s}^\dagger c_{k,s} + \frac{\lambda}{2} \int dx \left(\frac{du}{dx}(x) \right)^2 \quad (3.138)$$

whereas the interactions between the system comes in via the coupling

$$\mathcal{H}_{\text{int}} = -n_0 \sum_s \int dx dx' V(x-x') \frac{d}{dx} u(x) \hat{\Psi}_s^\dagger(x') \hat{\Psi}_s(x') \quad (3.139)$$

In the general theory of elastic media $\nabla \cdot \mathbf{u} = -\delta n/n_0$ describes density modulations, so that the second term in (3.137) models the coupling of the electrons to charge density fluctuations of

the positively charged background¹² mediated by the screened Coulomb interaction $V(x - x')$ (contact interaction). Consider the ground state of N electrons in a system of length L , leading to an electronic density $n_0 = N/L$. For a uniform background $u(x) = \text{const}$, the Fermi wavevector of free electrons is readily determined to be

$$N = \sum_s \frac{L}{2\pi} \int_{-k_F}^{+k_F} dk 1 = 2 \frac{L}{2\pi} 2k_F \quad (3.140)$$

leading to

$$k_F = \frac{\pi}{2} n_0. \quad (3.141)$$

Perturbative approach - instability

Now we consider the Kohn anomaly of this system. For a small background modulation $u(x) \neq \text{const}$, the interaction term \mathcal{H}_{int} can be treated perturbatively and will lead to a renormalization of the elastic modulus λ in (3.137). For that it will be useful to express the full Hamiltonian in momentum space,

$$\mathcal{H}_{\text{isol}} = \sum_{k,s} \frac{\hbar^2 k^2}{2m} c_{k,s}^\dagger c_{k,s} + \frac{\Omega \rho_0}{2} \sum_q \omega_q^2 u_q u_{-q} \quad (3.142)$$

$$\mathcal{H}_{\text{int}} = \frac{i}{2} \sum_{k,q,s} q [\tilde{V}_{-q} u_q \hat{c}_{k+q,s}^\dagger \hat{c}_{k,s} - \tilde{V}_q u_{-q} \hat{c}_{k,s}^\dagger \hat{c}_{k+q,s}], \quad (3.143)$$

where we used from previous considerations $\lambda q^2 = \rho_0 \omega_q^2$. Furthermore we defined

$$u(x) = \frac{1}{\sqrt{L}} \sum_q u_q e^{iqx}, \quad (3.144)$$

$$V(x) = \frac{1}{\sqrt{L}} \sum_q \tilde{V}_q e^{iqx}, \quad (3.145)$$

with $\tilde{V}_q = 4\pi e^2/q^2 \epsilon(q, 0) \approx \text{const}$. - we consider an effectively short-ranged potential. We compute the second order correction to the ground state energy using Rayleigh-Schrödinger perturbation theory (note that the linear energy shift vanishes)

$$\Delta E^{(2)} = \sum_{k,q,s} \frac{q^2 |\tilde{V}_q|^2}{4} u_q u_{-q} \sum_n \frac{|\langle \Psi_0 | \hat{c}_{k,s}^\dagger \hat{c}_{k+q,s} | n \rangle|^2 + |\langle \Psi_0 | \hat{c}_{k+q,s}^\dagger \hat{c}_{k,s} | n \rangle|^2}{E_0 - E_n} \quad (3.146)$$

$$= \sum_q \frac{q^2 |\tilde{V}_q|^2}{4} u_q u_{-q} \sum_k \frac{n_{k+q} - n_k}{\epsilon_{k+q} - \epsilon_k} \quad (3.147)$$

$$= \frac{\Omega}{4} \sum_q |\tilde{V}_q|^2 q^2 \chi_0(q, 0) u_q u_{-q} \quad (3.148)$$

where the virtual states $|n\rangle$ are electron-hole excitations of the filled Fermi sea. This term gives a correction to the elastic term in (3.142). In other words, the elastic modulus λ and, thus, the phonon frequency $\omega_q^2 = \lambda/\rho_0 q^2 = c_s^2 q^2$ is renormalized according to

$$(\omega_q^{\text{ren}})^2 \approx \omega_q^2 + \frac{|\tilde{V}_q|^2 q^2}{4\rho_0} \chi_0(q, 0) = \omega_q^2 - \frac{|\tilde{V}_q|^2 q}{8\pi\rho_0} \ln \left| \frac{q + 2k_F}{q - 2k_F} \right| \quad (3.149)$$

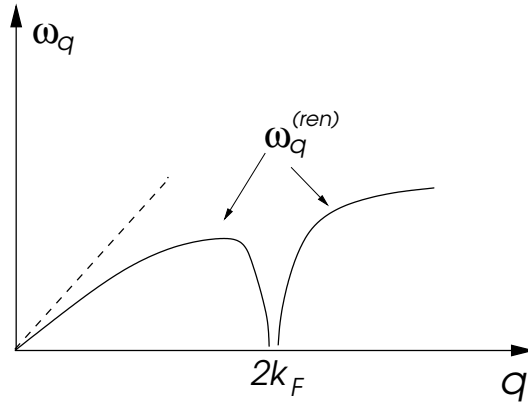


Figure 3.8: Kohn anomaly for the one-dimensional system with electron-phonon coupling. The renormalization of the phonon frequency is divergent at $q = 2k_F$.

From the behavior for $q \rightarrow 0$ we infer that the velocity of sound is renormalized. However, a much more drastic modification occurs at $q = 2k_F$. Here the phonon spectrum is 'softened', i.e. the frequency vanishes and even becomes negative. The latter effect is an artifact of the perturbation theory.¹³ This hints at an instability triggered by the Bose-Einstein condensation of phonons with a wave vector of $q = 2k_F$. This coherent superposition¹⁴ of many phonons corresponds classically to a static periodic deformation of the ionic background with wave vector $2k_F$. The unphysical behavior of the frequency ω_q indicates that in the vicinity of $2k_F$, the current problem can not be treated with the help of perturbation theory around the uniform state.

Peierls instability at $Q = 2k_F$

Instead of the perturbative approach, we assume that the background shows a periodic density modulation (coherent phonon state)

$$u(x) = u_0 \cos(Qx) \quad (3.154)$$

¹²Note that only phonon modes with a finite value of $\nabla \cdot \mathbf{u}$ couple in lowest order to the electrons. This is only possible of longitudinal modes. Transverse modes are defined by the condition $\nabla \cdot \mathbf{u} = 0$ and do not couple to electrons in lowest order.

¹³Note that indeed the expression

$$\omega_q^2 = \frac{\Omega_p^2}{\varepsilon(q, 0)} \quad (3.150)$$

in (3.135) does not yield negative energies but gives a zero of ω_q at $q = 2k_F$.

¹⁴We introduce the *coherent state*

$$|\Phi_Q^{\text{coh}}\rangle = e^{-|\alpha|^2/2} \sum_{n=0}^{\infty} \frac{(\hat{b}_Q^\dagger)^n}{n!} \alpha^n |0\rangle \quad (3.151)$$

which does not have a definite phonon number for the mode of wave vector Q . On the other hand, this mode is macroscopically occupied, since

$$n_Q = \langle \Phi_Q^{\text{coh}} | \hat{b}_Q^\dagger \hat{b}_Q | \Phi_Q^{\text{coh}} \rangle = |\alpha|^2 \quad (3.152)$$

and, moreover, we find

$$\langle \Phi_Q^{\text{coh}} | \hat{u}(x) | \Phi_Q^{\text{coh}} \rangle = \frac{1}{L} \frac{\hbar}{2\rho_0\omega_Q} \left[\alpha e^{iQx} + \alpha^* e^{-iQx} \right] = u_0 \cos(Qx) \quad (3.153)$$

with $u_0 = \hbar\alpha/\rho_0L\omega_Q$, assuming α being real.

where $Q = 2k_F$ and u_0 remains to be determined variationally. We investigate the effect of this modulation on the electron-phonon system. To this end we show that such a modulation lowers the energy of the electrons. Assuming that u_0 is small we can evaluate the electronic energy using the approximation of nearly free electrons, where Q appears as a reciprocal lattice vector. The electronic spectrum for $0 \leq k \leq Q$ is then approximately determined by the secular equation

$$\det \begin{pmatrix} \frac{\hbar^2 k^2}{2m} - E & \Delta \\ \Delta^* & \frac{\hbar^2 (k-Q)^2}{2m} - E \end{pmatrix} = 0 \quad (3.155)$$

where Δ derives from the Fourier transform of the potential $V(x)$,

$$\Delta = -iQ u_0 n \tilde{V}_Q \quad (3.156)$$

with

$$\tilde{V}_Q = \int dx e^{iQx} V(x). \quad (3.157)$$

The equation (3.155) leads to the energy eigenstates

$$E_k^\pm = \frac{\hbar^2}{4m} \left[(k-Q)^2 + k^2 \pm \sqrt{\{(k-Q)^2 - k^2\}^2 + 16m^2 |\Delta|^2 / \hbar^4} \right]. \quad (3.158)$$

The total energy of the electronic and ionic system is then given by

$$E_{\text{tot}}(u_0) = 2 \sum_{0 \leq k < Q} E_{k-} + \frac{\lambda L Q^2}{4} u_0^2 \quad (3.159)$$

where all electronic states of the lower band (E_{k-}) are occupied and all states of the upper band (E_{k+}) are empty. The amplitude u_0 of the modulation is found by minimizing E_{tot} with respect to u_0 :

$$0 = \frac{1}{L} \frac{dE_{\text{tot}}}{du_0} \quad (3.160)$$

$$= -\frac{\hbar^2}{2m} \frac{32Q^2 m^2 n^2 \tilde{V}_Q^2}{\hbar^4} u_0 \int_0^Q \frac{dk}{2\pi} \frac{1}{\sqrt{\{(k-Q)^2 - k^2\}^2 + 16m^2 Q^2 n^2 \tilde{V}_Q^2 u_0^2 / \hbar^4}} + \frac{\lambda}{2} Q^2 u_0 \quad (3.161)$$

$$= -u_0 \frac{4Qmn^2 \tilde{V}_Q^2}{\hbar^2 \pi} \int_{-k_F}^{+k_F} dq \frac{1}{\sqrt{q^2 + 4m^2 n^2 \tilde{V}_Q^2 u_0^2 / \hbar^4}} + \frac{\lambda}{2} Q^2 u_0 \quad (3.162)$$

$$= -u_0 \frac{8Qmn^2 \tilde{V}_Q^2}{\hbar^2 \pi} \text{arsinh} \left(\frac{\hbar^2 k_F}{2mn \tilde{V}_Q u_0} \right) + \frac{\lambda}{2} Q^2 u_0. \quad (3.163)$$

We solve this equation for u_0 using $\text{arsinh}(x) \approx \ln(2x)$ when $x \gg 1$.

$$u_0 = \frac{\hbar^2 k_F}{mn \tilde{V}_Q} \exp \left[-\frac{\hbar^2 k_F \pi \lambda}{8mn^2 \tilde{V}_Q^2} \right] = \frac{2}{k_F} \frac{\epsilon_F}{n \tilde{V}_Q} e^{-1/N(0)g} \quad (3.164)$$

where $\epsilon_F = \hbar^2 k_F^2 / 2m$ is the Fermi energy and $N(0) = 2m / \pi \hbar^2 k_F$ is the density of states at the Fermi energy. We introduced the coupling constant $g = 4n^2 \tilde{V}_Q^2 / \lambda$ that describes the phonon-induced effective electron-electron interaction. The coupling is the stronger the more polarizable

(softer) ionic background, i.e. when the elastic modulus λ is small. Note that the static displacement u_0 depends exponentially on the coupling and on the density of states. The underlying reason for this so-called *Peierls instability* to happen lies in the opening of an energy gap,

$$\Delta E = E_{k_F}^+ - E_{k_F}^- = 2|\Delta| = 8\epsilon_F \exp\left(-\frac{1}{N(0)g}\right), \quad (3.165)$$

at $k = \pm k_F$, i.e. at the Fermi energy. The gap is associated with a lowering of the energy of the electron states in the lower band in the vicinity of the Fermi energy. For this reason this kind of instability is called a Fermi surface instability. Due to the gap the metal has turned into a semiconductor with a finite energy gap for all electron-hole excitations.

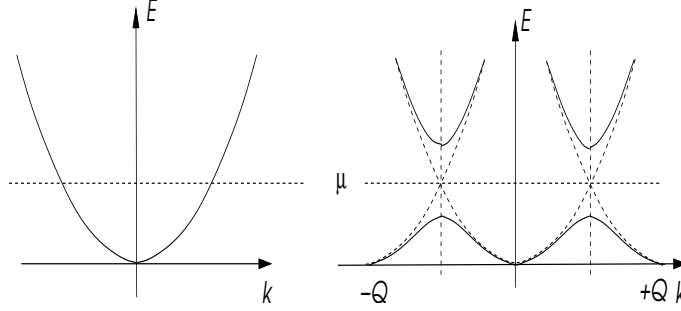


Figure 3.9: Change of the electron spectrum. The modulation of the ionic background yields gaps at the Fermi points and the system becomes an insulator.

The modulation of the electron density follows the charge modulation due to the ionic lattice deformation, which can be seen by expressing the wave function of the electronic states,

$$\psi'_k(x) = \frac{1}{\sqrt{\Omega}} \frac{\Delta e^{ikx} + (E_k - \epsilon_k) e^{i(k-Q)x}}{\sqrt{(E_k - \epsilon_k)^2 + |\Delta|^2}}, \quad (3.166)$$

which is a superposition of two plane waves with wave vectors k and $k - Q$, respectively. Hence the charge density reads

$$\rho_k(x) = -e|\psi'_k(x)|^2 = -\frac{e}{\Omega} \left[1 - \frac{2(\epsilon_k - E_k)|\Delta|}{(E_k - \epsilon_k)^2 + |\Delta|^2} \sin Qx \right] \quad (3.167)$$

and its modulation from the homogeneous distribution $-en$ is given by

$$\delta\rho(x) = \sum_k \rho_k(x) - (-en) = \frac{e}{2} \int_0^{k_F} \frac{dk'}{2\pi} \frac{m|\Delta| \sin Qx}{\sqrt{\hbar^4 k_F^2 k'^2 + m^2 |\Delta|^2}} \quad (3.168)$$

$$= \frac{en|\Delta|}{16\epsilon_F} \ln \left| \frac{2\epsilon_F}{|\Delta|} \right| \sin(2k_F x). \quad (3.169)$$

Such a state, with a spatially modulated electronic charge density, is called a *charge density wave* (CDW) state. This instability is important in quasi-one-dimensional metals which are for example realized in organic conductors such as TTF·TCNQ (tetrathiafulvalene tetracyanoquinomethane). In higher dimensions the effect of the Kohn anomaly is generally less pronounced, so that in this case spontaneous deformations rarely occur. As we will see later, a charge density wave instability can nevertheless be observed in multi-dimensional ($d > 1$) systems with a so-called nested Fermi surface. These systems resemble in some respects one-dimensional systems. Finally, notice that the electron-phonon interaction strongly contributes to another kind of Fermi surface instability, when metals exhibit superconductivity.

3.3.4 Dynamics of phonons and the dielectric function

We have seen that an external potential V_a is screened by the polarization of the electrons. As the positively charged ionic background is also polarizable, it should be included in the renormalization of the external potential. In general, the fully renormalized potential V_{ren} may be expressed via

$$\varepsilon V_{\text{ren}} = V_a, \quad (3.170)$$

with the full dielectric function ε . In order to determine V_{ren} and ε , we define the 'bare' (unrenormalized) electronic (ionic) dielectric function ε^{el} (ε^{ion}). The renormalized potential in (3.170) can be expressed considering three other points of view. First, if the ionic potential V_{ion} is added to the external potential V_a , the remaining screening is due to the electrons only, i.e.,

$$\varepsilon^{\text{el}} V_{\text{ren}} = V_a + V_{\text{ion}}. \quad (3.171)$$

Secondly, the electronic potential V_{el} may be added to the external potential V_a , so that the ions exclusively renormalize the new potential $V_{\text{el}} + V_a$, resulting in

$$\varepsilon^{\text{ion}} V_{\text{ren}} = V_a + V_{\text{el}}. \quad (3.172)$$

Note that in (3.172) all effects of electron polarization are included in V_{el} , so that the dielectric function results from the 'bare' ions. Finally we use the fact that V_{ren} may be expressed as

$$V_{\text{ren}} = V_a + V_{\text{el}} + V_{\text{ion}}. \quad (3.173)$$

Adding (3.171) to (3.172) and subtracting (3.170), we obtain

$$(\varepsilon^{\text{el}} + \varepsilon^{\text{ion}} - \varepsilon) V_{\text{ren}} = V_a + V_{\text{el}} + V_{\text{ion}} \quad (3.174)$$

which simplifies with (3.173) to

$$\varepsilon = \varepsilon^{\text{el}} + \varepsilon^{\text{ion}} - 1 \quad (3.175)$$

In order to find an alternative expression relating the renormalized potential V_{ren} to the external potential V_a , we make the Ansatz

$$V_{\text{ren}} = \frac{1}{\varepsilon} V_a = \frac{1}{\varepsilon_{\text{eff}}^{\text{ion}}} \frac{1}{\varepsilon^{\text{el}}} V_a \quad (3.176)$$

i.e. the potential $V_a/\varepsilon^{\text{el}}$ that results from bare screening of the polarizable electrons is additionally screened by an effective ionic dielectric function $\varepsilon_{\text{eff}}^{\text{ion}}$ which includes electron-phonon interactions. Using equation (3.175) and the definition of $\varepsilon_{\text{eff}}^{\text{ion}}$ via (3.176) we obtain

$$\varepsilon_{\text{eff}}^{\text{ion}} = 1 + \frac{1}{\varepsilon^{\text{el}}} (\varepsilon^{\text{ion}} - 1), \quad (3.177)$$

or using the definition (3.70)

$$\chi_{0,\text{eff}}^{\text{ion}} = \frac{\chi_0^{\text{ion}}}{\varepsilon^{\text{el}}}. \quad (3.178)$$

Taking into account the discussion of the plasma excitation of the bare ions in Eqs.(3.83, 3.84, and 3.131), and considering the long wave-length excitations ($\mathbf{k} \rightarrow 0$), we approximate

$$\varepsilon^{\text{ion}} = 1 - \frac{\Omega_p^2}{\omega^2}, \quad (3.179)$$

$$\varepsilon^{\text{el}} = 1 + \frac{k_{TF}^2}{k^2}. \quad (3.180)$$

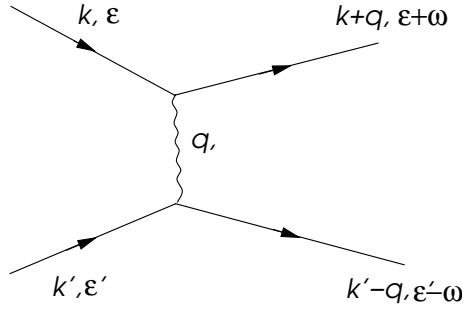


Figure 3.10: Diagram for the electron-electron interaction involving also electron-phonon coupling.

For the electrons we used the result from the quasi-static limit in (3.93). The full dielectric function now reads

$$\varepsilon = 1 + \frac{k_{TF}^2}{k^2} - \frac{\Omega_p^2}{\omega^2} = \left(1 + \frac{k_{TF}^2}{k^2}\right) \left(1 - \frac{\omega_{\mathbf{k}}^2}{\omega^2}\right). \quad (3.181)$$

The time-independent Coulomb interaction

$$V_a = \frac{4\pi e^2}{q^2} \quad (3.182)$$

between the electrons is replaced in a metal by an effective interaction

$$V_{\text{ren}}(\mathbf{q}, \omega) = \frac{4\pi e^2}{q^2 \varepsilon(\mathbf{q}, \omega)} \quad (3.183)$$

$$= \frac{4\pi e^2}{k_{TF}^2 + q^2} \left(\frac{\omega^2}{\omega^2 - \omega_{\mathbf{q}}^2} \right). \quad (3.184)$$

This interaction corresponds to the matrix element for a scattering process of two electrons with momentum exchange \mathbf{q} and energy exchange ω . The phonon frequency $\omega_{\mathbf{q}}$ is always less than the Debye frequency ω_D . Hence the effect of the phonons is almost irrelevant for energy exchanges ω that are much larger than ω_D . The time scale for such energies would be too short for the slow ions to move and influence the interaction. Interestingly, the repulsive bare Coulomb potential is renormalized to an interaction with an attractive channel for $\omega < \omega_D$ because of overcompensation by the ions. This aspect of the electron-phonon interaction is most important for superconductivity.

Chapter 4

Itinerant electrons in a magnetic field

Electrons couple through their orbital motion and their spin to external magnetic fields. In this chapter we focus on the case of orbital coupling which can be also used as a diagnostic tool to observe the presence of a Fermi surface in a metallic system and to map out the Fermi surface topology. A further most intriguing feature of electrons moving in a magnetic field is the Quantum Hall effect of a two-dimensional electronic system. In both case the Landau levels will play an important role and will be introduced here in a first step.

4.1 The de Haas-van Alphen effect

The ground state of a metal is characterized by the existence of a discontinuity of the occupation number in momentum space - the Fermi surface. The de Haas-van Alphen experiment is one of the best methods to verify its existence and to determine the shape of a Fermi surface. It is based on the behavior of electrons at low temperatures in a strong magnetic field.

4.1.1 Landau levels

Consider a free electron gas subject to a uniform magnetic field $\mathbf{B} = (0, 0, B)$. The one-particle Hamiltonian for an electron is given by

$$\mathcal{H} = \frac{1}{2m} \left(-i\hbar\nabla - \frac{e}{c}\mathbf{A} \right)^2 - \frac{g\mu_B}{\hbar} \hat{S}_z B. \quad (4.1)$$

We fix the gauge freedom of the vector potential \mathbf{A} by working in the Landau gauge, $\mathbf{A} = (0, Bx, 0)$, satisfying $\mathbf{B} = \nabla \times \mathbf{A}$. Hence the Hamiltonian (4.1) simplifies to

$$\mathcal{H} = \frac{1}{2m} \left[-\hbar^2 \frac{\partial^2}{\partial x^2} + \left(-i\hbar \frac{\partial}{\partial y} - \frac{e}{c} Bx \right)^2 - \hbar^2 \frac{\partial^2}{\partial z^2} \right] - \frac{g\mu_B}{\hbar} \hat{S}_z B. \quad (4.2)$$

In this gauge, the vector potential acts like a confining harmonic potential along the x -axis. As translational invariance in the y - and z -directions is preserved, the eigenfunctions separate in the three spacial components and take the form

$$\psi(\mathbf{r}) = e^{ik_z z} e^{ik_y y} \phi(x) \xi_s \quad (4.3)$$

where ξ_s is the spin wave function. The states $\phi(x)$ are found to be the eigenstates of the harmonic oscillator problem, so that we have

$$\phi_{n,k_y}(x) = \frac{1}{\sqrt{2^n n! 2\pi \ell^2}} H_n[(x - k_y \ell^2)/\ell] e^{-(x - k_y \ell^2)^2/2\ell^2} \quad (4.4)$$

where $H_n(x)$ are the Hermite polynomials and ℓ represents the *magnetic length* defined via $\ell^2 = \hbar c/|eB|$. The eigenenergies of the Hamiltonian (4.2) read

$$E_{n,k_z,s} = \frac{\hbar^2 k_z^2}{2m} + \hbar\omega_c \left(n + \frac{1}{2} \right) - \frac{g\mu_B}{\hbar} B s \quad (4.5)$$

where $s = \pm\hbar/2$, $n \in \mathbb{N}_0$ and we have introduced the cyclotron frequency $\omega_c = |eB|/mc$. Note that the energy (4.5) does not depend on k_y . The apparent differences in the spatial dependence of the wave functions for the x - and y -directions are merely a consequence of the chosen gauge.¹ The fact that the energy does not depend on k_y in the chosen gauge indicates a huge degeneracy of the eigenstates. To obtain the number of degenerate states we concentrate for simplicity on $k_z = 0$ and neglect the electron spin. We take the electrons to be confined to a cube of volume L^3 with periodic boundary conditions, i.e., $k_y = 2\pi n_y/L$ with $n_y \in \mathbb{N}_0$. As the wave function $\phi_{n,k_y}(x)$ is centered around $k_y \ell^2$, the condition

$$0 < k_y \ell^2 < L \quad (4.8)$$

fixes the maximal number N_{deg} of degenerate states

$$0 < n_y < N_{\text{deg}} = \frac{L^2}{2\pi\ell^2} = \frac{L^2 B}{hc/e} = \frac{\Phi}{\Phi_0}. \quad (4.9)$$

where $\Phi_0 = hc/e$ is the magnetic flux quantum (e.g. Aharonov-Bohm interference effect). Thus the degeneracy N_{deg} corresponds to the number of flux quanta included in the total magnetic flux Φ threading the system.

The energies correspond to a discrete set of one-dimensional systems, so that the density of states is determined by the structure of the one-dimensional dispersion (with square root singularities at the band edges) along the z -direction:

$$N_0(E, n, s) = \frac{N_{\text{deg}}}{\Omega} \sum_{k_z} \delta(E - E_{n,k_z,s}) \quad (4.10)$$

$$= \frac{1}{2\pi\ell^2} \int \frac{dk_z}{2\pi} \delta \left(E - \frac{\hbar^2 k_z^2}{2m} - \hbar\omega_c \left(n + \frac{1}{2} \right) + \frac{g\mu_B}{\hbar} B s \right) \quad (4.11)$$

$$= \frac{(2m)^{3/2} \omega_c}{8\pi^2 \hbar^2} \frac{1}{\sqrt{E - \hbar\omega_c(n + 1/2) + g\mu_B B s/\hbar}} \quad (4.12)$$

The total density of states $N_0(E)$ for a given energy E is obtained by summing over $n \in \mathbb{N}_0$ and $s = \pm\hbar/2$. This should be compared to the density of states without the magnetic field,

$$N_0(E, B = 0) = \frac{1}{\Omega} \sum_{\mathbf{k}, s} \delta \left(E - \frac{\hbar^2 \mathbf{k}^2}{2m} \right) = \frac{(2m)^{3/2}}{2\pi^2 \hbar^3} \sqrt{E}. \quad (4.13)$$

The density of states for finite applied field is shown in Fig. 4.1 for one spin-component.

¹Like the vector potential, the wave function is a gauge dependent quantity. To see this, observe that under a gauge transformation

$$\mathbf{A}(\mathbf{r}, t) \rightarrow \mathbf{A}'(\mathbf{r}, t) = \mathbf{A}(\mathbf{r}, t) + \nabla\chi(\mathbf{r}, t) \quad (4.6)$$

the wave function undergoes a position dependent phase shift

$$\psi(\mathbf{r}, t) \rightarrow \psi'(\mathbf{r}, t) = \psi(\mathbf{r}, t) e^{i\hbar c\chi(\mathbf{r}, t)/e}. \quad (4.7)$$

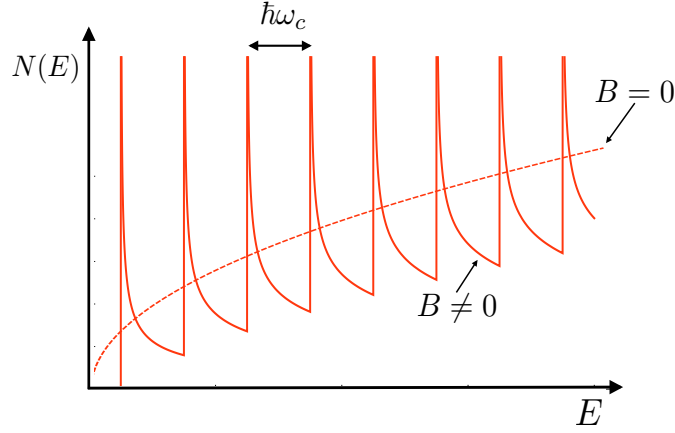


Figure 4.1: Density of states for electrons in a magnetic field due to Landau levels. The dashed line shows the density of states in the absence of a magnetic field.

4.1.2 Oscillatory behavior of the magnetization

In the presence of a magnetic field, the smooth density of states of the three-dimensional metal is replaced by a discontinuous form dominated by square root singularities. The position of the singularities depends on the strength of the magnetic field. In order to understand the resulting effect on the magnetization, we consider the free energy

$$F = N\mu - TS = N\mu - k_B T \sum_{k_z, k_y, n, s} \ln \left(1 + e^{-(E_{n, k_z, s} - \mu)/k_B T} \right) \quad (4.14)$$

and use the general thermodynamic relation $M = -\partial F/\partial B$. For the details of the somewhat tedious calculation, we refer to J. M. Ziman, *Principles of the Theory of Solids*² and merely present the result

$$M = N\chi_P B \left[1 + \frac{\chi_L}{\chi_P} + \frac{\pi k_B T}{\mu_B B} \sqrt{\frac{\epsilon_F}{\mu_B B}} \sum_{\nu=1}^{\infty} \frac{1}{\sqrt{\nu}} \frac{\sin\left(\frac{\pi}{4} - \frac{\pi\nu\epsilon_F}{\mu_B B}\right)}{\sinh\left(\frac{\pi^2\nu k_B T}{\mu_B B}\right)} \right]. \quad (4.15)$$

Here χ_P is the Pauli-spin susceptibility originating from the Zeeman-term and the second term $\chi_L = -\chi_P/3$ is the diamagnetic Landau susceptibility which is due to induced orbital currents (the Landau levels). For sufficiently low temperatures, $k_B T < \mu_B B \sim \hbar\omega_c$, the magnetization as a function of the applied field exhibits oscillatory behavior. The dominant contribution comes from the summand with $\nu = 1$. The oscillations are a consequence of the singularities in the density of states that influence the magnetic moment upon successively passing through the Fermi energy as the magnetic field is varied. The period in $1/B$ of the oscillations of the term $\nu = 1$ is easily found to be

$$\frac{\pi\epsilon_F}{\mu_B} \Delta \left(\frac{1}{B} \right) = 2\pi \quad (4.16)$$

or

$$\Delta \left(\frac{1}{B} \right) = \frac{2\pi e}{\hbar c} \frac{1}{A(k_F)} \quad (4.17)$$

where we used that $\mu_B = \hbar e/2mc$ and defined the cross sectional area $A(k_F) = \pi k_F^2$ of the Fermi sphere perpendicular to the magnetic field.

²German title : *Prinzipien der Festkörpertheorie*

4.1.3 Onsager equation

The behavior we have found above for a free electron gas, generalizes to systems with arbitrary band structures. In these cases there are usually no exact solutions available. Instead of generalizing the above treatment to such band systems, we discuss the behavior of electrons within the semiclassical approximation, as introduced in Section 1.7, and consider the closed orbits of a wave packet subject to a magnetic field. The semiclassical equations of motion for the center of mass of the wave packet (1.101, 1.102) simplify in the absence of an electric field to

$$\dot{\mathbf{r}} = \mathbf{v}_{\mathbf{k}} = \frac{\partial \epsilon_{\mathbf{k}}}{\partial \hbar \mathbf{k}} \quad (4.18)$$

$$\hbar \dot{\mathbf{k}} = -\frac{e}{c} \mathbf{v}_{\mathbf{k}} \times \mathbf{B}. \quad (4.19)$$

This defines a closed path in a plane perpendicular to the applied uniform field. Hence, we can apply the Bohr-Sommerfeld quantization scheme yielding quantized closed paths P_n ,

$$\oint_{P_n} \mathbf{p} \cdot d\mathbf{r} = h(n + \gamma) \quad (4.20)$$

with n being an integer and γ a system specific shift, irrelevant for the final result and $h = 2\pi\hbar$. The momentum within the semiclassical approach is expressed as

$$\mathbf{p} = \hbar \mathbf{k} - \frac{e}{c} \mathbf{A} = -\frac{e}{c} (\mathbf{r} \times \mathbf{B} + \mathbf{A}), \quad (4.21)$$

where we used Eq.(4.19) integrated over time. Thus, Eq.(4.20) can be now evaluated as

$$\oint_{P_n} \mathbf{p} \cdot d\mathbf{r} = -\frac{e}{c} \oint_{P_n} \{\mathbf{r} \times \mathbf{B} + \mathbf{A}\} \cdot d\mathbf{r} = -\frac{e}{c} \Phi_n + \underbrace{\frac{e}{c} \mathbf{B} \cdot \oint_{P_n} \mathbf{r} \times d\mathbf{r}}_{=2eB_{\perp} S_n/c=2e\Phi_n/c} = h(n + \gamma), \quad (4.22)$$

where S_n is the area encircled by the path P_n and $\Phi_n = B_{\perp} S_n$ the magnetic flux threading. With this we find

$$\Phi_n = (n + \gamma) \Phi_0. \quad (4.23)$$

Now we compare the areas of a given trajectory in real and reciprocal space, S_n and A_n , respectively. Considering $\hbar \mathbf{k} = e(\mathbf{r} \times \mathbf{B})/c$ yields

$$|d\mathbf{r}| = \frac{\Phi_0}{2\pi B_{\perp}} |d\mathbf{k}| \quad \Rightarrow \quad S_n = \left(\frac{\Phi_0}{2\pi B_{\perp}} \right)^2 A_n \quad (4.24)$$

With the flux quantization in Eq.(4.23) we obtain for a given magnetic field the area A_n ,

$$A_n = (n + \gamma) 4\pi^2 \frac{B_{\perp}}{\Phi_0} \quad (4.25)$$

while for a given area A we obtain,

$$A = (n + \gamma) 4\pi^2 \frac{B_n}{\Phi_0} = (n' + \gamma) \frac{4\pi^2}{\Phi_0} B_{n'}. \quad (4.26)$$

Thus changing the field B by a certain amount $B_n \rightarrow B_{n+1}$ would yield the same A and one period of changing density of states, i.e. magnetization. From this we conclude that there is a regular oscillation as a function of $1/B$ and the period is connected with the area A ,

$$\Delta \left(\frac{1}{B} \right) = \frac{1}{B_{n+1}} - \frac{1}{B_n} = \frac{4\pi^2}{A\Phi_0}. \quad (4.27)$$

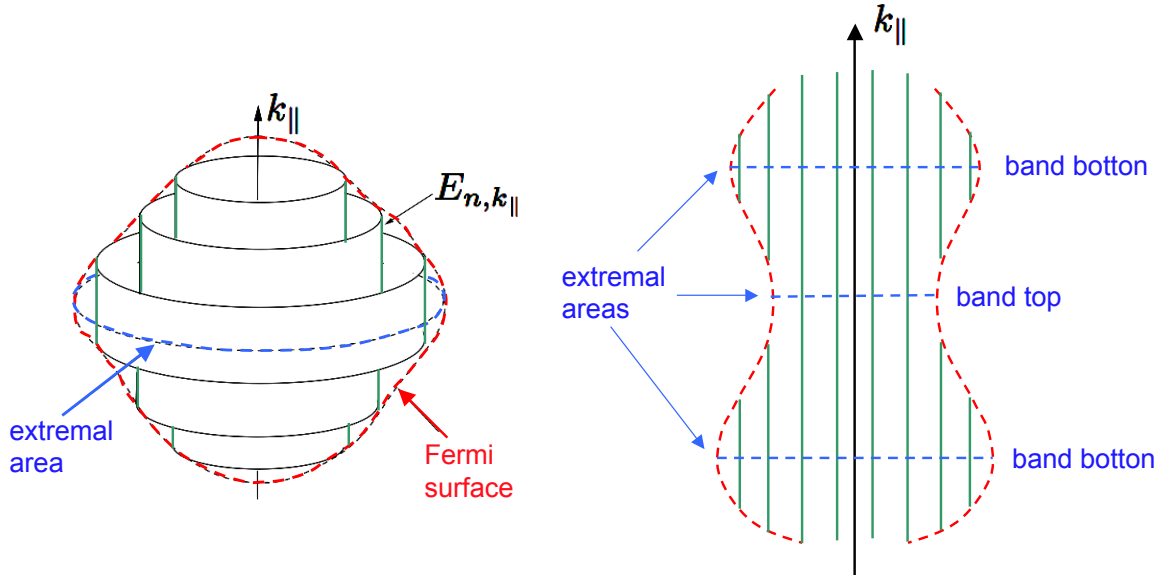


Figure 4.2: Concentric tubes represent the quantized orbits in the reciprocal space corresponding to the areas A_n embedded in the original Fermi surface which limits the height of the tubes, occupation along the k_{\parallel} -direction ($\mathbf{k}_{\parallel} \parallel \mathbf{B}$). Left panel: 3-dimensional view of system with a simple Fermi surface. Right panel: cross section including k_{\parallel} . Extremal areas represent the band edges (bottom: maximal A ; and top: minimal A).

As we have seen above (Eq.(4.12)) the Fermi energy passes through a singularity in the density of states at the band bottom of the one-dimensional motion of the electrons along k_z or $\mathbf{k}_{\parallel} \parallel \mathbf{B}$. This corresponds the extremal area $A(\mathbf{k}_{\parallel})$. Note, also a band top yields the same type of singularity and corresponds to a minimum of $A(\mathbf{k}_{\parallel})$. Therefore, in experiment the magnetization maxima oscillate with a period in the inverse magnetic field as given by Eq.(4.27).

The oscillations in the magnetization, thus, allow to measure the cross sectional area of the Fermi 'sphere'. By varying the orientation of the field the topology of the Fermi surface can be mapped. As an alternative to the measurement of magnetization oscillations one can also measure resistivity oscillations known under the name Schubnikov-de Haas effect. For both methods it is crucial that the Landau levels are sufficiently clearly recognizable. Apart from low temperatures this necessitates sufficiently clean samples. In this context, sufficiently clean means that the average life-time τ (average time between two scattering events) has to be much larger than the period of the cyclotron orbits, i.e. $\omega_c \tau \gg 1$. This condition follows from the uncertainty relation

$$\Delta \epsilon \sim \frac{\hbar}{\tau} \ll \hbar \omega_c. \quad (4.28)$$

4.2 Quantum Hall Effect

Classical Hall Effect

The Hall effect, discovered by Edwin Hall in 1879, originates from the Lorentz force exerted by a magnetic field on a moving charge. This force is perpendicular both to the velocity of the charged particle and to the magnetic field. In the presence of an electrical current, a Lorentz force produces a transverse voltage, whenever the applied magnetic field points in a direction non-collinear to the current in the conductor. This so-called *Hall effect* can be used to investigate some properties of the charge carriers. Before treating the quantum version, we briefly review

the original Hall effect. To this end we consider the classical equation of motion of an electron, subject to an electric and a magnetic field

$$m^* \frac{d\mathbf{v}}{dt} = -e \left(\mathbf{E} + \frac{\mathbf{v}}{c} \times \mathbf{B} \right), \quad (4.29)$$

where m^* is the effective electron mass. For this classical system, the steady state equation reads

$$\left(\mathbf{E} + \frac{\mathbf{v}}{c} \times \mathbf{B} \right) = 0. \quad (4.30)$$

For the Hall geometry shown in Fig. 4.3 with fixed current $\mathbf{j} = (0, j_y, 0) = (0, -n_0 e v, 0)$ and magnetic field $\mathbf{B} = B_z$, the steady state condition (4.30) simplifies to

$$E_x + \frac{v B_z}{c} = 0. \quad (4.31)$$

The solution $E_x = -v B_z / c$ yields the Hall voltage that compensates the Lorentz force. The Hall conductivity σ_H is defined as the ratio between the longitudinal current j_y and the transverse electric field E_x , leading to

$$\sigma_H = \sigma_{yx} = \frac{j_y}{E_x} = \frac{n_0 e c}{B_z} = \nu \frac{e^2}{h}, \quad (4.32)$$

where $\nu = n_0 h c / B e$.³ We infer from Eq.(4.32), that the measurements of the Hall conductivity can be used to determine both the charge density n_0 and the sign of the charge carriers, i.e. whether the Fermi surfaces encloses the Γ -point for electron-like, negative charges or a point on the boundary of the Brillouin zone for hole-like, positive charges.

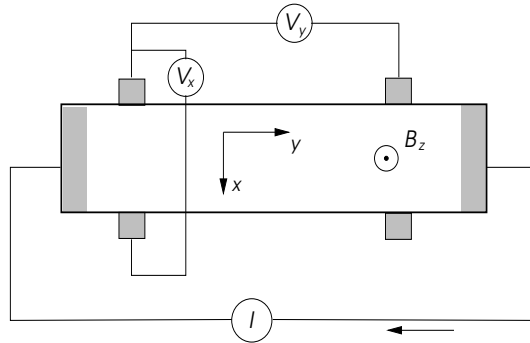


Figure 4.3: Schematic view of a Hall bar. The current runs along the y -direction and the magnetic field is applied along z -direction. The voltage V_y determines the conductance along the Hall bar, while V_x corresponds to the transverse Hall voltage.

Discovery of the Quantum Hall Effects

When measuring the Hall effect in a special two-dimensional electron system, Klaus von Klitzing and his collaborators made 1980 an astonishing discovery.⁴ The system was the inversion layer

³Note that the conductivity is a tensor,

$$j_a = \sum_{b=x,y,z} \sigma_{ab} E_b. \quad (4.33)$$

Following Eq.(4.30) yielding $\mathbf{E} \propto \mathbf{j} \times \mathbf{B}$, we conclude that the off-diagonal elements due to the Hall effect satisfy the relation $\sigma_{ab} = -\sigma_{ba}$.

⁴See [von Klitzing, Dorda, and Pepper, Phys. Rev. Lett. **45**, 494 (1980)] for the original paper.

of GaAs-MOSFET device with a sufficiently high gate voltage (see Section 2.4.3) which behaves like a two-dimensional electron gas with a high mobility $e\tau/m^*$ due to the mean free path $l \sim 10\text{\AA}$ and low density ($n_0 \sim 10^{11}\text{cm}^{-2}$). The two extended dimensions correspond to the interface of the MOSFET, whereas the electrons are confined in the third dimension like in a potential well (cf. Section 2.4.3). In high magnetic fields between 1 – 30T and at sufficiently low temperatures ($T < 4\text{K}$), von Klitzing and coworkers observed a quantization of the Hall conductivity corresponding to exact integer multiples of e^2/h

$$\sigma_H = \nu_n \frac{e^2}{h} \quad (4.34)$$

where $\nu_n \in \mathbb{N}$. By now, the integer quantization is so widely verified, that the von Klitzing constant (resistance quantum named after the discoverer of the Quantum Hall effect) $R_K = h/e^2 = 25812.807557\Omega$ is used in resistance calibrations. In the field range where the transverse conductivity shows integer plateaus in $\nu \propto 1/B$, the longitudinal conductivity σ_{yy} vanishes and takes finite values only when σ_H crossed over from one quantized value to the next (see Fig. 4.4).

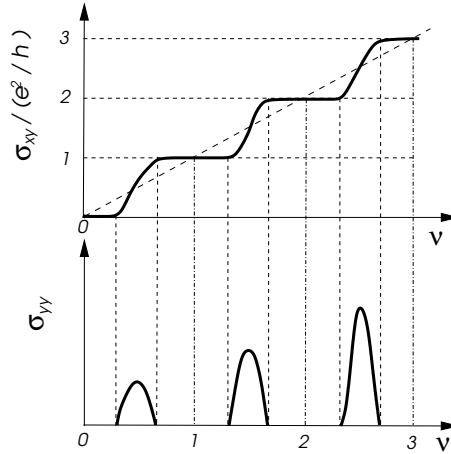


Figure 4.4: Integer Quantum Hall effect: As a function of the filling factor ν plateaus in σ_{xy} appear at multiples of e^2/h . The longitudinal conductance σ_{yy} is only finite for fillings where σ_{xy} changes between plateaus.

In 1982, Tsui, Störmer, and Gossard⁵ discovered an additional quantization of σ_H , corresponding to certain rational multiples of e^2/h . Correspondingly, one now distinguishes between the integer quantum Hall effect (IQHE) and the fractional quantum Hall effect (FQHE). These discoveries marked the beginning of a whole new field in solid state physics that continues to produce interesting results.

4.2.1 Hall effect of the two-dimensional electron gas

Here we first discuss the Hall effect in the quantum mechanical treatment. For this purpose we start with the Hamilton operator (4.1) and neglect the electron spin. Working again in the Landau gauge, $\mathbf{A} = (0, Bx, 0)$, and confining the electronic system to two dimensions, the Hamiltonian reduces to

$$\mathcal{H} = \frac{1}{2m} \left[-\hbar^2 \frac{\partial^2}{\partial x^2} + \left(-i\hbar \frac{\partial}{\partial y} - \frac{e}{c} Bx \right)^2 \right]. \quad (4.35)$$

⁵See [Tsui, Störmer and Gossard Phys. Rev. Lett. **48**, 1559 (1982)] for the original paper

For the two-dimensional gas there is no motion in the z -direction, so that the highly degenerate energy eigenvalues are given by the spectrum of a one-dimensional harmonic oscillator $E_n = \hbar\omega_c(n + 1/2)$, where again $\omega_c = |eB|/mc$. Here, we will concentrate on the lowest Landau level ($n = 0$) with the wave function

$$\phi_{0,k_y} = \frac{1}{\sqrt{2\pi\ell^2}} e^{-(x-x_0)^2/2\ell^2} e^{ik_y y}. \quad (4.36)$$

where the magnetic length $\ell = \sqrt{\hbar c/|eB|}$ gives the extension of the wave function in the presence of the magnetic field. In x -direction, the wave function is localized around $x_0 = k_y \ell^2$, whereas it takes the form of a plane wave in y -direction. As discussed previously, the energy does not depend on k_y .

We now introduce an electric field E_x along the x -direction. The Hamilton operator (4.35) is then modified by an additional potential $U(\mathbf{r}) = -eE_x x$. This term can easily be absorbed into the harmonic potential and leads to a shift of the center of the wave function,

$$x_0(k_y) \rightarrow x'_0(k_y) = k_y \ell^2 + \frac{eE_x}{m\omega_c^2}. \quad (4.37)$$

Moreover the degeneracy of the Landau level is lifted since the energy becomes k_y -dependent and (after completing the square) takes the form

$$E_{n=0}(k_y) = \frac{\hbar\omega_c}{2} - eE_x x'_0(k_y) + \frac{m}{2} \left(\frac{cE_x}{B} \right)^2. \quad (4.38)$$

The energy (4.38) corresponds to the wave function ϕ_{0k_y} from (4.36) where x_0 is replaced by x'_0 . The velocity of the electrons is then given by

$$v_y(k_y) = \frac{1}{\hbar} \frac{dE_{n=0}(k_y)}{dk_y} = -\frac{eE_x \ell^2}{\hbar} = -\frac{cE_x}{B}, \quad (4.39)$$

and from this, we determine the current density,

$$j_y = -en_0 v_y(k_y) = en_0 \frac{cE_x}{B} = \frac{e\nu}{2\pi\ell^2} \frac{cE_x}{B} = \nu \frac{e^2}{h} E_x = \sigma_H E_x \quad (4.40)$$

where $\nu = n_0 2\pi\ell^2$ is the filling of the Landau level.⁶ The Hall conductivity is then identical to the result (4.32) derived previously based on the quasiclassical approximation. There is a linear relation between the Hall conductivity σ_H and the index $\nu \propto B^{-1}$.

4.2.2 Integer Quantum Hall Effect

The plateaus observed by von Klitzing in the Hall conductivity σ_H of the two-dimensional electron gas as a function of the magnetic field correspond to the values $\sigma_H = \nu_n e^2/h$, as if $\nu = \nu_n \in \mathbb{N}$ was restricted to be an integer. Meanwhile, the longitudinal conductivity of the electron gas vanishes when a plateau of σ_H is realized

$$\sigma_{yy} = \frac{j_y}{E_y} = 0, \quad (4.41)$$

and only becomes finite at the transition points of σ_H between two plateaus (cf. Fig. 4.4). This fact seems to be in contradiction with the results from the consideration above. The solution to this mysterious behavior lies in the fact that disorder, which is always present in a real

⁶Note that $\nu^{-1} = B/n_0\Phi_0$ where $\Phi_0 = hc/e$ represents the flux quantum, i.e. $\nu^{-1} \propto B$ is the number of flux quanta Φ_0 per electron.

inversion layer, plays a crucial role and should not be neglected. In fact, due to the disorder, the electrons move in a randomly modulated potential landscape $U(x, y)$. As we will find out, even small amounts of disorder lead to the localization of electronic states in this two-dimensional system. To illustrate this new aspect we focus on the lowest Landau level in the symmetric gauge $\mathbf{A} = (-y, x, 0)B/2$. The Schrödinger equation in polar coordinates is given by

$$\frac{\hbar^2}{2m^*} \left[-\frac{1}{r} \frac{\partial}{\partial r} r \frac{\partial}{\partial r} - \left(\frac{1}{r} \frac{\partial}{\partial \varphi} - i \frac{e}{2\hbar c} Br \right)^2 \right] \psi(r, \varphi) + U(x, y)\psi(r, \varphi) = E\psi(r, \varphi). \quad (4.42)$$

Without the external potential $U(x, y)$ we find the ground state solutions

$$\psi_{n=0,m}(r, \varphi) = \frac{1}{\sqrt{2\pi\ell^2 2^m m!}} \left(\frac{r}{\ell} \right)^m e^{-im\varphi} e^{-r^2/4\ell^2} \quad (4.43)$$

where all values of $m \in \mathbb{N}_0$ correspond to the same energy $E_{n=0} = \hbar\omega_c/2$. One easily verifies, that the wave functions $|\psi_{n=0,m}(r, \varphi)|$ are peaked on circles of radius $r_m = \sqrt{2m} \ell$ (see Fig.4.5). Note that the magnetic flux threading such a circle is given by

$$\pi B r_m^2 = \pi B 2m \ell^2 = 2\pi m B \frac{\hbar c}{eB} = m \frac{\hbar c}{e} = m \Phi_0, \quad (4.44)$$

which is an integer multiple of the flux quantum $\Phi_0 = \hbar c/e$.

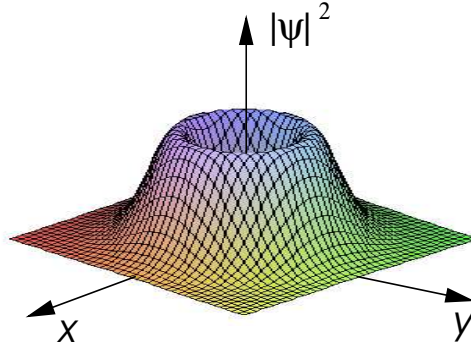


Figure 4.5: Wavefunction of a Landau level state in the symmetric gauge.

Now we consider the effect of the disorder potential. The gauge can be adjusted to the potential landscape. If, for simplicity, we assume the potential to be rotationally invariant around the origin, the symmetric gauge is already optimal. For the potential

$$U(x, y) = U(r) = \frac{C_1}{r^2} + C_2 r^2 + C_3, \quad (4.45)$$

the exact expression of all eigenstates of equation (4.42) in the lowest Landau level is obtained using the Ansatz

$$\tilde{\psi}_{0,m}(r, \varphi) = \frac{1}{\sqrt{2\pi\ell^{*2} 2^\alpha \Gamma(\alpha + 1)}} \left(\frac{r}{\ell^*} \right)^\alpha e^{-im\varphi} e^{-r^2/4\ell^{*2}}. \quad (4.46)$$

After introducing the dimensionless parameters $C_1^* = 2m^*C_1/\hbar^2$ and $C_2^* = 8\ell^4 m^* C_2/\hbar^2$, the quantities α and ℓ^* from equation (4.46) can be expressed via

$$\alpha^2 = m^2 + C_1^*, \quad (4.47)$$

$$(\ell^*)^{-2} = (\ell)^{-2} \sqrt{1 + C_2^*}. \quad (4.48)$$

Indeed, the Ansatz (4.46) describes eigenstates of the disordered problem (4.42). The degeneracy of the ground state energy (the lowest Landau level) is now lifted,

$$E_{0,m} = \frac{\hbar\omega_c}{2} \left[\frac{\ell^2}{\ell^{*2}}(\alpha + 1) - m \right] + C_3. \quad (4.49)$$

The wave functions are concentrated around the radii $r_m = \sqrt{2\alpha}\ell^*$. For weak potentials $C_1^*, C_2^* \ll 1$ and $m \gg 1$ the energy is approximatively given by

$$E_{0,m} \approx \frac{\hbar\omega_c}{2} + \frac{C_1}{r_m^2} + C_2 r_m^2 + C_3 + \dots, \quad (4.50)$$

i.e. the wave function adjusts itself to the potential landscape. It turns out that the same is true for arbitrarily structured weak potential landscapes. The wave function describes electrons on quasi-classical trajectories that trace the equipotential lines of the underlying disorder potential. Consequently the states described here are localized in the sense that they are attached to the structure of the potential. The application of an electric field cannot set the electrons in the concentric rings in motion. Therefore, the electrons are localized and do not contribute to electric transport.

Picture of the potential landscape

When the magnetic field is varied the filling $\nu = n_0 2\pi\ell^2$ of the Landau level is adjusted accordingly. While all states of a given level are degenerate in the transitionally invariant case, now, these states are spread over a certain energy range due to the disorder. In the quasi-classical approximation, these states correspond to equipotential trajectories that are either filled or empty depending on the strength of the magnetic field, i.e. they are either below or above the chemical potential. These considerations lead to an intuitive picture on localized (closed trajectories) and extended (percolating trajectories) states. We may consider the potential landscape like a real landscape where the trajectories are contour lines. Assume that we fill now water into such a landscape. The trajectories of the particles is restricted to the shore line. For small filling, we find lakes whose shores are closed and correspond to contour lines. They correspond to closed electron trajectories and represent localized electronic states. At very high water level, only the large mountains of the potential landscape would reach out of the water, forming islands in the sea. The coastlines again represent closed trajectories corresponding to localized electronic states. At some intermediate filling, a boundary between the lake and the island topology, there is a water level at which the coast lines become arbitrarily long and percolate through the whole landscape. Only these contour lines correspond to extended (non-localized) electron states. From this picture we conclude that when a Landau level of a system subject to a random potential is gradually filled, first all occupied state are localized (low filling). At some special intermediate filling level, the extended states are filled and contribute to the current transport. At higher chemical potential (filling) the states would be localized again. In the following argument, going back to Robert B. Laughlin, the presence of filled extended states plays an important role.

Laughlin's gauge argument

We consider a long rectangular Hall element that is deformed into a so-called *Corbino disc*, i.e. a circular disc with a hole in the middle as shown in Fig.4.7. The Hall element is threaded by a constant and uniform magnetic field B along the z -axis. In addition we can introduce an arbitrary flux Φ through the hole without influencing the uniform field in the disc. This flux is irrelevant for all localized electron trajectories since only extended (percolating) trajectories wind around the hole of the disc and by doing so receive an Aharonov-Bohm phase. When the

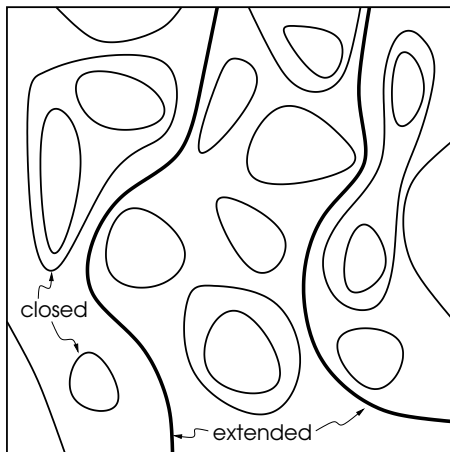


Figure 4.6: Contour plot of potential landscape. There are closed trajectories and extended percolating trajectories.

flux is increased adiabatically by $\delta\Phi$, the vector potential is changed according to

$$\mathbf{A} \rightarrow \mathbf{A} + \delta\mathbf{A} = \mathbf{A} + \nabla\chi,$$

which in our case means

$$(\delta A)_\varphi = \frac{\delta\Phi}{2\pi r}. \quad (4.51)$$

At the same time, the wave function acquires a phase factor

$$\psi \rightarrow \psi e^{ie\chi/\hbar c} = \psi e^{i(\delta\Phi/\Phi_0)\varphi}. \quad (4.52)$$

If the disc was translationally invariant, meaning that disorder is neglected and only extended states exist, we could use the wave functions $\psi_{0,m}$ from (4.43), so that $B\pi r_m^2 = m\Phi_0 + \delta\Phi$. The single-valuedness of the wave function implies that m has to be adjusted, $m \rightarrow m - \delta\Phi/\Phi_0$. This guarantees, that increasing Φ by one flux quantum leads to a decrease of m by 1. Hence, gauge invariance implies that the wave functions are shifted in their radius. This argument is also applicable to higher Landau levels.

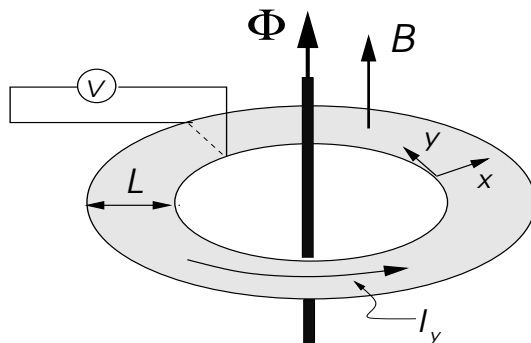


Figure 4.7: Corbino disk for Laughlin's argument. According to the Hall bar in Fig. 4.3, the radial (transverse) component of the Corbino disk is denoted by x , while the angular (longitudinal) component is termed as y . Both the homogeneous magnetic field B and the flux Φ point along the z -axis perpendicular to the plane of the disc.

Since this argument is topological in nature, it will not break down for independent electrons

when disorder is introduced. The transfer of one electron between neighboring extended states due to the change of Φ by Φ_0 leads to a net shift of one electron from the outer to the inner boundary. If an electric field E_x is applied in the radial direction (here denoted by x -direction, see Fig. 4.7), the transfer of this electron results in the energy change

$$\Delta\epsilon_V = -eE_x L \quad (4.53)$$

where L is the distance between the inner and the outer boundary of the Corbino disc. A further change in the electromagnetic energy

$$\Delta\epsilon_I = \frac{I_y \delta\Phi}{c}, \quad (4.54)$$

is caused by the constant current I_y (here the angular component is denoted by y , see Fig.4.7) in the disc when the magnetic flux is increased by $\delta\Phi$. Following the Aharonov-Bohm argument that the energy of the system is invariant under a flux change by integer multiples of Φ_0 , the two energies should compensate each other. Thus, setting $\delta\Phi = \Phi_0$ and demanding that $\Delta\epsilon_V + \Delta\epsilon_I = 0$ leads to

$$\sigma_H = \frac{j_y}{E_x} = \frac{I_y}{LE_x} = \frac{e^2}{h}. \quad (4.55)$$

We conclude from this argument, that each filled Landau level containing percolating states will contribute e^2/h to the total Hall conductivity. Hence, for $\nu_n \in \mathbb{N}_0$ filled levels the Hall conductivity is given by $\sigma_H = \nu_n e^2/h$. Note the importance of the topological nature of the Hall conductivity ensuring the universal character of the quantization.

Localized and extended states

The density of states of the two-dimensional electron gas (2DEG) in absence of an external magnetic field is given by

$$N_{\text{2DEG}}(E) = 2 \sum_{k_x, k_y} \delta\left(E - \frac{\hbar^2(k_x^2 + k_y^2)}{2m}\right) = \frac{L_x L_y m}{2\pi}, \quad (4.56)$$

with twice degenerate energy states for the spins, whereas for the Landau levels in a clean sample, we have

$$N_L(E) = \frac{L_x L_y}{2\pi\ell^2} \sum_{n,s} \delta(E - E_{n,s}). \quad (4.57)$$

Here the prefactor is given by the large degeneracy (4.9) of each Landau level.

According to our previous discussion, the main effect of a potential is to lift the degeneracy of the states comprising a Landau level. This remains true for random potential landscapes. Most of the states are then localized and do not contribute to electric transport. Only the few extended states contribute to the transport if they are filled (see Fig. 4.8). For partially filled extended states the Hall conductivity σ_H is not an integer multiple of e^2/h , since not all percolating states – necessary for transferring one electron from one edge to the other, when the flux is changed by Φ_0 (in Laughlin's argument) – are occupied. Thus, the charge transferred does not amount to a complete $-e$. The appearance of partially filled extended states marks the transition from one plateau to the next and is accompanied by a finite longitudinal conductivity σ_{yy} . When all extended states of a Landau level are occupied, the contribution to the longitudinal transport stops, i.e., in the range of a plateau σ_{yy} vanishes. Because of thermal occupation, the plateaus quickly shrink when the temperature of the system is increased. This is the reason why the Quantum Hall Effect is only observable for sufficiently low temperatures ($T < 4\text{K}$).

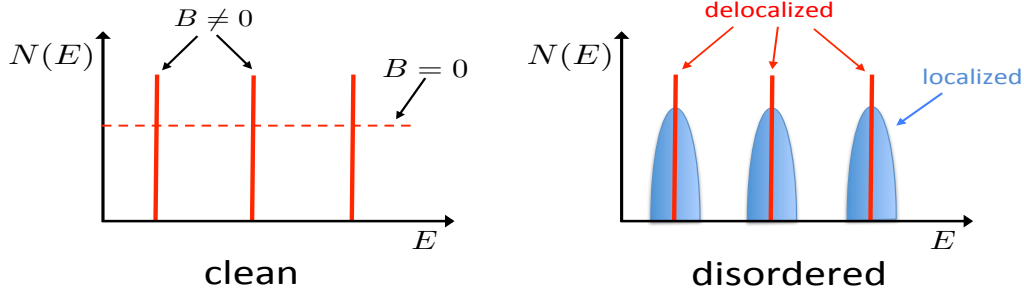


Figure 4.8: Density of states for the two-dimensional electron gas in three different cases. On the left panel, the system without and with applied magnetic field. Without magnetic field the density of states is flat (dashed line). If an external magnetic field is applied to a clean system, the Landau levels appear as infinitely sharp strongly degenerate peaks. The right panel visualizes the effect of disorder in the two-dimensional system with magnetic field; the Landau levels are spread and the density of state shows broadened peaks where most of the states are localized and only few states in the center percolate.

Edge states and Büttiker's argument

A confining potential prevents the electrons from leaving the metal. This potential at the edges of the sample has also to be considered in the potential landscape. Interestingly, equi-potential trajectories of states close to the edge are always extended and percolate along the edge. The corresponding wave functions have already been discussed in Section 4.2.1. From Eq.(4.38), we find that the energy is not symmetric in k_y , the wave vector along the edge, i.e. $E(k_y) \neq E(-k_y)$. This implies that the states are chiral and can move in one direction only for a given energy. The edge states on the opposing edges move in opposite directions, a fact that can be readily verified by inspection of (4.38) based on Fig.4.9. The total current flowing along the edge for a given Landau level is

$$I = \sum_{k_y} \frac{e}{L_y} v_y, \quad (4.58)$$

meaning that one state per k_y extends over the whole length L_y of the Hall element. Thus, the density is given by $1/L_y$. The wave vector is quantized according to the periodic boundary conditions; $k_y = 2\pi n_y/L_y$ with $n_y \in \mathbb{Z}$. The velocity v_y is given by equation (4.39). In summary, we have

$$I = \frac{e}{2\pi\hbar} \int_{\text{occupied}} dk_y \frac{dE_n(k_y)}{dk_y} = \frac{e}{h} \int_{\text{occupied}} dx_0 \frac{dE}{dx_0} = \frac{e}{h} (\mu - E_n^{(0)}) \quad (4.59)$$

where $x_0 = k_y \ell^2$ is the transversal position of the wave function and μ is the chemical potential. Sufficiently far away from the boundary E_n is independent of x_0 and approaches the value $E_n^{(0)} = \hbar\omega_c(1/2 + n)$ of a translationally invariant electron gas. The potential difference between the two opposing edges leads to a net current along the edge direction of the Hall bar,

$$\mu_A - \mu_B = eV_H = eE_x L_x = \frac{h}{e} (I_A + I_B) = \frac{h}{e} I_H, \quad (4.60)$$

and with that

$$\sigma_H = \frac{I_H}{E_x L_x} = \frac{e^2}{h}, \quad (4.61)$$

where for $\mu_A = \mu_B$ we have $I_A = -I_B$. Note that $I_H = I_A + I_B$ is only valid when no currents are present in the bulk of the system. The latter condition is ensured by the localization of the states at the chemical potential. This argument by Büttiker leads to the same quantization as derived before, namely every Landau level contributes one edge state and thus $\sigma_H = \nu_n e^2/h$ (ν_n is the number of occupied Landau levels). Note that this argument is independent of the precise shape of the confining edge potential.

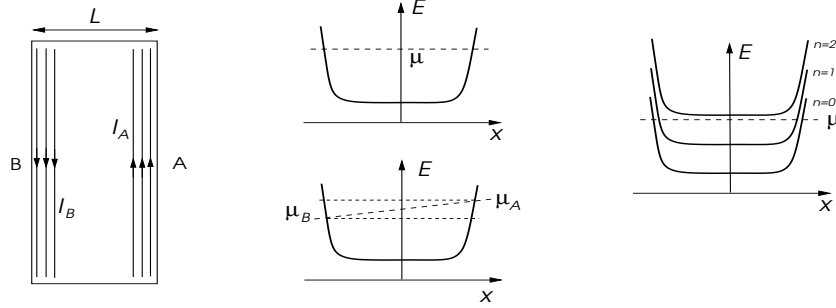


Figure 4.9: Edge state picture by Büttiker. The left panel gives a top view of the two dimensional system ($L = L_x$) where chiral edge states exist on both edges of the Hall bar with opposite chirality. On the middle panel, a single Landau level without and with transverse potential difference is shown, where the latter yields a finite net current due to current imbalance between left and right edge. The right panel visualizes the two lowest Landau levels which are occupied. All higher Landau levels are empty. This fixes the Hall conductance value ν_n to 2.

Within this argument we are able to understand why the longitudinal conductivity has to vanish at the Hall plateaus. For that we express Ohm's law. However it is simpler to discuss the resistivity. Like the conductivity $\hat{\sigma}$ the resistivity $\hat{\rho}$ is a tensor:

$$\mathbf{j} = \hat{\sigma} \mathbf{E} \quad (4.62)$$

$$\mathbf{E} = \hat{\rho} \mathbf{j} \quad (4.63)$$

where the conductivity $\hat{\sigma}$ and the resistivity $\hat{\rho}$ are both 2×2 tensors with $\sigma_{xx} = \sigma_{yy}$ ($\rho_{xx} = \rho_{yy}$) and $\sigma_{xy} = -\sigma_{yx}$ ($\rho_{xy} = -\rho_{yx}$). Therefore, we find

$$\sigma_{yy} = \frac{\rho_{yy}}{\rho_{yy}^2 + \rho_{xy}^2}, \quad (4.64)$$

$$\sigma_{xy} = \frac{\rho_{xy}}{\rho_{yy}^2 + \rho_{xy}^2}. \quad (4.65)$$

In the following argument, we explain why the longitudinal resistivity ρ_{yy} in two dimensions has to vanish in the presence of a finite Hall resistivity ρ_{xy} . Since the edge state electrons with a given energy can only move in one direction, there is no backward scattering by obstacles as long as the edges are far apart from each other. No scattering between the two edges implies $\rho_{yy} = 0$ and hence $\sigma_{yy} = 0$. A finite resistivity can only occur when extended states are present in the bulk, such that the edge states on opposite edges are no longer spatially separated from each other.

4.2.3 Fractional Quantum Hall Effect

Only two years after the discovery of the Integer Quantum Hall Effect, Störmer, Tsui and Gossard observed further series of plateaus of the Hall resistivity in a 2DEG realized with very high quality MOSFET inversion layers at low temperatures. The most pronounced of these

plateaus is observed at a filling of $\nu = 1/3$ ($\sigma_{xy} = \nu e^2/h$). Later, an entire hierarchy of plateaus at fractional values $\nu = \nu_{p,m} = p/m$ with $p, m \in \mathbb{N}$ has been discovered,

$$\nu_{p,m} \in \left\{ \frac{1}{3}, \frac{2}{3}, \frac{2}{5}, \frac{3}{5}, \frac{3}{7}, \dots \right\}. \quad (4.66)$$

The emergence of these new plateaus is a clear evidence of the so-called Fractional Quantum Hall Effect (FQHE).

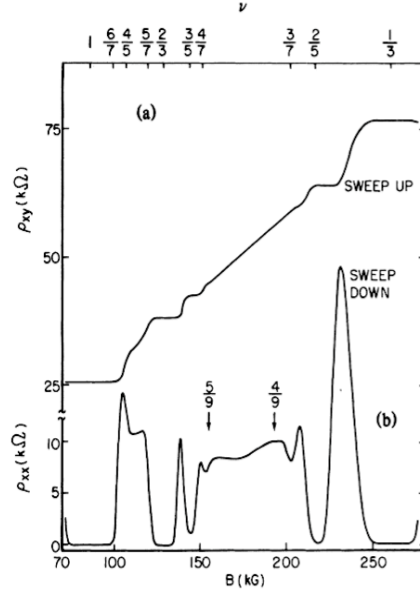


Figure 4.10: Experimental evidence of the Fractional Quantum Hall Effect.

It was again Laughlin who found the key concept to explain the FQHE. Unlike the IQHE, this new quantization feature can not be understood from a single-electron picture, but is based on the Coulomb repulsion among the electrons and the accompanying correlation effects. Laughlin specially investigated the case $\nu_{p,m} = 1/3$ and made the Ansatz

$$\Psi_{1/m}(z_1, \dots, z_N) \propto \prod_{i < j} (z_i - z_j)^m \exp \left(- \sum_i \frac{|z_i|^2}{4\ell^2} \right) \quad (4.67)$$

for the N -body wave function, where $z = x - iy$ is a complex number representing the coordinates of the two-dimensional system. Limiting ourselves to the consideration of the lowest Landau level, this state gives a stable plateau with $\sigma_H = (1/3)e^2/h$, when $m = 3$.

A heuristic interpretation of the Laughlin state was proposed by J. K. Jain and it is based on the concept of so-called composite fermions. In fact, Laughlin's state (4.67) can be written as

$$\Psi_{1/m} = \prod_{i < j} (z_i - z_j)^{m-1} \Psi_S \quad (4.68)$$

where Ψ_S is the Slater determinant⁷ describing the completely filled lowest Landau level. We see that the prefactor of Ψ_S in equation (4.68) acts as a so-called *Jastrow factor* that introduces

⁷The *Slater determinant* of the lowest Landau level is obtained from the states of the independent electrons. In symmetric gauge, the states are labelled by the quantum number $\tilde{m} \in \mathbb{N}_0$ and apart from the normalization (given in equation (4.43)) they are given by

$$\phi_{\tilde{m}}(z) = z^{\tilde{m}} e^{-|z|^2/4\ell^2}, \quad (4.69)$$

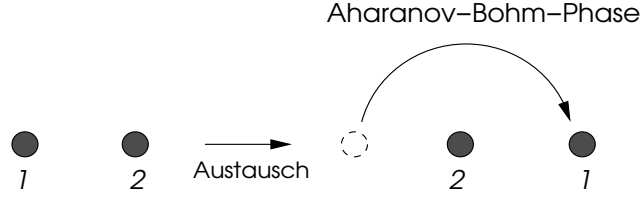


Figure 4.11: Exchange of two particles in two dimensions involves the motion of the particles around each other. There are two topologically distinct paths.

correlation effects into the wave function, since only the correlations due to the Pauli exclusion principle are contained in Ψ_S . The Jastrow factor treats the Coulomb repulsion among the electrons and consequently leads to an additional suppression of the wave function whenever two electrons approach each other. In the form introduced above, it produces an phase factor for the electrons encircling each other. In particular, exchanging two electrons (see Fig. 4.11) leads to a phase

$$\exp(i(m-1)\pi) = \exp\left(i\frac{e}{\hbar c}\frac{m-1}{2}\Phi_0\right), \quad (4.73)$$

since $\Phi_0 = 2\pi\hbar c/e$. This phase has to be unity since the Slater state Ψ_S is odd under exchange of two electrons. Therefore m is restricted to odd integer values. This guarantees that the total wave function $\Psi_{1/m}$ still changes sign when two electrons are exchanged.

According to the Footnote 6 (see equation (4.40)), the case $\nu_{p,m} = 1/3$ implies that there are three flux quanta Φ_0 per electron. In order to understand the FQHE, one constructs so-called *composite fermions* which do not interact with each other. Here, a composite fermion consists of an electron that has two (in fact $m-1$) negative flux quanta attached to it. These objects may be considered as independent fermions since the attached flux quanta compensate the Jastrow factor in equation 4.68 through factors of the type $(z_i - z_j)^{-(m-1)}$. The exchange of two such composite fermions in two dimensions leads to an Aharonov-Bohm phase that is just opposed to that in equation (4.73). Due to the presence of the flux $-2\Phi_0$ per electron, the composite fermions are subject to an effective field composed of the external field and the attached flux

where $z = x - iy$. The Slater determinant for N independent electrons is

$$\Psi_S(z_1, \dots, z_N) = \frac{1}{\sqrt{N!}} \det \begin{bmatrix} \phi_0(z_1) & \dots & \phi_{N-1}(z_1) \\ \vdots & & \vdots \\ \phi_0(z_N) & \dots & \phi_{N-1}(z_N) \end{bmatrix} \quad (4.70)$$

$$= \frac{1}{\sqrt{N!}} \det \begin{bmatrix} 1 & z_1 & z_1^2 & \dots & z_1^{N-1} \\ 1 & z_2 & z_2^2 & \dots & z_2^{N-1} \\ \vdots & \vdots & \vdots & & \vdots \\ 1 & z_N & z_N^2 & \dots & z_N^{N-1} \end{bmatrix} \exp\left(-\sum_i \frac{|z_i|^2}{4\ell^2}\right). \quad (4.71)$$

The remaining determinant is a so-called *Vandermonde determinant*, which can be reexpressed in the form of a product, such that

$$\Psi_S = \prod_{i < j} (z_i - z_j) \exp\left(-\sum_i \frac{|z_i|^2}{4\ell^2}\right). \quad (4.72)$$

The prefactor is a homogenous polynomial with roots whenever $z_i = z_j$, which is a manifestation of the Pauli exclusion principle. We also see that the state Ψ_S has a well defined total angular momentum $L_z = N\hbar$.

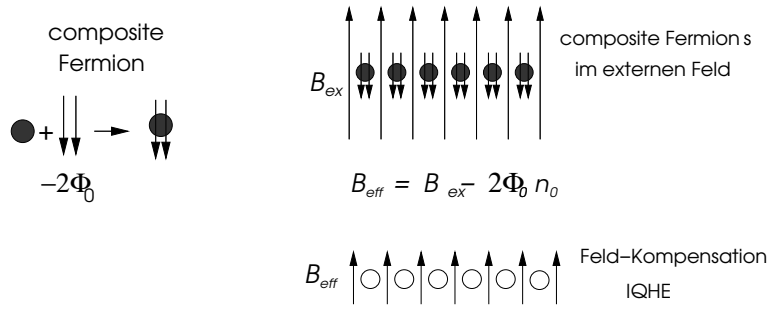


Figure 4.12: Sketch of the composite Fermion concept. Electrons with attached magnetic flux lines, here for the state of $\nu = 1/3$.

quanta:

$$B_{\text{eff}} = B - \sum_i 2\Phi_0(z_i) \quad (4.74)$$

$$= \frac{1}{3}B - \left(\sum_i 2\Phi_0(z_i) - \frac{2}{3}B \right) \quad (4.75)$$

For an external field $B = 3n_0\Phi_0$, the expression in the brackets of equation (4.75) vanishes and the composite fermions feel an effective field $B_{\text{eff}} = n_0\Phi_0$ (Fig. (4.12)). Thus, these fermions form an Integer Quantum Hall state with $\nu = 1$ (for $B = 3n_0\Phi_0$), as discussed previously. This way of interpretation is applicable to other Fractional Quantum Hall states, too, since for n filled Landau levels with composite fermions consisting of an electron with an attached flux of $-2k\Phi_0$, the effective field reads

$$B_{\text{eff}} = n_0 \frac{\Phi_0}{\nu_{p,m}} - 2kn_0\Phi_0 = n_0 \frac{\Phi_0}{n}. \quad (4.76)$$

From this we infer, that

$$\frac{1}{n} + 2k = \frac{1}{\nu_{p,m}} \quad (4.77)$$

or equivalently

$$\nu_{p,m} = \frac{p}{m} = \frac{n}{2kn + 1}. \quad (4.78)$$

Despite the apparent simplicity of the treatment in terms of independent composite fermions, one should keep in mind that one is dealing with a strongly correlated electron system. The structure of the composite fermions is a manifestation of the fact that the fermions are not independent electrons. No composite fermions can exist in the vacuum, they can only arise within a certain many-body state. The Fractional Quantum Hall state also exhibits unconventional excitations with fractional charges. For example in the case $\nu_{p,m} = 1/3$, there are excitations with effective charge $e^* = e/3$. These are so-called 'topological' excitations, that can only exist in correlated systems. The Fractional Quantum Hall system is a very peculiar 'ordered' state of a two-dimensional electron system that has many interesting and complex properties.⁸

⁸Additional literature on the quantum Hall effects. For the Integer quantum Hall effect consult

- K. von Klitzing et al., Physik Journal **4** (6), 37 (2005)

while detailed literature on the fractional quantum Hall effect is found in

- R. Morf, Physik in unserer Zeit **33**, 21 (2002)

- J.K. Jain, Advances in Physics **41**, 105 (1992).

Chapter 5

Landau's Theory of Fermi Liquids

In the previous chapters, we considered the electrons of the system as more or less independent particles. The effect of their mutual interactions only entered via the renormalization of potentials and collective excitations. The underlying assumptions of our earlier discussions were that electrons in the presence of interactions can still be described as particles with a well-defined energy-momentum relation, and that their groundstate is a filled Fermi sea with a sharp Fermi surface. Since there is no guarantee that this hypothesis holds in general (and in fact they do not), we have to show that in metals the description of electrons as quasiparticles is justified. This quasiparticle picture will lead us to Landau's phenomenological theory of Fermi liquids.

5.1 Lifetime of quasiparticles

We first consider the lifetime of a state consisting of a filled Fermi sea to which one electron is added. Let \mathbf{k} with $|\mathbf{k}| > k_F$ ($\epsilon_{\mathbf{k}} = \hbar^2 \mathbf{k}^2 / 2m$ with $\epsilon_{\mathbf{k}} > \epsilon_F$) be the momentum (energy) of the additional electron. Due to interactions between the electrons, this state will decay into a many-body state. In momentum space such an interaction takes the form

$$\mathcal{H}_{ee} = \sum_{\mathbf{k}, \mathbf{k}', \mathbf{q}} \sum_{s, s'} V(\mathbf{q}) \hat{c}_{\mathbf{k}-\mathbf{q}, s}^\dagger \hat{c}_{\mathbf{k}', s'}^\dagger \hat{c}_{\mathbf{k}', s'} \hat{c}_{\mathbf{k}, s}, \quad (5.1)$$

where $V(\mathbf{q})$ represents the electron-electron interaction in momentum space while \mathbf{q} indicates the momentum transfer in the scattering process. Below, the short-ranged Yukawa potential

$$V(\mathbf{q}) = \frac{4\pi e^2}{q^2 \epsilon(\mathbf{q}, 0)} = \frac{4\pi e^2}{q^2 + k_{TF}^2} \quad (5.2)$$

from equation (3.94) will be used. As we are only interested in very small energy transfers $\hbar\omega \ll \epsilon_F$, the static approximation is admissible.

In a perturbative treatment, the lowest order effect of the interaction is the creation of a particle-hole excitation in addition to the single electron above the Fermi energy. As the additional electron changes its momentum from \mathbf{k} to $\mathbf{k} - \mathbf{q}$, a hole appears at \mathbf{k}' and a second electron with wavevector $\mathbf{k}' + \mathbf{q}$ is created outside the Fermi sea. The transition is allowed whenever both energy and momentum are conserved, meaning

$$\mathbf{k} = (\mathbf{k} - \mathbf{q}) - \mathbf{k}' + (\mathbf{k}' + \mathbf{q}), \quad (5.3)$$

and

$$\epsilon_{\mathbf{k}} = \epsilon_{\mathbf{k}-\mathbf{q}} - \epsilon_{\mathbf{k}'} + \epsilon_{\mathbf{k}'+\mathbf{q}}. \quad (5.4)$$

We calculate the lifetime $\tau_{\mathbf{k}}$ of the initial state with momentum \mathbf{k} using Fermi's golden rule, yielding the transition rate from the initial state of a filled Fermi sea and one particle with

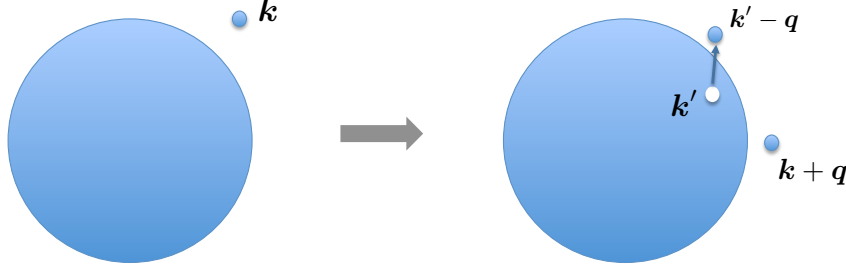


Figure 5.1: The decay of an electron state above the Fermi energy happens through scattering by creating particle-hole excitations.

momentum \mathbf{k} to a state with two electrons above the Fermi sea, with momenta $\mathbf{k} - \mathbf{q}$ and $\mathbf{k}' + \mathbf{q}$, and a hole with \mathbf{k}' , as shown in Fig. 5.1. Since neither the momenta \mathbf{k}' and \mathbf{q} , nor the spin of the created electron are fixed, a summation over the possible configuration has to be performed, leading to

$$\frac{1}{\tau_{\mathbf{k}}} = \frac{2\pi}{\hbar} \frac{1}{\Omega^2} \sum_{\mathbf{k}', \mathbf{q}} \sum_{s'} |V(\mathbf{q})|^2 n_{0, \mathbf{k}'} (1 - n_{0, \mathbf{k} - \mathbf{q}}) (1 - n_{0, \mathbf{k}' + \mathbf{q}}) \delta(\epsilon_{\mathbf{k} - \mathbf{q}} - \epsilon_{\mathbf{k}} - (\epsilon_{\mathbf{k}'} - \epsilon_{\mathbf{k}' + \mathbf{q}})). \quad (5.5)$$

Note that the term $n_{0, \mathbf{k}'} (1 - n_{0, \mathbf{k} - \mathbf{q}}) (1 - n_{0, \mathbf{k}' + \mathbf{q}})$ takes care of the Pauli principle, by ensuring that the final state after the scattering process exists, i.e. the hole state \mathbf{k}' lies inside and the two particle states $\mathbf{k} - \mathbf{q}$ and $\mathbf{k}' + \mathbf{q}$ lie outside the Fermi sea. First the integral over \mathbf{k}' is performed under the condition that the energy $\epsilon_{\mathbf{k}' + \mathbf{q}} - \epsilon_{\mathbf{k}'}$ of the excitation is small. With that, the integral reduces to

$$S(\omega_{\mathbf{q}, \mathbf{k}}, q) = \frac{1}{\Omega} \sum_{\mathbf{k}'} n_{0, \mathbf{k}'} (1 - n_{0, \mathbf{k}' + \mathbf{q}}) \delta(\epsilon_{\mathbf{k} - \mathbf{q}} - \epsilon_{\mathbf{k}} - (\epsilon_{\mathbf{k}'} - \epsilon_{\mathbf{k}' + \mathbf{q}})) \quad (5.6)$$

$$= \frac{1}{(2\pi)^3} \int d^3 k' n_{0, \mathbf{k}'} (1 - n_{0, \mathbf{k}' + \mathbf{q}}) \delta(\epsilon_{\mathbf{k}' + \mathbf{q}} - \epsilon_{\mathbf{k}'} - \hbar\omega_{\mathbf{q}, \mathbf{k}}) \quad (5.7)$$

$$= \frac{N(\epsilon_F)}{4} \frac{\omega_{\mathbf{q}, \mathbf{k}}}{qv_F} \quad (5.8)$$

where $N(\epsilon_F) = mk_F/\pi^2\hbar^2$ is the density of states of the electrons at the Fermi surface and $\hbar\omega_{\mathbf{q}, \mathbf{k}} = \hbar^2(2\mathbf{k} \cdot \mathbf{q} - q^2)/2m > 0$ is the energy loss of the decaying electron.¹ In order to compute the remaining integral over \mathbf{q} , we assume that the matrix element $|V(\mathbf{q})|^2$ depends only weakly on \mathbf{q} when $q \ll k_F$. This is especially true when the interaction is short-ranged. In spherical

¹Small ω are justified, because $\hbar\omega \leq (2k_F q - q^2)/2m$ for most allowed ω . The integral may be computed using cylindrical coordinates, where the vector \mathbf{q} points along the axis of the cylinder. It results in

$$S(\mathbf{q}, \omega) = \frac{1}{(2\pi)^2} \int_{k_2}^{k_1} dk_{\perp} k'_{\perp} \int_0^{k_F} dk'_{\parallel} \delta\left(\frac{\hbar^2 q^2}{2m} + \frac{\hbar^2 q k'_{\parallel}}{m} - \hbar\omega\right) \quad (5.9)$$

$$= \frac{m}{4\pi^2 \hbar^2 q} (k_1^2 - k_2^2), \quad (5.10)$$

with $k_1^2 = k_F^2 - k_{\parallel,0}^2$ and $k_2^2 = k_F^2 - (k_{\parallel,0} + q)^2$, where $k_{\parallel,0} = (2m\omega - \hbar q^2)/2\hbar q$ is enforced by the delta function.

coordinates, the integral reads

$$\frac{1}{\tau_{\mathbf{k}}} = \frac{2\pi}{\hbar} \cdot \frac{N(\epsilon_F)}{4v_F\Omega} \sum_{\mathbf{q}, s'} |V(\mathbf{q})|^2 \frac{\omega_{\mathbf{q}, \mathbf{k}}}{q} \quad (5.11)$$

$$= \frac{N(\epsilon_F)}{(2\pi)^2 2\hbar v_F} \int d^3\mathbf{q} |V(\mathbf{q})|^2 \frac{\omega_{\mathbf{q}, \mathbf{k}}}{q} \quad (5.12)$$

$$= \frac{N(\epsilon_F)}{(2\pi)4mv_F} \int dq |V(q)|^2 q^2 \int_{\theta_1}^{\theta_2} d\theta \sin\theta (2k \cos\theta - q) \quad (5.13)$$

$$= \frac{N(\epsilon_F)}{(2\pi)4mv_F} \int dq |V(q)|^2 q^2 \left[-\frac{1}{4k} (2k \cos\theta - q)^2 \right]_{\theta_1}^{\theta_2}. \quad (5.14)$$

The restriction of the domain of integration of θ follows from the two conditions $k^2 \geq (\mathbf{k} - \mathbf{q})^2 \geq k_F^2$ and $(\mathbf{k} - \mathbf{q})^2 = k^2 - 2kq \cos\theta + q^2$. From the first condition, $\cos\theta_2 = q/2k$, and from the second, $\cos\theta_1 = (k^2 - k_F^2 + q^2)/2kq$. Thus,

$$\frac{1}{\tau_{\mathbf{k}}} = \frac{N(\epsilon_F)}{(2\pi)4mv_F} \int dq |V(q)|^2 \frac{1}{4k} (k^2 - k_F^2)^2 \quad (5.15)$$

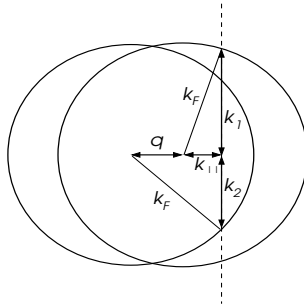
$$\approx \frac{N(\epsilon_F)}{(2\pi)4v_F} \frac{m}{k_F} \frac{1}{\hbar^4} (\epsilon_{\mathbf{k}} - \epsilon_F)^2 \int dq |V(q)|^2 \quad (5.16)$$

$$= \frac{1}{8\pi\hbar^3} \frac{N(\epsilon_F)}{v_F^2} (\epsilon_{\mathbf{k}} - \epsilon_F)^2 \int dq |V(q)|^2. \quad (5.17)$$

Note that convergence of the last integral over q requires that the integrand does not diverge stronger than q^α ($\alpha < 1$) for $q \rightarrow 0$. With the dielectric constant obtained in the previous chapter, this condition is certainly fulfilled. Essentially, the result states that

$$\frac{1}{\tau_{\mathbf{k}}} \propto (\epsilon_{\mathbf{k}} - \epsilon_F)^2 \quad (5.18)$$

for \mathbf{k} slightly above the Fermi surface. This implies that the state $|\mathbf{k}s\rangle$ occurs as a resonance of width $\hbar/\tau_{\mathbf{k}}$ and features a quasiparticle, which can be observed in the spectral function $A(E, \mathbf{k})$ as depicted in Fig.5.2.² The quasiparticle (coherent) part of the spectral function has a weight reduced from one (corresponding to the quasiparticle weight $Z_{\mathbf{k}}$). The remaining weight is shifted to higher energies as a so-called incoherent part (continuum without clear momentum-energy relation).



The wave vectors k_2 and k_1 are the upper and lower limits of integration determined from the condition $n_{0, \mathbf{k}'}(1 - n_{0, \mathbf{k}'+\mathbf{q}}) > 0$ and can be obtained by simple geometric considerations. equation (5.8) follows immediately.

²The spectral function is defined as

$$A(E, \mathbf{k}) \propto \sum_n |\langle \Psi_n | \hat{c}_{\mathbf{k}s} | \Psi_0 \rangle|^2 \delta(E - E_n) \quad (5.19)$$

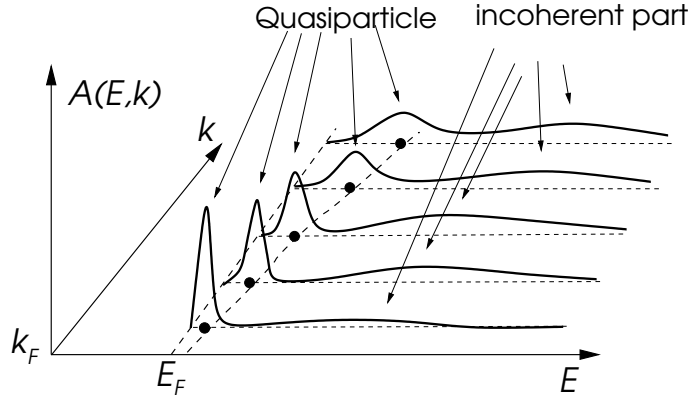


Figure 5.2: Quasiparticle spectrum: Quasiparticle peaks appear the sharper the closer the energy lies to the Fermi energy. The area under the “sharp” quasiparticle peak corresponds to the quasiparticle weight. The missing quasiparticle weight is transferred to higher energies.

The resonance becomes arbitrarily sharp as the Fermi surface is approached

$$\lim_{k \rightarrow k_F} \frac{\hbar/\tau_{\mathbf{k}}}{\epsilon_{\mathbf{k}} - \epsilon_F} = 0, \quad (5.21)$$

so that the quasiparticle concept is asymptotically valid. The equation (5.21) can also be seen as a verification of Heisenberg’s uncertainty principle. Consequently, the momentum of an electron is a good quantum number in the vicinity of the Fermi surface. Underlying this result is the Pauli exclusion principle, which restricts the phase space for decay processes of single particle states close to the Fermi surface. In addition, the assumption of short ranged interactions is crucial. Long ranged interactions can change the behavior drastically due to the larger number of decay channels.

5.2 Phenomenological Theory of Fermi Liquids

The existence of well-defined fermionic quasiparticles in spite of the underlying complex many-body physics inspired Landau to the following phenomenological theory. Just like the states of independent electrons, quasiparticle states shall be characterized by their momentum \mathbf{k} and spin σ . In fact, there is a one-to-one mapping between the free electrons and the quasiparticles. Consequently, the number of quasiparticles and the number of electrons coincide. The momentum distribution function of quasiparticles, defined as $n_{\sigma}(\mathbf{k})$, is subject to the condition

$$N = \sum_{\mathbf{k}, \sigma} n_{\sigma}(\mathbf{k}). \quad (5.22)$$

In analogy to the Fermi-Dirac distribution of free electrons, one demands, that the ground state distribution function $n_{\sigma}^{(0)}(\mathbf{k})$ for the quasiparticles is described by a simple step function

$$n_{\sigma}^{(0)}(\mathbf{k}) = \Theta(k_F - |\mathbf{k}|). \quad (5.23)$$

where $|\Psi_0\rangle$ is the exact (renormalized) ground state and $|\Psi_n\rangle$ are the corresponding exact excited states. The coherent part of the spectral function can be represented as a Lorentzian form

$$A_{\text{coh}}(E, \mathbf{k}) = \frac{Z_{\mathbf{k}} \hbar}{\pi \tau_{\mathbf{k}}} \frac{1}{(E - \tilde{\epsilon}_{\mathbf{k}})^2 + \frac{\hbar^2}{\tau_{\mathbf{k}}^2}}, \quad (5.20)$$

where $Z_{\mathbf{k}}$ is the quasiparticle weight, smaller than 1.

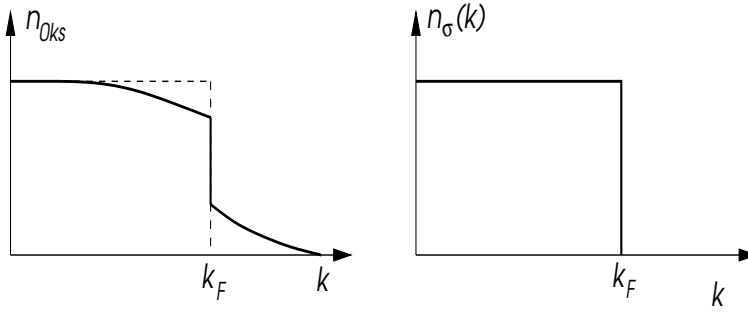


Figure 5.3: Schematic picture of the distribution function: Left panel: modified distribution function of the original electron states; right panel: distribution function of quasiparticle states making a simple step function.

For a spherically symmetric electron system, the quasiparticle Fermi surface is a sphere with the same radius as the one for free electrons of the same density. For a general point group symmetry, the Fermi surface may be deformed by the interactions without changing the underlying symmetry. The volume enclosed by the Fermi surface is always conserved despite the deformation.³ Note that the distribution $n_{\sigma}^{(0)}(\mathbf{k})$ of the quasiparticles in the ground state and that $n_{0\mathbf{k}s} = \langle \hat{c}_{\mathbf{k}\sigma}^{\dagger} \hat{c}_{\mathbf{k}\sigma} \rangle$ of the real electrons in the ground state are not identical (Figure 5.3). Interestingly, $n_{0\mathbf{k}s}$ is still discontinuous at the Fermi surface, but the height of the jump is, in general, smaller than unity. The modification of the electron distribution function from a step function to a “smoother” Fermi surface indicates the involvement of electron-hole excitations and the renormalization of the electronic properties, which deplete the Fermi sea and populate the states above the Fermi level. The reduced jump in $n_{0\mathbf{k}s}$ is a measure for the quasiparticle weight at the Fermi surface, $Z_{\mathbf{k}_F}$, i.e. the amplitude of the corresponding free electron state in the quasiparticle state.

In Landau’s theory of Fermi liquids, the essential information on the low-energy physics of the system shall be contained in the deviation of the quasiparticle distribution $n_{\sigma}(\mathbf{k})$ from its ground state distribution $n_{\sigma}^{(0)}(\mathbf{k})$,

$$\delta n_{\sigma}(\mathbf{k}) = n_{\sigma}(\mathbf{k}) - n_{\sigma}^{(0)}(\mathbf{k}). \quad (5.24)$$

The symbol δ is generally used in literature to denote this difference. Unfortunately this may suggest that the term $\delta n_{\sigma}(\mathbf{k})$ is small, which is not true in general. Indeed, $\delta n_{\sigma}(\mathbf{k})$ is concentrated on momenta \mathbf{k} very close to the Fermi energy only, where the quasiparticle concept is valid. This distribution function, describing the deviation from the ground state, enters a phenomenological energy functional of the form

$$E = E_0 + \sum_{\mathbf{k},\sigma} \epsilon_{\sigma}(\mathbf{k}) \delta n_{\sigma}(\mathbf{k}) + \frac{1}{2\Omega} \sum_{\mathbf{k},\mathbf{k}'} \sum_{\sigma,\sigma'} f_{\sigma\sigma'}(\mathbf{k},\mathbf{k}') \delta n_{\sigma}(\mathbf{k}) \delta n_{\sigma'}(\mathbf{k}') + O(\delta n^3) \quad (5.25)$$

where E_0 denotes the energy of the ground state. Moreover, the phenomenological parameters $\epsilon_{\sigma}(\mathbf{k})$ and $f_{\sigma\sigma'}(\mathbf{k},\mathbf{k}')$ have to be determined by experiments or by means of a microscopic theory. The variational derivative

$$\tilde{\epsilon}_{\sigma}(\mathbf{k}) = \frac{\delta E}{\delta n_{\sigma}(\mathbf{k})} = \epsilon_{\sigma}(\mathbf{k}) + \frac{1}{\Omega} \sum_{\mathbf{k}',\sigma'} f_{\sigma\sigma'}(\mathbf{k},\mathbf{k}') \delta n_{\sigma'}(\mathbf{k}') \quad (5.26)$$

yields an effective energy-momentum relation $\tilde{\epsilon}_{\sigma}(\mathbf{k})$, whose second term depends on the distribution of all quasiparticles. A quasiparticle moves in the “mean-field” of all other quasiparticles, so

³This is the content of the Luttinger theorem [J.M. Luttinger, Phys. Rev. **119**, 1153 (1960)].

that changes $\delta n_\sigma(\mathbf{k})$ in the distribution affect $\tilde{\epsilon}_\sigma(\mathbf{k})$. The second variational derivative describes the coupling between the quasiparticles

$$\frac{\delta^2 E}{\delta n_\sigma(\mathbf{k})\delta n_{\sigma'}(\mathbf{k}')} = \frac{1}{\Omega} f_{\sigma\sigma'}(\mathbf{k}, \mathbf{k}'). \quad (5.27)$$

We introduce a parametrization for these couplings $f_{\sigma\sigma'}(\mathbf{k}, \mathbf{k}')$ by assuming spherical symmetry of the system. Furthermore, the radial dependence is ignored, as we only consider quasiparticles in the vicinity of the Fermi surface where $|\mathbf{k}|, |\mathbf{k}'| \approx k_F$. Therefore the dependence of $f_{\sigma\sigma'}(\mathbf{k}, \mathbf{k}')$ on \mathbf{k}, \mathbf{k}' can be reduced to the relative angle $\theta_{\hat{k}, \hat{k}'}$

$$f_{\sigma\sigma'}(\mathbf{k}, \mathbf{k}') = f^s(\hat{k}, \hat{k}') + \sigma\sigma' f^a(\hat{k}, \hat{k}') \quad (5.28)$$

where $\hat{k} = \mathbf{k}/|\mathbf{k}|$. The symmetric (s) and antisymmetric (a) part of $f_{\sigma\sigma'}(\mathbf{k}, \mathbf{k}')$ can be expanded in Legendre-polynomials $P_l(z)$ ⁴, leading to

$$f^{s,a}(\hat{k}, \hat{k}') = \sum_{l=0}^{\infty} f_l^{s,a} P_l(\cos \theta_{\hat{k}, \hat{k}'}). \quad (5.31)$$

The density of states at the Fermi surface is defined as

$$N(\epsilon_F) = \frac{2}{\Omega} \sum_{\mathbf{k}} \delta(\epsilon(\mathbf{k}) - \epsilon_F) = \frac{k_F^2}{\pi^2 \hbar v_F} = \frac{m^* k_F}{\pi^2 \hbar^2} \quad (5.32)$$

and follows from the dispersion $\epsilon(\mathbf{k})$ of the bare quasiparticle energy

$$\nabla_{\mathbf{k}} \epsilon(\mathbf{k})|_{\mathbf{k}_F} = \mathbf{v}_F = \frac{\hbar \mathbf{k}_F}{m^*} \quad (5.33)$$

where for a fully rotation symmetric system we may write $\epsilon(\mathbf{k}) = \hbar^2 \mathbf{k}^2 / 2m^*$ with m^* as an "effective mass", although we will be only interested at the spectrum in the immediate vicinity of the Fermi energy. With this definition, we also introduce the so-called *Landau parameters*

$$F_l^s = N(\epsilon_F) f_l^s, \quad (5.34)$$

$$F_l^a = N(\epsilon_F) f_l^a, \quad (5.35)$$

commonly used in the literature.⁵ In the following, we want to study the relation between the different phenomenological parameters of Landau's theory of Fermi liquids and the experimentally accessible quantities of a real system, such as specific heat, compressibility, spin susceptibility among others.

5.2.1 Specific heat - Density of states

Since the quasiparticles are fermions, they obey Fermi-Dirac statistics

$$n_\sigma^{(0)}(T, \mathbf{k}) = \frac{1}{e^{[\tilde{\epsilon}(\mathbf{k}) - \mu]/k_B T} + 1} \quad (5.36)$$

⁴*Legendre-Polynomials:* The Legendre polynomials satisfy the orthogonality relation

$$\int \frac{d\Omega_k}{4\pi} P_l(\cos \theta_k) P_{l'}(\cos \theta_k) = \int_{-1}^{+1} \frac{dz}{2} P_l(z) P_{l'}(z) = \frac{\delta_{ll'}}{2l+1} \quad (5.29)$$

for all $l = 0, 1, 2, \dots$. The first few polynomials are

$$P_0(z) = 1, \quad P_1(z) = z, \quad P_2(z) = \frac{1}{2}(3z^2 - 1), \quad P_3(z) = \frac{1}{2}(5z^3 - 3z). \quad (5.30)$$

⁵Another frequently used notation for the Landau parameters in the literature is $F_l = F_l^s$ and $Z_l = F_l^a$.

with the chemical potential μ . For low temperatures, we find

$$\delta n_\sigma(\mathbf{k}) = n_\sigma^{(0)}(T, \mathbf{k}) - n_\sigma^{(0)}(0, \mathbf{k}) \quad (5.37)$$

which, using Eq.(5.26) leads to $\tilde{\epsilon}(\mathbf{k}) = \epsilon(\mathbf{k})$, because here

$$\frac{1}{\Omega} \sum_{\mathbf{k}', \sigma'} f_{\sigma\sigma'}(\mathbf{k}, \mathbf{k}') \delta n_{\sigma'}(\mathbf{k}') = 0. \quad (5.38)$$

In $\delta n_{\sigma'}(\mathbf{k}')$ there are as many particles (positive) as holes (negative) such that they cancel in the correction term. Therefore we rewrite the Fermi-Dirac distribution (5.36) as

$$n_\sigma(\mathbf{k}) = \frac{1}{e^{[\epsilon(\mathbf{k}) - \epsilon_F]/k_B T} + 1} \quad (5.39)$$

with the bare quasiparticle energy $\epsilon_\sigma(\mathbf{k})$ in place of the renormalized dispersion $\tilde{\epsilon}_\sigma(\mathbf{k})$. Furthermore, we replaced $\mu = \epsilon_F + O(T^2)$ by ϵ_F . When focussing on leading terms, which are usually of the order T^0 and T^1 , corrections of higher order may be neglected in the low-temperature regime. In order to discuss the specific heat, we employ the expression for the entropy of a fermion gas. For each quasiparticles with a given spin there is one state labelled by \mathbf{k} . The entropy density may be computed from the distribution function

$$S = -\frac{k_B}{\Omega} \sum_{\mathbf{k}, \sigma} [n_\sigma(\mathbf{k}) \ln(n_\sigma(\mathbf{k})) + (1 - n_\sigma(\mathbf{k})) \ln(1 - n_\sigma(\mathbf{k}))]. \quad (5.40)$$

Taking the derivative of the entropy S with respect to T , the specific heat

$$C(T) = T \frac{\partial S}{\partial T} \quad (5.41)$$

$$= -\frac{k_B T}{\Omega} \sum_{\mathbf{k}, \sigma} \frac{e^{\xi(\mathbf{k})/k_B T}}{(e^{\xi(\mathbf{k})/k_B T} + 1)^2} \frac{\xi(\mathbf{k})}{k_B T^2} \ln\left(\frac{n_\sigma(\mathbf{k})}{1 - n_\sigma(\mathbf{k})}\right) \quad (5.42)$$

$$= -\frac{k_B T}{\Omega} \sum_{\mathbf{k}, \sigma} \frac{1}{4 \cosh^2(\xi(\mathbf{k})/2k_B T)^2} \frac{\xi(\mathbf{k})}{k_B T^2} \frac{\xi(\mathbf{k})}{k_B T} \quad (5.43)$$

is obtained, where we introduced $\xi(\mathbf{k}) = \epsilon(\mathbf{k}) - \epsilon_F$. In the limit $T \rightarrow 0$ we find

$$\frac{C(T)}{T} \approx \frac{N(\epsilon_F)}{4k_B T^3} \int d\xi \frac{\xi^2}{\cosh^2(\xi/2k_B T)} \quad (5.44)$$

$$\approx \frac{k_B^2 N(\epsilon_F)}{4} \int_{-\infty}^{+\infty} dy \frac{y^2}{\cosh^2(y/2)} \quad (5.45)$$

$$= \frac{\pi^2 k_B^2 N(\epsilon_F)}{3}, \quad (5.46)$$

which is the well-known linear behavior $C(T) = \gamma T$ for the specific heat at low temperatures, with $\gamma = \pi^2 k_B^2 N(\epsilon_F)/3$. Since $N(\epsilon_F) = m^* k_F / \pi^2 \hbar^2$, the effective mass m^* of the quasiparticles can directly determined by measuring the specific heat of the system.

5.2.2 Compressibility - Landau parameter F_0^s

A Fermi gas has a finite compressibility because each fermion occupies a finite amount of space due to the Pauli principle. The compressibility κ is defined as⁶

$$\kappa = -\frac{1}{\Omega} \left(\frac{\partial \Omega}{\partial p} \right)_{T,N} \quad (5.48)$$

where p is the uniform hydrostatic pressure. The indices T, N mean, that the temperature T and the particle number N are kept fixed. We consider the response of the Fermi liquid upon application of uniform pressure p . The shift of the quasiparticle energies is given by

$$\delta \epsilon(\mathbf{k}) = \frac{\partial \epsilon(\mathbf{k})}{\partial p} \delta p = \frac{\partial \epsilon(\mathbf{k})}{\partial \mathbf{k}} \cdot \frac{\partial \mathbf{k}}{\partial \Omega} \frac{\partial \Omega}{\partial p} \delta p = \frac{\kappa^{(0)}}{3} \hbar \mathbf{v}_{\mathbf{k}} \cdot \mathbf{k} \delta p = \gamma_{\mathbf{k}} \kappa^{(0)} \delta p \quad (5.49)$$

with $\gamma_{\mathbf{k}} = \hbar \mathbf{v}_{\mathbf{k}} \cdot \mathbf{k} / 3 = 2\epsilon_{\sigma}(\mathbf{k}) / 3$. Analogous we introduce the shift of the renormalized quasiparticle energies,

$$\begin{aligned} \delta \tilde{\epsilon}_{\sigma}(\mathbf{k}) &= \gamma_{\mathbf{k}} \kappa \delta p = \gamma_{\mathbf{k}} \kappa^{(0)} \delta p + \frac{1}{\Omega} \sum_{\mathbf{k}', \sigma'} f_{\sigma, \sigma'}(\mathbf{k}, \mathbf{k}') \delta n_{\sigma'}(\mathbf{k}') \\ &= \gamma_{\mathbf{k}} \kappa^{(0)} \delta p + \frac{1}{\Omega} \sum_{\mathbf{k}', \sigma'} f_{\sigma, \sigma'}(\mathbf{k}, \mathbf{k}') \frac{\partial n_{\sigma'}(\mathbf{k}')}{\partial \tilde{\epsilon}_{\sigma'}(\mathbf{k}')} \delta \tilde{\epsilon}_{\sigma'}(\mathbf{k}') \\ &= \gamma_{\mathbf{k}} \kappa^{(0)} \delta p - \frac{1}{\Omega} \sum_{\mathbf{k}', \sigma'} f_{\sigma, \sigma'}(\mathbf{k}, \mathbf{k}') \delta(\tilde{\epsilon}_{\sigma'}(\mathbf{k}') - \epsilon_F) \gamma_{\mathbf{k}'} \kappa \delta p \end{aligned} \quad (5.50)$$

Changes are concentrated on the Fermi surface such that we can replace $\gamma_{\mathbf{k}} = 2\epsilon_F / 3$ so that

$$\kappa = \kappa^{(0)} - \kappa N(\epsilon_F) \int \frac{d\Omega_{\hat{k}'}}{4\pi} f^s(\hat{k}, \hat{k}') = \kappa^{(0)} - \kappa F_0^s. \quad (5.51)$$

Therefore we find

$$\kappa = \frac{\kappa^{(0)}}{1 + F_0^s}. \quad (5.52)$$

Now we determine $\kappa^{(0)}$ from the volume dependence of the energy

$$E^{(0)} = \sum_{\mathbf{k}, \sigma} \epsilon_{\sigma}(\mathbf{k}) = \frac{3}{5} N \epsilon_F = \frac{3}{5} N \frac{\hbar^2 k_F^2}{2m^*} = \frac{3}{10} \frac{\hbar^2 N}{m^*} \left(3\pi^2 \frac{N}{\Omega} \right)^{2/3}. \quad (5.53)$$

Then we determine the pressure

$$p = - \left(\frac{\partial E^{(0)}}{\partial \Omega} \right)_N = \frac{1}{5} \frac{\hbar^2 N}{m^*} \left(3\pi^2 \frac{N}{\Omega} \right)^{2/3} \frac{1}{\Omega} \quad (5.54)$$

and

$$\frac{1}{\kappa^{(0)}} = -\Omega \frac{\partial p}{\partial \Omega} = \frac{1}{3} \frac{\hbar^2 N}{m^* \Omega} (3\pi^2 n)^{2/3} = \frac{2}{3} n \epsilon_F. \quad (5.55)$$

⁶An alternative definition considers the change of particle number upon change of the chemical potential,

$$\kappa = \frac{1}{n^2} \left(\frac{\partial n}{\partial \mu} \right)_{T, \Omega} \quad (5.47)$$

with $n = N/\Omega$.

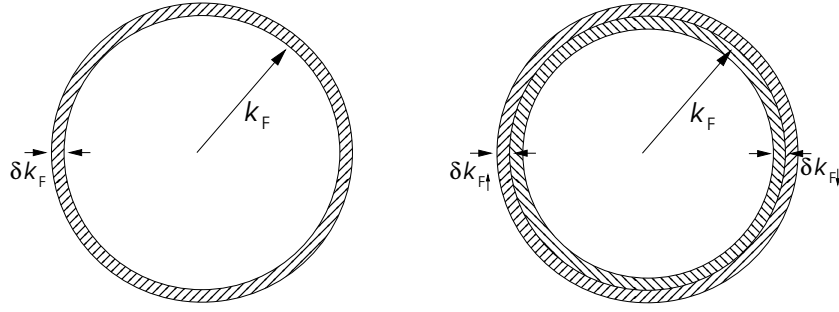


Figure 5.4: Deviations of the distribution functions: Left panel: isotropic increase of the Fermi surface as used for the uniform compressibility; right panel: spin dependent change of size of the Fermi surface as used for the uniform spin susceptibility.

5.2.3 Spin susceptibility - Landau parameter F_0^a

In a magnetic field H coupling to the electron spins the bare quasiparticle energy is supplemented by the Zeeman term,

$$\epsilon_\sigma(\mathbf{k}) = \frac{\hbar^2 \mathbf{k}^2}{2m^*} - g\mu_B H \frac{\sigma}{2} \quad (5.56)$$

where $\sigma = \pm 1$ denotes the spin component parallel to the applied field. The shift of the renormalized quasiparticle energy due to the applied field is

$$\begin{aligned} \delta\tilde{\epsilon}_\sigma(\mathbf{k}) &= \tilde{\epsilon}_\sigma(H, \mathbf{k}) - \tilde{\epsilon}(H=0, \mathbf{k}) \\ &= -g\mu_B H \frac{\sigma}{2} + \frac{1}{\Omega} \sum_{\mathbf{k}', \sigma'} f_{\sigma\sigma'}(\mathbf{k}, \mathbf{k}') \delta n_{\sigma'}(\mathbf{k}') \\ &= -\tilde{g}\mu_B H \frac{\sigma}{2}. \end{aligned} \quad (5.57)$$

Note that by symmetry, $\delta n_\sigma(\mathbf{k}) = -\delta n_{-\sigma}(-\mathbf{k})$. Due to interactions, the renormalized gyromagnetic factor \tilde{g} differs from the value of $g = 2$ for free electrons. We focus on the second term in Eq.(5.57), which can be reexpressed as

$$\begin{aligned} \frac{1}{\Omega} \sum_{\mathbf{k}', \sigma'} f_{\sigma\sigma'}(\mathbf{k}, \mathbf{k}') \delta n_{\sigma'}(\mathbf{k}') &= \frac{1}{\Omega} \sum_{\mathbf{k}', \sigma'} f_{\sigma\sigma'}(\mathbf{k}, \mathbf{k}') \frac{\partial n_{\sigma'}(\mathbf{k}')}{\partial \tilde{\epsilon}_{\sigma'}(\mathbf{k}')} \delta\tilde{\epsilon}_{\sigma'}(\mathbf{k}') \\ &= \frac{1}{\Omega} \sum_{\mathbf{k}', \sigma'} f_{\sigma\sigma'}(\mathbf{k}, \mathbf{k}') \delta(\tilde{\epsilon}_{\sigma'}(\mathbf{k}') - \epsilon_F) \tilde{g}\mu_B H \frac{\sigma'}{2} \end{aligned} \quad (5.58)$$

Combining this result with the Eqs. (5.57) and (5.58), we derive

$$\tilde{g} = g - \tilde{g}N(\epsilon_F) \int \frac{d\Omega_{\hat{k}'}}{4\pi} f^a(\hat{k}, \hat{k}') = g - \tilde{g}F_0^a, \quad (5.59)$$

or equivalently

$$\tilde{g} = \frac{g}{1 + F_0^a}. \quad (5.60)$$

The magnetization of the system can be computed from the distribution function,

$$\begin{aligned} M &= g\mu_B \sum_{\mathbf{k}, \sigma} \frac{\sigma}{2} \delta n_\sigma(\mathbf{k}) = g\mu_B \sum_{\mathbf{k}, \sigma} \frac{\sigma}{2} \frac{\partial n_\sigma(\mathbf{k})}{\partial \tilde{\epsilon}_\sigma(\mathbf{k})} \delta\tilde{\epsilon}_\sigma(\mathbf{k}) \\ &= g\mu_B \sum_{\mathbf{k}, \sigma} \frac{\sigma}{2} \delta(\tilde{\epsilon}_\sigma(\mathbf{k}) - \epsilon_F) \tilde{g}\mu_B H \frac{\sigma}{2} \end{aligned} \quad (5.61)$$

from which the susceptibility is immediately found to be

$$\chi = \frac{M}{H\Omega} = \frac{\mu_B^2 N(\epsilon_F)}{1 + F_0^a}. \quad (5.62)$$

The changes in the distribution function induced by the magnetic field feed back into the susceptibility, so that the latter may be either weakened ($F_0^a > 0$) or enhanced ($F_0^a < 0$). For the magnetic susceptibility, the Landau parameter F_0^a and the effective mass m^* (through $N(\epsilon_F)$) lead to a renormalization compared to the free electron susceptibility.

5.2.4 Galilei invariance - effective mass and F_1^s

We initially introduced by hand the effective mass of quasiparticles in $\epsilon_\sigma(\mathbf{k})$. In this section we show, that overall consistency of the phenomenological theory requires a relation between the effective mass and one Landau parameter (F_1^s). The reason is, that the effective mass is the result of the interactions among the electrons. This self-consistency is connected with the Galilean invariance of the system. When the momenta of all particles are shifted by $\hbar\mathbf{q}$ ($|\mathbf{q}|$ shall be very small compared to the Fermi momentum k_F in order to remain within the assumption-range of the Fermi liquid theory) the distribution function given by

$$\delta n_\sigma(\mathbf{k}) = n_\sigma^{(0)}(\mathbf{k} + \mathbf{q}) - n_\sigma^{(0)}(\mathbf{k}) \approx \mathbf{q} \cdot \nabla_{\mathbf{k}} n_\sigma^{(0)}(\mathbf{k}). \quad (5.63)$$

This function is strongly concentrated around the Fermi energy (see Figure 5.5).

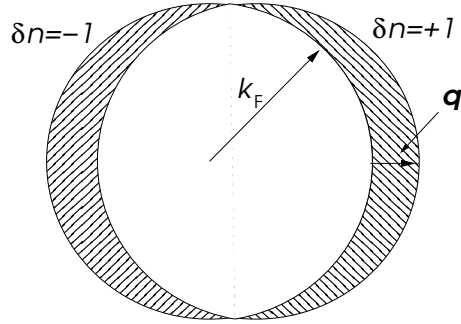


Figure 5.5: Distribution function due to a Fermi surface shift (Galilei transformation).

The current density can now be calculated, using the distribution function $n_\sigma(\mathbf{k}) = n_\sigma^{(0)}(\mathbf{k}) + \delta n_\sigma(\mathbf{k})$. Within the Fermi liquid theory this yields,

$$\mathbf{j}_q = \frac{1}{\Omega} \sum_{\mathbf{k}, \sigma} \mathbf{v}(\mathbf{k}) n_\sigma(\mathbf{k}) = \frac{1}{\Omega} \sum_{\mathbf{k}, \sigma} \mathbf{v}(\mathbf{k}) \delta n_\sigma(\mathbf{k}) \quad (5.64)$$

with

$$\begin{aligned} \mathbf{v}(\mathbf{k}) &= \frac{1}{\hbar} \nabla_{\mathbf{k}} \tilde{\epsilon}_\sigma(\mathbf{k}) \\ &= \frac{1}{\hbar} \left(\nabla_{\mathbf{k}} \epsilon_\sigma(\mathbf{k}) + \frac{1}{\Omega} \sum_{\mathbf{k}', \sigma'} \nabla_{\mathbf{k}} f_{\sigma\sigma'}(\mathbf{k}, \mathbf{k}') \delta n_\sigma(\mathbf{k}') \right). \end{aligned} \quad (5.65)$$

Thus we obtain for the current density,

$$\begin{aligned}
\mathbf{j}_q &= \frac{1}{\Omega} \sum_{\mathbf{k}, \sigma} \frac{\hbar \mathbf{k}}{m^*} n_\sigma(\mathbf{k}) + \frac{1}{\Omega^2} \sum_{\mathbf{k}, \sigma} \sum_{\mathbf{k}', \sigma'} [n_\sigma^{(0)}(\mathbf{k}) + \delta n_\sigma(\mathbf{k})] \frac{1}{\hbar} \nabla_{\mathbf{k}} f_{\sigma\sigma'}(\mathbf{k}, \mathbf{k}') \delta n_\sigma(\mathbf{k}') \\
&= \frac{1}{\Omega} \sum_{\mathbf{k}, \sigma} \frac{\hbar \mathbf{k}}{m^*} \delta n_\sigma(\mathbf{k}) - \frac{1}{\Omega^2} \sum_{\mathbf{k}, \sigma} \sum_{\mathbf{k}', \sigma'} \frac{1}{\hbar} [\nabla_{\mathbf{k}} n_\sigma^{(0)}(\mathbf{k})] f_{\sigma\sigma'}(\mathbf{k}, \mathbf{k}') \delta n_\sigma(\mathbf{k}') + O(q^2) \\
&= \frac{1}{\Omega} \sum_{\mathbf{k}, \sigma} \frac{\hbar \mathbf{k}}{m^*} \delta n_\sigma(\mathbf{k}) + \frac{1}{\Omega^2} \sum_{\mathbf{k}, \sigma} \sum_{\mathbf{k}', \sigma'} f_{\sigma\sigma'}(\mathbf{k}, \mathbf{k}') \delta(\epsilon_\sigma(\mathbf{k}') - \epsilon_F) \frac{\hbar \mathbf{k}'}{m^*} \delta n_\sigma(\mathbf{k}) + O(q^2) = \mathbf{j}_1 + \mathbf{j}_2.
\end{aligned} \tag{5.66}$$

where, for the second line, we performed an integration by parts and neglect terms quadratic in δn and, in the third line, used $f_{\sigma\sigma'}(\mathbf{k}, \mathbf{k}') = f_{\sigma'\sigma}(\mathbf{k}', \mathbf{k})$ and

$$\nabla_{\mathbf{k}} n_\sigma^{(0)}(\mathbf{k}) = \frac{\partial n_\sigma^{(0)}(\mathbf{k})}{\partial \epsilon_\sigma(\mathbf{k})} \nabla_{\mathbf{k}} \epsilon_\sigma(\mathbf{k}) = -\delta(\epsilon_\sigma(\mathbf{k}) - \epsilon_F) \nabla_{\mathbf{k}} \epsilon_\sigma(\mathbf{k}) = -\delta(\epsilon_\sigma(\mathbf{k}) - \epsilon_F) \frac{\hbar^2 \mathbf{k}}{m^*}. \tag{5.67}$$

The first term of equation (5.67) denotes quasiparticle current, \mathbf{j}_1 , while the second term can be interpreted as a drag current, \mathbf{j}_2 , an induced motion (backflow) of the other particles due to interactions.

From a different viewpoint, we consider the system as being in the inertial frame with a velocity $\hbar \mathbf{q}/m$, as all particles received the same momentum. Here m is the bare electron mass. The current density is then given by

$$\mathbf{j}_q = \frac{N \hbar \mathbf{q}}{\Omega m} = \frac{1}{\Omega} \sum_{\mathbf{k}, \sigma} \frac{\hbar \mathbf{k}}{m} n_\sigma(\mathbf{k}) = \frac{1}{\Omega} \sum_{\mathbf{k}, \sigma} \frac{\hbar \mathbf{k}}{m} \delta n_\sigma(\mathbf{k}). \tag{5.68}$$

Since these two viewpoints have to be equivalent, the resulting currents should be the same. Thus, we compare equation (5.67) and (5.68) and obtain the equation,

$$\frac{\hbar \mathbf{k}}{m} = \frac{\hbar \mathbf{k}}{m^*} + \frac{1}{\Omega} \sum_{\mathbf{k}', \sigma'} f_{\sigma\sigma'}(\mathbf{k}, \mathbf{k}') \delta(\epsilon_\sigma(\mathbf{k}') - \epsilon_F) \frac{\hbar \mathbf{k}'}{m^*} \tag{5.69}$$

which with $\hat{k} = \mathbf{k}/k_F$ then leads to

$$\frac{1}{m} = \frac{1}{m^*} + N(\epsilon_F) \int \frac{d\Omega_{\hat{k}'}}{4\pi} f^s(\hat{k}, \hat{k}') \frac{\hat{k} \cdot \hat{k}'}{m^*} = \frac{1}{m^*} + \frac{1}{m^*} \int \frac{d\Omega_{\hat{k}'}}{4\pi} \underbrace{N(\epsilon_F) f^s(\hat{k}, \hat{k}')}_{\sum_{l=0}^{\infty} F_l^s P_l(\cos \theta_{\hat{k}'})} \underbrace{\cos \theta_{\hat{k}'}}_{P_1(\cos \theta_{\hat{k}'})} \tag{5.70}$$

or by using the orthogonality of the Legendre polynomials,

$$\frac{m^*}{m} = 1 + \frac{1}{3} F_1^s. \tag{5.71}$$

where $1/3 = 1/(2l + 1)$ for $l = 1$ originates from the orthogonality relation of Legendre polynomials, as shown above. Therefore, the relation (5.71) has to couple m^* to F_1^s in order for Landau's theory of Fermi liquids to be self-consistent. Generally, we find that $F_1^s > 0$ so that quasiparticles in a Fermi liquid are effectively heavier than bare electrons.

5.2.5 Stability of the Fermi liquid

Upon inspection of the renormalization of the quantities treated previously

$$\frac{\gamma}{\gamma_0} = \frac{m^*}{m}, \tag{5.72}$$

$$\frac{\kappa}{\kappa_0} = \frac{m^*}{m} \frac{1}{1 + F_0^s}, \tag{5.73}$$

$$\frac{\chi}{\chi_0} = \frac{m^*}{m} \frac{1}{1 + F_0^a} \tag{5.74}$$

with

$$\frac{m^*}{m} = 1 + \frac{1}{3}F_1^s, \quad (5.75)$$

and the the response functions of the non-interacting system are given by

$$\gamma_0 = \frac{k_B^2 m k_F}{3\hbar^2}, \quad \kappa_0 = \frac{3m}{n\hbar^2 k_F^2} \quad \text{and} \quad \chi_0 = \mu_B^2 \frac{m k_F}{\pi^2 \hbar^2} \quad (5.76)$$

one notes that the compressibility κ (susceptibility χ) diverges for $F_0^s \rightarrow -1$ ($F_0^a \rightarrow -1$), indicating an instability of the system. A diverging spin susceptibility for example leads to a ferromagnetic state with a split Fermi surface, one for each spin direction. On the other hand, a diverging compressibility leads to a spontaneous contraction of the system. More generally, the deformation of the quasiparticle distribution function may vary over the Fermi surface, so that arbitrary deviations of the Fermi liquid ground state may be classified by the deformation

$$\delta n_\sigma(\hat{k}) = \sum_{l=0}^{\infty} \sum_{m=-l}^{+l} \delta n_{\sigma,l,m} Y_{lm}(\theta_{\mathbf{k}}, \phi_{\mathbf{k}}) \quad (5.77)$$

Note that we allow here formally for complex distribution functions. For pure charge density deformations we have $\delta n_{+,l,m}(\hat{k}) = \delta n_{-,l,m}(\hat{k})$, while pure spin density deformations are described by $\delta n_{+,l,m}(\hat{k}) = -\delta n_{-,l,m}(\hat{k})$. The general response function for a redistribution $\delta n_\sigma(\hat{k})$ with the anisotropy $Y_{lm}(\theta_{\mathbf{k}}, \phi_{\mathbf{k}})$ is given by ⁷

$$\chi_{l,m} = \frac{\chi_{l,m}^{(0)}}{1 + \frac{F_l^{s,a}}{2l+1}}. \quad (5.85)$$

⁷*General response and distribution deformations:* We consider a force field F with conjugate "polarisation" P which yields a modification of the quasiparticle dispersion,

$$\delta \epsilon_\sigma(\mathbf{k}) = -\alpha \lambda_\sigma(\mathbf{k}) F \quad \text{and} \quad \delta \tilde{\epsilon}_\sigma(\mathbf{k}) = -\tilde{\alpha} \lambda_\sigma(\mathbf{k}) F \quad (5.78)$$

where we assume that $\lambda_\sigma(\mathbf{k}) = Y_{l,m}(\theta_{\hat{k}}, \phi_{\hat{k}}) = (-1)^m Y_{l,-m}^*(\theta_{\hat{k}}, \phi_{\hat{k}})$ without spin dependence. Then we can write

$$\delta \tilde{\epsilon}_\sigma(\mathbf{k}) = \delta \epsilon_\sigma(\mathbf{k}) + \frac{1}{\Omega} \sum_{\mathbf{k}', \sigma'} f_{\sigma\sigma'}(\hat{k}, \hat{k}') \delta n_{\sigma'}(\mathbf{k}') = \delta \epsilon_\sigma(\mathbf{k}) + \frac{1}{\Omega} \sum_{\mathbf{k}', \sigma'} f_{\sigma\sigma'}(\hat{k}, \hat{k}') \frac{\partial n_{\sigma'}}{\partial \epsilon_{\sigma'}(\mathbf{k}')} \delta \tilde{\epsilon}_{\sigma'}(\mathbf{k}'). \quad (5.79)$$

In the last step we take for $\delta n_{\sigma'}(\mathbf{k}')$ the self-consistent value taking the feedback of the quasiparticle coupling into account. We now use the relation

$$f^{s,a}(\hat{k}, \hat{k}') = \sum_{l=0}^{\infty} f_l^{s,a} P_l(\hat{k} \cdot \hat{k}') = 4\pi \sum_{l=0}^{\infty} \frac{f_l^{s,a}}{2l+1} \sum_{m=-l}^{+l} Y_{lm}(\theta_{\hat{k}}, \phi_{\hat{k}}) Y_{lm}^*(\theta_{\hat{k}'}, \phi_{\hat{k}'}) \quad (5.80)$$

and insert Eq.(5.78) to find

$$\tilde{\alpha} \lambda_\sigma(\mathbf{k}) F = \alpha \lambda_\sigma(\mathbf{k}) F - N(\epsilon_F) \frac{f_l^s}{2l+1} Y_{lm}(\theta_{\hat{k}}, \phi_{\hat{k}}) \tilde{\alpha} \int d\Omega_{\mathbf{k}'} Y_{lm}^*(\theta_{\hat{k}'}, \phi_{\hat{k}'}) \lambda_\sigma(\mathbf{k}') F \quad (5.81)$$

which leads straightforwardly to

$$\tilde{\alpha} = \alpha - \tilde{\alpha} \frac{F_l^s}{2l+1} \quad \Rightarrow \quad \tilde{\alpha} = \frac{\alpha}{1 + \frac{F_l^s}{2l+1}}. \quad (5.82)$$

Now the polarisation is calculated which we may define as

$$P = -\frac{1}{\Omega} \sum_{\mathbf{k}, \sigma} \alpha \lambda_\sigma(\mathbf{k}) \delta n_\sigma(\mathbf{k}) = -\frac{1}{\Omega} \sum_{\mathbf{k}, \sigma} \alpha \lambda_\sigma(\mathbf{k}) \frac{\partial n_\sigma}{\partial \epsilon_\sigma(\mathbf{k})} \delta \tilde{\epsilon}_\sigma(\mathbf{k}) = \alpha \tilde{\alpha} N(\epsilon_F) F \quad (5.83)$$

such that the linear response is given by

$$\chi = \frac{P}{F} = \frac{\alpha^2 N(\epsilon_F)}{1 + \frac{F_l^s}{2l+1}}. \quad (5.84)$$

Stability of the Fermi liquid against any of these deformations requires

$$1 + \frac{F_l^{s,a}}{2l+1} > 0. \quad (5.86)$$

If for any deformation channel l this conditions is violated one talks about a "Pomeranchuk instability".⁸ Generally, the renormalization of the Fermi liquid leads to a change in the Wilson ratio, defined as

$$\frac{R}{R_0} = \frac{\chi}{\chi_0} \frac{\gamma_0}{\gamma} = \frac{1}{1 + F_0^a} \quad (5.87)$$

where $R_0 = \chi_0/\gamma_0 = 6\mu_B^2/\pi^2 k_B^2$. Note that the Wilson ratio does not depend on the effective mass. A remarkable feature of the Fermi liquid theory is that even very strongly interacting Fermions remain Fermi liquids, notably the quantum liquid ^3He and so-called heavy Fermion systems, which are compounds of transition metals and rare earths. Both are strongly renormalized Fermi liquids. For ^3He we give some of the parameters in Table 5.1 both for zero pressure and for pressures just below the critical pressure at which He solidifies ($p_c \approx 2.5\text{MPa} = 25\text{bar}$).

| pressure | m^*/m | F_0^s | F_0^a | F_1^s | κ/κ_0 | χ/χ_0 |
|-----------|---------|---------|---------|---------|-------------------|---------------|
| $p = 0$ | 3.0 | 10.1 | -0.52 | 6.0 | 0.27 | 6.3 |
| $p < p_c$ | 6.2 | 94 | -0.74 | 15.7 | 0.065 | 24 |

Table 5.1: List of the parameters of the Fermi liquid theory for ^3He at zero pressure and at a pressure just below solidification.

The trends show obviously, that the higher the applied pressure is, the denser the liquid becomes and the stronger the quasiparticles interact. Approaching the solidification the compressibility is reduced, the quasiparticles become heavier (slower) and the magnetic response increases drastically. Finally the heavy fermion systems are characterized by the extraordinary enhancements of the effective mass which for many of these compounds lie between 100 and 1000 times higher than the bare electron mass (e.g. CeAl_3 , UBe_{13} , etc.). This large masses lead the notion of almost localized Fermi liquids, since the large effective mass is induced by the hybridization of itinerant conduction electrons with strongly interacting (localized) electron states in partially filled $4f$ - or $5f$ -orbitals of Lanthanide and Actinide atoms, respectively.

5.3 Microscopic considerations

A rigorous derivation of Landau's Fermi liquid theory requires methods of quantum field theory and would go beyond the scope of these lectures. However, plain Rayleigh-Schrödinger theory applied to a simple model allows to gain some insights into the microscopic fundament of this phenomenologically based theory. In the following, we consider a model of fermions with contact interaction $U\delta(\mathbf{r} - \mathbf{r}')$, described by the Hamiltonian

$$\mathcal{H} = \sum_{\mathbf{k},s} \epsilon_{\mathbf{k}} \hat{c}_{\mathbf{k}s}^\dagger \hat{c}_{\mathbf{k}s} + \int d^3r d^3r' \hat{\Psi}_\uparrow(\mathbf{r})^\dagger \hat{\Psi}_\downarrow(\mathbf{r}')^\dagger U \delta(\mathbf{r} - \mathbf{r}') \hat{\Psi}_\downarrow(\mathbf{r}') \hat{\Psi}_\uparrow(\mathbf{r}) \quad (5.88)$$

$$= \sum_{\mathbf{k},s} \epsilon_{\mathbf{k}} \hat{c}_{\mathbf{k}s}^\dagger \hat{c}_{\mathbf{k}s} + \frac{U}{\Omega} \sum_{\mathbf{k},\mathbf{k}',\mathbf{q}} \hat{c}_{\mathbf{k}+\mathbf{q}\uparrow}^\dagger \hat{c}_{\mathbf{k}'-\mathbf{q}\downarrow}^\dagger \hat{c}_{\mathbf{k}'\downarrow} \hat{c}_{\mathbf{k}\uparrow}. \quad (5.89)$$

where $\epsilon_{\mathbf{k}} = \hbar^2 \mathbf{k}^2 / 2m$ is a parabolic dispersion of non-interacting electrons. We previously noticed that, in order to find well-defined quasiparticles, the interaction between the Fermions has to be short ranged. This specially holds for the contact interaction.

⁸I.J. Pomeranchuk, JETP 8, 361 (1958)

5.3.1 Landau parameters

Starting from the Hamiltonian (5.88), we will determine Landau parameters for a corresponding Fermi liquid theory. For a given momentum distribution $n_{\mathbf{k}s} = \langle c_{\mathbf{k}s}^\dagger c_{\mathbf{k}s} \rangle = n_{\mathbf{k}s}^{(0)} + \delta n_{\mathbf{k}s}$, we can expand the energy resulting from equation (5.89) following the Rayleigh-Schrödinger perturbation method,

$$E = E^{(0)} + E^{(1)} + E^{(2)} + \dots \quad (5.90)$$

with

$$E^{(0)} = \sum_{\mathbf{k},s} \epsilon_{\mathbf{k}} n_{\mathbf{k}s}, \quad (5.91)$$

$$E^{(1)} = \frac{U}{\Omega} \sum_{\mathbf{k},\mathbf{k}'} n_{\mathbf{k}\uparrow} n_{\mathbf{k}'\downarrow}, \quad (5.92)$$

$$E^{(2)} = \frac{U^2}{\Omega^2} \sum_{\mathbf{k},\mathbf{k}',\mathbf{q}} \frac{n_{\mathbf{k}\uparrow} n_{\mathbf{k}'\downarrow} (1 - n_{\mathbf{k}+\mathbf{q}\uparrow}) (1 - n_{\mathbf{k}'-\mathbf{q}\downarrow})}{\epsilon_{\mathbf{k}} + \epsilon_{\mathbf{k}'} - \epsilon_{\mathbf{k}+\mathbf{q}} - \epsilon_{\mathbf{k}'-\mathbf{q}}}. \quad (5.93)$$

The second order term $E^{(2)}$ describes virtual processes corresponding to a pair of particle-hole excitations. The numerator of this term can be split into four different contributions.

We first consider the term quadratic in $n_{\mathbf{k}}$ and combine it with the first order term $E^{(1)}$, which has the same structure,

$$\tilde{E}^{(1)} = E^{(1)} + \frac{U^2}{\Omega^2} \sum_{\mathbf{k},\mathbf{k}',\mathbf{q}} \frac{n_{\mathbf{k}\uparrow} n_{\mathbf{k}'\downarrow}}{\epsilon_{\mathbf{k}} + \epsilon_{\mathbf{k}'} - \epsilon_{\mathbf{k}+\mathbf{q}} - \epsilon_{\mathbf{k}'-\mathbf{q}}} \approx \frac{\tilde{U}}{\Omega} \sum_{\mathbf{k},\mathbf{k}'} n_{\mathbf{k}\uparrow} n_{\mathbf{k}'\downarrow}. \quad (5.94)$$

In the last step, we defined the renormalized interaction \tilde{U} through,

$$\tilde{U} = U + \frac{U^2}{\Omega} \sum_{\mathbf{q}} \frac{1}{\epsilon_{\mathbf{k}} + \epsilon_{\mathbf{k}'} - \epsilon_{\mathbf{k}+\mathbf{q}} - \epsilon_{\mathbf{k}'-\mathbf{q}}}. \quad (5.95)$$

In principle, \tilde{U} depends on the wave vectors \mathbf{k} and \mathbf{k}' . However, when the wave vectors are restricted to the Fermi surface ($|\mathbf{k}| = |\mathbf{k}'| = k_F$), and if the range of the interaction ℓ is small compared to the mean electron spacing, i.e., $k_F \ell \ll 1$,⁹ this dependency may be neglected.

Since the term quartic in $n_{\mathbf{k}}$ vanishes due to symmetry, the remaining contribution to $E^{(2)}$ is

⁹We should be careful with our choice of a contact interaction, since it would lead to a divergence in the large- q range. A cutoff for q of order $Q_c \sim \ell^{-1}$ would regularize the integral which is dominated by the large- q part. Thus we may use the following expansion,

$$\frac{1}{\Omega} \sum_{\mathbf{q}} \frac{1}{\epsilon_{\mathbf{k}} + \epsilon_{\mathbf{k}'} - \epsilon_{\mathbf{k}+\mathbf{q}} - \epsilon_{\mathbf{k}'-\mathbf{q}}} = \frac{1}{(2\pi)^3} \int_0^{Q_c} dq q^2 \int d\Omega_{\mathbf{q}} \frac{m}{(\mathbf{k}' - \mathbf{k}) \cdot \mathbf{q} - q^2} \quad (5.96)$$

$$= \frac{m}{(2\pi)^2} \int dq q \int_{-1}^+ \frac{d \cos \theta}{K \cos \theta - q} = \frac{m}{(2\pi)^2} \int_0^{Q_c} dq q \ln \left| \frac{q - K}{q + K} \right| \quad (5.97)$$

$$= -\frac{m}{(2\pi)^2} \left(Q_c + \frac{K^2 - Q_c^2}{2K} \ln \left| \frac{Q_c - K}{Q_c + K} \right| \right) \quad (5.98)$$

$$\approx -\frac{2mQ_c}{(2\pi)^2} \left(1 - \frac{K^2}{Q_c^2} + O\left(\frac{K^4}{Q_c^4}\right) \right), \quad (5.99)$$

where we use $K = |\mathbf{k}' - \mathbf{k}| \leq 2k_F \ll Q_c$. From this we conclude that the momentum dependence of \tilde{U} is indeed weak.

cubic in $n_{\mathbf{k}}$ and reads

$$\tilde{E}^{(2)} = -\frac{\tilde{U}^2}{\Omega^2} \sum_{\mathbf{k}, \mathbf{k}', \mathbf{q}} \frac{n_{\mathbf{k}\uparrow} n_{\mathbf{k}'\downarrow} (n_{\mathbf{k}+\mathbf{q}\uparrow} + n_{\mathbf{k}'-\mathbf{q}\downarrow})}{\epsilon_{\mathbf{k}} + \epsilon_{\mathbf{k}'} - \epsilon_{\mathbf{k}+\mathbf{q}} - \epsilon_{\mathbf{k}'-\mathbf{q}}}. \quad (5.100)$$

We replaced U^2 by \tilde{U}^2 , which is admissible at this order of the perturbative expansion. The variation of the energy E in Eq.(5.90) with respect to $\delta n_{\mathbf{k}\uparrow}$ can easily be calculated,

$$\tilde{\epsilon}_{\uparrow}(\mathbf{k}) = \epsilon_{\mathbf{k}} + \frac{\tilde{U}}{\Omega} \sum_{\mathbf{k}'} n_{\mathbf{k}'\downarrow} - \frac{\tilde{U}^2}{\Omega^2} \sum_{\mathbf{k}', \mathbf{q}} \frac{n_{\mathbf{k}'\downarrow} (n_{\mathbf{k}+\mathbf{q}\uparrow} + n_{\mathbf{k}'-\mathbf{q}\downarrow}) - n_{\mathbf{k}+\mathbf{q}\uparrow} n_{\mathbf{k}'-\mathbf{q}\downarrow}}{\epsilon_{\mathbf{k}} + \epsilon_{\mathbf{k}'} - \epsilon_{\mathbf{k}+\mathbf{q}} - \epsilon_{\mathbf{k}'-\mathbf{q}}}, \quad (5.101)$$

and an analogous expression is found for $\epsilon_{\downarrow}(\mathbf{k})$. The coupling parameters $f_{\sigma\sigma'}(\mathbf{k}, \mathbf{k}')$ may be determined using the definition (5.26). Starting with $f_{\uparrow\uparrow}(\mathbf{k}_F, \mathbf{k}'_F)$ with wave-vectors on the Fermi surface ($|\mathbf{k}_F| = |\mathbf{k}'_F| = k_F$), the terms contributing to the coupling can be written as

$$\frac{\tilde{U}^2}{\Omega^2} \sum_{\mathbf{k}', \mathbf{q}} n_{\mathbf{k}+\mathbf{q}\uparrow} \frac{n_{\mathbf{k}'-\mathbf{q}\downarrow} - n_{\mathbf{k}'\downarrow}}{\epsilon_{\mathbf{k}} + \epsilon_{\mathbf{k}'} - \epsilon_{\mathbf{k}+\mathbf{q}} - \epsilon_{\mathbf{k}'-\mathbf{q}}} \xrightarrow{\mathbf{k}+\mathbf{q} \rightarrow \mathbf{k}'_F} \frac{1}{\Omega} \sum_{\mathbf{k}'_F} n_{\mathbf{k}'_F\uparrow} \frac{\tilde{U}^2}{\Omega} \sum_{\mathbf{k}'} \frac{n_{\mathbf{k}'-\mathbf{q}\downarrow}^{(0)} - n_{\mathbf{k}'\downarrow}^{(0)}}{\epsilon_{\mathbf{k}'} - \epsilon_{\mathbf{k}'-\mathbf{q}}} \Big|_{\mathbf{q}=\mathbf{k}'_F-\mathbf{k}_F} \quad (5.102)$$

$$= -\frac{1}{\Omega} \sum_{\mathbf{k}'_F} n_{\mathbf{k}'_F\uparrow} \frac{\tilde{U}^2}{2} \chi_0(\mathbf{k}'_F - \mathbf{k}_F), \quad (5.103)$$

where we consider $n_{\mathbf{k}'_F\uparrow} = n_{\mathbf{k}'_F\uparrow}^{(0)} + \delta n_{\mathbf{k}'_F\uparrow}$. Note that the part in this term which depends on $n_{\mathbf{k}'_F\uparrow}^{(0)}$ will contribute the ground state energy in Landau's energy functional. Here, $\chi_0(\mathbf{q})$ is the static Lindhard susceptibility as it was defined in (3.63). With the help of equation (5.26), it follows immediately, that

$$f_{\uparrow\uparrow}(\mathbf{k}_F, \mathbf{k}'_F) = f_{\downarrow\downarrow}(\mathbf{k}_F, \mathbf{k}'_F) = \frac{\tilde{U}^2}{2} \chi_0(\mathbf{k}_F - \mathbf{k}'_F). \quad (5.104)$$

The other couplings are obtained in a similar way, resulting in

$$f_{\uparrow\downarrow}(\mathbf{k}_F, \mathbf{k}'_F) = f_{\downarrow\uparrow}(\mathbf{k}_F, \mathbf{k}'_F) = \tilde{U} - \frac{\tilde{U}^2}{2} [2\tilde{\chi}_0(\mathbf{k}_F + \mathbf{k}'_F) - \chi_0(\mathbf{k}_F - \mathbf{k}'_F)], \quad (5.105)$$

where the function $\tilde{\chi}_0(\mathbf{q})$ is defined as

$$\tilde{\chi}_0(\mathbf{q}) = \frac{1}{\Omega} \sum_{\mathbf{k}'} \frac{n_{\mathbf{k}'+\mathbf{q}\uparrow}^{(0)} + n_{\mathbf{k}'\downarrow}^{(0)}}{2\epsilon_{\mathbf{k}'} - \epsilon_{\mathbf{k}'+\mathbf{q}} - \epsilon_{\mathbf{k}'}} \quad (5.106)$$

If the couplings are parametrized by the angle θ between \mathbf{k}_F and \mathbf{k}'_F , they can be expressed as

$$f_{\sigma\sigma'}(\theta) = \frac{\tilde{U}}{2} \left[\left(1 + \frac{\tilde{U}N(\epsilon_F)}{4} \left(2 + \frac{\cos\theta}{2\sin(\theta/2)} \ln \frac{1 + \sin(\theta/2)}{1 - \sin(\theta/2)} \right) \right) \delta_{\sigma\sigma'} \right. \quad (5.107)$$

$$\left. - \left(1 + \frac{\tilde{U}N(\epsilon_F)}{4} \left(1 - \frac{\sin(\theta/2)}{2} \ln \frac{1 + \sin(\theta/2)}{1 - \sin(\theta/2)} \right) \right) \sigma\sigma' \right]. \quad (5.108)$$

Finally, we are in the position to determine the most important Landau parameters by matching the expressions (5.104) and (5.105) to the parametrization (5.107),

$$F_0^s = \tilde{u} \left[1 + \tilde{u} \left[1 + \frac{1}{6} (2 + \ln(2)) \right] \right] = \tilde{u} + 1.449 \tilde{u}^2, \quad (5.109)$$

$$F_0^a = -\tilde{u} \left[1 + \tilde{u} \left[1 - \frac{2}{3} (1 - \ln(2)) \right] \right] = -\tilde{u} - 0.895 \tilde{u}^2, \quad (5.110)$$

$$F_1^s = \tilde{u}^2 \frac{2}{15} (7 \ln(2) - 1) \approx 0.514 \tilde{u}^2, \quad (5.111)$$

where $\tilde{u} = \tilde{U}N(\epsilon_F)/2$ has been introduced for better readability. Since the Landau parameter F_1^s is responsible for the modification of the effective mass m^* compared to the bare mass m , m^* is enhanced compared to m for both attractive ($U < 0$) and repulsive ($U > 0$) interactions. Obviously, the sign of the interaction U does not affect the renormalization of the effective mass m^* . This is so, because the existence of an interaction (whatever sign it has) between the particles enforces the motion of many particles whenever one is moved. The behavior of the susceptibility and the compressibility depends on the sign of the interaction. If the interaction is repulsive ($\tilde{u} > 0$), the compressibility decreases ($F_0^s > 0$), implying that it is harder to compress the Fermi liquid. The susceptibility is enhanced ($F_0^a < 0$) in this case, so that it is easier to polarize the spins of the electrons. Conversely, for attractive interactions ($\tilde{u} < 0$), the compressibility is enhanced due to a negative Landau parameter F_0^s , whereas the susceptibility is suppressed with a factor $1/(1 + F_0^a)$, with $F_0^a > 0$. The attractive case is more subtle because the Fermi liquid becomes unstable at low temperatures, turning into a superfluid or superconductor, by forming so-called Cooper pairs. This represents another non-trivial Fermi surface instability.

5.3.2 Distribution function

Finally, we examine the effect of interactions on the ground state properties, using again Rayleigh-Schrödinger perturbation theory. The calculation of the corrections to the ground state $|\Psi_0\rangle$, the filled Fermi sea can be expressed as

$$|\Psi\rangle = |\Psi^{(0)}\rangle + |\Psi^{(1)}\rangle + \dots \quad (5.112)$$

where

$$|\Psi^{(0)}\rangle = |\Psi_0\rangle \quad (5.113)$$

$$|\Psi^{(1)}\rangle = \frac{U}{\Omega} \sum_{\mathbf{k}, \mathbf{k}', \mathbf{q}} \sum_{s, s'} \frac{\hat{c}_{\mathbf{k}+\mathbf{q}, s}^\dagger \hat{c}_{\mathbf{k}'-\mathbf{q}, s'}^\dagger \hat{c}_{\mathbf{k}', s'} \hat{c}_{\mathbf{k}, s}}{\epsilon_{\mathbf{k}} + \epsilon_{\mathbf{k}'} - \epsilon_{\mathbf{k}+\mathbf{q}} - \epsilon_{\mathbf{k}'-\mathbf{q}}} |\Psi_0\rangle. \quad (5.114)$$

The state $|\Psi_0\rangle$ represents the ground state of non-interacting fermions. The lowest order correction involves particle-hole excitations, depleting the Fermi sea by lifting particles virtually above the Fermi energy. How the correction (5.114) affects the distribution function, will be discussed next. The momentum distribution $n_{\mathbf{k}s} = \langle \hat{c}_{\mathbf{k}s}^\dagger \hat{c}_{\mathbf{k}s} \rangle$ is obtain as the expectation value,

$$n_{\mathbf{k}s} = \frac{\langle \Psi | \hat{c}_{\mathbf{k}s}^\dagger \hat{c}_{\mathbf{k}s} | \Psi \rangle}{\langle \Psi | \Psi \rangle} = n_{\mathbf{k}s}^{(0)} + \delta n_{\mathbf{k}s}^{(2)} + \dots \quad (5.115)$$

where $n_{\mathbf{k}s}^{(0)}$ is the unperturbed distribution $\Theta(k_F - |\mathbf{k}|)$, and

$$\delta n_{\mathbf{k}s}^{(2)} = \begin{cases} -\frac{U^2}{\Omega^2} \sum_{\mathbf{k}_1, \mathbf{k}_2, \mathbf{k}_3} \frac{(1 - n_{\mathbf{k}_1})(1 - n_{\mathbf{k}_2})n_{\mathbf{k}_3}}{(\epsilon_{\mathbf{k}} + \epsilon_{\mathbf{k}_3} - \epsilon_{\mathbf{k}_1} - \epsilon_{\mathbf{k}_2})^2} \delta_{\mathbf{k}+\mathbf{k}_3, \mathbf{k}_1+\mathbf{k}_2} & |\mathbf{k}| < k_F \\ \frac{U^2}{\Omega^2} \sum_{\mathbf{k}_1, \mathbf{k}_2, \mathbf{k}_3} \frac{n_{\mathbf{k}_1} n_{\mathbf{k}_2} (1 - n_{\mathbf{k}_3})}{(\epsilon_{\mathbf{k}_1} + \epsilon_{\mathbf{k}_2} - \epsilon_{\mathbf{k}} - \epsilon_{\mathbf{k}_3})^2} \delta_{\mathbf{k}+\mathbf{k}_3, \mathbf{k}_1+\mathbf{k}_2} & |\mathbf{k}| > k_F \end{cases}. \quad (5.116)$$

This yields the modification of the distribution functions as shown in Figure 5.6. It allows us also to determine the size of the discontinuity of the distribution function at the Fermi surface,

$$n_{\mathbf{k}_F^-} - n_{\mathbf{k}_F^+} = 1 - \left(\frac{UN(\epsilon_F)}{2} \right)^2 \ln(2), \quad (5.117)$$

where

$$n_{\mathbf{k}_F^\pm} = \lim_{|\mathbf{k}|-k_F \rightarrow 0^\pm} (n_{\mathbf{k}}^{(0)} + \delta n_{\mathbf{k}}^{(2)}). \quad (5.118)$$

The jump of $n_{\mathbf{k}}$ at the Fermi surface is reduced independently of the sign of the interaction. The reduction is quadratic in the perturbation parameter $UN(\epsilon_F)$. This jump is also a measure for the weight of the quasiparticle state at the Fermi surface.

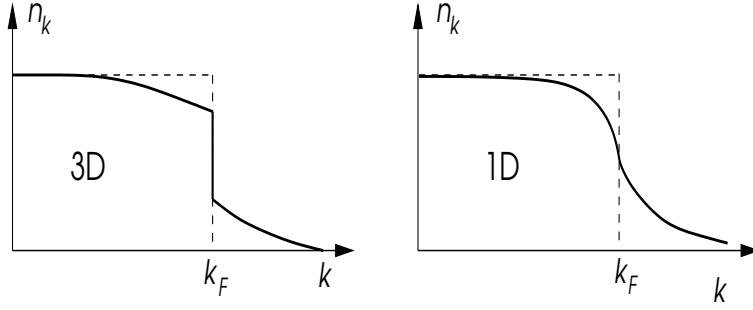


Figure 5.6: Momentum distribution functions of electrons for a three-dimensional (left panel) and one-dimensional (right panel) Fermion system.

5.3.3 Fermi liquid in one dimension?

Within a perturbative approach the Fermi liquid theory can be justified for a three-dimensional system and we recognize the one-to-one correspondence between bare electrons and quasiparticles renormalized by (short-ranged) interactions. Now we would like to show that within the same approach problems appear in one-dimensional systems, which are conceptual nature and hint that interaction Fermions in one dimension would not form a Fermi liquid, but a Luttinger liquid, as we will motivate briefly below.

The Landau parameters have been expressed above in terms of the response functions $\chi_0(\mathbf{q} = \mathbf{k}_F - \mathbf{k}'_F)$ and $\tilde{\chi}_0(\mathbf{q} = \mathbf{k}_F - \mathbf{k}'_F)$. For the one-dimensional system, as given in Eqs.(5.104 - 5.106), the relevant contributions come from two configurations, since there are two Fermi points only (instead of a two-dimensional Fermi surface),

$$(k_F, k'_F) \Rightarrow q = k_F - k'_F = 0, \pm 2k_F. \quad (5.119)$$

We find that the response functions show singularities for some of these momenta,¹⁰ and we obtain

$$f_{\uparrow\uparrow}(\pm k_F, \pm k_F) = f_{\downarrow\downarrow}(\pm k_F, \mp k_F) \rightarrow \infty \quad (5.122)$$

as well as

$$f_{\uparrow\downarrow}(k_F, \pm k_F) = f_{\downarrow\uparrow}(k_F, \mp k_F) \rightarrow \infty \quad (5.123)$$

giving rise to the divergence of all Landau parameters. Therefore the perturbative approach to a Landau Fermi liquid is not allowed for the one-dimensional Fermi system.

¹⁰While $\chi_0(q)$ is the Lindhard function given in Eq.(3.112) which diverges logarithmically at $q = \pm 2k_F$, we obtain for the other response function

$$\tilde{\chi}_0(q) = \begin{cases} -\frac{2m}{\hbar^2 \sqrt{4k_F^2 - q^2}} \ln \left(\frac{\sqrt{2k_F + q} - \sqrt{2k_F - q}}{\sqrt{2k_F + q} + \sqrt{2k_F - q}} \right) & |q| < 2k_F \\ -\frac{2m}{\hbar^2 \sqrt{q^2 - 4k_F^2}} \left(\arctan \sqrt{\frac{q + 2k_F}{q - 2k_F}} + \arctan \sqrt{\frac{q - 2k_F}{q + 2k_F}} \right) & |q| > 2k_F \end{cases} \quad (5.120)$$

which diverges as

$$\lim_{q \rightarrow 0_{\pm}} \tilde{\chi}_0(q) = -\frac{m}{\hbar^2 k_F} \ln \left(\frac{q}{2k_F} \right), \quad \lim_{q \rightarrow 2k_F^-} \tilde{\chi}_0(q) = \frac{m}{\hbar^2 k_F} \quad \text{and} \quad \lim_{q \rightarrow 2k_F^+} \tilde{\chi}_0(q) = \frac{\pi m}{\hbar^2 \sqrt{2k_F}} \frac{1}{\sqrt{q - 2k_F}}. \quad (5.121)$$

The same message is obtained when looking at the momentum distribution form which had in three dimensions a step giving a measure for the (reduced but finite) quasiparticle weight. The analogous calculation as in Sect.5.3.2 leads here to

$$n_{ks}^{(2)} \approx \begin{cases} \frac{1}{8\pi^2} \frac{U^2}{\hbar^2 v_F^2} \ln \frac{k_+}{k - k_F} & k > k_F \\ -\frac{1}{8\pi^2} \frac{U^2}{\hbar^2 v_F^2} \ln \frac{k_-}{k_F - k} & k < k_F \end{cases}. \quad (5.124)$$

Here, k_{\pm} are cutoff parameters of the order of the Fermi wave vector k_F . Apparently the quality of the perturbative calculation deteriorates as $k \rightarrow k_{F\pm}$, since we encounter a logarithmic divergence from both sides.

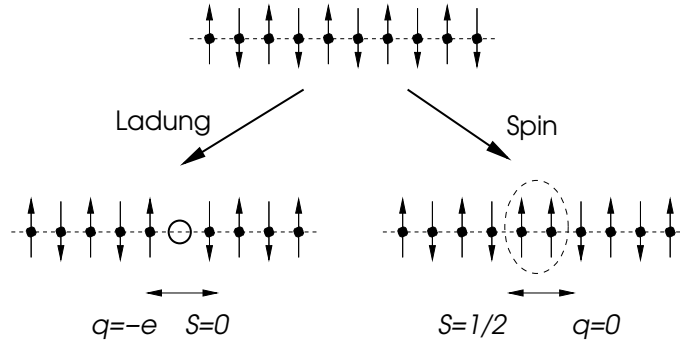


Figure 5.7: Visualization of spin-charge separation. The dominant anti-ferromagnetic spin correlation is staggered. A charge excitation is a vacancy which can move, while spin excitation may be considered as domain wall. Both excitations move independently.

Indeed, a more elaborated approach shows that the distribution function is continuous at $k = k_F$ in one dimension, without any jump. Correspondingly, the quasiparticle weight vanishes and the elementary excitations cannot be described by Fermionic quasiparticles but rather by collective modes. Landau's Theory of Fermi liquids is inappropriate for such systems. This kind of behavior, where the quasiparticle weight vanishes, can be described by the so-called bosonization of fermions in one dimension, a topic that is beyond the scope of these lectures. However, a result worth mentioning, shows that the fermionic excitations in one dimensions decay into independent charge and spin excitations, the so-called *spin-charge separation*. This behavior can be understood with the naive picture of a half-filled lattice with predominantly antiferromagnetic spin correlations. In this case both charge excitations (empty or doubly occupied lattice site) and spin excitations (two parallel neighboring spins) represent different kinds of domain walls, and are free to move at different velocities.

Chapter 6

Transport properties of metals

The ability to transport electrical current is one of the most remarkable and characteristic properties of metals. At zero temperature, a ideal pure metal is a perfect electrical conductor, i.e., its resistivity is zero. However, disorder due to impurities and lattice defects influence the transport and yield a finite *residual resistivity*, as found in real materials. At finite temperature, electron-electron and electron-phonon scattering lead to a temperature-dependent resistivity. Furthermore, an external magnetic field may influence the resistivity, a phenomenon called magnetoresistance, and also leads to the previously studied Hall effect. In this chapter, the effects of a magnetic field will not be considered. Finally, heat transport, which is also mostly mediated by electrons in metals, is going hand in hand with the electric transport. In this context, transport phenomena such as thermoelectricity (Seebeck and Peltier effect) will be analyzed here.

6.1 Electrical conductivity

In a normal metal, an electrical current density $\mathbf{j}(\mathbf{q}, \omega)$ (in \mathbf{q}, ω -space) is induced by an applied electrical field $\mathbf{E}(\mathbf{q}, \omega)$. For a homogeneous isotropic metal, we define the scalar¹ electrical conductivity $\sigma(\mathbf{q}, \omega)$ within linear response, through

$$\mathbf{j}(\mathbf{q}, \omega) = \sigma(\mathbf{q}, \omega)\mathbf{E}(\mathbf{q}, \omega). \quad (6.1)$$

The current density $\mathbf{j}(\mathbf{q}, \omega)$ is related to the charge density $\rho(\mathbf{r}, t) = -en(\mathbf{r}, t)$, via the continuity equation

$$\frac{\partial}{\partial t}\rho(\mathbf{r}, t) + \nabla \cdot \mathbf{j}(\mathbf{r}, t) = 0, \quad (6.2)$$

or, in Fourier transformed,

$$\omega\rho(\mathbf{q}, \omega) - \mathbf{q} \cdot \mathbf{j}(\mathbf{q}, \omega) = 0. \quad (6.3)$$

It is interesting to see that a relation between the conductivity $\sigma(\mathbf{q}, \omega)$ and the dynamical dielectric susceptibility $\chi_0(\mathbf{q}, \omega)$ defined in equation (3.68) of chapter 3 arises from the equations (6.1) and (6.3). For this, we can calculate

$$\begin{aligned} \chi_0(\mathbf{q}, \omega) &= -\frac{\rho(\mathbf{q}, \omega)}{eV(\mathbf{q}, \omega)} = -\frac{\mathbf{q} \cdot \mathbf{j}(\mathbf{q}, \omega)}{e\omega V(\mathbf{q}, \omega)} \\ &= -\frac{\sigma(\mathbf{q}, \omega)}{e} \frac{\mathbf{q} \cdot \mathbf{E}(\mathbf{q}, \omega)}{V(\mathbf{q}, \omega)} = -\frac{\sigma(\mathbf{q}, \omega)}{\omega} \frac{[i\mathbf{q}^2 V(\mathbf{q}, \omega)]}{e^2 V(\mathbf{q}, \omega)}. \end{aligned} \quad (6.4)$$

¹In an anisotropic material, the conductivity $\hat{\sigma}$ would be a full 3×3 tensor.

In the first line, we used the definition (3.68) of $\chi_0(\mathbf{q}, \omega)$ and the continuity equation (6.3). To the second line, we made use of the definition (6.1) of $\sigma(\mathbf{q}, \omega)$ and then replaced $\mathbf{E}(\mathbf{q}, \omega)$ by $-i\mathbf{q}V(\mathbf{q}, \omega)$, which is nothing else than the Fourier transform of the equation

$$-e\mathbf{E}(\mathbf{r}, t) = \nabla_{\mathbf{r}}V(\mathbf{r}, t). \quad (6.5)$$

From this calculations we conclude that

$$\chi_0(\mathbf{q}, \omega) = \frac{-iq^2}{e^2\omega}\sigma(\mathbf{q}, \omega), \quad (6.6)$$

and thus

$$\varepsilon(\mathbf{q}, \omega) = 1 - \frac{4\pi e^2}{q^2}\chi_0(\mathbf{q}, \omega) = 1 + \frac{4\pi i}{\omega}\sigma(\mathbf{q}, \omega). \quad (6.7)$$

In the limit of large wavelengths $q \ll k_F$, we know from previous discussions² that $\varepsilon(0, \omega) = 1 - \omega_p^2/\omega^2$. Then the conductivity simplifies to

$$\sigma(\omega) = \frac{i\omega_p^2}{4\pi\omega}. \quad (6.8)$$

One might conclude from this result that the conductivity is purely imaginary in the small- q limit. However, this conclusion is wrong, since the real part of $\sigma(\omega)$ is related to its imaginary part via the Kramers-Kronig relation. Defining σ_1 (σ_2) as the real (imaginary) part of σ , this relation states that

$$\sigma_1(\omega) = -\frac{1}{\pi} \mathcal{P} \left[\int_{-\infty}^{+\infty} d\omega' \frac{1}{\omega - \omega'} \sigma_2(\omega') \right] \quad (6.9)$$

and

$$\sigma_2(\omega) = \frac{1}{\pi} \mathcal{P} \left[\int_{-\infty}^{+\infty} d\omega' \frac{1}{\omega - \omega'} \sigma_1(\omega') \right]. \quad (6.10)$$

A simple calculation with σ_2 from equation (6.8), yields

$$\sigma_1(\omega) = \frac{\omega_p^2}{4}\delta(\omega), \quad (6.11)$$

$$\sigma_2(\omega) = \frac{\omega_p^2}{4\pi\omega}. \quad (6.12)$$

Obviously this metal is perfectly conducting ($\sigma \rightarrow \infty$ for $\omega \rightarrow 0$), which comes from the fact that we considered systems without dissipation so far.

An additional important property coming from complex analysis, is the existence of the so-called *f-sum rule*,

$$\int_0^{\infty} d\omega' \sigma_1(\omega') = \frac{1}{2} \int_{-\infty}^{+\infty} d\omega' \sigma_1(\omega') = \frac{\omega_p^2}{8} = \frac{\pi e^2 n}{2m}. \quad (6.13)$$

This relation is valid for all electronic systems (including semiconductors).

²In the small- q limit we approximate $\chi_0(\mathbf{q}, \omega) \approx nq^2/m\omega^2$ from equation (3.82).

6.2 Transport equations and relaxation time

We introduce here Boltzmann's transport theory as a rather simple and efficient way to deal with dissipation and momentum relaxation of non-stationary electronic states in metals.

6.2.1 The Boltzmann equation

In order to tackle the problem of a finite conductivity, we use a formalism similar to Landau's Fermi liquid theory, based on a distribution function of quasiparticles. In transport theory, the distribution function can be used to describe the deviation of the system from an equilibrium. If the system is isolated from external influence, equilibrium is reached through relaxation after some time, a process which is accompanied with an increase of entropy as discussed in statistical physics. Analogously to the theory of transport phenomena, let us introduce the distribution function³ $f(\mathbf{k}, \mathbf{r}, t)$, where

$$f(\mathbf{k}, \mathbf{r}, t) \frac{d^3k}{(2\pi)^3} d^3r \quad (6.14)$$

is the number of particles in the infinitesimal phase space volume $d^3r d^3k / (2\pi)^3$ centered at (\mathbf{k}, \mathbf{r}) , at time t . Such a description is only applicable if the temporal and spacial variations occur at long wavelengths and small frequencies, respectively, i.e., if typically $q \ll k_F$ and $\hbar\omega \ll \epsilon_F$. The total number of particles N is given by

$$N = 2 \int \frac{d^3k}{(2\pi)^3} d^3r f(\mathbf{k}, \mathbf{r}, t). \quad (6.15)$$

The equilibrium distribution f_0 for the fermionic quasiparticles is given by the Fermi-Dirac distribution,

$$f_0(\mathbf{k}, \mathbf{r}, t) = \frac{1}{e^{(\epsilon_{\mathbf{k}} - \mu)/k_B T} + 1}, \quad (6.16)$$

and is independent of space \mathbf{r} and time t . The general distribution function $f(\mathbf{k}, \mathbf{r}, t)$ obeys the *Boltzmann equation*

$$\frac{D}{Dt} f(\mathbf{k}, \mathbf{r}, t) = \left(\frac{\partial}{\partial t} + \dot{\mathbf{r}} \cdot \nabla_{\mathbf{r}} + \dot{\mathbf{k}} \cdot \nabla_{\mathbf{k}} \right) f(\mathbf{k}, \mathbf{r}, t) = \left(\frac{\partial f}{\partial t} \right)_{\text{coll}}, \quad (6.17)$$

where the substantial derivative in phase space D/Dt is defined as the total temporal derivative in a frame moving with the phase-space volume. The right-hand side is called *collision integral* and describes the rate of change in f due to collision processes. Without scattering, the equation (6.17) would represent a continuity equation for f . Now, consider the temporal derivatives of \mathbf{r} and \mathbf{k} from a quasi-classical viewpoint. In absence of a magnetic field, we find

$$\dot{\mathbf{r}} = \frac{\hbar \mathbf{k}}{m}, \quad (6.18)$$

$$\hbar \dot{\mathbf{k}} = -e \mathbf{E}, \quad (6.19)$$

i.e., the force $\hbar \dot{\mathbf{k}}$, which is our central interest, originates from the electric field. The collision integral may be expressed via the probability $W(\mathbf{k}, \mathbf{k}')$ to scatter a quasiparticle with wave vector \mathbf{k} to \mathbf{k}' . For simple scattering on static potentials, the collision integral is given by

$$\left(\frac{\partial f}{\partial t} \right)_{\text{coll}} = - \int \frac{d^3k'}{(2\pi)^3} [W(\mathbf{k}, \mathbf{k}') f(\mathbf{k}, \mathbf{r}, t) (1 - f(\mathbf{k}', \mathbf{r}, t)) \quad (6.20)$$

$$- W(\mathbf{k}', \mathbf{k}) f(\mathbf{k}', \mathbf{r}, t) (1 - f(\mathbf{k}, \mathbf{r}, t))]. \quad (6.21)$$

³For simplicity we neglect spin the electron spin. In general there would be a distribution function $f_{\sigma}(\mathbf{k}, \mathbf{r}, t)$ for each spin species σ .

The first term, describing the scattering⁴ from \mathbf{k} to \mathbf{k}' , requires a quasiparticle at \mathbf{k} , hence the factor $f(\mathbf{k}, \mathbf{r}, t)$, and the absence of a particle at \mathbf{k}' , therefore the factor $1 - f(\mathbf{k}', \mathbf{r}, t)$. This process describes the scattering out of the phase space volume $d^3k/(2\pi)^3$, i.e., reduces the number of particles in it. Therefore, it enters the collision integral with negative sign. The second term describes the opposite process and, according to its positive sign, increases the number of particles in the phase space volume $d^3k/(2\pi)^3$. For a system with time inversion symmetry, we have $W(\mathbf{k}, \mathbf{k}') = W(\mathbf{k}', \mathbf{k})$. Assuming this, we can combine both terms and end up with

$$\left(\frac{\partial f}{\partial t}\right)_{\text{coll}} = \int \frac{d^3k'}{(2\pi)^3} W(\mathbf{k}, \mathbf{k}') [f(\mathbf{k}', \mathbf{r}, t) - f(\mathbf{k}, \mathbf{r}, t)]. \quad (6.22)$$

The Boltzmann equation is a complicated integro-differential equation and suitable approximations are required. Usually, we study processes close to equilibrium, where the deviation $f(\mathbf{k}, \mathbf{r}, t) - f_0(\mathbf{k}, \mathbf{r}, t)$ is small compared to $f(\mathbf{k}, \mathbf{r}, t)$. Here, to generalize we assume $f_0(\mathbf{k}, \mathbf{r}, t)$ to be a *local* equilibrium distribution for which the temperature $T = T(\mathbf{r}, t)$ and the chemical potential $\mu = \mu(\mathbf{r}, t)$ vary slowly in \mathbf{r} and t , such that $f_0(\mathbf{k}, \mathbf{r}, t)$ can still be expressed via the local Fermi-Dirac distribution (6.16). At small deviations from equilibrium (or local equilibrium), we can approximate the collision integral by the *relaxation-time approximation*. For simplicity, we assume that the system is isotropic, such that the quasiparticle dispersion $\epsilon_{\mathbf{k}}$ only depends on $|\mathbf{k}|$ and, furthermore, that the scattering probabilities are elastic and depend on the angle between \mathbf{k} and \mathbf{k}' . Then, we make the Ansatz

$$\left(\frac{\partial f}{\partial t}\right)_{\text{coll}} = -\frac{f(\mathbf{k}, \mathbf{r}, t) - f_0(\mathbf{k}, \mathbf{r}, t)}{\tau(\epsilon_{\mathbf{k}})}. \quad (6.23)$$

The time scale $\tau(\epsilon_{\mathbf{k}})$ is called *relaxation time* and gives the characteristic time within which the system relaxes to equilibrium.

Consider the simplest case of a system at constant temperature subject to a small uniform electric field $\mathbf{E}(t)$. With $f(\mathbf{k}, \mathbf{r}, t) = f_0(\mathbf{k}, \mathbf{r}, t) + \delta f(\mathbf{k}, \mathbf{r}, t)$, we can calculate the Fourier-transform of Boltzmann equation (6.17) in relaxation-time approximation and find, after linearizing in δf ,

$$-i\omega \delta f(\mathbf{k}, \omega) - \frac{e\mathbf{E}(\omega)}{\hbar} \nabla_{\mathbf{k}} f_0(\mathbf{k}) = -\frac{\delta f(\mathbf{k}, \omega)}{\tau(\epsilon_{\mathbf{k}})} \quad (6.24)$$

with

$$f(\mathbf{k}, t) = \int_{-\infty}^{+\infty} \frac{d\omega}{2\pi} f(\mathbf{k}, \omega) e^{-i\omega t} \quad \text{and} \quad \mathbf{E}(\mathbf{k}, t) = \int_{-\infty}^{+\infty} \frac{d\omega}{2\pi} \mathbf{E}(\mathbf{k}, \omega) e^{-i\omega t}. \quad (6.25)$$

In order to come to this expression, we used that $f(\mathbf{k}, \mathbf{r}, t) = f(\mathbf{k}, t)$ for $E = E(t)$ are spacially uniform, and assumed for linearizing equation (6.24) that $\delta f \propto |\mathbf{E}|$. Thus, the equation (6.24) is consistent to linear order in $|\mathbf{E}|$ and can be easily solved as

$$\delta f(\mathbf{k}, \omega) = \frac{e\tau\mathbf{E}(\omega)}{\hbar(1 - i\omega\tau)} \nabla_{\mathbf{k}} f_0(\mathbf{k}) = \frac{e\tau\mathbf{E}(\omega)}{\hbar(1 - i\omega\tau)} \frac{\partial f_0(\epsilon)}{\partial \epsilon} \nabla_{\mathbf{k}} \epsilon_{\mathbf{k}}. \quad (6.26)$$

This result leads straightforwardly to the quasiparticle current $\mathbf{j}(\omega)$,

$$\mathbf{j}(\omega) = -2e \int \frac{d^3k}{(2\pi)^3} \mathbf{v}_{\mathbf{k}} f(\mathbf{k}, \omega) = -\frac{e^2}{4\pi^3} \int d^3k \frac{\tau(\epsilon_{\mathbf{k}}) [\mathbf{E}(\omega) \cdot \mathbf{v}_{\mathbf{k}}] \mathbf{v}_{\mathbf{k}}}{1 - i\omega\tau(\epsilon_{\mathbf{k}})} \frac{\partial f_0(\epsilon_{\mathbf{k}})}{\partial \epsilon_{\mathbf{k}}}, \quad (6.27)$$

⁴Note that if spin was considered here, this collision term would account for scattering processes where spin is conserved. However, there are in principle also scattering process where the electron spin can be transferred to the lattice (spin-orbit coupling) or an impurity (Kondo effect) and would not be conserved independently.

with $\hbar\mathbf{v}_k = \nabla_{\mathbf{k}}\epsilon_{\mathbf{k}}$, which in turn can be simplified to

$$j_\alpha(\omega) = \sum_{\beta} \sigma_{\alpha\beta}(\omega)E_\beta(\omega), \quad (6.28)$$

where the conductivity tensor $\sigma_{\alpha\beta}$ reads

$$\sigma_{\alpha\beta} = -\frac{e^2}{4\pi^3} \int d\epsilon \frac{\partial f_0(\epsilon)}{\partial \epsilon} \frac{\tau(\epsilon)}{1 - i\omega\tau(\epsilon)} \int d\Omega_{\mathbf{k}} k^2 \frac{v_{\alpha\mathbf{k}}v_{\beta\mathbf{k}}}{\hbar|\mathbf{v}_{\mathbf{k}}|}. \quad (6.29)$$

This corresponds to the Ohmic law. Note that $\sigma_{\alpha\beta} = \sigma\delta_{\alpha\beta}$ in isotropic systems. We recover in this case the expression (6.1) for the conductivity, which we introduced at the beginning of this chapter. It is also important to notice that $\partial f_0(\epsilon)/\partial\epsilon$ concentrates around $\epsilon = \mu$ for $T \ll T_F$. In the following, we consider the result (6.29) for an isotropic system in different limiting cases.

6.2.2 The Drude form

For $\omega\tau \gg 1$ equation (6.29) becomes independent on the relaxation time. In an isotropic system $\sigma_{\alpha\beta} = \sigma\delta_{\alpha\beta}$ at low temperatures $T \ll T_F$, this leads to

$$\sigma(\omega) \approx i \frac{e^2 m^2 v_F}{4\pi^3 \hbar^3 \omega} \int d\Omega_{\mathbf{k}} v_{Fz}^2 = i \frac{e^2 n}{m\omega} = i \frac{\omega_p^2}{4\pi\omega}, \quad (6.30)$$

which reproduces the result from equation (6.8). However now, this does not mean that our system is a perfect conductor, as becomes clear when we turn towards small ω ($\omega\tau \ll 1$). We are actually interested in the static limit, where the "dc conductivity" ($\omega = 0$; "dc" means "direct current") reduces to

$$\sigma = -\frac{e^2 n}{m} \int d\epsilon \frac{\partial f_0}{\partial \epsilon} \tau(\epsilon) = \frac{e^2 n \bar{\tau}}{m} = \frac{\omega_p^2 \bar{\tau}}{4\pi}. \quad (6.31)$$

Since the function $\partial f_0/\partial\epsilon$ is strongly peaked around the Fermi energy ϵ_F , we introduced a mean relaxation time $\bar{\tau} = \int d\epsilon \tau(\epsilon) \partial f_0/\partial\epsilon$. In the form (6.31), the result recovers the well-known Drude⁵ form of the conductivity.

If the relaxation time τ depends only weakly on energy, we can simply calculate the optical conductivity at finite frequency,

$$\sigma(\omega) = \frac{\omega_p^2}{4\pi} \frac{\bar{\tau}}{1 - i\omega\bar{\tau}} = \frac{\omega_p^2}{4\pi} \left(\frac{\bar{\tau}}{1 + \omega^2 \bar{\tau}^2} + \frac{i\bar{\tau}^2 \omega}{1 + \omega^2 \bar{\tau}^2} \right) = \sigma_1 + i\sigma_2. \quad (6.32)$$

Note that the real part satisfies the f -sum rule,

$$\int_0^\infty d\omega \sigma_1(\omega) = \int_0^\infty d\omega \frac{\omega_p^2}{4\pi} \frac{\bar{\tau}}{1 + \omega^2 \bar{\tau}^2} = \frac{\omega_p^2}{8} \quad (6.33)$$

and that $\sigma(\omega)$ recovers the behavior of equation (6.12) in the limit $\bar{\tau} \rightarrow \infty$.⁶ This form of the conductivity yields the dielectric function

$$\epsilon(\omega) = 1 - \frac{\omega_p^2 \bar{\tau}}{\omega(i + \omega\bar{\tau})} = 1 - \frac{\omega_p^2 \bar{\tau}^2}{1 + \omega^2 \bar{\tau}^2} + \frac{i}{\omega} \frac{\omega_p^2 \bar{\tau}}{1 + \omega^2 \bar{\tau}^2}, \quad (6.35)$$

⁵Note, that the phenomenological Drude theory of electron transport can be deduced from purely classical considerations.

⁶Note that $\sigma_1(\omega)$ has Lorentzian form and naturally leads to a delta function:

$$\sigma_1(\omega) = \frac{\omega_p^2}{4\pi} \frac{\bar{\tau}}{1 + \omega^2 \bar{\tau}^2} \xrightarrow{\bar{\tau} \rightarrow \infty} \frac{\omega_p^2}{4} \delta(\omega). \quad (6.34)$$

which can be used to discuss the optical properties of metals. The complex index of refraction $n + ik$ is given through $(n + i\kappa)^2 = \varepsilon$. Next, we discuss three important regimes of frequency. To probe optical properties we consider the reflectivity of light hitting a metal surface perpendicularly. Then the reflectivity is given by

$$R = \frac{(n - 1)^2 + \kappa^2}{(n + 1)^2 + \kappa^2}. \quad (6.36)$$

Inside the metal the light propagation is renormalised by $k \rightarrow k(n + i\kappa)$ with $k = \omega/c$ such that

$$e^{ik(n+i\kappa)z} = e^{iknz} e^{-\kappa kz} = e^{iknz} e^{-z/\delta} \quad (6.37)$$

defining the penetration length

$$\delta = \frac{c}{\omega\kappa}. \quad (6.38)$$

Relaxation-free regime ($\omega\bar{\tau} \ll 1 \ll \omega_p\bar{\tau}$)

In this limit, the real (ε_1) and imaginary (ε_2) part of the dielectric function (6.35) read

$$\varepsilon_1(\omega) \approx -\omega_p^2 \bar{\tau}^2, \quad (6.39)$$

$$\varepsilon_2(\omega) \approx \frac{\omega_p^2 \bar{\tau}}{\omega}. \quad (6.40)$$

The real part ε_1 is constant and negative, whereas the imaginary part ε_2 becomes singular in the limit $\omega \rightarrow 0$. Thus, the refractive index turns out to be dominated by ε_2

$$n(\omega) \approx \kappa(\omega) \approx \sqrt{\frac{\varepsilon_2(\omega)}{2}} \approx \sqrt{\frac{\omega_p^2 \bar{\tau}}{2\omega}} \gg 1, \quad (6.41)$$

As a result, the reflectivity R is practically 100%. The absorption index $\kappa(\omega)$ determines the penetration depth δ through

$$\delta(\omega) = \frac{c}{\omega\kappa(\omega)} \approx \frac{c}{\omega_p} \sqrt{\frac{2}{\omega\bar{\tau}}}. \quad (6.42)$$

With this, the skin depth of a metal with the famous relation $\delta(\omega) \propto \omega^{-1/2}$ is reproduced within the relaxation time approximation of the Boltzmann equation. While length $\delta(\omega)$ is in the centimeter range for frequencies of the order of 10 – 100Hz, the Debye length c/ω_p , is only of the order of 100Å for $\hbar\omega_p = 10$ eV. (cf. Figure 6.1).

Relaxation regime ($1 \ll \omega\bar{\tau} \ll \omega_p\bar{\tau}$)

Here, we can expand the dielectric function (6.35) in $(\omega\bar{\tau})^{-1}$, yielding

$$\varepsilon(\omega) = 1 - \frac{\omega_p^2}{\omega^2} + i \frac{\omega_p^2}{\omega^3 \bar{\tau}}. \quad (6.43)$$

The real part $\varepsilon_1 \approx -\omega_p^2/\omega^2$ is large and negative and dominates in magnitude over ε_2 . For the optical properties, we obtain

$$\kappa(\omega) \approx \frac{\omega_p}{\omega} \quad (6.44)$$

$$n(\omega) \approx \frac{\omega_p}{2\omega^2 \bar{\tau}}. \quad (6.45)$$

We find $\kappa(\omega) \gg n(\omega) \gg 1$, which implies a large reflectivity of metals in this frequency range as well. Note that visible frequencies are part of this regime (see Figures 6.2 and 6.3). The frequency dependence of the penetration depth becomes weak, and its magnitude is approximately given by the Debye length, $\delta \sim c/\omega_p$.

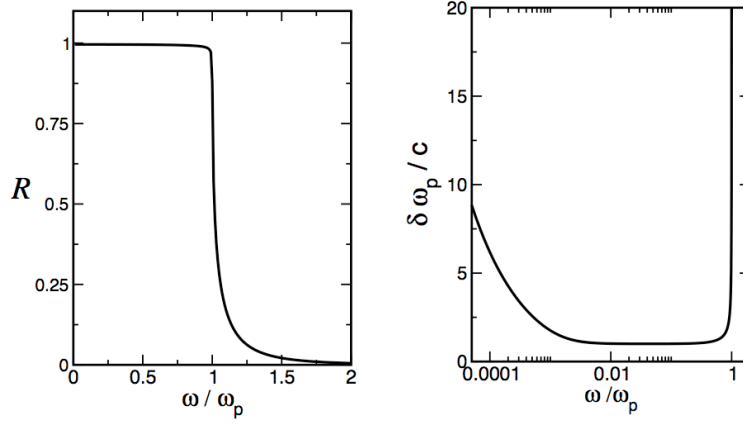


Figure 6.1: The frequency dependent reflectivity and penetration depth for $\omega_p \bar{\tau} = 500$.

Ultraviolet regime ($\omega \approx \omega_p$ and $\omega > \omega_p$)

In this regime, the imaginary part of ε is approximately zero and the real part has the well known form

$$\varepsilon_1(\omega) = 1 - \frac{\omega_p^2}{\omega^2}, \quad (6.46)$$

such that the reflectivity drops drastically, from close to unity towards zero (cf. Figure 6.1). Metals become nearly transparent in the range $\omega > \omega_p$. In Figure 6.1, one also notices the rapid increase in the penetration depth δ , showing the transparency of the metal.

In all these considerations, we have neglected the contributions to the dielectric function due to the ion cores (core electrons and nuclei). This may be incorporated in Eq.(6.46) in the following approximate way:

$$\varepsilon_1(\omega) = \varepsilon_\infty - \frac{\omega_p^2}{\omega^2}, \quad (6.47)$$

This influences the reflecting properties of metals; particularly, the value of ω_p is reduced to $\omega'_p = \omega_p / \sqrt{\varepsilon_\infty}$, where ε_∞ is the frequency-independent part of the dielectric function. With this, the reflectivity for frequencies above ω'_p approaches $R_\infty = (\varepsilon_\infty - 1)^2 / (\varepsilon_\infty + 1)^2$, and $0 < R_\infty < 1$ (see Figure 6.2 and 6.3).

Color of metals

The practically full reflectance for frequencies below ω_p is a typical feature of metals. Since for most metals, the plasma frequency lies well above the range of visible light ($\hbar\omega = 1.5 - 3.5\text{eV}$), they appear shiny to our eye. While most polished metal surfaces appear shiny white, like silver, there are some metals with a color, like gold which is yellow and copper which is reddish. White shininess results from reflectance on the whole visible frequency range, while for colored metals there is a certain threshold above which the reflectance drops and frequencies towards blue are not or much weaker reflected. In most cases this drop is not connected with the plasma frequency, but with light absorption due to interband transitions. Note that the single band metal which was used for the Drude theory does not allow for optical absorption apart from the plasma excitation. Interband transition play a particularly important role for the noble metals, Cu, Ag and Au. For these metals, the reflectance drop is caused by the transition from the

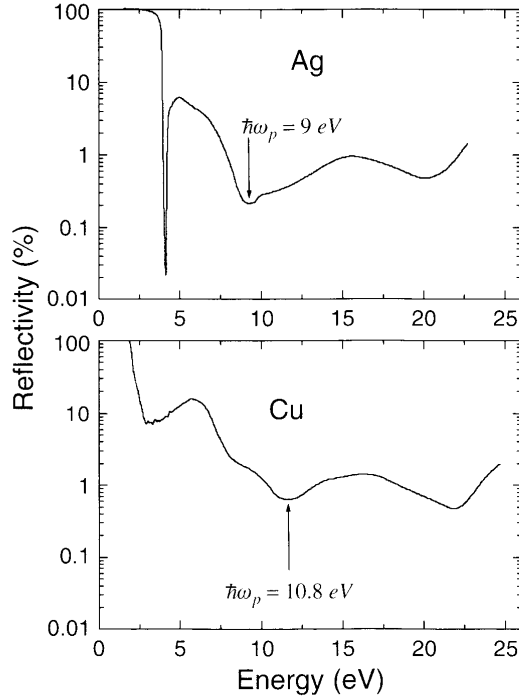


Figure 6.2: Reflectance spectra for silver and copper. In both cases the drop of reflectance is due to optical transition between the completely filled d -band and the partially filled s -band. Note the logarithmic scale for the reflectivity. (Source: *An introduction to the optical spectroscopy of inorganic solids*, J. García Solé, L.E. Bausá and D. Jaque, Wiley (2005))

completely occupied d -band to the partially filled s -band, $3d \rightarrow 4s$ in case of Cu. For copper, this drop appears below 2.5eV so that predominantly red light is reflected (see Figure 6.2). For gold, this threshold frequency is slightly higher, but still in the visible, while for silver, it lies beyond the visible range (see Figure 6.2). For all these cases, the plasma frequency is not so easily recognizable in the reflectance. On the other hand, aluminum shows a reflectance rather close to the expected behavior (see. Figure 6.3). Also here, there is a small reduction of the reflection due to interband absorption. However, this effect is weak and the strong drop occurs at the plasma frequency of $\hbar\omega_p = 15.8\text{eV}$. Like silver also polished aluminum is white shiny.

6.2.3 The relaxation time

By replacing the collision integral by a relaxation time approximation, we implicitly introduced a connection between the scattering rate $W(\mathbf{k}, \mathbf{k}')$ and the relaxation time τ . This relation,

$$\frac{f(\mathbf{k}) - f_0(\mathbf{k})}{\tau(\epsilon_{\mathbf{k}})} = \int \frac{d^3k'}{(2\pi)^3} W(\mathbf{k}, \mathbf{k}') \{f(\mathbf{k}) - f(\mathbf{k}')\}, \quad (6.48)$$

will be studied for an isotropic system, with elastic scattering, and a small external field \mathbf{E} . The solution of equation (6.24) is of the form

$$f(\mathbf{k}) = f_0(\mathbf{k}) + A(k)\mathbf{k} \cdot \mathbf{E}, \quad (6.49)$$

such that

$$f(\mathbf{k}) - f(\mathbf{k}') = A(k)(\mathbf{k} - \mathbf{k}') \cdot \mathbf{E}. \quad (6.50)$$

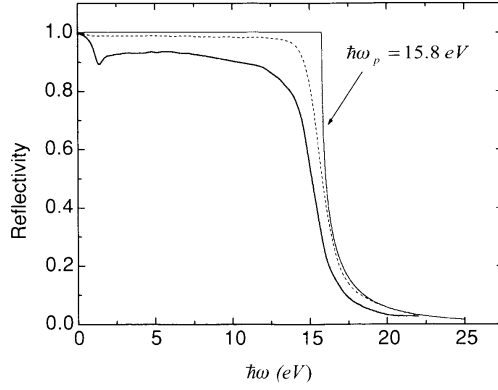


Figure 6.3: Reflectance spectrum of aluminum. The slight reduction of reflectivity below ω_p is due to interband transitions. The thin solid line is the theoretical behavior for $\tau = 0$ and the dashed line for finite τ . (Source: *An introduction to the optical spectroscopy of inorganic solids*, J. García Solé, L.E. Bausá and D. Jaque, Wiley (2005))

Without loss of generality, we define $\hat{z} \parallel \mathbf{k}$, and introduce the parametrization of the angles θ , polar angle of \mathbf{E} and θ' (ϕ') polar (azimuth) angle of \mathbf{k}' , leading to

$$\mathbf{k} \cdot \mathbf{E} = kE \cos \theta, \quad (6.51)$$

$$\mathbf{k} \cdot \mathbf{k}' = kk' \cos \theta', \quad (6.52)$$

$$\mathbf{k}' \cdot \mathbf{E} = k'E(\cos \theta \cos \theta' + \sin \theta \sin \theta' \cos \phi'). \quad (6.53)$$

For elastic scattering, $k = k'$, we obtain

$$f(\mathbf{k}) - f(\mathbf{k}') = A(k)kE[\cos \theta(1 - \cos \theta') - \sin \theta \sin \theta' \cos \phi']. \quad (6.54)$$

Inserting this into the right-hand side of equation (6.48), the ϕ' -dependent part of the integration vanishes for an isotropic system, and we are left with

$$\frac{f(\mathbf{k}) - f_0(\mathbf{k})}{\tau(\epsilon_{\mathbf{k}})} = \int d\Omega_{\mathbf{k}'} [f(\mathbf{k}) - f(\mathbf{k}')] W(\mathbf{k}, \mathbf{k}') \quad (6.55)$$

$$= A(k)kE \cos \theta \int d\Omega_{\mathbf{k}'} (1 - \cos \theta') W(\mathbf{k}, \mathbf{k}') \quad (6.56)$$

$$= [f(\mathbf{k}) - f_0(\mathbf{k})] \int d\Omega_{\mathbf{k}'} (1 - \cos \theta') W(\mathbf{k}, \mathbf{k}'). \quad (6.57)$$

The factor $[f(\mathbf{k}) - f_0(\mathbf{k})]$ can be dropped on both sides of the equation, resulting in

$$\frac{1}{\tau(\epsilon_{\mathbf{k}})} = \int \frac{d^3 k'}{(2\pi)^3} W(\mathbf{k}, \mathbf{k}') (1 - \cos \theta'), \quad (6.58)$$

where one should remember that, for elastic scattering, the quasiparticle energy $\epsilon_{\mathbf{k}} = \epsilon_{\mathbf{k}'}$ is conserved in the collision process. The scattering probability $W(\mathbf{k}, \mathbf{k}')$ accounts for this restriction. In the next few sections we discuss different scattering processes, looking at collision probabilities, relaxation times and the resulting conductivity and resistivity contributions.

6.3 Impurity scattering

6.3.1 Potential scattering

Every deviation from the perfect periodicity of the ionic lattice is a source of quasiparticle scattering, leading to the loss of their original momentum. Without translational invariance,

the conservation of momentum is lost, the energy, however, is still conserved. Possible static scatterers are among others vacancies, dislocations, and impurity atoms. The scattering rate $W(\mathbf{k}, \mathbf{k}')$ for a potential \widehat{V} can be determined applying Fermi's golden rule,⁷

$$W(\mathbf{k}, \mathbf{k}') = \frac{2\pi}{\hbar} n_{\text{imp}} |\langle \mathbf{k}' | \widehat{V} | \mathbf{k} \rangle|^2 \delta(\epsilon_{\mathbf{k}} - \epsilon_{\mathbf{k}'}). \quad (6.59)$$

By n_{imp} we denote the density of impurities, assuming only one species of them. For small densities n_{imp} , it is reasonable to neglect interference effects between different impurities. According to equation (6.58), the relaxation time τ of a quasiparticle with momentum $\hbar\mathbf{k}$ is given by

$$\frac{1}{\tau(\epsilon_{\mathbf{k}})} = \frac{2\pi}{\hbar} n_{\text{imp}} \int \frac{d^3k'}{(2\pi)^3} |\langle \mathbf{k}' | \widehat{V} | \mathbf{k} \rangle|^2 (1 - \hat{k} \cdot \hat{k}') \delta(\epsilon_{\mathbf{k}} - \epsilon_{\mathbf{k}'}) \quad (6.60)$$

$$= n_{\text{imp}} (\hat{k} \cdot \mathbf{v}_{\mathbf{k}}) \int \frac{d\sigma}{d\Omega}(\mathbf{k}, \mathbf{k}') (1 - \hat{k} \cdot \hat{k}') \frac{d\Omega_{\mathbf{k}'}}{4\pi}, \quad (6.61)$$

with the differential scattering cross section $d\sigma/d\Omega$ and $\hat{k} = \mathbf{k}/|\mathbf{k}|$. Here, we used the connection⁸ between Fermi's golden rule and the Born approximation. Note the difference in the expressions for the relaxation time τ in equation (6.58) and for the lifetime $\tilde{\tau}$,

$$\frac{1}{\tilde{\tau}} = \int \frac{d^3k}{(2\pi)^3} W(\mathbf{k}, \mathbf{k}'), \quad (6.65)$$

given by Fermi's golden rule. The factor $(1 - \cos\theta')$ in equation (6.58) gives more weight to backscattering ($\theta' \approx \pi$) compared to forward scattering ($\theta' \approx 0$), since the former has more influence in impeding transport. This explains why τ is also termed *transport lifetime*.

Assuming defects in the form of point charges Ze , whose screened potential is

$$\langle \mathbf{k}' | \widehat{V} | \mathbf{k} \rangle = \frac{4\pi Ze^2}{|\mathbf{k} - \mathbf{k}'|^2 + k_{\text{TF}}^2}. \quad (6.66)$$

In the limit of very strong screening, $k_{\text{TF}} \gg k_F$, the differential cross section becomes independent of the deviation $(\mathbf{k} - \mathbf{k}')$, the transport and the usual lifetime become equal, $\tau = \tilde{\tau}$,⁹ and

$$\frac{1}{\tau} \approx \frac{\pi}{\hbar} N(\epsilon_F) n_{\text{imp}} \left(\frac{4\pi Ze^2}{k_{\text{TF}}^2} \right)^2. \quad (6.67)$$

With this, we are now able to determine the conductivity for scattering on Coulomb defects, assuming *s*-wave scattering only. Then, since $\tau(\epsilon)$ depends weakly on energy, equation (6.31) yields

$$\sigma = \frac{e^2 n \tau(\epsilon_F)}{m}, \quad (6.68)$$

⁷This corresponds to the first Born approximation in scattering theory. Note, that this approximation is insufficient to describe resonant scattering.

⁸The scattering of particles with momentum $\hbar\mathbf{k}$ into the solid angle $d\Omega_{\mathbf{k}'}$ around \mathbf{k}' yields

$$W(\mathbf{k}, \mathbf{k}') d\Omega_{\mathbf{k}'} = \frac{2\pi}{\hbar} \sum_{\mathbf{k}' \in d\Omega_{\mathbf{k}'}} |\langle \mathbf{k}' | \widehat{V} | \mathbf{k} \rangle|^2 \delta(\epsilon_{\mathbf{k}} - \epsilon_{\mathbf{k}'}) \quad (6.62)$$

$$= \frac{2\pi}{\hbar} d\Omega_{\mathbf{k}'} \int \frac{d^3k'}{(2\pi)^3} |\langle \mathbf{k}' | \widehat{V} | \mathbf{k} \rangle|^2 \delta(\epsilon_{\mathbf{k}} - \epsilon_{\mathbf{k}'}) = \frac{2\pi}{\hbar} d\Omega_{\mathbf{k}'} N(\epsilon) |\langle \mathbf{k}' | \widehat{V} | \mathbf{k} \rangle|^2. \quad (6.63)$$

The scattering per incoming particle current $j_{\text{in}} d\sigma(\mathbf{k}, \mathbf{k}') = W(\mathbf{k}, \mathbf{k}') d\Omega_{\mathbf{k}'}$ determines the differential cross section

$$\hat{k} \cdot \mathbf{v}_{\mathbf{k}} \frac{d\sigma}{d\Omega}(\mathbf{k}, \mathbf{k}') = \frac{2\pi}{\hbar} \frac{N(\epsilon)}{4\pi} |\langle \mathbf{k}' | \widehat{V} | \mathbf{k} \rangle|^2. \quad (6.64)$$

leading to equation (6.61).

⁹In the context of partial wave expansion, one speaks of *s*-wave scattering, i.e., $\delta_{l>0} \rightarrow 0$.

or, for the specific resistivity $\rho = 1/\sigma$,

$$\rho = \frac{m}{e^2 n \tau(\epsilon_F)}. \quad (6.69)$$

Both σ and ρ are independent of temperature. This contribution is called the *residual resistivity* of a metal, which approaches zero for a perfect material. The temperature dependence of the resistivity is induced in other scattering processes like electron-phonon scattering and electron-electron scattering, which will be considered below. The so-called *residual resistance ratio* $RRR = R(T = 300K)/R(T = 0)$ is an often used quantity to benchmark the quality of a material. It is defined as the ratio between the resistance R at room temperature and the resistance at zero temperature. The bigger the RRR , the better the quality of the material. The typical value of RRR for common copper is 40-50, while the RRR for very clean aluminum reaches values up to 20000.

6.3.2 Kondo effect

There are impurity atoms inducing so-called *resonant scattering*. If the resonance occurs close to the Fermi energy, the scattering rate is strongly energy dependent, inducing a more pronounced temperature dependence of the resistivity. An important example is the scattering off magnetic impurities with a spin degree of freedom, yielding a dramatic energy dependence of the scattering rate. This problem was first studied by Kondo in 1964 in order to explain the peculiar minima in resistivity in some materials. The coupling between the local spin impurities \mathbf{S}_i at \mathbf{R}_i and the quasiparticle spin \mathbf{s} has the exchange form

$$\hat{V}_K = \sum_i (\hat{V}_K)_i = J \sum_i \hat{\mathbf{S}}_i \cdot \hat{\mathbf{s}}(\mathbf{r}) \delta(\mathbf{r} - \mathbf{R}_i) \quad (6.70)$$

$$= J \sum_i \left(\hat{S}_i^z \hat{s}^z(\mathbf{r}) + \frac{1}{2} \hat{S}_i^+ \hat{s}^-(\mathbf{r}) + \frac{1}{2} \hat{S}_i^- \hat{s}^+(\mathbf{r}) \right) \delta(\mathbf{r} - \mathbf{R}_i) \quad (6.71)$$

$$= \frac{J\hbar}{2\Omega} \sum_{\mathbf{k}, \mathbf{k}', i} \left[\hat{S}_i^z (\hat{c}_{\mathbf{k}\uparrow}^\dagger \hat{c}_{\mathbf{k}'\uparrow} - \hat{c}_{\mathbf{k}\downarrow}^\dagger \hat{c}_{\mathbf{k}'\downarrow}) + S_i^+ \hat{c}_{\mathbf{k}\downarrow}^\dagger \hat{c}_{\mathbf{k}'\uparrow} + S_i^- \hat{c}_{\mathbf{k}\uparrow}^\dagger \hat{c}_{\mathbf{k}'\downarrow} \right] e^{-i(\mathbf{k}-\mathbf{k}') \cdot \mathbf{R}_i}. \quad (6.72)$$

Here, it becomes important that spin flip processes, which change the spin state of the impurity and that of the scattered electron, are enabled. The results for the scattering rate are presented here without derivation,

$$W(\mathbf{k}, \mathbf{k}') \approx J^2 S(S+1) \left[1 + 2JN(\epsilon_F) \ln \left(\frac{D}{|\epsilon_{\mathbf{k}} - \epsilon_F|} \right) \right], \quad (6.73)$$

where D is the bandwidth and we have assumed that $JN(\epsilon_F) \ll 1$. The relaxation time is found to be

$$\frac{1}{\tau(\epsilon_{\mathbf{k}})} \approx \frac{J^2 S(S+1)}{\hbar} N(\epsilon) \left[1 + 2JN(\epsilon_F) \ln \left(\frac{D}{|\epsilon_{\mathbf{k}} - \epsilon_F|} \right) \right]. \quad (6.74)$$

Note that $W(\mathbf{k}, \mathbf{k}')$ does not depend on angle, meaning that the process is described by s -wave scattering. The energy dependence is singular at the Fermi energy, indicating that we are not dealing with simple resonant potential scattering, but with a much more subtle many-particle effect involving the electrons very near the Fermi surface. The fact that the local spins \mathbf{S}_i can flip, makes the scattering center dynamical, because the scatterer is constantly changing. The scattering process of an electron is influenced by previous scattering events, leading to the singularity at ϵ_F . This cannot be described within the first Born approximation, but requires at least the second approximation or the full solution.¹⁰ As mentioned before, the resonant

¹⁰We refer to J.M. Ziman, *Principles of the Theory of Solids*, and A.C. Hewson, *The Kondo Problem to Heavy Fermions* for more details.

behavior induces a strong temperature dependence of the conductivity. Indeed,

$$\sigma(T) = \frac{e^2 k_F^3}{6\pi^2 m} \int d\epsilon \frac{1}{4k_B T \cosh^2(\epsilon - \epsilon_F)/2k_B T} \tau(\epsilon) \quad (6.75)$$

$$\approx \frac{e^2 n}{8mk_B T} \int d\tilde{\epsilon} \frac{J^2 S(S+1)[1 - 2JN(\epsilon_F) \ln(D/\tilde{\epsilon})]}{\cosh^2(\tilde{\epsilon}/2k_B T)}. \quad (6.76)$$

A simple substitution in the integral leads to

$$\sigma(T) \approx \frac{e^2 n}{2m} J^2 S(S+1) \left[1 - 2JN(\epsilon_F) \ln\left(\frac{D}{k_B T}\right) \right]. \quad (6.77)$$

Usual contributions to the resistance, like electron-phonon scattering discussed below, typically decrease with temperature. The contribution (6.77) to the conductivity is strongly increasing, inducing a minimum in the resistance, when we crossover from the decreasing behavior at high temperatures to the low-temperature increase of $\rho(T)$. At even lower temperatures, the conductivity would decrease and eventually even turn negative which is an artifact of our approximation. In reality, the conductivity saturates at a finite value when the temperature is lowered below a characteristic Kondo temperature T_K ,

$$k_B T_K = D e^{-1/JN(\epsilon_F)}, \quad (6.78)$$

a characteristic energy scale of this system. The real behavior of the conductivity at temperatures $T \ll T_K$ is not accessible by simple perturbation theory. This regime, known as the Kondo problem, represents one of the most interesting correlation phenomena of many-particle physics.

6.4 Electron-phonon interaction

Even in perfect metals, the conductivity becomes non-zero at finite temperature. The thermally induced distortions of the lattice, phonons, act as fluctuating scattering centers. In the language of electron-phonon interaction, electrons are scattered via absorption and emission of phonons, which induce local fluctuations in volume (cf. Chapter 3). The corresponding coupling term was given in equation (3.143) and simplifies with the definition (3.130) to

$$\mathcal{H}_{\text{int}} = 2i \sum_{\mathbf{k}, \mathbf{q}, s} \tilde{V}_{\mathbf{q}} \sqrt{\frac{\hbar}{2\rho_0 \omega_{\mathbf{q}}}} |\mathbf{q}| (\hat{b}_{\mathbf{q}} - \hat{b}_{-\mathbf{q}}^\dagger) \hat{c}_{\mathbf{k}+\mathbf{q}, s}^\dagger \hat{c}_{\mathbf{k} s}. \quad (6.79)$$

The interaction is formally similar to the coupling between electrons and photons. The dominant processes consist of single-phonon processes, i.e., the absorption or emission of one phonon. Energy and momentum are conserved, such that, for the scattering of an electron from momentum \mathbf{k} to \mathbf{k}' due to the emission of a phonon with momentum \mathbf{q} , we have

$$\mathbf{k} = \mathbf{k}' + \mathbf{q} + \mathbf{G}, \quad (6.80)$$

$$\epsilon_{\mathbf{k}} = \hbar\omega_{\mathbf{q}} + \epsilon_{\mathbf{k}'}, \quad (6.81)$$

Here, $\omega_{\mathbf{q}} = c_s q$ is the phonon spectrum, while the reciprocal lattice vector \mathbf{G} allows for scattering¹¹ in nearby Brillouin zones. By this, the phase space available for scattering is strongly reduced, especially near the Fermi energy. Note that $\hbar\omega_{\mathbf{q}} \leq \hbar\omega_D \ll \epsilon_F$. In order to calculate

¹¹This so-called *Umklapp phenomenon* will be discussed in some more detail later in this chapter.

the scattering rates, the matrix elements¹² of the available processes,

$$\langle \mathbf{k} + \mathbf{q}; N_{\mathbf{q}'} | (\hat{b}_{\mathbf{q}} - \hat{b}_{-\mathbf{q}}^\dagger) \hat{c}_{\mathbf{k}+\mathbf{q},s}^\dagger \hat{c}_{\mathbf{k},s} | \mathbf{k}; N_{\mathbf{q}'} \rangle = \langle \mathbf{k} + \mathbf{q} | \hat{c}_{\mathbf{k}+\mathbf{q},s}^\dagger \hat{c}_{\mathbf{k},s} | \mathbf{k} \rangle \left(\sqrt{N_{\mathbf{q}'}} \delta_{N_{\mathbf{q}'}, N_{\mathbf{q}'}-1} \delta_{\mathbf{q}, \mathbf{q}'} - \sqrt{N_{\mathbf{q}'} + 1} \delta_{N_{\mathbf{q}'}, N_{\mathbf{q}'}+1} \delta_{\mathbf{q}, -\mathbf{q}'} \right), \quad (6.82)$$

need to be calculated. From Fermi's golden rule we obtain

$$\left(\frac{\partial f}{\partial t} \right)_{\text{coll}} = -\frac{2\pi}{\hbar} \sum_{\mathbf{q}} |g(\mathbf{q})|^2 \left[[f(\mathbf{k})(1 - f(\mathbf{k} + \mathbf{q}))(N_{-\mathbf{q}} + 1) - f(\mathbf{k} + \mathbf{q})(1 - f(\mathbf{k}))N_{-\mathbf{q}}] \delta(\epsilon_{\mathbf{k}+\mathbf{q}} - \epsilon_{\mathbf{k}} + \hbar\omega_{-\mathbf{q}}) - [f(\mathbf{k} + \mathbf{q})(1 - f(\mathbf{k}))N_{\mathbf{q}} + 1 - f(\mathbf{k})(1 - f(\mathbf{k} + \mathbf{q}))N_{\mathbf{q}}] \delta(\epsilon_{\mathbf{k}+\mathbf{q}} - \epsilon_{\mathbf{k}} - \hbar\omega_{\mathbf{q}}) \right], \quad (6.83)$$

where $g(\mathbf{q}) = \tilde{V}_{\mathbf{q}} |\mathbf{q}| \sqrt{2\hbar/\rho_0\omega_{\mathbf{q}}}$. Each of these four terms describes one of the single phonon scattering processes depicted in Figure 6.4.

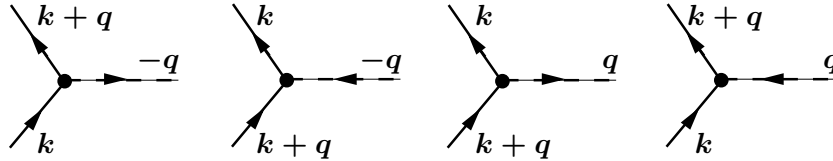


Figure 6.4: The four single-phonon electron-phonon scattering processes.

The collision integral leads to a complicated integro-differential equation, whose solution is tedious and would involve the solution of the non-equilibrium phonon-problem as well. Instead of a full rigorous calculation including the non-equilibrium redistribution of phonons, we will consider the behavior in various temperature regimes by an approximate treatment of the phonons. The characteristic temperature of phonons, the Debye temperature $\Theta_D \ll T_F$, is much smaller than the Fermi temperature. Hence, the phonon energy is virtually unimportant for the energy conservation, $\epsilon_{\mathbf{k}'=\mathbf{k}+\mathbf{q}} \approx \epsilon_{\mathbf{k}}$. Therefore we are allowed to impose momentum conservation $\epsilon_{\mathbf{k}+\mathbf{q}} = \epsilon_{\mathbf{k}}$ and consider the lattice distortion as being essentially static, in the sense of an adiabatic Born-Oppenheimer approximation. The approximate collision integral then reads

$$\left(\frac{\partial f}{\partial t} \right)_{\text{coll}} = \frac{2\pi}{\hbar} \sum_{\mathbf{q}} |g(\mathbf{q})|^2 2N(\omega_{\mathbf{q}}) [f(\mathbf{k} + \mathbf{q}) - f(\mathbf{k})] \delta(\epsilon_{\mathbf{k}+\mathbf{q}} - \epsilon_{\mathbf{k}}), \quad (6.84)$$

where we assume the occupation of phonon states according to the equilibrium distribution for bosons,

$$N(\omega_{\mathbf{q}}) = \frac{1}{e^{\hbar\omega_{\mathbf{q}}/k_B T} - 1}. \quad (6.85)$$

This approximation includes all important aspects of the electron-phonon scattering we need to derive the temperature dependence of $\rho(T)$.

¹²In analogy to the discussion on electromagnetic radiation, the phenomenon of *spontaneous phonon emission* due to zero-point fluctuations appears. It is formally visible in the additional “+1” in the factors $(N_{\pm\mathbf{q}} + 1)$.

In analogy to previous approaches, we obtain with relaxation-time Ansatz

$$\frac{1}{\tau(\epsilon_{\mathbf{k}})} = \frac{2\pi}{\hbar} \frac{\lambda}{N(\epsilon_F)} \int \frac{d^3q}{(2\pi)^3} \hbar\omega_{\mathbf{q}} N(\omega_{\mathbf{q}}) (1 - \cos\theta) \delta(\epsilon_{\mathbf{k}+\mathbf{q}} - \epsilon_{\mathbf{k}}), \quad (6.86)$$

where $|\mathbf{k}| = |\mathbf{k} + \mathbf{q}| = k_F$, meaning that only the electrons in a thin shell close to the Fermi surface are relevant. Furthermore, we parametrized $g(\mathbf{q})$ according to

$$|g(\mathbf{q})|^2 = \frac{\lambda}{2N(\epsilon_F)\Omega} \hbar\omega_{\mathbf{q}}, \quad (6.87)$$

where λ is a dimensionless electron-phonon coupling constant. In usual metals $\lambda < 1$. As in the case of defect scattering, the relaxation time depends only weakly on the electron energy. But, unlike previously, the direct temperature dependence enters via the dependence on temperature of the phonon occupation $N(\omega_{\mathbf{q}})$.

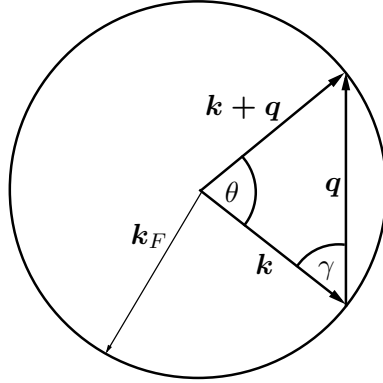


Figure 6.5: The geometry of electron-phonon scattering.

In order to perform the integration in equation (6.86), we have to re-express $\delta(\epsilon_{\mathbf{k}+\mathbf{q}} - \epsilon_{\mathbf{k}})$ by writing

$$\delta(\epsilon_{\mathbf{k}+\mathbf{q}} - \epsilon_{\mathbf{k}}) = \delta\left(\frac{\hbar^2}{2m}(q^2 - 2k_F q \cos\gamma)\right) = \frac{m}{\hbar^2 k_F q} \delta\left(\frac{q}{2k_F} - \cos\gamma\right), \quad (6.88)$$

where γ is defined in Figure 6.5. From there, we also see that $2\gamma + \theta = \pi$, and thus, find the relation

$$1 - \cos\theta = 1 + \cos(2\gamma) = 2\cos^2(\gamma). \quad (6.89)$$

Obviously, we have to integrate q over the range $[0, 2k_F]$ on the right-hand side of equation (6.86), which can be reformulated to

$$\frac{1}{\tau(\epsilon_F, T)} = \frac{-\lambda}{N(\epsilon_F)} \frac{m}{\hbar^2 \pi k_F} \int_0^{2k_F} dq q \omega_{\mathbf{q}} N(\omega_{\mathbf{q}}) \int_0^{\pi/2} d\gamma \sin\gamma \cos^2(\gamma) \delta\left(\frac{q}{2k_F} - \cos\gamma\right) \quad (6.90)$$

$$= \frac{\lambda}{4N(\epsilon_F)} \frac{mc_s}{\hbar^2 \pi k_F^3} \int_0^{2k_F} \frac{q^4 dq}{e^{\hbar c_s q / k_B T} - 1} \quad (6.91)$$

$$= \frac{\lambda}{4N(\epsilon_F)} \frac{mc_s k_F^2}{\hbar^2 \pi} \left(\frac{T}{\Theta_D}\right)^5 \int_0^{2\Theta_D/T} \frac{y^4 dy}{e^y - 1}, \quad (6.92)$$

where we have approximated the Debye temperature by $k_B\Theta_D \approx \hbar c_s k_F$. We notice the two distinct characteristic temperature regimes,

$$\frac{1}{\tau} = \begin{cases} 6\zeta(5)\lambda\pi\frac{k_B\Theta_D}{\hbar}\left(\frac{T}{\Theta_D}\right)^5, & T \ll \Theta_D, \\ \lambda\pi\frac{k_B\Theta_D}{\hbar}\left(\frac{T}{\Theta_D}\right), & T \gg \Theta_D. \end{cases} \quad (6.93)$$

The prefactors depend on the details of the approximation, whereas the qualitative temperature dependence does not. We finally obtain the conductivity and resistivity from equation (6.29),

$$\sigma = \frac{e^2 n}{m} \tau(T), \quad (6.94)$$

$$\rho = \frac{m}{e^2 n} \frac{1}{\tau(T)}, \quad (6.95)$$

where we used the weak energy dependence of $\tau(\epsilon \approx \epsilon_F, T)$. With this, we obtain the well-known Bloch-Grüneisen form

$$\rho(T) \propto \begin{cases} T^5, & T \ll \Theta_D, \\ T, & T \gg \Theta_D. \end{cases} \quad (6.96)$$

At high temperatures, ρ is determined by the occupation of phonon states

$$N(\omega_q) \approx \frac{k_B T}{\hbar \omega_q} \quad (6.97)$$

which change the scattering strength (amplitude) of the lattice modulation linear in T . At low temperature only the lowest phonon states are occupied $\hbar\omega_q < k_B T$ yield $q < k_B T / \hbar c_s$. Thus, at low temperatures only long-wave length modulations of the lattice generate a scattering potentials which deflects electrons only slightly from their trajectories (forward scattering dominates). This represents a restriction of the scattering phase space becoming ever smaller with decreasing temperature.

6.5 Electron-electron scattering

In Chapter 5 we have learned, that, taking a short-ranged electron-electron interaction into account, scattering rate for electrons decreases strongly close to the Fermi surface. The basic reason for this lies in the constraint of the scattering phase space imposed by the Pauli principle. The lifetime, which we identify with the relaxation time here, has the form

$$\frac{1}{\tau(\epsilon)} = \frac{1}{\tau_e} \left(\frac{\epsilon}{\epsilon_F} - 1 \right)^2 \quad (6.98)$$

where energy and momentum conservation is taken into account and τ_e is a constant of unit time. We may now calculate the mean relaxation time $\bar{\tau}$ as introduced in Sect.6.2.2. To regularize the integrals we take here also impurity scattering into account by adding a constant to the scattering rate in Eq.(6.98) and obtain for the resistivity¹³

$$\rho(T) = \rho_0 + \frac{\pi^2}{3} \frac{m}{ne^2 \tau_e} \left(\frac{k_B T}{\epsilon_F} \right)^2 \quad (6.102)$$

Electron-electron scattering introduces a quadratic temperature dependence to resistivity. This is a key property of a Fermi liquid and is often considered an identifying criterion.

¹³ *Calculation of mean scattering time $\bar{\tau}$:* We use Matthiessen's rule to add the scattering rates of electron-electron and impurity scattering to the form

$$\frac{1}{\tau(\epsilon)} = \frac{1}{\tau_e} \left(\frac{\epsilon}{\epsilon_F} - 1 \right)^2 + \frac{1}{\tau_0}. \quad (6.99)$$

Umklapp process

An important point, kept quiet so far, requires some explanation. One could argue, that the momentum of the Fermi liquid is conserved upon the collision of two electrons. With this argument, it is not quite clear what causes a finite resistance. This argument, however, is based on translational invariance and ignores the existence of the underlying lattice. In the sense that the kinematics (momentum conservation) is also satisfied for electrons being scattered from the Fermi surface of one Brillouin zone to the one of another Brillouin zone, while incorporating a reciprocal lattice vector. The equation of momentum conservation,

$$\mathbf{k} = \mathbf{k}' + \mathbf{G}, \quad (6.103)$$

where \mathbf{G} is a reciprocal vector of the lattice, allows for scattering to other Brillouin zones ($\mathbf{G} \neq 0$). By this, the momentum is transferred to a static deformation of the lattice. Such processes are termed *Umklapp* processes and play an important role in electron-phonon scattering as well (see equation (6.80)).

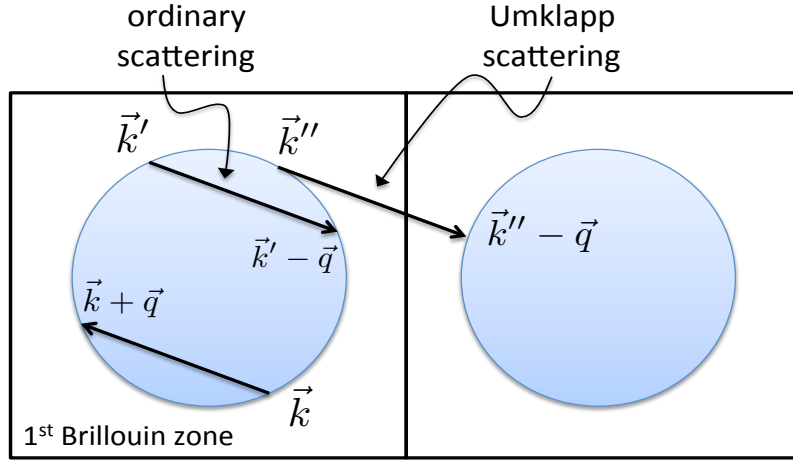


Figure 6.6: Considering energy and momentum conservation in two-electron collision there are ordinary scattering processes $(\mathbf{k}, \mathbf{k}') \rightarrow (\mathbf{k} + \mathbf{q}, \mathbf{k}' - \mathbf{q})$ which does not lead to a momentum relaxation, and there are Umklapp scattering processes $(\mathbf{k}, \mathbf{k}'') \rightarrow (\mathbf{k} + \mathbf{q}, \mathbf{k}'' - \mathbf{q})$ leading to a neighbouring Brillouin zone, here visualized by an extended Brillouin zone scheme.

Restricting to the small temperature limit, we determine $\bar{\tau}$ by

$$\begin{aligned} \bar{\tau} &= \int d\epsilon \tau(\epsilon) \partial f_0 / \partial \epsilon = \int_{-\infty}^{+\infty} dE \frac{\tau(E)}{4k_B T \cosh^2(E/2k_B T)} \approx \int_{-\infty}^{+\infty} dE \frac{1}{4k_B T \cosh^2(E/2k_B T)} \left\{ \tau_0 - \frac{\tau_0^2 E^2}{\tau_e \epsilon_F^2} \right\} \\ &= \tau_0 - \frac{\pi^2}{3} \frac{\tau_0^2}{\tau_e} \left(\frac{k_B T}{\epsilon_F} \right)^2 \end{aligned} \quad (6.100)$$

where $E = \epsilon - \epsilon_F$. The resistivity is given by

$$\rho(T) = \frac{m}{ne^2 \bar{\tau}(T)} \approx \frac{m}{ne^2 \tau_0} \left\{ 1 + \frac{\pi^2}{3} \frac{\tau_0}{\tau_e} \left(\frac{k_B T}{\epsilon_F} \right)^2 \right\}, \quad (6.101)$$

and with $\rho_0 = m/ne^2 \tau_0$ as the residual resistivity leads to $\rho(T)$ in Eq.(6.102).

6.6 Matthiessen's rule and the Ioffe-Regel limit

Matthiessen's rule states, that the scattering rates of different scattering processes can simply be added, leading to

$$W(\mathbf{k}, \mathbf{k}') = W_1(\mathbf{k}, \mathbf{k}') + W_2(\mathbf{k}, \mathbf{k}'), \quad (6.104)$$

or, expressed in the relaxation time approximation,

$$\frac{1}{\tau} = \frac{1}{\tau_1} + \frac{1}{\tau_2}, \quad (6.105)$$

and

$$\rho = \frac{m}{ne^2\tau} = \frac{m}{ne^2} \left(\frac{1}{\tau_1} + \frac{1}{\tau_2} \right) = \rho_1 + \rho_2. \quad (6.106)$$

This rule is not a theorem and corresponds effectively to a serial coupling of resistors in a classical circuit. It is applicable, if the different scattering processes are independent. Actually, the assumption that the impurity scattering rate depends linearly on the impurity density n_{imp} is already an application of Matthiessen's rule. Mutual influences of impurities, e.g., through interference effects due to the coherent scattering of an electron at different impurities, would invalidate this simplification. An example where Matthiessen's rule is violated is a one-dimensional system, where a single scatterer i induces a finite resistance R_i . Two serial scatterers then lead to a total resistance

$$R = R_1 + R_2 + \frac{2e^2}{h} R_1 R_2 \geq R_1 + R_2. \quad (6.107)$$

The reason is, that in one-dimensional systems, the interference of backscattered waves is unavoidable and no impurity can be treated as isolated. Furthermore, every particle traversing the whole system has to pass all scatterers. The more general Matthiessen's rule,

$$\rho \geq \rho_1 + \rho_2, \quad (6.108)$$

is still valid. Another source of deviation from Matthiessen's rule arises, if the relaxation time depends on \mathbf{k} , since then the averaging is not the same for all scattering processes. The electron-phonon coupling can be modified by the scattering on impurities, most importantly in the presence of anisotropic Fermi surfaces. For the analysis of resistance data of simple metals, we often assume the validity of Matthiessen's rule. A typical example is the resistance minimum explained by Kondo, where

$$\rho(T) = \rho_0 + \rho_{e-p}(T) + \rho_K(T) + \rho_{e-e}(T) \quad (6.109)$$

$$= \rho_0 + \alpha T^5 + \beta(1 + 2JN(\epsilon_F) \ln(D/k_B T)) + \gamma T^2, \quad (6.110)$$

where α , β , and γ are numerical constants. Upon decreasing temperature, the Kondo term is increasing, whereas the electron-phonon and electron-electron contributions decrease. Consequently, there is a minimum.

We now turn to the discussion of resistivity in the high-temperature limit. Believing the previous considerations entirely, the electrical resistivity would grow indefinitely with temperature. In most cases, however, the resistivity will saturate at a finite limiting value. We can understand this from simple considerations writing the mean free path $\ell = v_F \tau(\epsilon_F)$ as the mean distance an electron travels freely between two collisions. The lattice constant a is a natural lower boundary to ℓ in the crystal lattice. Furthermore, we assumed so far that scattering occurs between two states with sharp momenta \mathbf{k} and \mathbf{k}' . If the de Broglie wavelength becomes comparable to the mean free path, the framework becomes unfounded and k_F^{-1} would become a boundary for ℓ . In

most systems a and k_F^{-1} are comparable lengths. Empirically, the resistivity is described via the formula

$$\frac{1}{\rho(T)} = \frac{1}{\rho_{BT}(T)} + \frac{1}{\rho_{\max}}, \quad (6.111)$$

corresponding to the parallel addition of two resistivities; on one hand, $\rho_{BT}(T)$, which we have investigated using the Boltzmann transport theory, and on the other hand the limiting value ρ_{\max} . This is in clear disagreement to Matthiessen's rule, which is to be expected, since for $k_F \ell \sim 1$, complex interference effects will arise. The saturated resistivity ρ_{\max} can be estimated from the Jellium model,

$$\rho_{\max} = \frac{m}{e^2 n \tau(\epsilon_F)} = \frac{3\pi^2 m}{e^2 k_F^3 \tau(\epsilon_F)} = \frac{h}{e^2} \frac{3\pi}{2k_F^2 \ell} \quad (6.112)$$

$$\sim \frac{h}{e^2} \frac{3\pi}{2k_F}, \quad (6.113)$$

where we used $\ell^{-1} \sim k_F$. For a typical value $k_F \sim 10^8 \text{cm}^{-1}$ of the Fermi wave vector, we find $\rho_{\max} \sim 1 \text{m}\Omega\text{cm}$, which is called the Ioffe-Regel¹⁴ limit. Establishing a quantitative estimate of ρ_{\max} for a given material is often difficult. There are even materials whose resistivity surpasses the Ioffe-Regel limit.

6.7 General transport coefficients

Simultaneously with charge, electrons will also transport energy, i.e., heat and entropy. This is why charge and heat transport are naturally interconnected. In the following, we generalize the transport theory set up above to include this interplay.

6.7.1 Generalized Boltzmann equation

We consider a metal with weakly space-dependent temperature $T(\mathbf{r})$ and chemical potential $\mu(\mathbf{r})$. The distribution function then reads

$$\delta f(\mathbf{k}; \mathbf{r}) = f(\mathbf{k}; \mathbf{r}) - f_0(\mathbf{k}, T(\mathbf{r}), \mu(\mathbf{r})), \quad (6.114)$$

where

$$f_0(\mathbf{k}, T(\mathbf{r}), \mu(\mathbf{r})) = \frac{1}{e^{(\epsilon_{\mathbf{k}} - \mu(\mathbf{r}))/k_B T(\mathbf{r})} + 1}. \quad (6.115)$$

In addition, we require the charge density to remain constant in space, i.e.,

$$\int \frac{d^3k}{(2\pi)^3} f(\mathbf{k}; \mathbf{r}) = n_0 \quad (6.116)$$

for all \mathbf{r} . In this section, we introduce the *electrochemical potential* $\eta(\mathbf{r}) = -e\phi(\mathbf{r}) + \mu(\mathbf{r})$ generating the general force field $\mathcal{E} = -\nabla(e\phi + \mu)$, where $\phi(\mathbf{r})$ denotes the electrostatic potential which produces the electric field $\mathbf{E} = -\nabla\phi$. With this, the Boltzmann equation for the

¹⁴The saturated resistivity $\rho_{\max} \sim 1 \text{m}\Omega\text{cm} = 1000 \mu\Omega\text{cm}$ should be compared to the room-temperature resistivity of good conductors,

| metal | Cu | Au | Ag | Pt | Al | Sn | Na | Fe | Ni | Pb |
|---------------------------------|-----|-----|-----|------|-----|----|-----|-----|----|----|
| ρ [$\mu\Omega\text{cm}$] | 1.7 | 2.2 | 1.6 | 10.5 | 2.7 | 11 | 4.6 | 9.8 | 7 | 21 |

which are all well below ρ_{\max} .

stationary situation reads

$$\left(\frac{\partial f}{\partial t}\right)_{\text{coll}} = \mathbf{v}_{\mathbf{k}} \cdot \nabla_{\mathbf{r}} f + \dot{\mathbf{k}} \cdot \nabla_{\mathbf{k}} f \quad (6.117)$$

$$= -\frac{\partial f}{\partial \epsilon_{\mathbf{k}}} \mathbf{v}_{\mathbf{k}} \cdot \left(\frac{\epsilon_{\mathbf{k}} - \mu}{T} \nabla_{\mathbf{r}} T - \boldsymbol{\mathcal{E}} \right). \quad (6.118)$$

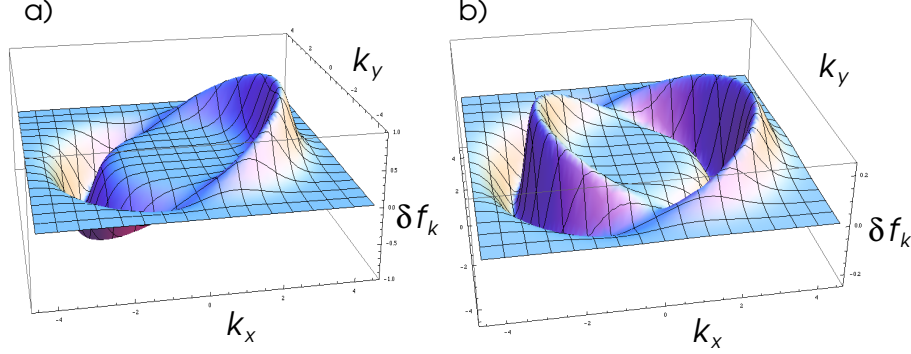


Figure 6.7: Schematic view of the distribution functions $\delta f(\mathbf{k})$ on a slice cut through the k -space ($k_z = 0$) with a circular Fermi surface for two situations. On the left panel (a), for an applied electric field along the negative x -direction, on the right panel (b) for a temperature gradient in x -direction.

In the relaxation time approximation for the collision integral, we obtain the solution

$$\delta f(\mathbf{k}) = -\frac{\partial f_0}{\partial \epsilon_{\mathbf{k}}} \tau(\epsilon_{\mathbf{k}}) \mathbf{v}_{\mathbf{k}} \cdot \left(\boldsymbol{\mathcal{E}} - \frac{\epsilon_{\mathbf{k}} - \mu}{T} \nabla_{\mathbf{r}} T \right), \quad (6.119)$$

which allows us to calculate the charge and heat currents,

$$\mathbf{J}_e = -2e \int \frac{d^3 k}{(2\pi)^3} \mathbf{v}_{\mathbf{k}} \delta f(\mathbf{k}), \quad (6.120)$$

$$\mathbf{J}_q = 2 \int \frac{d^3 k}{(2\pi)^3} (\epsilon_{\mathbf{k}} - \mu) \mathbf{v}_{\mathbf{k}} \delta f(\mathbf{k}), \quad (6.121)$$

respectively. Inserting the solution (6.119) into the two definitions above yields

$$\mathbf{J}_e = e \hat{K}^{(0)} \boldsymbol{\mathcal{E}} - \frac{e}{T} \hat{K}^{(1)} (-\nabla T), \quad (6.122)$$

$$\mathbf{J}_q = -\hat{K}^{(1)} \boldsymbol{\mathcal{E}} + \frac{1}{T} \hat{K}^{(2)} (-\nabla T), \quad (6.123)$$

where ∇ should be understood as $\nabla_{\mathbf{r}}$ and the tensors $\hat{K}^{(n)}$ ($n \in \mathbb{N}_0$) are defined as

$$K_{\alpha\beta}^{(n)} = -\frac{1}{4\pi^3} \int d\epsilon \frac{\partial f_0}{\partial \epsilon} \tau(\epsilon) (\epsilon - \mu)^n \int d\Omega_{\mathbf{k}} \frac{v_{F\alpha} v_{F\beta}}{\hbar |\mathbf{v}_F|} k_F^2. \quad (6.124)$$

For an isotropic system these transport coefficients are no longer tensors but represented by scalars,

$$K^{(n)} = -\frac{n_0}{m} \int d\epsilon \frac{\partial f_0}{\partial \epsilon} \tau(\epsilon) (\epsilon - \mu)^n \quad (6.125)$$

In the case $T \ll T_F$ we can calculate the coefficients,¹⁵

$$K^{(0)}(\epsilon_F) = \frac{n_0(\epsilon_F)\tau(\epsilon_F)}{m} \quad (6.128)$$

$$K^{(1)}(\epsilon_F) = \frac{\pi^2}{3}(k_B T)^2 \left. \frac{\partial}{\partial \epsilon} K^{(0)}(\epsilon) \right|_{\epsilon=\epsilon_F}, \quad (6.129)$$

$$K^{(2)}(\epsilon_F) = \frac{\pi^2}{3}(k_B T)^2 K^{(0)}(\epsilon_F). \quad (6.130)$$

We measure the electrical resistivity assuming thermal equilibrium, $\nabla T = 0$ for all \mathbf{r} . With this, we find the expression

$$\sigma = e^2 K^{(0)}. \quad (6.131)$$

In order to determine the thermal conductivity $\hat{\kappa}$ relating the heat current \mathbf{J}_q to ∇T when no external electric field \mathbf{E} is applied, we set $\mathbf{J}_e = 0$ as for an open circuit. Then, the equations (6.122) and (6.123) reveal the appearance of an general force field

$$\mathcal{E} = -\frac{K^{(1)}}{TK^{(0)}} \nabla T. \quad (6.132)$$

Thus, the heat current is given by

$$\mathbf{J}_q = -\frac{1}{T} \left(K^{(2)} - \frac{K^{(1)2}}{K^{(0)}} \right) \nabla T = -\hat{\kappa} \nabla T. \quad (6.133)$$

In simple metals, the second term in (6.133) is often negligible as compared to the first one and we obtain in this case

$$\hat{\kappa} = \frac{1}{T} \hat{K}^{(2)} = \frac{\pi^2 k_B^2}{3} T \hat{K}^{(0)} = \frac{\pi^2}{3} \frac{k_B^2}{e^2} T \hat{\sigma}, \quad (6.134)$$

which is the well-known *Wiedemann-Franz law*. Note, that we can write the thermal conductivity in the form

$$\hat{\kappa} = \frac{C}{e^2 N(\epsilon_F)} \hat{\sigma}, \quad (6.135)$$

where $C = \pi^2 N(\epsilon_F) k_B^2 T / 3$ denotes the electronic specific heat.

6.7.2 Thermoelectric effect

Equation (6.132) shows, that a temperature gradient induces an electric field. For a simple, isotropic system, this relation reduces to

$$\mathcal{E} = Q \nabla T = -\frac{K^{(1)}}{TK^{(0)}} \nabla T, \quad (6.136)$$

¹⁵If a function $g(\epsilon)$ depends only weakly on ϵ in the vicinity of ϵ_F , we can use the Sommerfeld (Taylor) expansion to derive a general approximation for following integrals

$$-\int d\epsilon g(\epsilon) \frac{\partial f_0}{\partial \epsilon} = g(\epsilon_F) + \frac{\pi^2}{6} (k_B T)^2 \left. \frac{\partial^2 g(\epsilon)}{\partial \epsilon^2} \right|_{\epsilon=\epsilon_F} + \dots \quad (6.126)$$

and

$$-\int d\epsilon g(\epsilon) (\epsilon - \epsilon_F) \frac{\partial f_0}{\partial \epsilon} = \frac{\pi^2}{3} (k_B T)^2 \left. \frac{\partial g(\epsilon)}{\partial \epsilon} \right|_{\epsilon=\epsilon_F} + \dots, \quad (6.127)$$

in the limit $T \rightarrow 0$. We used that $\mu \rightarrow \epsilon_F$ in that asymptotic case.

with the *Seebeck coefficient*

$$Q = - \left. \frac{\pi^2 k_B^2 T}{3} \frac{\sigma'(\epsilon)}{e \sigma(\epsilon)} \right|_{\epsilon=\epsilon_F}. \quad (6.137)$$

This is the so-called Mott formula which loses its validity at high-temperatures or very anisotropic scattering. Using $\sigma(\epsilon) = n(\epsilon)e^2\tau(\epsilon)/m$, we investigate $\sigma'(\epsilon)$,

$$\sigma'(\epsilon) = \frac{\tau'(\epsilon)}{\tau(\epsilon)}\sigma(\epsilon) + \frac{n'(\epsilon)}{n(\epsilon)}\sigma(\epsilon) = \frac{\tau'(\epsilon)}{\tau(\epsilon)}\sigma(\epsilon) + \frac{N(\epsilon)}{n(\epsilon)}\sigma(\epsilon), \quad (6.138)$$

and obtain an additional contribution to Q , if the relaxation time depends strongly on energy. This is most prominent in collision processes in which resonant scattering is involved (e.g., the Kondo effect). In the opposite situation, namely, when the first term is irrelevant, the Seebeck coefficient

$$Q = - \frac{\pi^2 k_B^2 T}{3} \frac{N(\epsilon_F)}{e n(\epsilon_F)} = - \frac{S}{ne} \quad (6.139)$$

is simply reduced to the entropy per electron. For simple metals such as the alkali metals we may estimate the low-temperature values using equation (6.139)

$$Q = - \frac{\pi^2 k_B^2 T}{2 e \epsilon_F} = - \frac{\pi^2 k_B T}{2 e T_F} \quad (6.140)$$

which for $T_F(\text{Na}, K) \approx 3 \times 10^4 K$ leads to $Q = -14nVK^{-1} \times T[K]$. A comparison with experiments in Fig.6.8 shows that the order of magnitude works reasonably well for Na and K. However, for Li and Cs even the sign is different. Differences occur through phonon effects, such as the so-called phonon drag which we have neglected here.

In the following, we consider two different types of thermoelectric effects.

Seebeck effect

The first is the *Seebeck effect*, where a thermoelectric voltage appears in a bi-metallic system (cf. Figure 6.9). With equation (6.136), a temperature gradient across metal B induces an electromotive force¹⁶

$$U_{\text{EMF}} = \int d\mathbf{l} \cdot \boldsymbol{\mathcal{E}} \quad (6.141)$$

$$= Q_A \int_{T_0}^{T_1} d\mathbf{l} \cdot \nabla T + Q_B \int_{T_1}^{T_2} d\mathbf{l} \cdot \nabla T + Q_A \int_{T_2}^{T_0} d\mathbf{l} \cdot \nabla T \quad (6.142)$$

$$= (Q_B - Q_A)(T_2 - T_1). \quad (6.143)$$

The resulting voltage $V_{\text{therm}} = U_{\text{EMF}}$ appears between the two ends of a second metal A , whose contacts are kept at the same temperature T_0 . Here, a bi-metallic configuration was chosen to reveal voltage differences across the contacts which are absent in a single metal.

Peltier effect

The second phenomenon, termed *Peltier effect*, emerges in a system kept at the same temperature everywhere. Here, an electric current J_e between the two contacts of the metal A (see Figure 6.9) induces a heat current in the bi-metallic system, such that heat is transferred from

¹⁶The term *electromotive force*, first introduced by Alessandro Volta, is misleading in the sense, that it measures a voltage instead of a force.

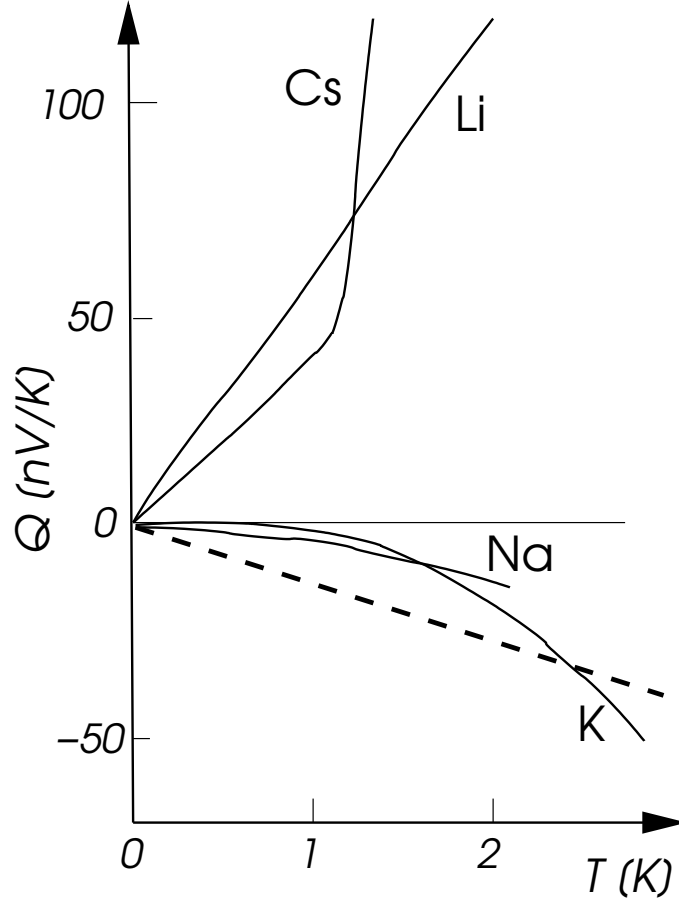


Figure 6.8: Seebeck coefficient for the Alkali metals Li, Na, K, and Cs at low temperatures. The dashed line represents the estimate for Na and K following Eq.(6.140). (adapted from D.K.C. MacDonald, *Thermoelectricity: an introduction to the principles*, Dover (2006).)

one reservoir (top) to another (bottom). This follows from the equations (6.122) and (6.123) by assuming $\nabla T = 0$, where

$$\begin{cases} J_e = e^2 K^{(0)} E \\ J_q = -K^{(1)} E \end{cases} \quad (6.144)$$

implies

$$J_q = -\frac{K^{(1)}}{K^{(0)}} J_e = \Pi J_e = QT J_e. \quad (6.145)$$

The coupling $\Pi = TQ$ between J_q and J_e is called *Peltier coefficient*. According to Figure 6.9, a contribution to the heat current is to be expected from both metals A and B ,

$$J_q = (\Pi_A - \Pi_B) J_e = T_0(Q_A - Q_B) J_e. \quad (6.146)$$

This means, that the heat transfer between reservoirs can be controlled by electrical current.

It has to be emphasized here that the bi-metal design of the devices in Fig. 6.9 serves the observation of the two effects which both represent bulk effects of the two metals A and B . By no means, it should be mistaken as an effect originating from the inter-metal contacts.

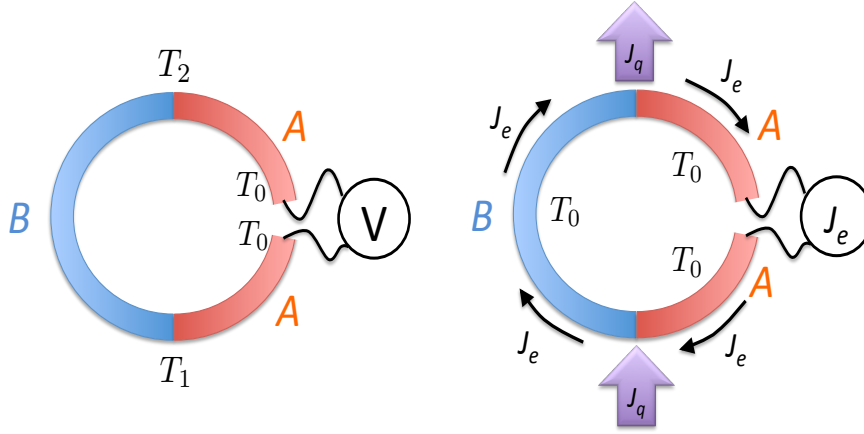


Figure 6.9: Schematic design of bi-metallic device to measure the Seebeck and Peltier effect: On the left panel (a) a representation of Seebeck effect is given, where the symbol E is used instead of \mathcal{E} . On the right panel (b) the Peltier effect is represented. In our analysis, both systems were effectively one-dimensional.

6.8 Anderson localization in one-dimensional systems

Transport in one spatial dimension is very special, since there are only two different directions to go: forward and backward. We introduce the transfer matrix formalism and use it to express the conductivity through the Landauer formula. We will then investigate the effects of multiple scattering at different obstacles, leading to the so-called *Anderson localization*, which turns a metal into an insulator.

6.8.1 Landauer Formula for a single impurity

The transmission and reflection at an arbitrary potential with finite support¹⁷ in one dimension can be described by a transfer matrix T .

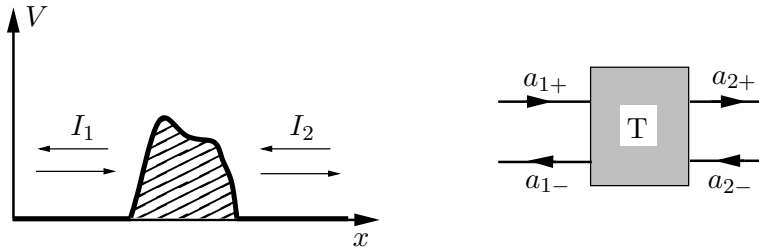


Figure 6.10: Transfer matrices are sufficient to describe potential scattering in one dimension.

In this situation, a suitable choice for a basis of the electron states is the set of plane waves $\{e^{\pm ikx}\}$ (cf. Figure 6.10) moving in the positive (negative) x -direction with wave vector $+k$ ($-k$). Only plane waves with the same $|k|$ on the left (I_1) and right (I_2) side of the scatterer are interconnected. Therefore, we write

$$\psi_1(x) = a_{1+} e^{ikx} + a_{1-} e^{-ikx}, \quad (6.147)$$

$$\psi_2(x) = a_{2+} e^{ikx} + a_{2-} e^{-ikx}, \quad (6.148)$$

¹⁷The support (dt. Träger) of a function is the set of all points, where the function takes non zero values.

where ψ_1 (ψ_2) is defined in the area I_1 (I_2). The vectors $a_i = (a_{i+}, a_{i-})$ $i \in \{1, 2\}$ are connected via the linear relation,

$$a_2 = \hat{T}a_1 = \begin{pmatrix} T_{11} & T_{12} \\ T_{21} & T_{22} \end{pmatrix} a_1, \quad (6.149)$$

with the 2×2 transfer matrix \hat{T} . The conservation of current ($J_1 = J_2$) requires that \hat{T} is unimodular, i.e., $\det T = 1$. Here,

$$J = \frac{i\hbar}{2m} \left(\frac{d\psi^*(x)}{dx} \psi(x) - \psi^*(x) \frac{d\psi(x)}{dx} \right), \quad (6.150)$$

such that, for a plane wave $\psi(x) = (1/\sqrt{L})e^{ikx}$ in a system of length L , the current results in

$$J = v/L \quad (6.151)$$

with the velocity v defined as $v = \hbar k/m$. Time reversal symmetry implies that, simultaneously with $\psi(x)$, the complex conjugate $\psi^*(x)$ is a solution of the stationary Schrödinger equation. From this, we find $T_{11} = T_{22}^*$ and $T_{12} = T_{21}^*$, such that

$$\hat{T} = \begin{pmatrix} T_{11} & T_{12} \\ T_{12}^* & T_{11}^* \end{pmatrix}. \quad (6.152)$$

It is easily shown that a shift of the scattering potential by a distance x_0 changes the coefficient T_{12} of \hat{T} by a phase factor e^{i2kx_0} . Meanwhile, the coefficient T_{11} remains unchanged.

With the Ansatz for a right moving incoming wave ($\propto e^{ikx}$), producing a reflected ($\propto r e^{-ikx}$) and transmitted ($\propto t e^{ikx}$) part, the wave functions on both sides of the scatterer read

$$\psi_1(x) = \frac{1}{\sqrt{L}} (e^{ikx} + r e^{-ikx}), \quad (6.153)$$

$$\psi_2(x) = \frac{1}{\sqrt{L}} (t e^{ikx}). \quad (6.154)$$

The coefficients of \hat{T} can be determined explicitly in this situation, resulting in

$$\hat{T} = \begin{pmatrix} \frac{1}{t^*} & -\frac{r^*}{t^*} \\ -\frac{r}{t} & \frac{1}{t} \end{pmatrix}. \quad (6.155)$$

Here, the conservation of currents imposes the condition $1 = |r|^2 + |t|^2$. Furthermore, we can find a relation between the parameters (r, t) of the potential barrier and the electric resistivity. For this, we notice that the incoming current density J_0 is split into a reflected J_r and transmitted J_t part, all given by

$$J_0 = -\frac{1}{L} v e = -n_0 v e, \quad (6.156)$$

$$J_r = -\frac{|r|^2}{L} v e = -n_r v e, \quad (6.157)$$

$$J_t = -\frac{|t|^2}{L} v e = -n_t v e, \quad (6.158)$$

with the velocity $v = \hbar k/m$, the electron charge $-e$, and the particle densities n_0 , n_r , and n_t corresponding to the incoming, reflected and transmitted particles respectively. The electron density on the two sides of the barrier is given by

$$n_1 = n_0 + n_r = \frac{1 + |r|^2}{L}, \quad (6.159)$$

$$n_2 = n_t = \frac{|t|^2}{L}. \quad (6.160)$$

From this consideration, a density difference $\delta n = n_1 - n_2 = (1 + |r|^2 - |t|^2)/L = 2|r|^2/L$ results between the left and the right side of the scatterer. The resistance R of the barrier is defined by the ratio between the voltage drop over the resistor δV and the transmitted current J_t , i.e.

$$R = \frac{\delta V}{J_t} \quad (6.161)$$

Consequently, a relation between δV and the electron density δn remains to be established to determine R . The connection is easily found via the existing energy difference $\delta E = -e\delta V$ between the two sides of the resistor, such that the expression

$$\delta n = \frac{dn}{dE} \delta E \quad (6.162)$$

$$= \frac{dn}{dE} (-e\delta V) \quad (6.163)$$

produces the wished relation. Here, $\frac{dn}{dE} dE$ is the number of states per unit length in the energy interval $[E, E + dE]$ and we find

$$\frac{dn}{dE} = \frac{1}{L} \sum_{\mathbf{k}, s} \delta \left(E - \frac{\hbar^2 k^2}{2m} \right) = 2 \int \frac{dk}{2\pi} \delta \left(E - \frac{\hbar^2 k^2}{2m} \right) = \frac{1}{\pi \hbar v(E)}. \quad (6.164)$$

The resistance R is finally obtained from the equations (6.161), (6.162), and (6.164), leading to

$$R = \frac{h}{e^2} \frac{|r|^2}{|t|^2}, \quad (6.165)$$

The *Klitzing constant* $R_K = h/e^2 \approx 25.8k\Omega$ is a resistance quantum named after the discoverer of the Quantum Hall Effect. The result (6.165) is the famous *Landauer formula*, which is valid for all one-dimensional systems and whose application often extends to the description of mesoscopic systems and quantum wires.

6.8.2 Scattering at two impurities

We consider now two spatially separated scattering potentials, represented by \hat{T}_1 and \hat{T}_2 each determined by r_1, t_1 and r_2, t_2 respectively.

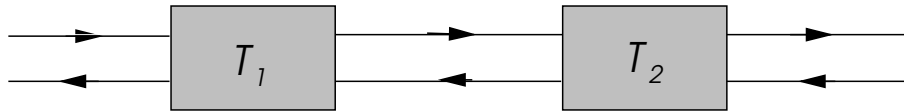


Figure 6.11: Two spatially separated scattering potentials with transmission matrices \hat{T}_1 and \hat{T}_2 respectively.

The particles are multiply scattered at these potentials in a unknown manner, but the global result can again be expressed via a simple transfer matrix $\hat{T} = \hat{T}_1 \hat{T}_2$, given by the matrix multiplication of each transfer matrix. All previously found properties remain valid for the new matrix \hat{T} , given by

$$\hat{T} = \begin{pmatrix} \frac{1}{t_1^* t_2^*} + \frac{r_1^* r_2}{t_1^* t_2} & -\frac{r_2^*}{t_1^* t_2^*} - \frac{r_1^*}{t_1^* t_2} \\ -\frac{r_1}{t_1 t_2^*} - \frac{r_2}{t_1 t_2} & \frac{1}{t_1 t_2} + \frac{r_1 r_2^*}{t_1 t_2^*} \end{pmatrix} = \begin{pmatrix} \frac{1}{t^*} & -\frac{r^*}{t^*} \\ -\frac{r}{t} & \frac{1}{t} \end{pmatrix}. \quad (6.166)$$

For the ratio between reflection and transmission probability we find

$$\frac{|r|^2}{|t|^2} = \frac{1}{|t|^2} - 1 \quad (6.167)$$

$$= \frac{1}{|t_1|^2 |t_2|^2} \left| 1 + \frac{r_1 r_2^* t_2}{t_2^*} \right|^2 - 1 \quad (6.168)$$

$$= \frac{1}{|t_1|^2 |t_2|^2} \left(1 + |r_1|^2 |r_2|^2 + \frac{r_1 r_2^* t_2}{t_2^*} + \frac{r_1^* r_2 t_2^*}{t_2} \right) - 1. \quad (6.169)$$

Assuming a (random) distance $d = x_2 - x_1$ between the two potential barriers, we may average over this distance. Note, that for $x_1 = 0$, we find $r_2 \propto e^{-2ikd}$, while r_1 , t_1 , and t_2 are independent on d . Consequently, all terms containing an odd power of r_2 or r_2^* vanish after averaging over d . The remainders of equation (6.169) can be collected to

$$\left. \frac{|r|^2}{|t|^2} \right|_{\text{avg}} = \frac{1}{|t_1|^2 |t_2|^2} (1 + |r_1|^2 |r_2|^2) - 1 \quad (6.170)$$

$$= \frac{|r_1|^2}{|t_1|^2} + \frac{|r_2|^2}{|t_2|^2} + 2 \frac{|r_1|^2 |r_2|^2}{|t_1|^2 |t_2|^2}. \quad (6.171)$$

Even though two scattering potentials are added in series, an additional non-linear combination emerges beside the sum of the two ratios $|r_i|^2/|t_i|^2$. It results from the Landauer formula applied to two scatterers, that resistances do not add linearly to the total resistance. Adding R_1 and R_2 serially, the total resistance is not given by $R = R_1 + R_2$, but by

$$R = R_1 + R_2 + 2 \frac{R_1 R_2}{R_K} > R_1 + R_2, \quad (6.172)$$

with $R_K = h/e^2$. This result is a consequence of the unavoidable multiple scattering in one dimensions. This effect is particularly prominent if $R_i \gg h/e^2$ for $i \in \{1, 2\}$, where resistances are then multiplied instead of summed.

6.8.3 Anderson localization

Let us consider a system with many arbitrarily distributed scatterers, and let ρ be a mean resistance per unit length. $R(\ell)$ shall be the resistance between points 0 and ℓ . The change in resistance by advancing an infinitesimal $\delta\ell$ is found from equation (6.172), resulting in

$$dR = \rho d\ell + 2 \frac{R(\ell)}{R_K} \rho d\ell, \quad (6.173)$$

which yields

$$\int_0^\ell \rho d\ell = \int_0^{R(\ell)} \frac{dR}{1 + 2R/R_K}, \quad (6.174)$$

and thus,

$$\rho\ell = \frac{h}{2e^2} \ln(1 + 2R(\ell)/R_K). \quad (6.175)$$

Finally, solving this equation for $R(\ell)$, we find

$$R(\ell) = \frac{R_K}{2} \left(e^{2\rho\ell/R_K} - 1 \right). \quad (6.176)$$

Obviously, R grows almost exponentially fast for increasing ℓ . This means, that for large ℓ , the system is an insulator for arbitrarily small but finite $\rho > 0$. The reason for this is that, in one dimension, all states are bound states in the presence of disorder. This phenomenon is called *Anderson localization*. Even though all states are localized, the energy spectrum is continuous, as infinitely many bound states with different energy exist. The mean localization length ξ of individual states, related to the mean extension of a wave function, is found from equation (6.176) to be $\xi = \rho/R_K$. The transmission amplitude is reduced¹⁸ on this length scale, since $|t| \approx 2e^{-\ell/\xi}$ for $\ell \gg \xi$. In one dimension, there is no linearly increasing electric resistance, $R(\ell) \approx \rho\ell$. For non-interacting particles, only two extreme situations are possible. Either, the potential is perfectly periodic and the states correspond to Bloch waves. Then, coherent constructive interference produces extended states¹⁹ that propagate freely throughout the system, resulting in a perfect conductor without resistance. On the other hand, if the scattering potential is disordered, all states are strictly localized. In this case, there is no propagation and the system is an insulator. In three-dimensional systems, the effects of multiple scattering are far less drastic and the Ohmic law is applicable. Localization effects in two dimensions is a very subtle topic and part of today's research in solid state physics.

¹⁸For an expanded discussion of this topic, the article [P.W. Anderson, D.J. Thouless, E. Abrahams, and D.S. Fisher, *New method for a scaling theory of localization*, Physical Review B **22**, 3519 (1980)] is recommended.

¹⁹We have also seen in the context of chiral edge states in the Quantum Hall state, that perfect conductance in a one-dimensional channel is obtained if there is no backscattering due to the lack of states moving in the opposite direction. In chiral states, particles move only in one direction.

Chapter 7

Magnetism in metals

Magnetic ordering in metals can be viewed as an instability of the Fermi liquid state. We introduce this new phase of metals through the description of the Stoner ferromagnetism. The discussion of antiferromagnetism and spin density wave phases will be only brief in this chapter. In Stoner ferromagnets the magnetic moment is provided by the spin of itinerant electrons. Magnetism due to localized magnetic moments will be considered in the context of Mott insulators which are subject of the next chapter.

Well-known examples of elemental ferromagnetic metals are iron (Fe), cobalt (Co) and nickel (Ni) belonging to the $3d$ transition metals, where the $3d$ -orbital character is dominant for the conduction electrons at the Fermi energy. These orbitals are rather tightly bound to the atomic cores such that the electron mobility is reduced, enhancing the effect of interaction which is essential for the formation of a magnetic state. Other forms of magnetism, such as antiferromagnetism and the spin density wave state are found in the $3d$ transition metals Cr and Mn.

Note, $4d$ and $5d$ transition metals within the same columns of the periodic system are not magnetic. Their d -orbitals are more extended, leading to a higher mobility of the electrons, such that the mutual interaction is insufficient to trigger magnetism. It is, however, possible to find ferromagnetism in $ZrZn_2$ where zink (Zn) may act as a spacer reducing the mobility of the $4d$ -electrons of zirconium (Zr). The $4d$ -elements Pd and Rh and the $5d$ -element Pt are, however, nearly ferromagnetic. Going further in the periodic table, the $4f$ -orbitals appearing in the lanthanides are nearly localized and can lead to ferromagnetism, as illustrated by the elements going from Gd through Tm in the periodic system.

Magnetism appears through a phase transition, meaning that the metal is non-magnetic at temperatures above a critical temperature T_c , the Curie-temperature (cf. Table 7.1). In many cases, magnetism appears at T_c as a continuous, second order phase transition involving the spontaneous violation of symmetry. This transition is lacking latent heat (no discontinuity in entropy and volume) but instead features a discontinuity in the specific heat.

| element | T_c (K) | type | element | T_c (K) | type |
|----------|-----------|------------------|--------------|-----------|------------------------|
| Fe | 1043 | ferromagnet (3d) | Gd | 293 | ferromagnet (4f) |
| Co | 1388 | ferromagnet (3d) | Dy | 85 | ferromagnet (4f) |
| Ni | 627 | ferromagnet (3d) | Cr | 312 | spin density wave (3d) |
| $ZrZn_2$ | 22 | ferromagnet | α -Mn | 100 | antiferromagnet |
| Pd | – | paramagnet | Pt | – | paramagnet |
| $HfZn_2$ | – | paramagnet | | | |

Table 7.1: Selection of (ferro)magnetic materials with their respective form of magnetism and the critical temperature T_c .

7.1 Stoner instability

In the following section, we study the emergence of the metallic ferromagnetism originating from the Stoner mechanism. In close analogy to the first Hund's rule, the exchange interaction among the electrons plays a crucial role here. The alignment of the electronic spins in a favored direction allows the system to reduce the energy contribution due to Coulomb repulsion. According to Landau's theory of Fermi liquids, the interaction between electrons renormalizes the spin susceptibility χ_0 to

$$\chi = \frac{m^*}{m} \frac{\chi_0}{1 + F_0^a}, \quad (7.1)$$

which obviously diverges for $F_0^a \rightarrow -1$ and leads to a ferromagnetic instability of the Fermi liquid. Using Eq.(5.110), $F_0^a \approx -UN(\epsilon_F)/2$ provides a critical value for the interaction $U_c = 2/N(\epsilon_F)$ such that $F_0^a = -1$ and χ diverges. We will see below that this corresponds to a value we will derive also by a mean field theory.

7.1.1 Stoner model within the mean field approximation

Consider the following model for conduction electrons with a repulsive contact interaction,

$$\mathcal{H} = \sum_{\mathbf{k}, s} \epsilon_{\mathbf{k}} \hat{c}_{\mathbf{k}s}^\dagger \hat{c}_{\mathbf{k}s} + U \int d^3r d^3r' \hat{\rho}_\uparrow(\mathbf{r}) \delta(\mathbf{r} - \mathbf{r}') \hat{\rho}_\downarrow(\mathbf{r}'), \quad (7.2)$$

where we use the electron density $\hat{\rho}_s(\mathbf{r}) = \hat{\Psi}_s^\dagger(\mathbf{r}) \hat{\Psi}_s(\mathbf{r})$ and the field operator $\hat{\Psi}_s^\dagger$ ($\hat{\Psi}_s$) follows from the definition (3.28) [(3.29)]. The contact interaction is an approximation of the screened Coulomb interaction. Due to the Pauli exclusion principle, the contact interaction is only active between electrons with opposite spins. This is a consequence of the exchange hole in the two-particle correlation between electrons of identical spin (cf. Figure 3.1). We obtain a useful insight into mechanisms leading to ferromagnetism by means of a mean field approximation¹. We rewrite,

$$\hat{\rho}_s(\mathbf{r}) = n_s + [\hat{\rho}_s(\mathbf{r}) - n_s], \quad (7.3)$$

where

$$n_s = \langle \hat{\rho}_s(\mathbf{r}) \rangle, \quad (7.4)$$

and $\langle \cdot \rangle$ represents the thermal average. We stipulate that the deviation from the mean value n_s is small in the sense that

$$\langle [\hat{\rho}_\uparrow(\mathbf{r}) - n_\uparrow][\hat{\rho}_\downarrow(\mathbf{r}) - n_\downarrow] \rangle \ll n_\uparrow n_\downarrow. \quad (7.5)$$

Inserting equation (7.3) into the Hamiltonian (7.2), we obtain

$$\mathcal{H}_{\text{mf}} = \sum_{\mathbf{k}, s} \epsilon_{\mathbf{k}} \hat{c}_{\mathbf{k}s}^\dagger \hat{c}_{\mathbf{k}s} + U \int d^3r [\hat{\rho}_\uparrow(\mathbf{r}) n_\downarrow + \hat{\rho}_\downarrow(\mathbf{r}) n_\uparrow - n_\uparrow n_\downarrow] \quad (7.6)$$

$$= \sum_{\mathbf{k}, s} (\epsilon_{\mathbf{k}} + U n_{\bar{s}}) \hat{c}_{\mathbf{k}s}^\dagger \hat{c}_{\mathbf{k}s} - U \Omega n_\uparrow n_\downarrow, \quad (7.7)$$

the *mean field Hamiltonian*, describing electrons which move in the uniform background of electrons of opposite spin coupling via the spin dependent exchange interaction (\bar{s} denotes to opposite spin s). Fluctuations of the form $\langle [\hat{\rho}_\uparrow(\mathbf{r}) - n_\uparrow][\hat{\rho}_\downarrow(\mathbf{r}) - n_\downarrow] \rangle$ are neglected here. The

¹Note that the following mean field calculation is equivalent to a variational approach using simple many-body wavefunction (Slater determinant) with different concentrations of up and down spins.

advantage of this approximation is, that the many-body problem is now reduced to an effective one-particle problem, where only the mean electron interaction is taken into account. This is equivalent to a generalized Hartree-Fock approximation and enables us to calculate certain expectation values, such as the density of one spin species, e.g.;

$$n_{\uparrow} = \frac{1}{\Omega} \sum_{\mathbf{k}} \langle \hat{c}_{\mathbf{k}\uparrow}^{\dagger} \hat{c}_{\mathbf{k}\uparrow} \rangle = \frac{1}{\Omega} \sum_{\mathbf{k}} f(\epsilon_{\mathbf{k}} + Un_{\downarrow}) \quad (7.8)$$

$$= \int d\epsilon \frac{1}{\Omega} \sum_{\mathbf{k}} \delta(\epsilon - \epsilon_{\mathbf{k}} - Un_{\downarrow}) f(\epsilon) \quad (7.9)$$

$$= \int d\epsilon \frac{1}{2} N(\epsilon - Un_{\downarrow}) f(\epsilon), \quad (7.10)$$

where $f(\epsilon)$ is the Fermi-Dirac distribution function. An analogous result is found for the opposite spin direction. These mean densities are determined self-consistently, namely such that the insertion of n_s in into the mean field Hamiltonian (7.7) provides the correct output according to the expectation values given in equation (7.8). Furthermore, the constraint that the total number of electrons is conserved, must be implemented. The real magnetization $M = \mu_B m$ is proportional to m which is defined via

$$n_s = \frac{1}{2} [(n_{\uparrow} + n_{\downarrow}) + s(n_{\uparrow} - n_{\downarrow})] = \frac{n_0 + sm}{2}, \quad (7.11)$$

where n_0 is the total particle density. This leads to the two coupled equations

$$n_0 = \frac{1}{2} \int d\epsilon \left(N(\epsilon - Un_{\downarrow}) + N(\epsilon - Un_{\uparrow}) \right) f(\epsilon), \quad (7.12)$$

$$m = \frac{1}{2} \int d\epsilon \left(N(\epsilon - Un_{\downarrow}) - N(\epsilon - Un_{\uparrow}) \right) f(\epsilon), \quad (7.13)$$

or equivalently

$$n_0 = \frac{1}{2} \sum_s \int d\epsilon N \left(\epsilon - \frac{Un_0}{2} - s \frac{Um}{2} \right) f(\epsilon), \quad (7.14)$$

$$m = -\frac{1}{2} \sum_s s \int d\epsilon N \left(\epsilon - \frac{Un_0}{2} - s \frac{Um}{2} \right) f(\epsilon), \quad (7.15)$$

which usually can not be solved analytically and must be treated numerically.

7.1.2 Stoner criterion

An approximate solution can be found if $m \ll n_0$. Eqs.(7.14) and (7.15) are solved by adapting the chemical potential μ . For low temperatures and small magnetization we can expand μ as

$$\mu(m, T) = \epsilon_F + \Delta\mu(m, T). \quad (7.16)$$

The constant energy shift $-Un_0/2$ appearing in Eqs.(7.14) and (7.15) can be absorbed into ϵ_F . The Fermi-Dirac distribution takes the form

$$f(\epsilon) = \frac{1}{e^{\beta[\epsilon - \mu(m, T)]} + 1}, \quad (7.17)$$

where $\beta = (k_B T)^{-1}$. After expanding equation (7.14) for small m , one obtains using the Sommerfeld expansion,

$$n_0 \approx \int d\epsilon f(\epsilon) \left[N(\epsilon) + \frac{1}{2} \left(\frac{Um}{2} \right)^2 N''(\epsilon) \right] \quad (7.18)$$

$$\approx \int_0^{\epsilon_F} d\epsilon [N(\epsilon)] + N(\epsilon_F) \Delta\mu + \frac{\pi^2}{6} (k_B T)^2 N'(\epsilon_F) + \frac{1}{2} \left(\frac{Um}{2} \right)^2 N'(\epsilon_F), \quad (7.19)$$

where we introduced the abbreviations $N'(\epsilon) = dN(\epsilon)/d\epsilon$ and $N''(\epsilon) = d^2N(\epsilon)/d\epsilon^2$. Since the first term on the right side of Eq.(7.19) is identical to n_0 , $\Delta\mu(m, T)$ is immediately found to be given by

$$\Delta\mu(m, T) \approx -\frac{N'(\epsilon_F)}{N(\epsilon_F)} \left[\frac{\pi^2}{6} (k_B T)^2 + \frac{1}{2} \left(\frac{Um}{2} \right)^2 \right]. \quad (7.20)$$

Analogously, the expansion of Eq.(7.15) in m and T , results in

$$m \approx \int d\epsilon f(\epsilon) \left[N'(\epsilon) \frac{Um}{2} + \frac{1}{3!} N'''(\epsilon) \left(\frac{Um}{2} \right)^3 \right] \quad (7.21)$$

$$\approx \left[N(\epsilon_F) + \frac{\pi^2}{6} (k_B T)^2 N''(\epsilon_F) + \frac{1}{3!} \left(\frac{Um}{2} \right)^2 N'''(\epsilon_F) + \Delta\mu N'(\epsilon_F) \right] \left(\frac{Um}{2} \right), \quad (7.22)$$

and, finally, inserting the result for $\Delta\mu$ of Eq.(7.20) into (7.22), we find

$$m = N(\epsilon_F) \left[1 - \frac{\pi^2}{6} (k_B T)^2 \Lambda_1^2(\epsilon_F) \right] \left(\frac{Um}{2} \right) - N(\epsilon_F) \Lambda_2^2(\epsilon_F) \left(\frac{Um}{2} \right)^3, \quad (7.23)$$

where

$$\Lambda_1^2(\epsilon_F) = \left(\frac{N'(\epsilon_F)}{N(\epsilon_F)} \right)^2 - \frac{N''(\epsilon_F)}{N(\epsilon_F)}, \quad \text{and} \quad \Lambda_2^2(\epsilon_F) = \frac{1}{2} \left(\frac{N'(\epsilon_F)}{N(\epsilon_F)} \right)^2 - \frac{N''(\epsilon_F)}{3!N(\epsilon_F)}. \quad (7.24)$$

The structure of Eq.(7.23) is $m = am + bm^3$, where b is assumed to be negative. Thus, two types of solutions emerge

$$m^2 = \begin{cases} 0, & a < 1, \\ \frac{1-a}{b}, & a \geq 1. \end{cases} \quad (7.25)$$

With this, $a = 1$ corresponds to a critical value.

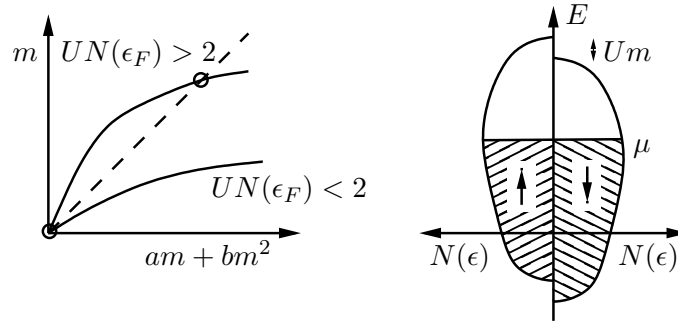


Figure 7.1: Graphical solution of equation (7.23) and the resulting magnetization. The Fermi sea of each spin configuration is shifted by $\pm Um/2$, resulting in a finite total magnetization.

Here, this condition corresponds to

$$1 = \frac{1}{2} UN(\epsilon_F) \left[1 - \frac{\pi^2}{6} (k_B T_C)^2 \Lambda_1^2(\epsilon_F) \right], \quad (7.26)$$

yielding

$$k_B T_C = \frac{\sqrt{6}}{\pi \Lambda_1(\epsilon_F)} \sqrt{1 - \frac{2}{UN(\epsilon_F)}} \propto \sqrt{1 - \frac{U_c}{U}} \quad (7.27)$$

for $U > U_c = 2/N(\epsilon_F)$. This is an instability condition for the paramagnetic Fermi liquid state with $m = 0$, and T_C is the *Curie temperature*, below which the ferromagnetic state appears (see Figure 7.1). The temperature dependence of the magnetization M of the ferromagnetic state ($T < T_C$) is given by

$$M(T) = \mu_B m(T) \propto \sqrt{T_C - T}, \quad (7.28)$$

close to the phase transition ($T_C - T \ll T_C$). Note that the Curie temperature T_C is nonzero for $UN(\epsilon_F) > 2$, and $T_C \rightarrow 0$ in the limit $UN(\epsilon_F) \rightarrow 2_+$. For $UN(\epsilon_F) < 2$ no phase transition occurs. This condition for a finite transition temperature T_C is known as the *Stoner criterion*. This simple model also describes a so-called *quantum phase transition*, i.e., a phase transition that appears at $T = 0$ as a function of system parameters, which in our case are the density of states $N(\epsilon_F)$ and the Coulomb repulsion U . While thermal fluctuations destroy the ordered state at finite temperature via entropy increase, entropy is irrelevant at $T = 0$. Here, the order is suppressed by quantum fluctuations (Heisenberg's uncertainty principle).

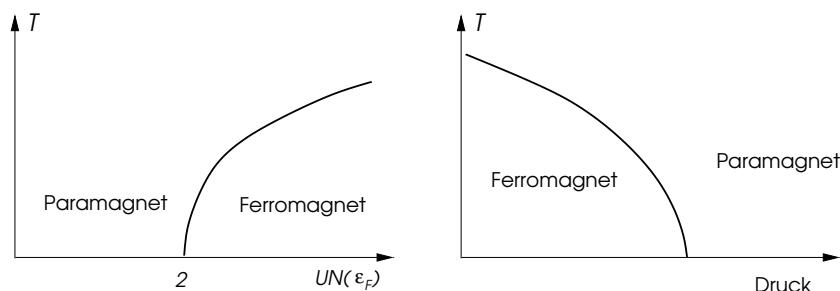


Figure 7.2: Phase diagram of a Stoner ferromagnet in the T - $UN(\epsilon_F)$ and T - p plane, respectively.

The density of states as an internal parameter can, for example, be changed by applying a pressure. By reducing the lattice constant, pressure may facilitate the motion of the conduction electrons and increase the Fermi velocity. Consequently, the density of states is reduced (cf. Figure 7.2). Indeed, pressure is able to destroy ferromagnetism in weakly ferromagnetic materials as ZrZn_2 , MnSi , and UGe_2 . In other materials, the Curie temperature is high enough, such that the technologically applicable pressure is insufficient to suppress magnetism. It is, however, possible, that pressure leads to other transitions, such as structural phase transitions, that eventually destroy magnetism. This is seen in iron (Fe), where a pressure of about 12 GPa induces a transition from magnetic iron with body-centered crystal (bcc) structure to a nonmagnetic, hexagonal close packed (hcp) structure (cf. Figure 7.3).

While this structural transition is a quantum phase transition as well, it appears as a discontin-

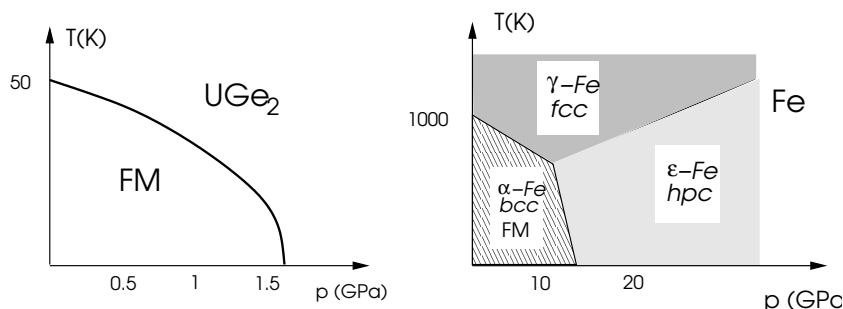


Figure 7.3: Phase diagrams of UGe_2 and Fe.

uous, first order² transition. In some cases, pressure can also induce an increase in $N(\epsilon_F)$, for example in metals with multiple bands, where compression leads to a redistribution of charge. One example is the ruthenate $\text{Sr}_3\text{Ru}_2\text{O}_7$ for which uniaxial pressure along the z -axis leads to magnetism.

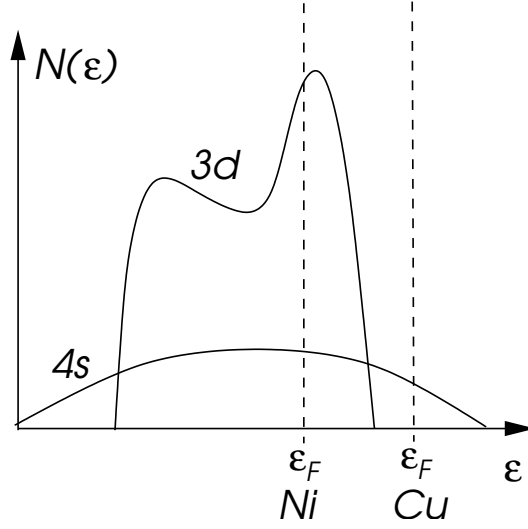


Figure 7.4: The position of the Fermi energy of Cu and Ni, respectively.

Finally, let us turn to the question, why Cu, being a direct neighbor of Ni in the 3d-row of the periodic table, is not ferromagnetic, even though both elemental metals share the same fcc crystal structure. The answer is given by the Stoner criterion $UN(\epsilon_F) = 2$. While the conduction electrons at the Fermi level of Ni have 3d-character and belong to a narrow band with a large density of states, the Fermi energy of Cu is situated in the broad 4s-band and constitutes a much smaller density of states (cf. Figure 7.4). With this, the Cu conduction electrons are much less localized and feature a weaker tendency towards ferromagnetic order.

7.1.3 Spin susceptibility for $T > T_C$

Next we study the response of the metallic system in the paramagnetic state when we apply a small magnetic field H along the z -axis, which induces a spin polarization due to the Zeeman coupling,

$$H_Z = -g\mu_B \int d^3r H \frac{1}{2} \{ \hat{\rho}_\uparrow(\mathbf{r}) - \hat{\rho}_\downarrow(\mathbf{r}) \}. \quad (7.29)$$

From the self-consistency equations (7.14) and (7.15) we obtain

$$m = -\frac{1}{2} \int d\epsilon f(\epsilon) \sum_s s N \left(\epsilon - \mu_B s H - s \frac{Um}{2} \right) \quad (7.30)$$

$$\approx \int d\epsilon f(\epsilon) N'(\epsilon) \left(\frac{Um}{2} + \mu_B H \right) \quad (7.31)$$

$$= N(\epsilon_F) \left[1 - \frac{\pi^2}{6} (k_B T)^2 \Lambda_1(\epsilon_F)^2 \right] \left(\frac{Um}{2} + \mu_B H \right) \quad (7.32)$$

to lowest order in m and H . Solving this equation for m yields

$$M = \mu_B m = \frac{\chi_0(T)}{1 - U\chi_0(T)/2\mu_B^2} H, \quad (7.33)$$

²The Stoner instability is a simplification of the quantum phase transition. In most cases, a discontinuous phase transition originates in the band structure or in fluctuation effects, which were ignored here. For more details consult [D. Belitz and T.R. Kirkpatrick, Phys. Rev. Lett. **89**, 247202 (2002)].

and, consequently, the magnetic susceptibility χ reads

$$\chi = \frac{M}{H} = \frac{\chi_0(T)}{1 - U\chi_0(T)/2\mu_B^2}, \quad (7.34)$$

where the bare susceptibility χ_0 is given by

$$\chi_0(T) = \mu_B^2 N(\epsilon_F) \left[1 - \frac{\pi^2}{6} (k_B T)^2 \Lambda_1(\epsilon_F)^2 \right]. \quad (7.35)$$

We see, that the denominator of the susceptibility $\chi(T)$ vanishes exactly when the Stoner instability criterion for finite temperatures is fulfilled (see Eq.(7.26)). The susceptibility

$$\chi(T) \approx \frac{\chi_0(T_C)}{\frac{T_C^2}{T^2} - 1}, \quad (7.36)$$

diverging at T_c defined through Eq.(7.26) indicates the instability. Note that for $T \rightarrow T_c$ from the paramagnetic side, the susceptibility diverges like $\chi(T) \propto |T_c - T|^{-1}$ corresponding to the mean field behavior, since the mean field critical exponent γ for the susceptibility takes the value $\gamma = 1$.

7.2 General spin susceptibility and magnetic instabilities

The ferromagnetic state is characterized by a uniform magnetization. There are, however, magnetically ordered states which do not feature a nonzero net magnetization but spacially modulated magnetic moments.. Examples are spin density wave (SDW) states, antiferromagnets and spin spiral states. In this section, we analyze general instability conditions for metallic systems to some magnetically ordering.

7.2.1 General dynamic spin susceptibility

We consider a magnetic field, oscillating in time and with spacial modulation

$$\mathbf{H}(\mathbf{r}, t) = \mathbf{H}_0 e^{i\mathbf{q}\cdot\mathbf{r} - i\omega t} e^{\eta t}, \quad (7.37)$$

where $\eta \rightarrow 0_+$ yields an adiabatic switching on the field. We calculate the resulting magnetization, for the corresponding Fourier component. For that, we proceed analogous to the discussion in Chapter 3 and define the spin density operator $\widehat{\mathbf{S}}(\mathbf{r})$ in real space,

$$\widehat{\mathbf{S}}(\mathbf{r}) = \frac{\hbar}{2} \sum_{s,s'} \widehat{\Psi}_s^\dagger(\mathbf{r}) \boldsymbol{\sigma}_{ss'} \widehat{\Psi}_{s'}(\mathbf{r}) = \frac{\hbar}{2} \begin{pmatrix} \widehat{\Psi}_\uparrow^\dagger(\mathbf{r}) \widehat{\Psi}_\downarrow(\mathbf{r}) + \widehat{\Psi}_\downarrow^\dagger(\mathbf{r}) \widehat{\Psi}_\uparrow(\mathbf{r}) \\ -i \widehat{\Psi}_\uparrow^\dagger(\mathbf{r}) \widehat{\Psi}_\downarrow(\mathbf{r}) + i \widehat{\Psi}_\downarrow^\dagger(\mathbf{r}) \widehat{\Psi}_\uparrow(\mathbf{r}) \\ \widehat{\Psi}_\uparrow^\dagger(\mathbf{r}) \widehat{\Psi}_\uparrow(\mathbf{r}) - \widehat{\Psi}_\downarrow^\dagger(\mathbf{r}) \widehat{\Psi}_\downarrow(\mathbf{r}) \end{pmatrix} \quad (7.38)$$

with momentum space representation

$$\widehat{\mathbf{S}}_{\mathbf{q}} = \int d^3r \widehat{\mathbf{S}}(\mathbf{r}) e^{-i\mathbf{q}\cdot\mathbf{r}} = \frac{\hbar}{2\Omega} \sum_{\mathbf{k},s,s'} c_{\mathbf{k},s}^\dagger \boldsymbol{\sigma}_{ss'} c_{\mathbf{k}+\mathbf{q},s'} = \frac{1}{\Omega} \sum_{\mathbf{k}} \widehat{\mathbf{S}}_{\mathbf{k},\mathbf{q}}, \quad (7.39)$$

where $\widehat{\mathbf{S}}_{\mathbf{k},\mathbf{q}} = (\hbar/2) c_{\mathbf{k},s}^\dagger \boldsymbol{\sigma}_{ss'} c_{\mathbf{k}+\mathbf{q},s'}$. The Hamiltonian of the electronic system with contact interaction is given by

$$\mathcal{H} = \mathcal{H}_0 + \mathcal{H}_Z + \mathcal{H}_{\text{int}}, \quad (7.40)$$

where

$$\mathcal{H}_0 = \sum_{\mathbf{k},s} \epsilon_{\mathbf{k}} \hat{c}_{\mathbf{k}s}^\dagger \hat{c}_{\mathbf{k}s}, \quad (7.41)$$

$$\mathcal{H}_Z = -\frac{g\mu_B}{\hbar} \int d^3r \mathbf{H}(\mathbf{r}, t) \cdot \hat{\mathbf{S}}(\mathbf{r}), \quad (7.42)$$

$$\mathcal{H}_{\text{int}} = U \int d^3r \hat{\rho}_\uparrow(\mathbf{r}) \hat{\rho}_\downarrow(\mathbf{r}). \quad (7.43)$$

The operator \mathcal{H}_Z describes the *Zeeman coupling* between the electrons of the metal and the perturbing field. We investigate a magnetic field

$$\mathbf{H} = \frac{1}{2} H^+(\mathbf{q}, \omega) e^{i\mathbf{q}\cdot\mathbf{r} - i\omega t} e^{\eta t} \begin{pmatrix} 1 \\ -i \\ 0 \end{pmatrix} \quad (7.44)$$

in the x - y -plane. The Zeeman term then simplifies to

$$\mathcal{H}_Z = -\frac{g\mu_B}{\hbar} H^+(\mathbf{q}, \omega) \hat{S}_{-\mathbf{q}}^- + \text{h.c.}, \quad (7.45)$$

where $\hat{S}_{-\mathbf{q}}^\pm = \hat{S}_{-\mathbf{q}}^x \pm i\hat{S}_{-\mathbf{q}}^y$. In the following the Hermitian conjugate (h.c.) part of Eq.(7.45) will be ignored. We use

$$\hat{S}_{-\mathbf{q}}^- = \frac{\hbar}{\Omega} \sum_{\mathbf{k}} \hat{c}_{\mathbf{k}\downarrow}^\dagger \hat{c}_{\mathbf{k}-\mathbf{q}\uparrow}, \quad (7.46)$$

in the c -operator representation. In the framework of linear response theory, this coupling will induce a magnetization $M_{\text{ind}}^+(\mathbf{q}, t) = (\mu_B/\hbar) \langle \hat{S}_{\mathbf{q}}^+(t) \rangle \propto e^{-i\omega t + \eta t}$. Using the same equations of motion as in Section 3.2,

$$i\hbar \frac{\partial}{\partial t} \hat{S}_{\mathbf{k},\mathbf{q}}^+ = [\hat{S}_{\mathbf{k},\mathbf{q}}^+, \mathcal{H}], \quad (7.47)$$

with $\hat{S}_{\mathbf{k},\mathbf{q}}^+ = \hat{c}_{\mathbf{k}\uparrow}^\dagger \hat{c}_{\mathbf{k}+\mathbf{q}\downarrow}$, we can determine this induced magnetization, first without the interaction term ($U=0$). We obtain for the given Fourier component,

$$i\hbar \frac{\partial}{\partial t} \hat{S}_{\mathbf{k},\mathbf{q}}^+(t)_{\mathbf{k},\mathbf{q}} = (\epsilon_{\mathbf{k}+\mathbf{q}} - \epsilon_{\mathbf{k}}) \hat{S}_{\mathbf{k},\mathbf{q}}^+(t) - g\hbar\mu_B (\hat{c}_{\mathbf{k}\downarrow}^\dagger \hat{c}_{\mathbf{k}\downarrow} - \hat{c}_{\mathbf{k}+\mathbf{q}\uparrow}^\dagger \hat{c}_{\mathbf{k}+\mathbf{q}\uparrow}) H^+(\mathbf{q}, \omega) e^{-i\omega t + \eta t}. \quad (7.48)$$

Using the monochromatic time dependence of the field and the response ($e^{-i\omega t + \eta t}$) and applying the thermal average we obtain,

$$(\epsilon_{\mathbf{k}+\mathbf{q}} - \epsilon_{\mathbf{k}} - \hbar\omega - i\hbar\eta) \langle S_{\mathbf{k},\mathbf{q}}^+(t) \rangle = -g\hbar\mu_B (n_{\mathbf{k}+\mathbf{q}\uparrow} - n_{\mathbf{k}\downarrow}) H^+(\mathbf{q}, \omega) e^{-i\omega t + \eta t}, \quad (7.49)$$

which then leads to the induced spin density - magnetization,

$$\begin{aligned} \frac{\hbar}{\mu_B} M_{\text{ind}}^+(\mathbf{q}, \omega) e^{-i\omega t + \eta t} &= \langle S_{\text{ind}}^+(\mathbf{q}, \omega) \rangle e^{-i\omega t + \eta t} = \frac{1}{\Omega} \sum_{\mathbf{k}} \langle S_{\mathbf{k},\mathbf{q}}^+(t) \rangle \\ &= \frac{\hbar}{\mu_B} \chi_0(\mathbf{q}, \omega) H^+(\mathbf{q}, \omega) e^{-i\omega t + \eta t}, \end{aligned} \quad (7.50)$$

with

$$\chi_0(\mathbf{q}, \omega) = -\frac{g\mu_B^2}{\Omega} \sum_{\mathbf{k}} \frac{n_{\mathbf{k}+\mathbf{q}\uparrow} - n_{\mathbf{k}\downarrow}}{\epsilon_{\mathbf{k}+\mathbf{q}} - \epsilon_{\mathbf{k}} - \hbar\omega - i\hbar\eta}. \quad (7.51)$$

Note that the form of the bare susceptibility $\chi_0(\mathbf{q}, \omega)$ is similar to the Lindhard function (3.63), actually identical, if there is no spin polarization. The result (7.50) describes the induced spin density within linear response approximation.

In a next step, we want to include the effects of the interaction. Analogously to the induced charge modulation found in Section 3.2, the induced spin density generates an effective field on the spin of the electrons ("mean field"). The induced spin polarization may be represented as an effective magnetic field through the exchange interaction. To implement this feature let us rewrite the contact interaction term in Eq.(7.40) in the form

$$\begin{aligned}\mathcal{H}_{\text{int}} &= \frac{U}{\Omega} \sum_{\mathbf{k}, \mathbf{k}', \mathbf{q}'} \hat{c}_{\mathbf{k}+\mathbf{q}'\uparrow}^\dagger \hat{c}_{\mathbf{k}\uparrow} \hat{c}_{\mathbf{k}'-\mathbf{q}'\downarrow}^\dagger \hat{c}_{\mathbf{k}'\downarrow} \\ &= -\frac{U}{\Omega} \sum_{\mathbf{k}, \mathbf{k}', \mathbf{q}'} \hat{c}_{\mathbf{k}\uparrow}^\dagger \hat{c}_{\mathbf{k}+\mathbf{q}'\downarrow} \hat{c}_{\mathbf{k}'\downarrow}^\dagger \hat{c}_{\mathbf{k}'-\mathbf{q}'\uparrow} + \text{const.} \\ &= -\frac{U}{\Omega \hbar^2} \sum_{\mathbf{q}'} \hat{S}_{\mathbf{q}'}^+ \hat{S}_{-\mathbf{q}'}^-\end{aligned}\quad (7.52)$$

The induced spin polarization $\langle S_{\text{ind}}^+(\mathbf{q}, \omega) \rangle$ acts through the exchange interaction as an effective (local) field, as can be seen by replacing $\hat{S}_{\mathbf{q}'}^+ \rightarrow \langle S_{\text{ind}}^+(\mathbf{q}, \omega) \rangle \delta_{\mathbf{q}, \mathbf{q}'}$ in Eq.(7.53) ,

$$-\frac{U}{\Omega \hbar^2} \sum_{\mathbf{q}'} \hat{S}_{\mathbf{q}'}^+ \hat{S}_{-\mathbf{q}'}^- \rightarrow -\frac{U}{\hbar^2} \langle S^+(\mathbf{q}, \omega) \rangle \hat{S}_{-\mathbf{q}}^- = -\frac{g\mu_B}{\hbar} H_{\text{ind}}^+(\mathbf{q}, \omega) \hat{S}_{-\mathbf{q}}^- \quad (7.53)$$

where the effective magnetic field $H_{\text{ind}}^+(\mathbf{q}, \omega)$ finally reads

$$H_{\text{ind}}^+(\mathbf{q}, \omega) = \frac{U}{g\mu_B \hbar} \langle S^+(\mathbf{q}, \omega) \rangle, \quad (7.54)$$

with the same monochromatic time dependence as above. This induced field acts on the spins as well, such that the total response of the spin density on the external field becomes

$$\begin{aligned}M^+(\mathbf{q}, \omega) &= \frac{\mu_B}{\hbar} \langle S^+(\mathbf{q}, \omega) \rangle \\ &= \chi_0(\mathbf{q}, \omega) [H^+(\mathbf{q}, \omega) + H_{\text{ind}}^+(\mathbf{q}, \omega)] \\ &= \chi_0(\mathbf{q}, \omega) H^+(\mathbf{q}, \omega) + \chi_0(\mathbf{q}, \omega) \frac{U}{g\mu_B \hbar} \langle S^+(\mathbf{q}, \omega) \rangle \\ &= \chi_0(\mathbf{q}, \omega) H^+(\mathbf{q}, \omega) + \chi_0(\mathbf{q}, \omega) \frac{U}{g\mu_B^2} M^+(\mathbf{q}, \omega).\end{aligned}\quad (7.55)$$

In the last step we introduce self-consistency taking the induced magnetization as the real magnetization. With the definition

$$M^+(\mathbf{q}, \omega) = \chi(\mathbf{q}, \omega) H^+(\mathbf{q}, \omega) \quad (7.56)$$

of the susceptibility we find

$$\chi(\mathbf{q}, \omega) = \frac{\chi_0(\mathbf{q}, \omega)}{1 - \frac{U}{2\mu_B^2} \chi_0(\mathbf{q}, \omega)}. \quad (7.57)$$

which corresponds to the random phase approximation (RPA) (see Section 3.2). This form of the susceptibility is found to be valid for all field directions, as long as spin-orbit coupling is neglected. Within the random phase approximation, the generalization of the Stoner criterion for the appearance of an instability of the system at finite temperature reads

$$1 = \frac{U}{2\mu_B^2} \chi_0(\mathbf{q}, \omega). \quad (7.58)$$

For the limiting case $(\mathbf{q}, \omega) \rightarrow (\mathbf{0}, 0)$ corresponding to a uniform, static external field, we obtain for the bare susceptibility

$$\begin{aligned}\chi_0(\mathbf{q}, 0) &= -\frac{2\mu_B^2}{\Omega} \sum_{\mathbf{k}} \frac{n_{\mathbf{k}+\mathbf{q}\uparrow} - n_{\mathbf{k}\downarrow}}{\epsilon_{\mathbf{k}+\mathbf{q}} - \epsilon_{\mathbf{k}}} \\ \xrightarrow{\mathbf{q} \rightarrow 0} &-\frac{2\mu_B^2}{\Omega} \sum_{\mathbf{k}} \frac{\partial f(\epsilon_{\mathbf{k}})}{\partial \epsilon_{\mathbf{k}}} = \chi_0(T),\end{aligned}\quad (7.59)$$

which corresponds to the Pauli susceptibility ($g = 2$). Then, $\chi(T)$ from equation (7.57) is again cast into the form (7.34) and describes the instability of the metal with respect to ferromagnetic spin polarization, when the denominator vanishes. Similar to the charge density wave, the isotropic deformation for $\mathbf{q} = \mathbf{0}$ is not the leading instability, when $\chi_0(\mathbf{Q}, 0) > \chi_0(\mathbf{0}, 0)$ for a finite \mathbf{Q} . Then, another form of magnetic order is more favored.

7.2.2 Instability with finite wave vector \mathbf{Q}

In order to show that, indeed, the Stoner instability does not always prevail among all possible magnetic instabilities, we first go through a simple argument based on the local susceptibility. For that, we define the local magnetic moment along the z -axis, $M(\mathbf{r}) = \mu_B \langle \hat{\rho}_\uparrow(\mathbf{r}) - \hat{\rho}_\downarrow(\mathbf{r}) \rangle$, and consider the nonlocal relation

$$M(\mathbf{r}) = \int d^3r' \tilde{\chi}_0(\mathbf{r} - \mathbf{r}') H_z(\mathbf{r}'), \quad (7.60)$$

within the linear response approximation. In Fourier space, the same relation reads

$$M_{\mathbf{q}} = \chi_0(\mathbf{q}) H_{\mathbf{q}}, \quad (7.61)$$

with

$$\chi_0(\mathbf{q}) = \int d^3r \tilde{\chi}_0(\mathbf{r}) e^{-i\mathbf{q}\cdot\mathbf{r}}. \quad (7.62)$$

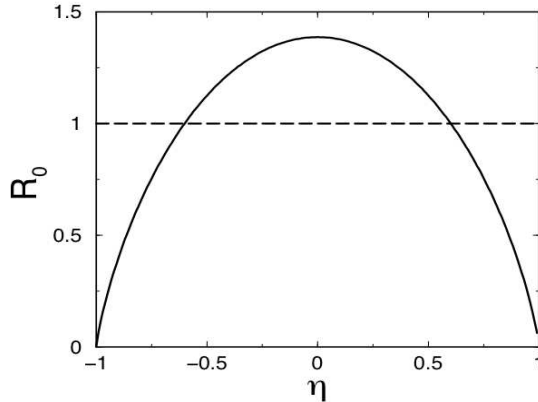


Figure 7.5: R_0 , the ratio between the local and the extended susceptibility, plotted for a box-shaped band with width $2D$. Depending where the Fermi energy lies $\eta = \epsilon_F/D$, the susceptibility is dominated by the contribution $\chi_0(\mathbf{q} = 0)$ or by the susceptibility at finite \mathbf{q} .

Now, compare $\chi_0(\mathbf{q} = 0)$ with $\overline{\chi_0(\mathbf{q})}$ defined as

$$\overline{\chi_0(\mathbf{q})} = \frac{1}{\Omega} \sum_{\mathbf{q}} \chi_0(\mathbf{q}) = \frac{1}{\Omega} \sum_{\mathbf{q}} \int d^3r \tilde{\chi}_0(\mathbf{r}) e^{-i\mathbf{q}\cdot\mathbf{r}} = \int d^3r \tilde{\chi}_0(\mathbf{r}) \delta(\mathbf{r}) = \tilde{\chi}_0(\mathbf{r} = 0). \quad (7.63)$$

This \mathbf{q} -averaged susceptibility corresponds to the local susceptibility. For a paramagnetic metal at $T = 0$ we may write

$$\overline{\chi_0(\mathbf{q})} = \frac{2\mu_B^2}{\Omega^2} \sum_{\mathbf{k}, \mathbf{q}} \frac{n_{\mathbf{k}+\mathbf{q}\uparrow} - n_{\mathbf{k}\downarrow}}{\epsilon_{\mathbf{k}} - \epsilon_{\mathbf{k}+\mathbf{q}}} = \frac{\mu_B^2}{2} \int d\epsilon N(\epsilon) \int d\epsilon' N(\epsilon') \frac{f(\epsilon) - f(\epsilon')}{\epsilon' - \epsilon}, \quad (7.64)$$

and must be compared to $\chi_0(\mathbf{q} = 0) = \mu_B^2 N(\epsilon_F)$ ($f(\epsilon) = \Theta(\epsilon_F - \epsilon)$). The local susceptibility depends on the density of states and the Fermi energy of the system. A very good qualitative understanding can be obtained by a very simple form

$$N(\epsilon) = \begin{cases} \frac{1}{D}, & -D \leq \epsilon \leq D, \\ 0, & |\epsilon| > D, \end{cases} \quad (7.65)$$

for the density of states which does not correspond to particular band structure but mimics a band of width $2D$. With this rough approximation, the integral in equation (7.64) is easily evaluated. The ratio between $\overline{\chi(\mathbf{q})}$ and $\chi_0(\mathbf{q} = 0)$ is then found to be

$$R_0 = \frac{\overline{\chi_0(\mathbf{q})}}{\chi_0(\mathbf{q} = 0)} = \ln \left(\frac{4}{1 - \eta^2} \right) + \eta \ln \left(\frac{1 - \eta}{1 + \eta} \right), \quad (7.66)$$

with $\eta = \epsilon_F/D$ where $-D < \epsilon_F < +D$. For both small and large band fillings (ϵ_F close to the band edges), the tendency towards ferromagnetism dominates (cf. Figure 7.5), whereas when ϵ_F lies in the center of the band, the susceptibility $\chi_0(\mathbf{q})$ is not maximal at $\mathbf{q} = 0$ anymore, and magnetic ordering with a well-defined finite $\mathbf{q} = \mathbf{Q}$ becomes more probable.

7.2.3 Influence of the band structure

Whether magnetic order arises at finite \mathbf{q} or not depends strongly on the details of the band structure. The argument given above, comparing the local ($\mathbf{r} = 0$) to the uniform ($\mathbf{q} = 0$) susceptibility is nothing more than a vague indicator for a possible instability at nonzero \mathbf{q} . A crucial ingredient for the appearance of magnetic order at a given $\mathbf{q} = \mathbf{Q}$ is the so-called *nesting* of the Fermi surface. Within extended areas of the Fermi surface the energy dispersion satisfies the nesting condition,

$$\xi_{\mathbf{k}+\mathbf{Q}} = -\xi_{\mathbf{k}} \quad (7.67)$$

where $\xi_{\mathbf{k}} = \epsilon_{\mathbf{k}} - \epsilon_F$ and \mathbf{Q} is some fixed vector. The nesting condition connects for given \mathbf{k} an electron- and hole-like band states (at $T = 0$ filled and empty states, respectively). If the Fermi surface of a material features such a nesting trait, the susceptibility will be dominated by the contribution from this vector \mathbf{Q} . In order to see this, let us investigate the static susceptibility $\chi_0(\mathbf{q})$ for $\mathbf{q} = \mathbf{Q}$ under the assumption, that equation (7.67) holds for all \mathbf{k} (see tight-binding example below). Thus,

$$\chi_0(\mathbf{Q}; T) = \frac{2\mu_B^2}{\Omega} \sum_{\mathbf{k}} \frac{n_{\mathbf{k}+\mathbf{Q}} - n_{\mathbf{k}}}{\xi_{\mathbf{k}} - \xi_{\mathbf{k}+\mathbf{Q}}} = \mu_B^2 \int \frac{d^3k}{(2\pi)^3} \frac{\tilde{f}(-\xi_{\mathbf{k}}) - \tilde{f}(\xi_{\mathbf{k}})}{\xi_{\mathbf{k}}}, \quad (7.68)$$

where $\tilde{f}(\xi) = f(\xi + \epsilon_F) = f(\epsilon) = [\exp(\xi/k_B T) + 1]^{-1}$ and f is the Fermi-Dirac distribution. Under the further assumption that $\xi_{\mathbf{k}}$ is weakly angle dependent, we find

$$\chi_0(\mathbf{Q}; T) = \mu_B^2 \int \frac{d^3k}{(2\pi)^3} \frac{\tanh(\xi_{\mathbf{k}}/2k_B T)}{\xi_{\mathbf{k}}} = \frac{\mu_B^2}{2} \int d\xi N(\xi + \epsilon_F) \frac{\tanh(\xi/2k_B T)}{\xi}. \quad (7.69)$$

In order to approximate this integral properly, we notice that the integral has a logarithmic divergence at infinite energies ξ . The band width gives a natural cutoff. Let us, therefore, take the density of states in Eq.(7.65) with $\epsilon_F = 0$,

$$\chi_0(\mathbf{Q}; T) \approx \mu_B^2 N(\epsilon_F) \int_0^D d\xi \frac{\tanh(\xi/2k_B T)}{\xi} \quad (7.70)$$

$$= \mu_B^2 N(\epsilon_F) \left(\ln \left(\frac{D}{2k_B T} \right) + \ln \left(\frac{4e^\gamma}{\pi} \right) \right) \approx \mu_B^2 N(\epsilon_F) \ln \left(\frac{1.14D}{2k_B T} \right), \quad (7.71)$$

where we assumed $D \gg k_B T$, and where $\gamma \approx 0.57721$ is the Euler constant. The bare susceptibility χ_0 diverges logarithmically at zero temperatures. Inserting the result (7.71) into the generalized Stoner relation (7.58), results in

$$0 = 1 - \frac{UN(\epsilon_F)}{2} \ln \left(\frac{1.14\epsilon_0}{2k_B T_c} \right), \quad (7.72)$$

with the critical temperature

$$k_B T_c = 1.14\epsilon_0 e^{-2/UN(\epsilon_F)}. \quad (7.73)$$

A finite critical temperature persists for arbitrarily small positive values of $UN(\epsilon_F)$. The nesting condition for a given \mathbf{Q} leads to a maximum of $\chi_0(\mathbf{q}, 0; T)$ at $\mathbf{q} = \mathbf{Q}$ and triggers the relevant instability in the system. The latter finally stabilizes in a magnetic ordered phase with wave vector \mathbf{Q} , the so-called *spin density wave*. The spin density distribution takes, for example, the form

$$\mathbf{S}(\mathbf{r}) = \hat{z} S \cos(\mathbf{Q} \cdot \mathbf{r}), \quad (7.74)$$

without a uniform component. In comparison, the charge density wave was a modulation of the charge density with a much smaller amplitude than the height of the uniform density, i.e.,

$$\rho(\mathbf{r}) = \rho_0 + \delta\rho \cos(\mathbf{Q} \cdot \mathbf{r}), \quad (7.75)$$

with $\delta\rho \ll \rho_0$. The spin density state frequently appear in low-dimensional systems like organic conductors, or in transition metals such as chromium (Cr) for example. In all cases, nesting plays an important role (cf. Figure 7.6).

In quasi-one-dimensional electron systems, a main direction of motion dominates over two other directions with weak dispersion. In this case, the nesting condition is very probable to be fulfilled, as it is schematically shown in the center panel of Figure 7.6. Chromium is a three-dimensional metal, where nesting occurs between a electron-like Fermi surface around the Γ -point and a hole-like Fermi surface at the Brillouin zone boundary (H -point). These Fermi surfaces originate in different bands (right panel in Figure 7.6). Chromium has a cubic body centered crystal structure, where the H -point at $(\pi/a, 0, 0)$ leads to the nesting vector $\mathbf{Q}_x \parallel (1, 0, 0)$ and equivalent vectors in y - and z -direction, which are incommensurable with the lattice.

The textbook example of nesting is found in a tight-binding model of a simple cubic lattice with nearest-neighbor hopping at half filling. The band structure is given by

$$\epsilon_{\mathbf{k}} = -2t[\cos(k_x a) + \cos(k_y a) + \cos(k_z a)], \quad (7.76)$$

where a is the lattice constant and t the hopping term. Because of half filling, the chemical potential $\mu = \epsilon_F$ lies at $\mu = 0$ such that $\xi_{\mathbf{k}} = \epsilon_{\mathbf{k}}$. Obviously, $\epsilon_{\mathbf{k}+\mathbf{Q}} = -\epsilon_{\mathbf{k}}$ holds for all \mathbf{k} , for the nesting vector $\mathbf{Q} = (\pi/a)(1, 1, 1)$. This full nesting trait is a signature of the total particle-hole symmetry, i.e. in the ground state there are as many occupied as empty states. Analogously to the Peierls instability, the spin density wave induces the opening of a gap at the Fermi surface. This is another example of a Fermi surface instability. In this situation, the gap is confined to the areas of the Fermi surface obeying the nesting condition. Contrarily to the ferromagnetic order, the material can become insulating when forming the spin density wave state.

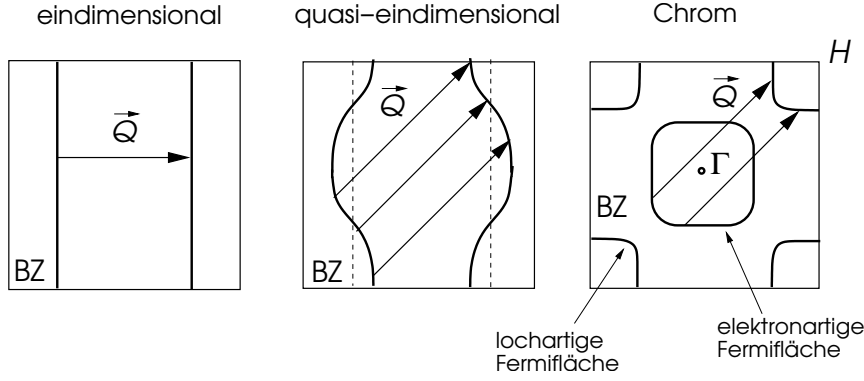


Figure 7.6: Sketch of Fermi surfaces favorable for nesting. In purely one-dimensional systems (left panel) there is a well-defined nesting vector pointing from one end of the Fermi surface to the other one. In quasi-one-dimensional systems nesting is almost perfect (central panel). In special cases (e.g. Cr) the Fermi surface(s) of three-dimensional systems show nesting properties (right panel) promoting an instability of the susceptibility at finite \mathbf{q} .

7.3 Stoner excitations

In this last section, we discuss the elementary excitations of the ferromagnetic ground state with $n_\uparrow > n_\downarrow$, including both particle-hole excitations and collective modes. We focus on spin excitations, for which we make the Ansatz

$$|\psi_{\mathbf{q}}\rangle = \sum_{\mathbf{k}} f_{\mathbf{k}} \hat{c}_{\mathbf{k}+\mathbf{q}\downarrow}^\dagger \hat{c}_{\mathbf{k}\uparrow} |\psi_g\rangle. \quad (7.77)$$

In this excitation, an electron is extracted from the ground state $|\psi_g\rangle$ and is replaced by an electron with opposite spin. We consider excitations with a fixed momentum transfer \mathbf{q} . We have to ensure that an electron with (\mathbf{k}, \downarrow) is available to be removed, and that the state $(\mathbf{k} + \mathbf{q}, \uparrow)$ is unoccupied. The excitation energy can be obtained by solving the following Schrödinger equation

$$\mathcal{H}|\psi_{\mathbf{q}}\rangle = (E_g + \hbar\omega_{\mathbf{q}})|\psi_{\mathbf{q}}\rangle, \quad (7.78)$$

with E_g as the ground state energy ($\mathcal{H}|\psi_g\rangle = E_g|\psi_g\rangle$). Actually it is more convenient to rearrange this equation into the following form eliminating E_g ,

$$\hbar\omega_{\mathbf{q}}|\psi_{\mathbf{q}}\rangle = \sum_{\mathbf{k}} f_{\mathbf{k}} [\mathcal{H}, \hat{c}_{\mathbf{k}+\mathbf{q}\downarrow}^\dagger \hat{c}_{\mathbf{k}\uparrow}] |\psi_g\rangle \quad (7.79)$$

with the Hamiltonian

$$\mathcal{H} = \sum_{\mathbf{k}, s} \epsilon_{\mathbf{k}} \hat{c}_{\mathbf{k}s}^\dagger \hat{c}_{\mathbf{k}s} + \frac{U}{\Omega} \sum_{\mathbf{k}, \mathbf{k}', \mathbf{q}'} \hat{c}_{\mathbf{k}+\mathbf{q}'\uparrow}^\dagger \hat{c}_{\mathbf{k}\uparrow} \hat{c}_{\mathbf{k}'-\mathbf{q}'\downarrow}^\dagger \hat{c}_{\mathbf{k}'\downarrow}. \quad (7.80)$$

Evaluating the commutator in Eq.(7.79) we obtain

$$\begin{aligned} \hbar\omega_{\mathbf{q}}|\psi_{\mathbf{q}}\rangle &= (\epsilon_{\mathbf{k}+\mathbf{q}} - \epsilon_{\mathbf{k}})|\psi_{\mathbf{q}}\rangle \\ &+ \frac{U}{\Omega} \sum_{\mathbf{k}} f_{\mathbf{k}} \sum_{\mathbf{k}', \mathbf{q}'} \left\{ \hat{c}_{\mathbf{k}'+\mathbf{q}'\uparrow}^\dagger \hat{c}_{\mathbf{k}'\uparrow} \hat{c}_{\mathbf{k}+\mathbf{q}-\mathbf{q}'\downarrow}^\dagger \hat{c}_{\mathbf{k}\uparrow} - \hat{c}_{\mathbf{k}+\mathbf{q}\downarrow}^\dagger \hat{c}_{\mathbf{k}-\mathbf{q}'\uparrow} \hat{c}_{\mathbf{k}'-\mathbf{q}'\downarrow}^\dagger \hat{c}_{\mathbf{k}'\downarrow} \right\} |\psi_g\rangle. \end{aligned} \quad (7.81)$$

The four- \hat{c} -operator terms are not so easy to handle. Therefore we decouple them through the following approximation,

$$\begin{aligned} & \hat{c}_{\mathbf{k}'+\mathbf{q}\uparrow}^\dagger \hat{c}_{\mathbf{k}'\uparrow} \hat{c}_{\mathbf{k}+\mathbf{q}\downarrow}^\dagger \hat{c}_{\mathbf{k}\downarrow} - \hat{c}_{\mathbf{k}+\mathbf{q}\downarrow}^\dagger \hat{c}_{\mathbf{k}-\mathbf{q}\uparrow} \hat{c}_{\mathbf{k}'-\mathbf{q}\downarrow}^\dagger \hat{c}_{\mathbf{k}'\downarrow} \\ \longrightarrow & \delta_{\mathbf{q}',0} (n_{\mathbf{k}'\uparrow} - n_{\mathbf{k}'\downarrow}) \hat{c}_{\mathbf{k}+\mathbf{q}\downarrow}^\dagger \hat{c}_{\mathbf{k}\downarrow} + (n_{\mathbf{k}+\mathbf{q}\downarrow} \delta_{\mathbf{k}',\mathbf{k}+\mathbf{q}} - n_{\mathbf{k}\uparrow} \delta_{\mathbf{k},\mathbf{k}'+\mathbf{q}'}) \hat{c}_{\mathbf{k}-\mathbf{q}'+\mathbf{q}\downarrow}^\dagger \hat{c}_{\mathbf{k}-\mathbf{q}'\uparrow} \end{aligned} \quad (7.82)$$

where $n_{\mathbf{k}s}$ is the Fermi-Dirac distribution for electrons of spin s with the energy $\epsilon_{\mathbf{k}s}$. We insert this approximation now into the Schrödinger equation (7.79) and multiply from the left with $\langle \psi_g | \hat{c}_{\mathbf{k}\uparrow}^\dagger \hat{c}_{\mathbf{k}+\mathbf{q}\downarrow}$ to obtain the projected equation,

$$f_{\mathbf{k}} \left\{ \hbar\omega_{\mathbf{q}} - \epsilon_{\tilde{\mathbf{k}}+\mathbf{q}} + \epsilon_{\tilde{\mathbf{k}}} - U(n_{\uparrow} - n_{\downarrow}) \right\} = \frac{U}{\Omega} \sum_{\mathbf{k}} f_{\mathbf{k}} (n_{\mathbf{k}+\mathbf{q}\downarrow} - n_{\mathbf{k}\uparrow}) = R_{\mathbf{q}} \quad (7.83)$$

where we used that the density of electrons of spin s is given by

$$n_s = \frac{1}{\Omega} \sum_{\mathbf{k}'} n_{\mathbf{k}'s}. \quad (7.84)$$

and we defined $R_{\mathbf{q}}$. We solve now Eq.(7.83) for the wave function $f_{\mathbf{k}}$ and obtain

$$f_{\mathbf{k}} = \frac{R_{\mathbf{q}}}{\hbar\omega_{\mathbf{q}} - \epsilon_{\mathbf{k}+\mathbf{q}\downarrow} + \epsilon_{\mathbf{k}\uparrow}} \quad (7.85)$$

with $\epsilon_{\mathbf{k}s} = \epsilon_{\mathbf{k}} + U n_{\bar{s}}$. We use now $f_{\mathbf{k}}$ to reexpress $R_{\mathbf{q}}$ which yields the implicit equation for the excitation energies $\hbar\omega_{\mathbf{q}}$,

$$R_{\mathbf{q}} = U R_{\mathbf{q}} \frac{1}{\Omega} \sum_{\mathbf{k}} \frac{n_{\mathbf{k}+\mathbf{q}\downarrow} - n_{\mathbf{k}\uparrow}}{\hbar\omega_{\mathbf{q}} - \epsilon_{\mathbf{k}+\mathbf{q}\downarrow} + \epsilon_{\mathbf{k}\uparrow}} \quad (7.86)$$

where we may divide by $R_{\mathbf{q}} \neq 0$. This equation contains a continuum of states corresponding to the electron-hole excitations given by

$$\hbar\omega_{\mathbf{q}} = \epsilon_{\mathbf{k}+\mathbf{q}\downarrow} - \epsilon_{\mathbf{k}\uparrow} = \epsilon_{\mathbf{k}+\mathbf{q}} - \epsilon_{\mathbf{k}} + U(n_{\uparrow} - n_{\downarrow}) = \epsilon_{\mathbf{k}+\mathbf{q}} - \epsilon_{\mathbf{k}} + \Delta. \quad (7.87)$$

This part of the spectrum is depicted by the shaded region in Fig.7.7. Note that the spin splitting of the spectrum opens a window in the low-energy low-momentum transfer sector of the excitations.

There is also a collective mode. It is easy to see from Eq.(7.86) that in the $\mathbf{q} \rightarrow 0$ limit we find

$$1 = \frac{U(n_{\downarrow} - n_{\uparrow})}{\hbar\omega_0 - U(n_{\uparrow} - n_{\downarrow})} \quad \Rightarrow \quad \hbar\omega_0 = 0 \quad (7.88)$$

indicating that there are excitations in the mentioned window. We calculate now the dispersion for small \mathbf{q} ($\ll k_F$). Using the fact that $\hbar\omega_{\mathbf{q}} \ll \Delta$ we can expand Eq.(7.86) leading to

$$\hbar\omega_{\mathbf{q}} \approx \left[1 + \frac{U}{\Omega} \sum_{\mathbf{k}} \frac{n_{\mathbf{k}+\mathbf{q}\downarrow} - n_{\mathbf{k}\uparrow}}{\epsilon_{\mathbf{k}+\mathbf{q}\downarrow} - \epsilon_{\mathbf{k}\uparrow}} \right] \left[-\frac{U}{\Omega} \sum_{\mathbf{k}} \frac{n_{\mathbf{k}+\mathbf{q}\downarrow} - n_{\mathbf{k}\uparrow}}{(\epsilon_{\mathbf{k}+\mathbf{q}\downarrow} - \epsilon_{\mathbf{k}\uparrow})^2} \right]^{-1}. \quad (7.89)$$

For small q we expand up order q^2 (actually q -linear contributions cancel),

$$\begin{aligned} \frac{U}{\Omega} \sum_{\mathbf{k}} \frac{n_{\mathbf{k}+\mathbf{q}\downarrow} - n_{\mathbf{k}\uparrow}}{\epsilon_{\mathbf{k}+\mathbf{q}} - \epsilon_{\mathbf{k}} + \Delta} & \approx \frac{U}{\Omega} \sum_{\mathbf{k}} \frac{n_{\mathbf{k}+\mathbf{q}\downarrow} - n_{\mathbf{k}\uparrow}}{\Delta} \left\{ 1 - \frac{\epsilon_{\mathbf{k}+\mathbf{q}} - \epsilon_{\mathbf{k}}}{\Delta} + \left(\frac{\epsilon_{\mathbf{k}+\mathbf{q}} - \epsilon_{\mathbf{k}}}{\Delta} \right)^2 \right\} \\ & \approx -1 + \frac{U}{\Omega} \sum_{\mathbf{k}} \left\{ \frac{n_{\mathbf{k}\uparrow} + n_{\mathbf{k}\downarrow}}{\Delta^2} \frac{\hbar^2 q^2}{2m} - \frac{n_{\mathbf{k}\uparrow} - n_{\mathbf{k}\downarrow}}{\Delta^2} \frac{(2\hbar^2 \mathbf{k} \cdot \mathbf{q})^2}{4m^2 \Delta} \right\} \\ & \approx -1 + \frac{\hbar^2 q^2}{2m\Delta^2} \left(U n_0 - \frac{4\epsilon_F}{3} \right) \end{aligned} \quad (7.90)$$

and analogously

$$\frac{U}{\Omega} \sum_{\mathbf{k}} \frac{n_{\mathbf{k}+\mathbf{q}\downarrow} - n_{\mathbf{k}\uparrow}}{(\epsilon_{\mathbf{k}+\mathbf{q}} - \epsilon_{\mathbf{k}} + \Delta)^2} \approx -\frac{1}{\Delta} \quad (7.91)$$

such that we obtain

$$\hbar\omega_{\mathbf{q}} \approx \frac{\hbar^2 q^2}{2m\Delta} \frac{2\epsilon_F}{3} (UN(\epsilon_F) - 2) \propto \frac{\hbar^2 q^2}{2m} \left(\frac{U}{U_c} - 1\right)^{1/2}. \quad (7.92)$$

Were we use that $\Delta \propto (U - U_c)^{1/2}$ for $U \rightarrow U_c$. Hence, if $U > U_c = 2/N(\epsilon_F)$ we find $\hbar\omega_{\mathbf{q}} > 0$. This collective excitation features a q^2 -dependent dispersion, vanishing in the limit $\mathbf{q} \rightarrow 0$. This is a consequence of the ferromagnetic state breaking a continuous symmetry. The continuous rotation symmetry is broken by the choice of a given direction of magnetization. A uniform $\mathbf{q} = 0$ rotation of the magnetization does not cost any energy $\omega_0 = 0$. This result was already found in equation (7.88) and is predicted by the so-called *Goldstone theorem*.³ Such an infinitesimal rotation is induced by a global spin rotation,

$$\sum_{\mathbf{k}} \hat{c}_{\mathbf{k}\downarrow}^\dagger \hat{c}_{\mathbf{k}\uparrow} = \hat{S}_{tot}^- \quad (7.93)$$

which acting on the ground state $|\psi_g\rangle$ leads to a degenerate state and corresponds to the state (7.77) with a wave function $f_{\mathbf{k}} = const.$. Since the elementary excitations have an energy gap of the order of Δ at small \mathbf{q} , the collective excitations, which are termed *magnons*, are well-defined quasiparticles describing propagating spin waves. When these modes enter the electron-hole continuum, they are damped in the same way as plasmons decaying into electrons and holes (see Figure 7.7). Being a bound state composed of an electron and a hole, magnons are bosonic quasiparticles.

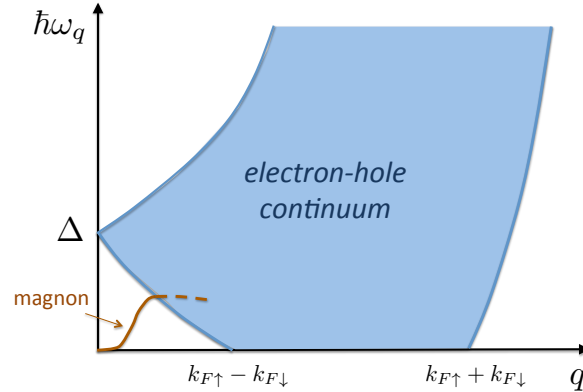


Figure 7.7: Schematic diagram of the elementary spin excitation spectrum (light gray) and collective modes (magnons, solid line) of the Stoner ferromagnet.

³The Goldstone theorem states that, in a system with a short-ranged interaction, a phase which is reached by the breaking of a continuous symmetry features a collective excitation with arbitrarily small energy, so-called *Goldstone modes*. These modes have bosonic character. In the case of the Stoner ferromagnet, these modes are the magnons or spin waves.

Chapter 8

Magnetism of localized moments

Up to now, we have mostly assumed that the interaction between electrons leads to secondary effects. This was, essentially, the message of the Fermi liquid theory, the standard model of condensed matter physics. There, the interactions of course renormalize the properties of a metal, but their description is still possible by using a language of nearly independent fermionic quasiparticles with a few modifications. Even in connection with the magnetism of itinerant electrons, where interactions proved to be crucial, the description in terms of extended Bloch states. Many properties were determined by the band structure of the electrons in the lattice, i.e., the electrons were preferably described in k -space.

However, in this chapter, we will consider situations, where it is less clear whether we should describe the electrons in momentum or in real space. The problem becomes obvious with the following Gedanken experiment: We look at a regular lattice of H-atoms. The lattice constant should be large enough such that the atoms can be considered to be independent for now. In the ground state, each H-atom contains exactly one electron in the $1s$ -state, which is the only atomic orbital we consider at the moment. The transfer of one electron to another atom would cost the relatively high energy of $E(H^+) + E(H^-) - 2E(H) \sim 15\text{eV}$, since it corresponds to an ionization. Therefore, the electrons remain localized on the individual H-atoms and the description of the electron states is obviously best done in real space. The reduction of the lattice constant will gradually increase the overlap of the electron wave functions of neighboring atoms. In analogy to the H_2 molecule, the electrons can now extend on neighboring atoms, but the cost in energy remains that of an “ionization”. Thus, transfer processes are only possible virtually, there are not yet itinerant electrons in the sense of a metal.

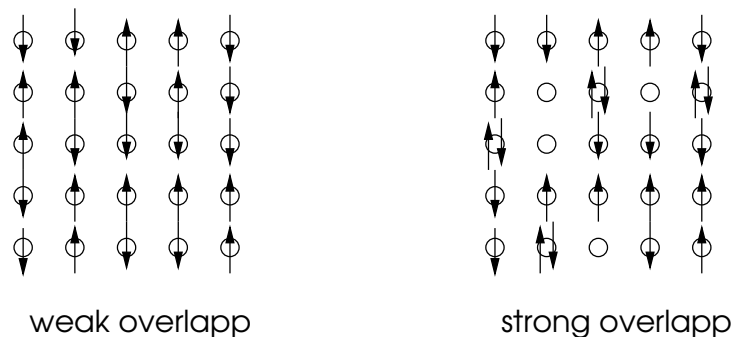


Figure 8.1: Possible states of the electrons in a lattice with weak or strong overlap of the electron wave functions, respectively.

On the other hand, we know the example of the alkali metals, which release their outermost n -electron into an extended Bloch state and build a metallic (half-filled) band. This would actually

work well for the H-atoms for sufficiently small lattice constant too.¹ Obviously, a transition between the two limiting behaviors should exist. This metal-insulator transition, which occurs, if the gain of kinetic energy surpasses the energy costs for the charge transfer. The insulating side is known as a Mott insulator.

While the obviously metallic state is reliably described by the band picture and can be sufficiently well approximated by the previously discussed methods, this point of view becomes obsolete when approaching the metal-insulator transition. According to band theory, a half-filled band must produce a metal, which definitely turns wrong when entering the insulating side of the transition. Unfortunately, no well controlled approximation for the description of this metal-insulator transition exists, since there are no small parameters for a perturbation theory.

Another important aspect is the fact, that in a standard Mott insulator each atom features an electron in the outermost occupied orbital and, hence, a degree of freedom in the form of a localized spin $s = 1/2$, in the simplest case. While charge degrees of freedom (motion of electrons) are frozen at small temperatures, the same does not apply to these spin degrees of freedom. Many interesting magnetic phenomena are produced by the coupling of these spins. Other, more general forms of Mott insulators exist as well, which include more complex forms of localized degrees of freedom, e.g., partially occupied degenerate orbital states.

8.1 Mott transition

First, we investigate the metal-insulator transition. Its description is difficult, since it does not constitute a transition between an ordered and a disordered state in the usual sense. We will, however, use some simple considerations which will allow us to gain some insight into the behavior of such systems.

8.1.1 Hubbard model

We introduce a model, which is based on the tight-binding approximation we have introduced in chapter 1. It is inevitable to go back to a description based on a lattice and give up continuity. The model describes the motion of electrons, if their wave functions on neighboring lattice sites only weakly overlap. Furthermore, the Coulomb repulsion, leading to an increase in energy, if a site is doubly occupied, is taken into account. We include this with the lattice analogue of the contact interaction. The model, called *Hubbard model*, has the form

$$\mathcal{H} = -t \sum_{\langle i,j \rangle, s} (\hat{c}_{is}^\dagger \hat{c}_{js} + \text{h.c.}) + U \sum_i \hat{n}_{i\uparrow} \hat{n}_{i\downarrow}, \quad (8.1)$$

where we consider hopping between nearest neighbors only, via the matrix element $-t$. Note, that \hat{c}_{is}^\dagger are real-space field operators on the lattice (site index i) and $\hat{n}_{is} = \hat{c}_{is}^\dagger \hat{c}_{is}$ is the density operator. We focus on half filling, $n = 1$, one electron per site on average. There are two obvious limiting cases:

- *Insulating atomic limit:* We put $t = 0$. The ground state has exactly one electron on each lattice site. This state is, however, highly degenerate. In fact, the degeneracy is 2^N (number of sites N), since each electron has spin $1/2$, i.e.,

$$|\Phi_{A0}\{s_i\}\rangle = \prod_i \hat{c}_{i,s_i}^\dagger |0\rangle, \quad (8.2)$$

where the spin configuration $\{s_i\}$ can be chosen arbitrarily. We will deal with the lifting of this degeneracy later. The first excited states feature one lattice site without electron

¹In nature, this can only be induced by enormous pressures metallic hydrogen probably exists in the centers of the large gas planets Jupiter and Saturn due to the gravitational pressure.

and one doubly occupied site. This state has energy U and its degeneracy is even higher, i.e., $2^{N-2}N(N-1)$. Even higher excited states correspond to more empty and doubly occupied sites. The system is an insulator and the density of states is shown in Figure 8.2.

- *Metallic band limit:* We set $U = 0$. The electrons are independent and move freely via hopping processes. The band energy is found through a Fourier transform of the Hamiltonian. With

$$\hat{c}_{is} = \frac{1}{\sqrt{N}} \sum_{\mathbf{k}} \hat{c}_{\mathbf{k}s} e^{i\mathbf{k}\cdot\mathbf{r}_i}, \quad (8.3)$$

we can rewrite

$$-t \sum_{\langle i,j \rangle, s} (\hat{c}_{is}^\dagger \hat{c}_{js} + h.c.) = \sum_{\mathbf{k}, s} \epsilon_{\mathbf{k}} \hat{c}_{\mathbf{k}s}^\dagger \hat{c}_{\mathbf{k}s}, \quad (8.4)$$

where

$$\epsilon_{\mathbf{k}} = -t \sum_{\mathbf{a}} e^{i\mathbf{k}\cdot\mathbf{a}} = -2t (\cos k_x a + \cos k_y a + \cos k_z a), \quad (8.5)$$

and the sum runs over all vectors \mathbf{a} connecting nearest neighbors. The density of states is also shown in Figure 8.2. Obviously, this system is metallic, with a unique ground state

$$|\Phi_{B0}\rangle = \prod_{\mathbf{k}} \Theta(-\epsilon_{\mathbf{k}}) \hat{c}_{\mathbf{k}\uparrow}^\dagger \hat{c}_{\mathbf{k}\downarrow}^\dagger |0\rangle. \quad (8.6)$$

Note, that $\epsilon_{\mathbf{F}} = 0$ at half filling, whereas the bandwidth $2D = 12t$.

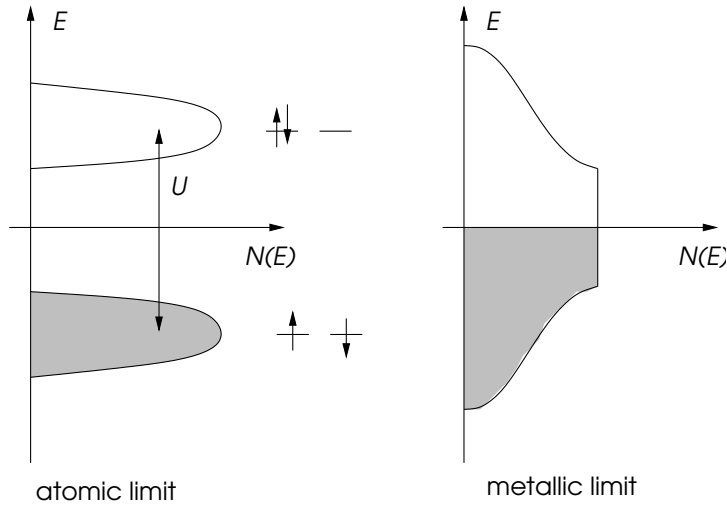


Figure 8.2: Density of states of the Hubbard model in the atomic limit (left) and in the free limit (right).

8.1.2 Insulating state

We consider the two lowest energy sectors for the case $t \ll U$. The ground state sector α has already been defined: one electron sits on each lattice site. The lowest excited states create the sector β with one empty and one doubly occupied site (cf. Figure 8.3). With the finite hopping matrix element, the empty (holon) and the doubly occupied (doublon) site become “mobile”. A

fraction of the degeneracy ($2^{N-2}N(N-1)$) is herewith lifted and the energy obtains a momentum dependence,

$$E_{\mathbf{k},\mathbf{k}'} = U + \epsilon_{\mathbf{k}} + \epsilon_{\mathbf{k}'} > U - 12t. \quad (8.7)$$

Even though ignoring the spin configurations here is a daring approximation, we obtain a qualitatively good picture of the situation.² One notices that, with increasing $|t|$, the two energy sectors approach each other, until they finally overlap. In the left panel Figure 8.2 the holon-doublon excitation spectrum is depicted by two bands, the lower and upper Hubbard bands, where the holon is a hole in the lower and the doublon a particle in the upper Hubbard band. The excitation gap is the gap between the two bands and we may interpret this system as an insulator, called a Mott insulator. (Note, however, that this band structure depends strongly on the correlation effects (e.g. spin correlation) and is not rigid as the band structure of a semiconductor.) The band overlap (closing of the gap) indicates a transition, after which a perturbative treatment is definitely inapplicable. This is, in fact, the metal-insulator transition.

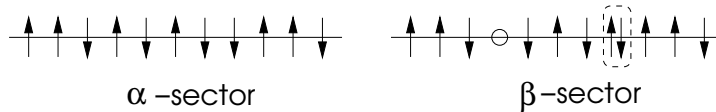


Figure 8.3: Illustration of the two energy sectors, α and β .

8.1.3 The metallic state

On the metallic side, the initial state is better defined since the ground state is a filled Fermi sea without degeneracy. The treatment of the Coulomb repulsion U turns out to become difficult, once we approach the Mott transition, where the electrons suffer a strong impediment in their mobility. In this region, there is no straight-forward way of a perturbative treatment. The so-called Gutzwiller approximation, however, provides a qualitative and very instructive insights into the properties of the strongly correlated electrons.

For this approximation we introduce the following important densities:

1: electron density

s_{\uparrow} : density of the singly occupied lattice sites with spin \uparrow

s_{\downarrow} : density of the singly occupied lattice sites with spin \downarrow

d : density of the doubly occupied sites

h : density of the empty sites

It is easily seen, that $h = d$ and $s_{\uparrow} = s_{\downarrow} = s/2$, as long as no uniform magnetization is present. Note, that d determines the energy contribution of the interaction term to Ud , which we regard as the index of fixed interaction energy sectors. Furthermore,

$$1 = s + 2d \quad (8.8)$$

holds. The view point of the Gutzwiller approximation is based on the renormalization of the probability of the hopping process due to the correlation of the electrons, exceeding restrictions

²Note that the motion of an empty site (holon) or doubly occupied site (doublon) is not independent of the spin configuration which is altered through moving these objects. As a consequence, the holon/doublon motion is not entirely free leading to a reduction of the band width. Therefore the band width seen in Figure 8.2 (left panel) is smaller than 2D, in general. The motion of a single hole was in detail discussed by Brinkman and Rice (Phys. Rev. B 2, 1324 (1970)).

due to the Pauli principle. With this, the importance of the spatial configuration of the electrons is enhanced. In the Gutzwiller approximation, the latter is taken into account statistically by simple probabilities for the occupation of lattice sites.

We fix the density of the doubly occupied sites d and investigate the hopping processes which keep d constant. First, we consider an electron hopping from a singly occupied to an empty site ($i \rightarrow j$). Hopping probability depends on the availability of the initial configuration. We compare the probability to find this initial state for the correlated (P) and the uncorrelated (P_0) case and write

$$P(\uparrow 0) + P(\downarrow 0) = g_t [P_0(\uparrow 0) + P_0(\downarrow 0)]. \quad (8.9)$$

The factor g_t will eventually appear as the renormalization of the hopping probability and, thus, leads to an effective kinetic energy of the system due to correlations. We determine both sides statistically. In the correlated case, the joint probability for i to be singly occupied and j to be empty is obviously

$$P(\uparrow 0) + P(\downarrow 0) = sh = sd = d(1 - 2d). \quad (8.10)$$

where we used equation (8.8). In the uncorrelated case (where d is not fixed), we have

$$P_0(\uparrow 0) = n_{i\uparrow}(1 - n_{i\downarrow})(1 - n_{j\uparrow})(1 - n_{j\downarrow}) = \frac{1}{16}. \quad (8.11)$$

The case for \downarrow follows accordingly. In order to collect the total result for hopping processes which keep d constant, we have to do the same calculation for the hopping process $(\uparrow\downarrow, \uparrow) \rightarrow (\uparrow, \uparrow\downarrow)$, which leads to the same result. Processes of the kind $(\uparrow\downarrow, 0) \rightarrow (\uparrow, \downarrow)$ leave the sector of fixed d and are ignored.³ With this, we obtain in all cases the same renormalization factor for the kinetic energy,

$$g_t = 8d(1 - 2d), \quad (8.12)$$

i.e., $t \rightarrow g_t t$. We consider the correlations by treating the electrons as independent but with a renormalized matrix element $g_t t$. The energy in the sector d becomes

$$E(d) = g_t \epsilon_{\text{kin}} + Ud = 8d(1 - 2d)\epsilon_{\text{kin}} + Ud, \quad \epsilon_{\text{kin}} = \frac{1}{N} \int_{-D}^0 d\epsilon N(\epsilon)\epsilon. \quad (8.13)$$

For fixed U and t , we can minimize this with respect to d (note that this is not a variational calculation in a strict sense, the resulting energy is not an upper bound to the ground state energy), and find

$$d = \frac{1}{4} \left(1 - \frac{U}{U_c} \right) \quad \text{and} \quad g_t = 1 - \left(\frac{U}{U_c} \right)^2, \quad (8.14)$$

with the critical value

$$U_c = 8|\epsilon_{\text{kin}}| \approx 25t \sim 4D. \quad (8.15)$$

For $u \geq U_c$, double occupancy and, thus, hopping is completely suppressed, i.e., electrons become localized. This observation by Brinkman and Rice [Phys. Rev. B **2**, 4302 (1970)] provides a qualitative description of the metal-insulator transition to a Mott insulator, but

³This formulation is based on plausible arguments. A more rigorous derivation can be found in the literature, e.g., in D. Vollhardt, Rev. Mod. Phys. **56**, 99 (1984); T. Ogawa et al., Prog. Theor. Phys. **53**, 614 (1975); S. Huber, *Gutzwiller-Approximation to the Hubbard-Model* (Proseminar SS02, <http://www.itp.phys.ethz.ch/proseminar/condmat02>).

takes into account only local correlations, while correlations between different lattice sites are not considered. Moreover, correlations between the spin degrees of freedom are entirely neglected. The charge excitations contain contributions between different energy scales: (1) a metallic part, described via the renormalized effective Hamiltonian

$$\mathcal{H}_{\text{ren}} = \sum_{\mathbf{k},s} g_t \epsilon_{\mathbf{k}} \hat{c}_{\mathbf{k}s}^\dagger \hat{c}_{\mathbf{k}s} + U d, \quad (8.16)$$

and (2) a part with higher energy, corresponding to charge excitations on the energy scale U , i.e., to excitations raising the number of doubly occupied sites by one (or more).

We can estimate the contribution to the metallic conduction. Since in the tight-binding description the current operator contains the hopping matrix element and is thus subject to the same renormalization as the kinetic energy, we obtain

$$\sigma_1(\omega) = \frac{\omega_p^{*2}}{4} \delta(\omega) + \sigma_1^{\text{high energy}}(\omega), \quad (8.17)$$

where we have used equation (6.12) for a perfect conductor (no residual resistivity in a perfect lattice). There is a high-energy part which we do not specify here. The plasma frequency is renormalized, $\omega_p^{*2} = g_t \omega_p^2$, such that the f -sum rule in equation (6.13) yields

$$I = \int_0^\infty d\omega \sigma_1(\omega) = \frac{\omega_p^2}{8} g_t + I_{\text{high energy}} = \frac{\omega_p^2}{8}. \quad (8.18)$$

For $U \rightarrow U_c$, the coherent metallic part becomes weaker and weaker,

$$\frac{\omega_p^2}{8} g_t = \left(1 - \left(\frac{U}{U_c}\right)^2\right) \frac{\omega_p^2}{8}. \quad (8.19)$$

According to the f -sum rule, the lost weight must gradually be transferred to the “high-energy” contribution.

8.1.4 Fermi liquid properties of the metallic state

The just discussed approximation allows us to discuss a few Fermi liquid properties of the metallic state close to metal-insulator transition in a simplified way. Let us investigate the momentum distribution. According to the above definition,

$$\epsilon_{\text{kin}} = \frac{1}{N} \sum_{\mathbf{k} \in \text{FS}} \epsilon_{\mathbf{k}}, \quad (8.20)$$

where the sum runs over all \mathbf{k} in the Fermi sea (FS). One can show within the above approximation, that the distribution is a constant within (n_{in}) and outside (n_{out}) the Fermi surface for finite U , such that, for \mathbf{k} in the first Brillouin zone,

$$\frac{1}{2} = \frac{1}{N} \sum_{\mathbf{k} \in \text{FS}} n_{\text{in}} + \frac{1}{N} \sum_{\mathbf{k} \notin \text{FS}} n_{\text{out}} = \frac{1}{2} (n_{\text{in}} + n_{\text{out}}) \quad (8.21)$$

and

$$g_t \epsilon_{\text{kin}} = \frac{1}{N} \sum_{\mathbf{k} \in \text{FS}} n_{\text{in}} \epsilon_{\mathbf{k}} + \frac{1}{N} \sum_{\mathbf{k} \notin \text{FS}} n_{\text{out}} \epsilon_{\mathbf{k}}. \quad (8.22)$$

Taking into account particle-hole symmetry, i.e.,

$$\sum_{\mathbf{k}} \epsilon_{\mathbf{k}} = \sum_{\mathbf{k} \in \text{FS}} \epsilon_{\mathbf{k}} + \sum_{\mathbf{k} \notin \text{FS}} \epsilon_{\mathbf{k}} = 0, \quad (8.23)$$

we are able to determine n_{in} and n_{out} ,

$$\left. \begin{array}{l} n_{\text{in}} + n_{\text{out}} = 1 \\ n_{\text{in}} - n_{\text{out}} = g_t \end{array} \right\} \Rightarrow \begin{cases} n_{\text{in}} = (1 + g_t)/2 \\ n_{\text{out}} = (1 - g_t)/2 \end{cases}. \quad (8.24)$$

With this, the jump in the distribution at the Fermi energy is equal to g_t , which, as previously, corresponds to the quasiparticle weight (cf. Figure 8.4). For $U \rightarrow U_c$ it vanishes, i.e., the quasiparticles cease to exist for $U = U_c$.

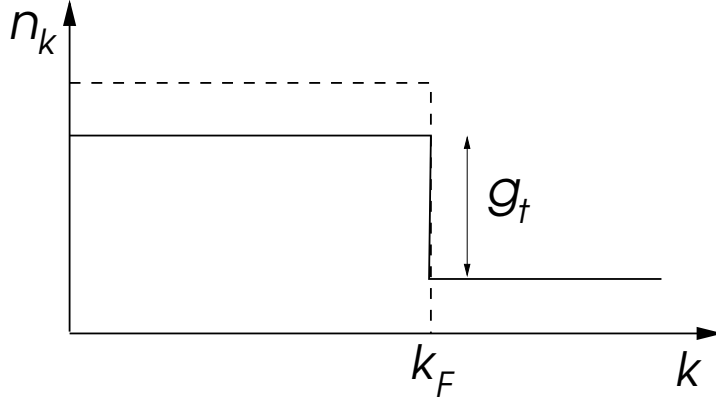


Figure 8.4: The distribution function in the Gutzwiller approximation, displaying the jump at the Fermi energy.

Without going into the details of the calculation, we provide a few Fermi liquid parameters. It is easy to see that the effective mass

$$\frac{m}{m^*} = g_t, \quad (8.25)$$

and thus

$$F_1^s = 3(g_t^{-1} - 1) = \frac{3U^2}{U_c^2 - U^2}, \quad (8.26)$$

where $t = 1/2m$ and the density of states $N(\epsilon_F)^* = N(\epsilon_F)g_t^{-1}$. Furthermore,

$$F_0^a = -\frac{UN(\epsilon_F)}{4} \frac{2U_c + U}{(U + U_c)^2} U_c, \quad \Rightarrow \quad \chi = \frac{\mu_B^2 N(\epsilon_F)^*}{1 + F_0^a}, \quad (8.27)$$

$$F_0^s = \frac{UN(\epsilon_F)}{4} \frac{2U_c - U}{(U - U_c)^2} U_c, \quad \Rightarrow \quad \kappa = \frac{N(\epsilon_F)^*}{n^2(1 + F_0^s)}. \quad (8.28)$$

It follows, that the compressibility κ vanishes for $U \rightarrow U_c$ as expected, since it becomes more and more difficult to compress the electrons or to add more electrons, respectively. The insulator is, of course, incompressible. The spin susceptibility diverges because of the diverging density of states $N(\epsilon_F)^*$. This indicates, that local spins form, which exist as completely independent degrees of freedom at $U = U_c$. Only the antiferromagnetic correlation between the spins would lead to a renormalization, which turns χ finite. This correlation is, as mentioned above, neglected in the Gutzwiller approximation. The effective mass diverges and shows that the quasiparticles are more and more localized close to the transition, since the occupation of a lattice site is getting more rigidly fixed to 1.⁴ As a last remark, it turns out that the Gutzwiller approximation is well suited to describe the strongly correlated Fermi liquid ³He (cf. [D. Vollhardt, Rev. Mod. Phys. **56**, 99 (1984)]).

⁴This can be observed within the Gutzwiller approximation in the form of local fluctuations of the particle number. For this, we introduce the density matrix of the electron states on an arbitrary lattice site,

$$\hat{\rho} = h|0\rangle\langle 0| + d|\uparrow\downarrow\rangle\langle\uparrow\downarrow| + \frac{s}{2}(|\uparrow\rangle\langle\uparrow| + |\downarrow\rangle\langle\downarrow|), \quad (8.29)$$

8.2 The Mott insulator as a quantum spin system

One of the most important characteristics of the Mott insulator is the presence of spin degrees of freedom after the freezing of the charge. This is one of the most profound features distinguishing a Mott insulator from a band insulator. In our simple discussion, we have seen that the atomic limit of the Mott insulator provides us with a highly degenerate ground state, where a spin-1/2 degree of freedom is present on each lattice site. We lift this degeneracy by taking into account the kinetic energy term \mathcal{H}_{kin} ($t \ll U$). In this way new physics appears on a low-energy scale, which can be described by an effective spin Hamiltonian. Prominent examples for such spin systems are transition-metal oxides like the cuprates La_2CuO_4 , SrCu_2O_3 or vanadates CaV_4O_9 , NaV_2O_5 .

8.2.1 The effective Hamiltonian

In order to employ our perturbative considerations, it is sufficient to observe the spins of two neighboring lattice sites and to consider perturbation theory for discrete degenerate states. Here, this is preferably done in real space. There are 4 degenerate configurations, $\{|\uparrow, \uparrow\rangle, |\uparrow, \downarrow\rangle, |\downarrow, \uparrow\rangle, |\downarrow, \downarrow\rangle\}$. The application of \mathcal{H}_{kin} yields

$$\mathcal{H}_{\text{kin}}|\uparrow, \uparrow\rangle = \mathcal{H}_{\text{kin}}|\downarrow, \downarrow\rangle = 0, \quad (8.31)$$

$$\mathcal{H}_{\text{kin}}|\uparrow, \downarrow\rangle = -\mathcal{H}_{\text{kin}}|\downarrow, \uparrow\rangle = -t|\uparrow\downarrow, 0\rangle - t|0, \uparrow\downarrow\rangle, \quad (8.32)$$

where, in the last two cases, the resulting states have an energy higher by U and lie outside the ground state sector. Thus, it becomes clear that we have to proceed to second order perturbation, where the states of higher energy will appear only virtually (cf. Figure 8.5).

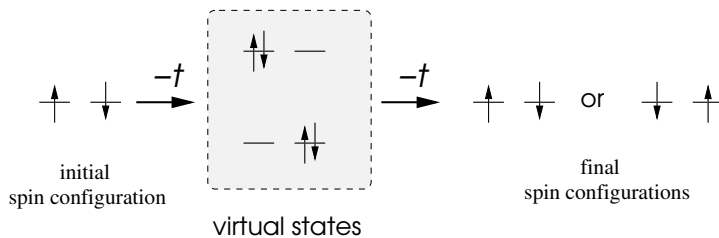


Figure 8.5: Illustration of the origin of the superexchange.

We obtain the matrix elements

$$M_{s_1, s_2; s'_1, s'_2} = - \sum_n \langle s_1, s_2 | \mathcal{H}_{\text{kin}} | n \rangle \frac{1}{\langle n | \mathcal{H}_{\text{Coul}} | n \rangle} \langle n | \mathcal{H}_{\text{kin}} | s'_1, s'_2 \rangle, \quad (8.33)$$

where $|n\rangle = |\uparrow\downarrow, 0\rangle$ or $|0, \uparrow\downarrow\rangle$, such that the denominator is always U . We end up with

$$M_{\uparrow\downarrow, \uparrow\downarrow} = M_{\downarrow\uparrow, \downarrow\uparrow} = -M_{\uparrow\downarrow, \downarrow\uparrow} = -M_{\downarrow\uparrow, \uparrow\downarrow} = -\frac{2t^2}{U}. \quad (8.34)$$

from which we deduce the variance of the occupation number,

$$\langle n^2 \rangle - \langle n \rangle^2 = \langle n^2 \rangle - 1 = \text{tr}(\hat{\rho} n^2) - 1 = 4d + s - 1 = 2d. \quad (8.30)$$

The deviation from single occupation vanishes with d , i.e., with the approach of the metal-insulator transition. Note that the dissipation-fluctuation theorem connects $\langle n^2 \rangle - \langle n \rangle^2$ to the compressibility.

Note that the signs originates from the anti-commutation properties of the Fermion operators. In the subspace $\{|\uparrow, \downarrow\rangle, |\downarrow, \uparrow\rangle\}$ we find the eigenstates of the respective secular equations,

$$\frac{1}{\sqrt{2}}(|\uparrow, \downarrow\rangle + |\downarrow, \uparrow\rangle), \quad E = 0, \quad (8.35)$$

$$\frac{1}{\sqrt{2}}(|\uparrow, \downarrow\rangle - |\downarrow, \uparrow\rangle), \quad E = -\frac{4t^2}{U}. \quad (8.36)$$

Since the states $|\uparrow, \uparrow\rangle$ and $|\downarrow, \downarrow\rangle$ have energy $E = 0$, the sector with total spin $S = 1$ is degenerate (spin triplet). The spin sector $S = 0$ with the energy $-4t^2/U$ is the ground state (spin singlet).

An effective Hamiltonian with the same energy spectrum for the spin configurations can be written with the help of the spin operators $\widehat{\mathbf{S}}_1$ and $\widehat{\mathbf{S}}_2$ on the two lattice sites

$$\mathcal{H}_{\text{eff}} = J \left(\widehat{\mathbf{S}}_1 \cdot \widehat{\mathbf{S}}_2 - \frac{\hbar^2}{4} \right), \quad J = \frac{4t^2}{U\hbar^2} > 0. \quad (8.37)$$

This mechanism of spin-spin coupling is called *superexchange* and introduced by P.W. Anderson [Phys. Rev. **79**, 350 (1950)].

Since this relation is valid between all neighboring lattice sites, we can write the total Hamiltonian as

$$\mathcal{H}_H = J \sum_{\langle i,j \rangle} \widehat{\mathbf{S}}_i \cdot \widehat{\mathbf{S}}_j + \text{const.} \quad (8.38)$$

This model, reduced to spins only, is called *Heisenberg model*. The Hamiltonian is invariant under a global $SU(2)$ spin rotation,

$$U_s(\boldsymbol{\theta}) = e^{-i\widehat{\mathbf{S}} \cdot \boldsymbol{\theta}}, \quad \widehat{\mathbf{S}} = \sum_j \widehat{\mathbf{S}}_j. \quad (8.39)$$

Thus, the total spin is a good quantum number, as we have seen in the two-spin case. The coupling constant is positive and favors an antiparallel alignment of neighboring spins. The ground state is therefore not ferromagnetic.

8.2.2 Mean field approximation of the anti-ferromagnet

There are a few exact results for the Heisenberg model, but not even the ground state energy can be calculated exactly (except in the case of the one-dimensional spin chain which can be solved by means of a Bethe Ansatz). The difficulty lies predominantly in the treatment of quantum fluctuations, i.e., the zero-point motion of coupled spins. It is easiest seen already with two spins, where the ground state is a singlet and maximally entangled. The ground state of all antiferromagnetic systems is a spin singlet ($S_{\text{tot}} = 0$). In the so-called thermodynamic limit ($N \rightarrow \infty$) there is long-ranged anti-ferromagnetic order in the ground state for dimensions $D \geq 2$. Contrarily, the fully polarized ferromagnetic state (ground state for a model with $J < 0$) is known exactly, and as a state with maximal spin quantum number \mathbf{S}^2 it features no quantum fluctuations.

In order to describe the antiferromagnetic state anyway, we apply the mean field approximation again. We can characterize the equilibrium state of the classical Heisenberg model (spins as simple vectors without quantum properties) by splitting the lattice into two sublattices A and B , where each A -site has only B -sites as neighbors, and vice-versa.⁵ On the A -(B -)sublattice, the spins point up (down). This is unique up to a global spin rotations. Note, that this spin

⁵Lattices which allow for such a separation are called *bipartite*. There are lattices, where this is not possible, e.g., triangular or cubic face centered lattices. There, frustration phenomena appear, a further complication of anti-ferromagnetically coupled systems.

configuration doubles the unit cell.

We introduce the respective mean field,

$$\widehat{S}_i^z = \begin{cases} m + (\widehat{S}_i^z - m) & i \in A \\ -m + (\widehat{S}_i^z + m) & i \in B \end{cases}. \quad (8.40)$$

This leads to the mean field Hamiltonian

$$\mathcal{H}_{\text{mf}} = \mathcal{H}_A + \mathcal{H}_B = -Jzm \sum_{i \in A} \widehat{S}_i^z + Jzm \sum_{i \in B} \widehat{S}_i^z + Jz \frac{m^2}{2} N + \dots, \quad (8.41)$$

with the coordination number z , the number of nearest neighbors ($z = 6$ in a simple cubic lattice). It is simple to calculate the partition sum of this Hamiltonian,

$$Z = \text{tr} \left(e^{-\beta \mathcal{H}_{\text{mf}}} \right) = \left[\left(e^{\beta Jzm\hbar/2} + e^{-\beta Jzm\hbar/2} \right) e^{-\beta Jzm^2/2} \right]^N. \quad (8.42)$$

The free energy per spin is consequently given by

$$F(m, T) = -\frac{1}{N} k_B T \ln Z = Jz \frac{m^2}{2} - k_B T \ln (2 \cosh(\beta Jzm\hbar/2)). \quad (8.43)$$

At fixed temperature, we minimize the free energy with respect to m to determine the thermal equilibrium state,⁶ i.e., set $\partial F/\partial m = 0$ and find

$$m = \frac{\hbar}{2} \tanh \left(\frac{Jzm\hbar}{2k_B T} \right). \quad (8.44)$$

This is the self-consistency equation of the mean field theory. It provides a critical temperature T_N (Néel temperature), below which the mean moment m is finite. For $T \rightarrow T_{N-}$, m approaches 0 continuously. Thus, T_N can be found from a linearized self-consistency equation,

$$m = \frac{Jzm\hbar^2}{4k_B T} \Big|_{T=T_N}, \quad (8.45)$$

and thus

$$T_N = \frac{Jz\hbar^2}{4k_B}. \quad (8.46)$$

This means, that T_N scales with the coupling constant and with z . The larger J and the more neighbors are present, the more stable is the ordered state.⁷ For T close to T_N , we can expand the free energy in m ,

$$F(m, T) = F_0 + \frac{Jz}{2} \left[\left(1 - \frac{T_N}{T} \right) m^2 + \frac{2}{3\hbar^2} \left(\frac{T_N}{T} \right)^3 m^4 \dots \right]. \quad (8.47)$$

This is a Landau theory for a phase transition of second order, where a symmetry is spontaneously broken. The breaking of the symmetry (from the high-temperature phase with high symmetry to the low-temperature phase with low symmetry) is described by the order parameter m . The minimization of F with respect to m yields (cf. Figure 8.6)

$$m(T) = \begin{cases} 0, & T > T_N, \\ \frac{\hbar}{2} \sqrt{3(T_N/T - 1)}, & T \leq T_N. \end{cases} \quad (8.48)$$

⁶Actually, a magnetic field pointing into the opposite direction on each site would be another equilibrium variable (next to the temperature). We set it to zero.

⁷At infinite z , the mean field approximation becomes exact.

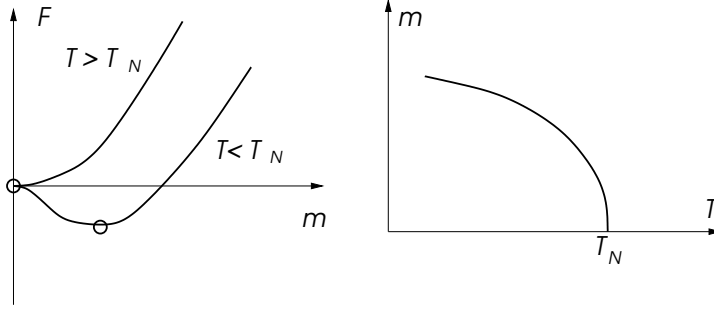


Figure 8.6: The free energy and magnetization of the anti-ferromagnet above and below T_N .

8.3 Collective modes – spin wave excitations

Besides its favorable properties, the mean field approximation also has a number of insufficiencies. Quantum and some part of thermal fluctuations are neglected, and the insight into the low-energy excitations remains vague. As a matter of fact, as in the case of the ferromagnet, collective excitations exist here. In order to investigate these, we write the Heisenberg model in its spin components, i.e.,

$$\mathcal{H}_H = J \sum_{\langle i,j \rangle} \left(\hat{S}_i^z \hat{S}_j^z + \frac{1}{2} \left(\hat{S}_i^+ \hat{S}_j^- + \hat{S}_i^- \hat{S}_j^+ \right) \right). \quad (8.49)$$

In the ordered state, the moments shall be aligned along the z -axis.

To observe the dynamics of a flipped spin, we apply the operator $\widehat{W} = \sum_{l=0}^N f_l \widehat{S}_l^-$ on the ground state $|\Phi_0\rangle$, and determine the spectrum, by solving the resulting eigenvalue equation

$$(\mathcal{H}_H - E_0) \widehat{W} |\Phi_0\rangle = [\mathcal{H}_H, \widehat{W}] |\Phi_0\rangle = \hbar\omega \widehat{W} |\Phi_0\rangle, \quad (8.50)$$

with the ground state energy E_0 . Using the spin-commutation relations

$$[\hat{S}_j^+, \hat{S}_j^-] = 2\hat{S}_j^z \delta_{ij}, \quad (8.51)$$

$$[\hat{S}_j^z, \hat{S}_j^\pm] = \pm \hat{S}_j^\pm \delta_{ij}, \quad (8.52)$$

then yields the equation

$$\sum_l \left[-J \sum_j' \hat{S}_j^z \hat{S}_l^- + J \sum_j' \hat{S}_j^- \hat{S}_l^z - \hbar\omega \hat{S}_l^- \right] |\Phi_0\rangle = 0, \quad (8.53)$$

where \sum_j' runs over all neighbors of l . We decouple this complicated problem by replacing the operators \hat{S}^z by their mean fields. Therefore, we have to distinguish between A and B sublattices, such that we end up with two equations,

$$\sum_{l \in A} f_l^A \left(Jmz \hat{S}_l^- + Jm \sum_{\mathbf{a}} \hat{S}_{l+\mathbf{a}}^- - \hbar\omega \hat{S}_l^- \right) |\Phi_0\rangle = 0, \quad l \in A, \quad (8.54)$$

$$\sum_{l' \in B} f_{l'}^B \left(-Jmz \hat{S}_{l'}^- - Jm \sum_{\mathbf{a}} \hat{S}_{l'+\mathbf{a}}^- - \hbar\omega \hat{S}_{l'}^- \right) |\Phi_0\rangle = 0, \quad l' \in B. \quad (8.55)$$

Choosing

$$f_l^A = \sqrt{\frac{2}{N}} e^{-i\mathbf{q} \cdot \mathbf{r}_l} \quad l \in A, \quad (8.56)$$

$$f_{l'}^B = \sqrt{\frac{2}{N}} e^{-i\mathbf{q} \cdot \mathbf{r}_{l'}} \quad l' \in B,$$

we introduce the operators

$$\widehat{S}_l^- = \sqrt{\frac{2}{N}} \sum_{\mathbf{q}} \widehat{a}_{\mathbf{q}}^\dagger e^{i\mathbf{q}\cdot\mathbf{r}_l}, \quad (8.57)$$

$$\widehat{S}_{l'}^- = \sqrt{\frac{2}{N}} \sum_{\mathbf{q}} \widehat{b}_{\mathbf{q}}^\dagger e^{i\mathbf{q}\cdot\mathbf{r}_{l'}}, \quad (8.58)$$

with $l \in A$ and $l' \in B$, and, vice versa,

$$\widehat{a}_{\mathbf{q}}^\dagger = \sqrt{\frac{2}{N}} \sum_{l \in A} \widehat{S}_l^- e^{-i\mathbf{q}\cdot\mathbf{r}_l}, \quad (8.59)$$

$$\widehat{b}_{\mathbf{q}}^\dagger = \sqrt{\frac{2}{N}} \sum_{l' \in B} \widehat{S}_{l'}^- e^{-i\mathbf{q}\cdot\mathbf{r}_{l'}}, \quad (8.60)$$

and insert them into the equation and obtain,

$$\left((Jmz - \hbar\omega) \sum_{l \in A} \widehat{S}_l^- e^{-i\mathbf{q}\cdot\mathbf{r}_l} + Jm \sum_{\mathbf{a}} e^{i\mathbf{q}\cdot\mathbf{a}} \sum_{l' \in B} \widehat{S}_{l'}^- e^{-i\mathbf{q}\cdot\mathbf{r}_{l'}} \right) |\Phi_0\rangle = 0, \quad (8.61)$$

$$\left((-Jmz - \hbar\omega) \sum_{l' \in B} \widehat{S}_{l'}^- e^{-i\mathbf{q}\cdot\mathbf{r}_{l'}} - Jm \sum_{\mathbf{a}} e^{i\mathbf{q}\cdot\mathbf{a}} \sum_{l \in A} \widehat{S}_l^- e^{-i\mathbf{q}\cdot\mathbf{r}_l} \right) |\Phi_0\rangle = 0. \quad (8.62)$$

From this follows that

$$\left((Jmz - \hbar\omega) \widehat{a}_{\mathbf{q}}^\dagger + Jm\gamma_{\mathbf{q}} \widehat{b}_{\mathbf{q}}^\dagger \right) |\Phi_0\rangle = 0, \quad (8.63)$$

$$\left((-Jmz - \hbar\omega) \widehat{b}_{\mathbf{q}}^\dagger - Jm\gamma_{\mathbf{q}} \widehat{a}_{\mathbf{q}}^\dagger \right) |\Phi_0\rangle = 0, \quad (8.64)$$

with $\gamma_{\mathbf{q}} = \sum_{\mathbf{a}} e^{i\mathbf{q}\cdot\mathbf{a}} = 2(\cos q_x a + \cos q_y a + \cos q_z a)$. This eigenvalue equation is easily solved leading to the description of spin waves in the antiferromagnet. The energy spectrum is given by

$$\hbar\omega_{\mathbf{q}} = \pm Jm\sqrt{z^2 - \gamma_{\mathbf{q}}^2}. \quad (8.65)$$

Note, that only the positive energies make sense. It is interesting to investigate the limit of small \mathbf{q} ,

$$z^2 - \gamma_{\mathbf{q}}^2 \rightarrow z^2 \mathbf{q}^2 + O(q^4), \quad (8.66)$$

where

$$\hbar\omega_{\mathbf{q}} = Jmz|\mathbf{q}| + \dots. \quad (8.67)$$

This means that, in contrast to the ferromagnet, the spin waves of the antiferromagnet have a linear low-energy spectrum (cf. Figure 8.7). The same applies here if we expand the spectrum around $\mathbf{Q} = (1, 1, 1)\pi/a$ (folding of the Brillouin zone due to the doubling of the unit cell).

After a suitable normalization, the operators $\widehat{a}_{\mathbf{q}}$ and $\widehat{b}_{\mathbf{q}}$ are of bosonic nature; this comes about since, due to the mean field approximation, the \widehat{S}_l^\pm are bosonic as well,

$$[\widehat{S}_l^+, \widehat{S}_j^-] = 2\widehat{S}_l^z \delta_{lj} \approx \pm 2m\delta_{lj}, \quad (8.68)$$

where the sign depends on the sublattice. The zero-point fluctuations of these bosons yield quantum fluctuations, which reduce the moment m from its mean field value. In a one-dimensional

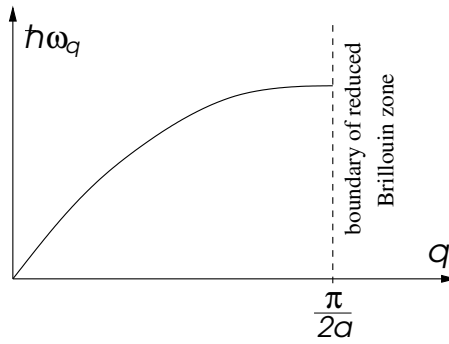


Figure 8.7: Spectrum of the spin waves in the antiferromagnet.

spin chain these fluctuations are strong enough to suppress antiferromagnetic order even for the ground state. The fact that the spectrum starts at zero has to do with the infinite degeneracy of the ground state. The ordered moments can be turned into any direction globally. This property is known under the name *Goldstone theorem*, which tells that each ordered state that breaks a continuous symmetry has collective excitations with arbitrary small (positive) energies. The linear spectrum is normal for collective excitations of this kind; the quadratic spectrum of the ferromagnet has to do with the fact that the state breaks time-inversion symmetry.

These spin excitations show the difference between a band and a Mott insulator very clearly. While in the band insulator both charge and spin excitations have an energy gap and are inert, the Mott insulator has only gapped charge excitation. However, the spin degrees of freedom for a low-energy sector which can even form gapless excitations as shown just above.